RADIO ENGINEERING
and
ELECTRONIC PHYSICS

English Edition of

РАДИОТЕХНИКА
И
ЭЛЕКТРОНИКА

Published by the American Institute of Electrical Engineers
with the aid of a grant from the National Science Foundation

No.5 May 1961

Translated and Produced by Royer and Roger, Inc.

AMERICAN INSTITUTE OF ELECTRICAL ENGINEERS

Established 1884

345 East Forty-Seventh Street
New York 17, N. Y.

Warren H. Chase, President
N.S. Hibshman, Executive Secretary
C.E. Dean, Technical Vice President, Communications
W.F. Denkhaus, Director of Publications
L.G. Abraham, Chairman, Communications Division

The English edition of RADIO ENGINEERING AND ELECTRONIC PHYSICS is published by the American Institute of Electrical Engineers with the aid of a grant from the National Science Foundation. © 1961 by American Institute of Electrical Engineers. Also published under the same arrangement are the Russian electronic journals RADIO ENGINEERING and TELECOMMUNICATIONS.

RADIO ENGINEERING AND ELECTRONIC PHYSICS

(РАДИОТЕХНИКА И ЭЛЕКТРОНИКА)

Publication of the Institute of Radio Engineering and Electronic Physics,
Academy of Sciences of the USSR

Translated and Produced
by
Royer and Roger, Inc.

Translation Editor: Ivo Herzer, Columbia University

AIEE REVIEW COMMITTEE FOR RADIO ENGINEERING AND ELECTRONIC PHYSICS
Leonard S. Schwartz
New York University College of Engineering
Chairman

A.W. Bickley
W.P. Birkemeier
T.T.W. Bucher
J.L. Callahan
G.R. Cooper
W.A. Depp
R.G. Enticknay
A. Burr Fontaine
F.E. Froelich
Paul H. Gleichauf
G.S. Glinski
Bernard Harris
R.K. Hellmann
D.E. Higginbotham
W.Miller
Harry Rowe Mimno
W.W. Peterson
B. Reiffen
W.G. Schmidt
Herbert Sherman
D.L. Solomon
C.A. Stutt
G.C. Sziklai
Joseph Vogelman
G.M. White
F.B. Wood
H.L. Yudkin

Subscriptions to Radio Engineering and Electronic Physics should be sent to AIEE
Special Subscription Department
41 East 28th Street, New York 16, New York

1961 Subscription rates:

	$	£
Individuals	28.50	10
Libraries, institutes, govt. agencies	57.00	20

12 issues per annum comprising approximately 1900 pages

THE KINETIC POWER THEOREM AND ITS APPLICATION TO ELECTRON BEAM DEVICES

V.M. Lopukhin

The application of the kinetic-power theorem to the operation of several microwave electron-beam devices, such as the transit klystron, the traveling-wave tube, and the double-beam tube is considered.

The possibility of extracting energy from a fast space-charge wave and the possibility of reducing the noise in electron-beam devices are discussed.

INTRODUCTION

The question of increased sensitivity (that is, reduced noise figure) of devices such as traveling wave tubes (TWT) has been under continual discussion in recent published papers.

It has been established that the noise figure of a TWT with longitudinal interaction between beam and field is determined by the properties and the operating conditions of the cathode and by the potential distribution in the gun. To reduce the noise figure of a TWT at a certain frequency, it is necessary that the noise waves, which are excited in the beam by shot processes of the same frequency in the cathode, induce a minimum noise emf in the TWT input antenna, which also receives the amplified signal. A review of the work done prior to 1957 is found in references [1,2], which contain an appropriate bibliography.

References [3,4] describe TWT amplifiers for the 10-cm band with a noise figure less than 4 db. These tubes incorporate guns with a tubular electron beam and a special distribution of the static field in the gun, the field build up being quite slow and deviating from the Langmuir law. The minimum measured noise figure is 3.5 db.

Reference [5] reported a 10-cm TWT tube with a minimum noise figure also of 3.5 db. The beam was in the form of a solid cylinder, and the field varied very smoothly in the gun.

Backward wave tubes with 2.9 db minimum noise figure and with guns of the same type as in references [3,4] have been investigated by Currie et al. [6].

We recall that the minimum noise figure of a TWT is 6.3 db according to the single-velocity theory, a figure which is much higher than the noise figure of experimental tubes. The apparent reason for this is that near the cathode of the experimental tube, where the potential builds up rather slowly, there is a long multi-velocity region which acts as a transformer to reduce the noise in the beam.

The question of the noise figure of a TWT with transverse high-frequency field is studied in [8,9].

Longitudinal random currents do not interact with the transverse fields and, consequently hardly influence the noise figure.

Transverse random electron displacements occurring in the electron gun are partially reduced with a collimator — a narrow slit restricting the passage of the electron beam from the gun.

The minimum noise figure obtained in a TWT of this type is 6 db, while the rated minimum noise figure is 2 db.

Further reduction in the TWT noise figure can be attained by a more detailed investigation of the waves in the electron beam, waves excited by current and velocity fluctuations and also by the amplified signal. It is known [10, 11] that the time-varying quantities characterizing the current, velocity, and current density in an electron beam can be represented as a superposition of fast and slow electron-beam waves. The fast waves are associated with the predominance of fast electrons in the beam, and the slow waves are due to the slow electrons. These waves have interesting properties. Thus, for example a fast wave, including one excited by shot-noise current or velocity fluctuations, can be extracted from the electron beam by means of some slow-wave system or resonator, whereas a slow wave cannot be extracted. At the same time, the operation of a traveling wave tube, that is, the appearance of growing waves in the slow-wave system, is due to slowing down of the electrons, that is, to an increase in the amplitude of the slow electron wave.

The use of these properties of electron waves has been proposed to "render the electron beam noiseless," or more accurately speaking, to reduce the amplitude of the fast electron waves excited in the electron beam by the shot fluctuations of the current of velocity density. The signal wave is introduced into the electron beam instead of the fast noise wave. Such a wave, however, cannot be amplified by the usual operating mechanism of the traveling wave tube. It has been proposed that the amplification be effected by parametric action on the electron beam.

An electron beam receives, in addition, a signal consisting of a fast space-charge wave and noise in the form of a slow electron wave in the beam, but also pumping power of frequency $\omega_p \neq \omega$ (ω is the signal frequency). Under these conditions, solutions that increase with the coordinate are possible for the fast signal wave, providing certain relationships exist between the problem parameters. The power source in this case is the pumping wave.

Amplifiers of this type are called parametric electron-beam amplifiers. Articles [12 — 14] are devoted to a theoretical investigation of electron-beam parametric amplifiers with longitudinal interaction. The problem is most fully treated in [14], where all the combination frequencies produced in the electron beam by the pumping are taken into account. References [15 — 18] report on experimental investigations of the amplification associated with the parametric interaction in an electron beam in the absence of a slow-wave system [15,16], in a backward wave tube [17], and in a TWT [18]. Articles [19,20] are devoted to a theoretical study of the transformation of the waves in a slow-wave system surrounding an electron beam. It is shown that the fast wave of the electron beam can be converted into the slow wave and then absorbed by a matched load. At the same time, the signal from the slow-wave system can be converted into a fast beam wave.

Experimental investigations of the noise figure of parametric TWT with longitudinal interaction have thus far not yielded good results: There are no descriptions of tubes of this type with low noise coefficient in the literature.

The most effective noise-figure reduction has been produced by parametric TWT with transverse field [21 — 24]. Some tubes of this type have a noise coefficient of 1.3 db, which is much less than the noise coefficient of even the best types of nonparametric TWT.

The theory of a parametric transverse-field amplifier is developed in references [25, 26].

It is the purpose of the present review to discuss several problems connected with the energy flow in electron beams and with the application of the kinetic power theorem to electron-beam devices. This theorem, formulated by Chu [27,28], is closely connected with the problem of extraction of noise power from an electron beam. This theory also explains the mechanism whereby the electrons interact with the field and gives a criterion for the reality of expressions that rise exponentially with the coordinate for fields that appear in the simultaneous solution of the equation of motion of the electrons and of the electromagnetic field.

This theorem was generalized by Haus [29] for a parametric electron beam. It is connected with the Manly-Row [30] relations, which describe the flow of energy in nonlinear systems with reactance elements.

1. KINETIC POWER THEOREM FOR N-RAY BEAM

The law of conservation of energy in an electron beam, as applied to the theory of small amplitudes, has been cast in the form of a kinetic-power theorem.

This theorem was derived by Chu [27,28] for a single beam. We give below a derivation of this theorem for a beam with N rays.

We consider a volume V, bounded by a closed surface S (see Figure 1). Assume that N electron beams penetrate through this volume and propagate in the z direction with average velocity v_{0n}(n , 1, 2, . . . , N). The beams are considered to be intermixed over the cross section, and the average electronic charge is assumed to be compensated by the ion background

Let the electron velocity, the charge density, and the current density of the electrons in beam number n have the form

$$\vec{v}_{0n} + \vec{v}_n \exp i\omega t, \tag{1}$$

$$\rho_{0n} + \rho_n \exp i\omega t, \tag{2}$$

$$\vec{j}_{0n} + \vec{j}_n \exp i\omega t, \tag{3}$$

where $\vec{v}_{0n}$, ρ_{0n}, and $\vec{j}_{0n}$ are the dc components of the corresponding quantities, independent of either the coordinates or the time, while v_n, ρ_n, and $\vec{j}_n$ are the amplitudes of the variable coordinates, which are independent of the time but may depend on the coordinates: ω is the angular frequency.

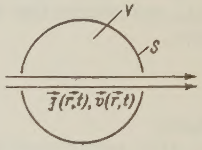

Figure 1. Cavity of volume V, bounded by a surface S, transversed by an electron beam whose density is $\vec{j}(\vec{r}, t)$ and velocity is $\vec{v}(\vec{r}, t)$.

We assume that the theory of small amplitudes is in force, so that

$$|v_n| \ll v_{0n}, \tag{4}$$

$$|\rho_n| \ll \rho_{0n}, \tag{5}$$

$$|j_h| \ll j_{0n}. \tag{6}$$

We start from Maxwell's equations, the continuity equation, and the electron equation of motion

$$[\nabla \vec{E}] = -i\omega\mu\vec{H}, \tag{7}$$

$$[\nabla \vec{H}] = i\omega\varepsilon\vec{E} + \sum_{n=1}^{N} \vec{j}_n, \tag{8}$$

$$\nabla \vec{j}_n = -i\omega\rho_n, \tag{9}$$

$$i\omega\vec{v}_n + (\vec{v}_{0n}\nabla)\vec{v}_n = \frac{e}{m}\vec{E}, \tag{10}$$

where $\vec{E}$ and $\vec{H}$ are the intensities of the electric and magnetic fields, μ and ϵ are the permeability and the dielectric constant of the substance filling the volume V, while e and m are the charge and mass of the electron.

Multiplying (7) by $\vec{H}^*$, multiplying the equation conjugate to (8) by $\vec{E}$, and then subtracting respectively the left and right halves of the resultant equations (8) and (7), we obtain

$$\nabla [\vec{E}\vec{H}^*] = -i\omega\mu\vec{H}\vec{H}^* + i\omega\varepsilon EE^* - \sum_{n=1}^{N} \vec{E}\vec{j}_n^*. \tag{11}$$

Multiplying (11) by $\vec{j}_n^*$, we get

$$i\omega\vec{v}_n\vec{j}_n^* + \vec{j}_n^*(\vec{v}_{0n}\nabla)\vec{v}_n = \frac{e}{m}\vec{E}\vec{j}_n^*. \tag{12}$$

Using the small-amplitude condition, we get

$$\vec{j}_n = \rho_{0n}\vec{v}_n + \vec{v}_{0n}\rho_n. \tag{13}$$

We assume henceforth that the electrons move only along the z-axis, that is, $j = j_z$ and $v = v_z$. Substituting in (12) the value of $\vec{j}_n^*$ calculated with the aid of (13) and the value of ρ_n from (9), we get

$$\vec{E}\vec{j}_n^* = \frac{m}{e}\,[i\omega v_n v_n^* \rho_{0n} + \nabla\,(\vec{j}_n^* v_{0n} v_n)]. \tag{14}$$

Substituting (12) in (11) we have

$$\nabla\left([\vec{E}\vec{H}^*] + \sum_{n=1}^{N} \vec{j}_n^* \frac{m}{e} v_{0n} v_n\right) = i\omega\left[(\varepsilon\vec{E}\,\vec{E}^* - \mu\vec{H}\vec{H}^*) - \sum_{n=1}^{N}\frac{m}{e}\rho_{0n} v_n v_n^*\right]. \tag{15}$$

Integrating both halves of (15) over the volume V, transforming further in the left half to the surface integral over the surface S, and evaluating the real part of the resultant equation, we obtain the mathematical formulation of the kinetic-power theorem for a N-beam tube:

$$\{P_{\text{rad}}\} + \{P_{\text{к}}\} = 0, \tag{16}$$

where

$$\{P_{\text{rad}}\} = \frac{1}{2}\,\mathrm{Re}\int_S [\vec{E}\vec{H}^*]\,d\vec{S}; \tag{17}$$

$$\{P_{\text{к}}\} = \frac{1}{2}\,\mathrm{Re}\sum_{n=1}^{N}\int V_{\text{к}n}\,\vec{j}_n^*\,d\vec{S}; \tag{18}$$

$\{P_{\text{rad}}\}$ is the power radiated through the surface S, averaged over the cycle; when $\{P_{\text{rad}}\} > > 0$, the energy flows out of the volume V; $\{P_k\}$ is the kinetic power of the N-ray beam, averaged over the cycle; $V_{kn} = (m/e)v_{0n}v_n$ is the kinetic potential of beam number n.

It is clear from relations (15) and (16) that $\{P_k\} = \{P_e\}$, where $\{P_e\}$ is the electronic power of the interaction between the beam and the field, averaged over the cycle and given by the equation

$$\{P_e\} = \frac{1}{2}\,\mathrm{Re}\int_V \vec{j}^*\,\vec{E}\,dV. \tag{19}$$

Let us modify somewhat the expression (18) for kinetic power. Let S_0 be the section of the electron beam, and let $\vec{j}_n$ and V_{kn} have the form

$$\vec{j}_n = \psi(x, y)\, j_n(z)\,\vec{z}_0, \quad V_{\text{к}n} = \psi(x, y)\, V_{\text{к}n}(z),$$

where ψ (x,y) is a function characterizing the distribution of the current density and of the kinetic potential over the section of the beam.

Let us examine the portion of the electron beam contained between the planes z = 0 and z = l. The surface is made up of the sum $S_1 + S_2 + S_3$, where S_1 and S_3 are the end surfaces and S_2 the side surface of the cylindrical electron beam. Integrating in (19) over the surface S, we obtain

$$\{P_{\text{к}}\} = \frac{1}{2}\,\mathrm{Re}\left[\sum_{n=1}^{N}\hat{I}_n(l)\,V_{\text{к}n}(l) - \sum_{n=1}^{N}\hat{I}_n(0)\,V_{\text{к}n}(0)\right], \tag{20}$$

where $I_n(l) = \hat{S}j(l)$; $\hat{S} = \int_{S_0}\psi^2\,dx\,dy$; $j_n(0)$, $V_{\text{к}n}(0)$, $j_n(l)$, $V_{\text{к}n}(l)$ are the values of j_n and V_{kn} in the initial and final sections of the electron beam. The next task is to calculate the value of $\{P_e\} = \{P_k\}$ for different waves in the electron beams and to determine the conditions under which $\{P_k\} < 0$.

2. WAVES IN ELECTRON BEAM AND THE KINETIC POWER THEOREM

Let us apply the kinetic-power theorem to waves in an electron beam. It is known (see for example, [11]) that in an electron beam having an average velocity v_0 and a charge density ρ_0, there can propagate at a frequency ω, in the linear approximation, two waves with propagation constants β_1 and β_2

$$\beta_1 = \beta_e - \beta_p, \tag{21}$$

$$\beta_2 = \beta_e + \beta_p, \tag{22}$$

where

$$\beta_e = \frac{\omega}{v_0}; \quad \beta_p = \frac{\omega_0}{v_0}; \quad \omega_0^2 = \frac{e\rho_0}{m\varepsilon_0}.$$

These waves have phase velocities

$$v_{\text{ph1}} = v_0\left(1 - \frac{\omega_0}{\omega}\right)^{-1} > v_0 \tag{23}$$

and

$$v_{\text{ph2}} = v_0\left(1 + \frac{\omega_0}{\omega}\right)^{-1} < v_0. \tag{24}$$

Thus, β_1 corresponds to the fast wave in the beam while β_2 to the slow one.

The expressions for the field intensity E, the current density j, and the electron velocity v have the following form

$$E = (E_1 e^{i\beta_p z} + E_2 e^{-i\beta_p z})\, e^{-i\beta_e z}, \tag{25}$$

$$j = -i\omega\varepsilon_0 (E_1 e^{i\beta_p z} + E_2 e^{-i\beta_p z})\, e^{-i\beta_e z}, \tag{26}$$

$$v = e\,(mi\omega_p)^{-1} (E_1 e^{i\beta_p z} - E_2 e^{-i\beta_p z})\, e^{-i\beta_e z}. \tag{27}$$

It follows from (25) — (27) that E, j, and v are superpositions of two waves with propagation constants β_1 and β_2. The amplitudes of the waves of field intensities E_1 and E_2 are determined by the initial conditions, that is, by the values of v(0) and j(0) at the input to the system.

Actually, putting z = 0 in (26) and (27), we get

$$j(0) = -i\omega\varepsilon_0 (E_1 + E_2), \tag{28}$$

$$v(0) = e\,(mi\omega_p)^{-1} (E_1 - E_2). \tag{29}$$

Solving (28) and (29) with respect to E_1 and E_2, we get

$$E_1 = \frac{1}{2}\left[-j(0)\,(i\omega\varepsilon_0)^{-1} + \frac{m}{e}\, i\omega_p\, v(0)\right], \tag{30}$$

$$E_2 = \frac{1}{2}\left[-j(0)\,(i\omega\varepsilon_0)^{-1} - \frac{m}{e}\, i\omega_p\, v(0)\right]. \tag{31}$$

j(0) and v(0) are complex quantities, which depend on the method used to modulate the beam at the section z = 0. In the general case $E_1 \neq E_2$.

Introducint the kinetic potential $V_k(z) = mv_0 v/e$ and using (27), we get

$$V_k(z) = (i\beta_p)^{-1} e^{-i\beta_e z} (E_1 e^{i\beta_p z} - E_2 e^{-i\beta_p z}). \tag{32}$$

For the convection current in the cross section S_0 we obtain the expression

$$I = S_0 j = -i\omega\varepsilon_0 S_0 e^{-i\beta_e z} (E_1 e^{i\beta_p z} + E_2 e^{-i\beta_p z}). \tag{33}$$

Let us find the equivalent impedance Z of the electron beam at the cross section z:

$$Z = \frac{V_k}{I} = Z_0 \frac{E_1 e^{i\beta_p z} - E_2 e^{-i\beta_p z}}{E_1 e^{i\beta_p z} + E_2 e^{-i\beta_p z}}, \tag{34}$$

where

$$Z_0 = (\beta_p\, \omega\, \varepsilon_0 S_0)^{-1}. \tag{35}$$

Formula (34) is equivalent to the expression for the impedance of a two-conductor line with wave impedance Z_0 and propagation constant β_p. If the conditions for the excitation of the electron beam at the cross section z = 0 are such that $E_2 = 0$, we find from (34) that $Z = Z_0 > 0$. Thus, the current and the electron velocity are in phase in the fast wave.

For the case $E_1 = 0$ and $E_2 \neq 0$, when only the slow wave is excited in the beam, we have $Z = -Z_0 < 0$. The current and the electron velocity are in phase opposition in the slow wave.

Let us calculate the power, averaged over the cycle, of the interaction between the

the current and the kinetic potential V_k at the cross section z:

$$\{\hat{P}\} = \frac{1}{2}\operatorname{Re} I^* V_k = \frac{1}{2}\operatorname{Re} Z I I^* = \{\operatorname{Re} I \operatorname{Re} V_k\}.$$

Putting in lieu of $\operatorname{Re} I$ and $\operatorname{Re} V_k$ the expressions $\operatorname{Re} I = S_0(\rho_0 \operatorname{Re} \tilde{v} + v_0 \operatorname{Re} \tilde{\rho})$, where S_0 is the cross section of the beam, and $\operatorname{Re} V_k = \frac{m v_0}{e} \operatorname{Re} \tilde{v}$,, we obtain

$$\{\hat{P}\} = \frac{S_0 m v_0}{e}[\rho_0 \{(\operatorname{Re} \tilde{v})^2\} + \tilde{v}_0 \{\operatorname{Re} \tilde{\rho} \operatorname{Re} \tilde{v}\}]. \tag{36}$$

It follows from (36) that the average value of the kinetic-power flux in the wave $\{\hat{P}\}$ consists of two terms. One is positive and proportional to $\{(\operatorname{Re} v)^2\}$, and is connected with the kinetic energy of the electrons in the given cross section, while the second is proportional to $\{(\operatorname{Re} \tilde{\rho} \operatorname{Re} \tilde{v}\}$ and can be either positive or negative. Let $\{\operatorname{Re} \rho \operatorname{Re} v\} < 0$. Then two cases are possible: 1) $\operatorname{Re} \tilde{\rho} > 0$, $\operatorname{Re} \tilde{v} < 0$, 2) $\operatorname{Re} \tilde{\rho} < 0$, $\operatorname{Re} \tilde{v} > 0$. In the first case the increase in concentration of particles above the average level is accompanied by a reduction in particle velocity. In the second case the reduction in charge-particle concentration is accompanied by an increase in their velocity. Consequently, when $\{\operatorname{Re} \tilde{\rho} \operatorname{Re} \tilde{v}\} < 0$ the wave contains on the average more slow electrons than fast ones. By analogous reasons we can show that when $\{\operatorname{Re} \tilde{\rho} \operatorname{Re} \tilde{v}\} > 0$ the wave has on the average more fast electrons than slow ones.

Let us return to expression (36). We consider the case $\{\hat{P}\} < 0$. With this, $\{\operatorname{Re} \tilde{\rho} \operatorname{Re} \tilde{v}\} < -\frac{\rho_0}{v_0}\{(\operatorname{Re} \tilde{v})^2\} < 0$ and consequently the wave has an excess of slow electrons and a shortage of fast ones. To the contrary, if $\{\operatorname{Re} \tilde{\rho} \operatorname{Re} \tilde{v}\} > 0$, which corresponds to an excess of fast electrons, we have $\{\hat{P}\} > 0$, as follows from (36). We note that the condition $\{\operatorname{Re} \tilde{\rho} \operatorname{Re} \tilde{v}\} > 0$ is not necessary to obtain $\{\hat{P}\} > 0$, in view of the presence of a term proportional to $\{(\operatorname{Re} \tilde{v})^2\}$. This, however, is unessential for our qualitative argument, since usually the inequality $\rho_0 \{(\operatorname{Re} \tilde{v})^2\} \ll \{\operatorname{Re} \tilde{\rho} \operatorname{Re} \tilde{v}\}$ is satisfied. That this inequality holds for space-charge waves can be readily verified by using the expression for $\rho = -\frac{1}{i\omega}\frac{\partial j}{\partial z}$, and also formulas (26) and (27).

Our arguments concern beams of positively charged particles. The conclusions remain the same for electron beams, since the negative sign of the electron charge leads to the need for simultaneous reversal of the signe of I and V_k.

Substituting (32) and (33) in (36), we obtain

$$\{\hat{P}\} = (2 Z_0 \beta_p^2)^{-1}(E_1 E_1^* - E_2 E_2^*). \tag{37}$$

The average power of interaction between the current I and the kinetic potential V_k is thus the sum of the power fluxes produced by the fast and slow waves. The fast wave carries a positive power

$$\{\hat{P}_1\} = (2 Z_0 \beta_p^2)^{-1} E_1 E_1^* > 0. \tag{38}$$

This is due to the excess electron kinetic energy, that is, to the fast electrons. The slow wave carries a negative power

$$\{\hat{P}_2\} = -(2 Z_0 \beta_p^2)^{-1} E_2 E_2^* < 0. \tag{39}$$

The physical meaning of this inequality is that slow electrons predominate in the slow waves. In the general case $\{\hat{P}_1\} \neq \{\hat{P}_2\}$, since $E_1 \neq E_2$ [see expressions (30) and (31)] . We note that the kinetic power of $\{\hat{P}\}$ of the electron beam must not be confused with the electromagnetic power $\{P_{em}\}$ of the field in the beam. The value of $\{P_{em}\}$ is given by the expression $\{P_{em}\} = \frac{1}{2}\operatorname{Re} V I^*$, where I is the electron current in the beam and V is the high frequency potential, connected with the longitudinal field E_z by the relation $E_z = -\partial V/\partial z$. Reference [31] gives for space-charge waves in an electron beam the relation $\{P_{em}\}/\{\hat{P}\} = \pm\omega_p/\omega$, where ω and ω_p are the operating frequency and the plasma frequency respectively; the plus and minus sign correspond to the fast and slow waves. Usually $\omega_p \ll \omega$; thus, the electromagnetic-field power in the space-charge wave is much lower than the kinetic power. The energy exchange between the beam and the resonator or else between the beam and the slow-wave system is due to the change in the kinetic power. The fact that the electron beam has a finite cross section with area S_0 was introduced formally above; the problem was essentially regarded as one-dimensional. A correct account of the finite cross section of the electron beam is found in references [32 — 34], where it is shown that if an electron beam of radius a passes along the axis of a waveguide of radius b ($a \leqslant b$), it is necessary to replace β_p in the formulas of the linear theory (for example (25) — (27)) by $\beta_{ef}(\beta_e a, a/b)$. Plots of the function $\beta_{ef}/\beta_p = \omega_{ef}/\omega_p$ are listed in [33, 34].

The fact that the beam has a finite cross section and the presence of the waveguide lead to a reduction in the effective plasma frequency.

3. THE KINETIC POWER THEOREM AS APPLIED TO THE PROBLEM OF RESONATOR EXCITATION

Let us apply the kinetic power theorem to the following problem. An electron beam passes through a cavity (see Fig 2) in which the electric field varies as $\mathcal{E}e^{i\omega t}$.

The current density on the electron velocity at the entrance to the cavity is known, with values $j_0 = j(0)e^{i\omega t}$ and $v_0 + v(0)e^{i\omega t}$. The corresponding values at the exit from the cavity are $j_0 + j(\varphi_0)\, e^{i\omega t}$ and $v_0 + v(\varphi_0)e^{i\omega t}$, where $\varphi_0 = \omega d / v_0$; d is the length of the interaction space in the cavity. Let the surface S encompass the cavity. The kinetic power theorem then assumes the form

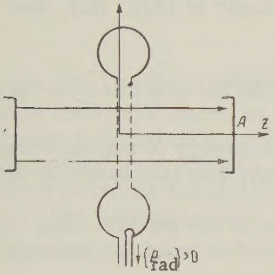

Figure 2. A toroidal type cavity is traversed by an electron beam. K — cathode, A — Collector; the surface S encloses the cavity, the input section corresponds to z = 0, while the output section corresponds to z = = d. If energy is radiated out of the cavity, then $\{P_{rad}\} >$ > 0.

$$\{P_{rad}\} + \{\hat{P}(\varphi_0)\} - \{\hat{P}(0)\} = 0, \qquad (40)$$

where $\{P_{rad}\}$ is the radiated power averaged over the cycle; $\{\hat{P}(\varphi_0)\}$ and $\{\hat{P}(0)\}$ are the kinetic power fluxes, averaged over the cycle, through the entrance and exit sections of the cavity, and on the basis of (37) we have

$$\{\hat{P}(0)\} = (2Z_0\beta_p^2)^{-1}[E_1(0)\, E_1^*(0) - E_2(0)\, E_2^*(0)], \qquad (41)$$

$$\{\hat{P}(\varphi_0)\} = (2Z_0\beta_p^2)^{-1}[E_1(\varphi_0)\, E_1^*(\varphi_0) - E_2(\varphi_0)\, E_2^*(\varphi_0)], \qquad (42)$$

where $E_1(0)$ and $E_2(0)$ are the amplitudes of the fast and slow waves in the beam at the cross section z = 0; $E_1(\varphi_0)$ and $E_2(\varphi_0)$ are the amplitudes of the same waves at the section z = d (the asterisk denotes the complex conjugate); Z_0 is the impedance of the beam; $\beta_p = \omega_p / v_0$. In accordance with (30) and (31) we have

$$E_1(0) = \frac{1}{2}\left(-\frac{j(0)}{i\omega\varepsilon_0} + \frac{m}{e}v(0)\, i\omega_p\right), \qquad (43)$$

$$F_2(0) = \frac{1}{2}\left(-\frac{j(0)}{i\omega\varepsilon_0} - \frac{m}{e}v(0)\, i\omega_p\right), \qquad (44)$$

$$E_1(\varphi_0) = \frac{1}{2}\left(-\frac{j(\varphi_0)}{i\omega\varepsilon_0} + \frac{m}{e}v(\varphi_0)\, i\omega_p\right), \qquad (45)$$

$$E_2(\varphi_0) = \frac{1}{2}\left(-\frac{j(\varphi_0)}{i\omega\varepsilon_0} - \frac{m}{e}v(\varphi_0)\, i\omega_p\right). \qquad (46)$$

It follows from (41) — (46) that the kinetic power flux in the electron beam is in general different from 0, since $E_1(0) = E_2(0)$ and $E_1(\varphi_0) = E_2(\varphi_0)$ only if the parameters of the problem are especially chosen.

Comparing (40) with the equation of energy conservation

$$\{P_{rad}\} + \{P_e\} = 0, \qquad (47)$$

we obtain

$$\{\hat{P}(\varphi_0)\} - \{\hat{P}(0)\} = \{P_e\}, \qquad (48)$$

that is, the change in the kinetic power flux due to the passage of the electrons through the cavity is equal to the average electron power of interaction between the beam and the field $\{P_e\}$, which was calculated earlier (see, for example [32, 35, 36]).

Let us examine several particular cases.

1) $\{P_e\} < 0$; the electron beam transfers power to the cavity; $\{P_{rad}\} > 0$, the electromagnetic energy is radiated from the cavity. On the basis of (41), (42). and (48) we have

$$E_1(\varphi_0)E_1^*(\varphi_0) - E_1(0)E_1^*(0) < E_2(\varphi_0)E_2^*(\varphi_0) - E_2(0)E_2^*(0), \tag{49}$$

that is, the passage through the cavity causes the amplitude of the slow wave, which carries negative power, to grow more intensely than the amplitude of the fast wave. In other words, the content of the slow wave in the beam has increased after passage through the cavity.

2) $\{P_e\} = 0$; $\{P_{rad}\} = 0$; no electromagnetic energy is radiated from the cavity. With the aid of (41), (42), and (48) we obtain

$$E_1(\varphi_0)E_1^*(\varphi_0) - E_1(0)E_1^*(0) = E_2(\varphi_0)E_2^*(\varphi_0) - E_2(0)E_2^*(0), \tag{50}$$

that is, the energies of the fast and slow waves experience equal changes as a result of passage through the cavity.

3) $\{P_e\} > 0$; the electron beam takes power from the cavity; $\{P_{rad}\} < 0$, the power should be pumped into the cavity from the external source. On the basis of (41), (42), and (48) we obtain

$$E_1(\varphi_0)E_1^*(\varphi_0) - E_1(0)E_1^*(0) > E_2(\varphi_0)E_2^*(\varphi_0) - E_2(0)E_2^*(0), \tag{51}$$

that is, the energy of the fast wave increases more strongly than the energy of the slow wave. As a result of passage through the cavity, the content of the fast wave has increased in the beam, and consequently the contents of the slow one has decreased.

Thus, the kinetic power theorem makes it possible to estimate in the general case the change in the amplitudes of the fast and slow waves in the beam resulting from the passage through the cavity.

Assume that waves of frequency ω are excited in the beam by shot fluctuations. We shall henceforth call these waves, for brevity, noise waves.

From the foregoing argument it follows that passage of an electron beam through the cavity enables us to reduce the amplitude of the fast noise wave but not to reduce the amplitude of a slow noise wave.

4. ENERGY FLOW IN A DOUBLE CAVITY KLYSTRON AMPLIFIER

The flow of energy in a double-cavity klystron amplifier is considered in reference [10]. The construction of a double-cavity klystron amplifier is shown in Figure 3a. The electron beam produced by the cathode K is accelerated to a potential $V_0 = mv_0^2/2e$ and then passes through the interaction spaces of cavities I and II. The length of the interaction space of the two cavities is regarded as small, so that passage through the interaction spaces of the cavities results in a jump in the electron velocity, while the current density remains the same on both sides of the cavity.

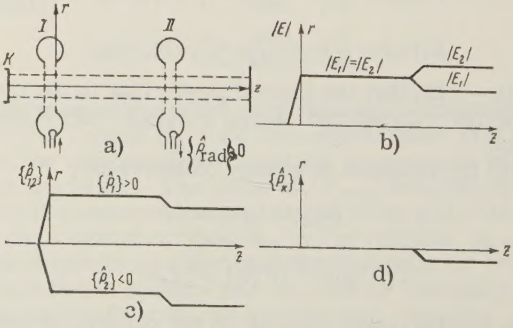

Figure 3. Flow of energy in a two-cavity klystron amplifier for the case $\{P_e\} < 0$, $\{P_{rad}\} > 0$.

High-frequency power is fed to cavity I through a coaxial cable and induces in the cavity a voltage $V_1 e^{i\omega t}$, where V_1 is the voltage amplitude and ω is the angular frequency. This voltage velocity-modulates the beam. The initial velocity-modulation amplitude is $v(0)e^{i\omega t} = \frac{1}{2} v_0 V_1 V_0^{-1} e^{i\omega t}$, and the initial current velocity is neglected, so that $j(0) = 0$. Applying to the klystron drift space the formulas (30) and (31), we obtain

$$E_1 = -E_2 = \frac{m}{2e} v(0) i\omega_p . \tag{52}$$

Using (41), (42), as well as (52), we reach the conclusion that the kinetic power flux in the drift space is zero. This is due to the fact that velocity-modulation of the beam in its pure form entails no power loss over the cycle: the electron velocity increases during the accelerating signal-voltage half-cycles and decreases during the retarding half-cycles.

Using (25) — (27) and (52), we obtain the following expressions for $v(z,t)$ and $j(z,t)$ in the drift space:

$$v(z, t) = v(0) \cos \beta_p z e^{i(\omega t - \beta_e z)}, \tag{53}$$

$$j(z, t) = i \frac{\omega}{\omega_p} j_0 \frac{v(0)}{v_0} \sin \beta_p z e^{i(\omega t - \beta_e z)} \tag{54}$$

From (53) and (54) it follows that in the linear theory the current and the velocity in the drift space are out of phase by $\pi/2$. Putting $z = l$ in these formulas we obtain the values for the velocity and electron current density at the entrance to cavity II. Let the voltage on cavity II vary as $V_2 e^{i(\chi + \omega t)}$ where V_2 is the voltage amplitude and χ is the phase shift of the oscillations in cavity II relative to those in cavity I.

The electron power of interaction between the beam and the field is given by

$$\{P_e\} = \frac{1}{2} S_0 \operatorname{Re} j^*(l) V_2 e^{i\chi}, \tag{55}$$

where S_0 is the cross-sectional area of the beam.

In this case, if $\{P_e\} < 0$, the electrons are slowed down on the average and the amplitude of the slow wave builds up, while that of the fast wave decreases. On the other hand, if $\{P_e\} > 0$, the electrons are accelerated on the average and passage through cavity II brings about an increase in the amplitude of the fast wave, while that of the slow wave decreases.

The change in the amplitudes of the fast and slow waves in the electron beam can be illustrated graphically (see Figures 3 and 4). Figure 3 shows the case when $\{P_e\} < 0$, the energy is radiated from the second cavity, and $\{P_{rad}\} > 0$. Figure 3b shows the behavior of the amplitudes of the fast and slow waves as functions of the coordinate z. When $z < 0$, there are no waves in the beam to the left of the modulating cavity and $E_1 = E_2 = 0$.

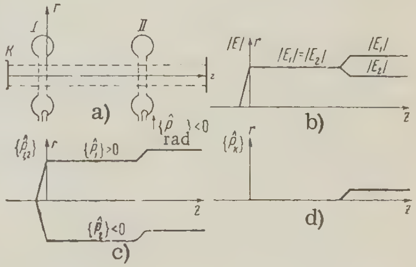

Figure 4. Flow of energy in a two-cavity klystron amplifier for the case $\{P_e\} < 0$, $\{P_{rad}\} > 0$.

Fast and slow waves are excited in the drift space $0 < z < l$, with amplitudes $|E_1| = |E_2|$. Beyond the receiving cavity $z > l$, the amplitude of the slow wave increases while that of the fast wave decreases, so we have $|E_2| > |E_1|$ beyond the cavity.

Figure 3c shows the kinetic power fluxes for the fast and slow waves, connected with the amplitudes of these waves by the relations $\{\hat{P}_1\} = (2Z_0 \beta_p^2)^{-1} E_1 E_1^* > 0$, $\{\hat{P}_2\} = -(2Z_0 \beta_p^2)^{-1} E_2 E_2^* < 0$, where Z_0 is the beam impedance; $Z_0 = (S_0 \omega \varepsilon_0 \beta_p)^{-1}$; $\beta_p = \omega_p / v_0$. To the left of the modulating cavity we have $z < 0 \{\hat{P}_1\} = \{\hat{P}_2\} = 0$ when $z < 0$. In the drift space $0 < z < l$ we have $\{\hat{P}_1\} = -\{\hat{P}_2\}$ and after passage through the receiving cavity, where $z > l$, we have $\{\hat{P}_1\} | < | \{\hat{P}_2\}|$. The total flux of kinetic power through a certain cross section z = const is equal to the sum of the fluxes carried by the fast and slow waves: $\{\hat{P}_K\} = \{\hat{P}_1\} + \{\hat{P}_2\}$. This is shown in Figure 3d. In the drift space $0 < z < l$, the total flux of kinetic power is 0. Beyond the receiving cavity, $\{\hat{P}_1\} < -\{\hat{P}_2\}$, and therefore $\{\hat{P}_k\} = \{\hat{P}_1\} + \{P_2\} < 0$. The electronic power of interaction between the beam and the field in the receiving cavity, $\{P_e\}$, is, in accordance with (40), equal to the change in the total flux of kinetic power $\{\hat{P}_k\}$ due to the passage of the electrons through cavity II. Recognizing that $\{\hat{P}_K\} = 0$ to the left of cavity II, we reach the conclusion that $\{P_e\} = \{P_K\} < 0$.

The plots in Figure 3 confirm the following conclusion. If the cavity is excited by an electron beam, the amplitude of the slow wave increases beyond the cavity, and the amplitude of the fast wave decreases.

Consequently, a passive cavity in the path of the beam supresses the fast wave, but cannot suppress the slow wave.

Figure 4 shows the behavior of fast and slow waves and the related power fluxes for the case when $\{P_e\} > 0$, that is, the field of the second cavity performs positive work on the beam: $\{P_{rad}\} < 0$, $\{P_e\} > 0$, the total flux of kinetic power beyond the cavity is $\{P_k\} = \{P_e\} > 0$, and the fast-wave amplitude increases beyond the receiving cavity while the slow-wave amplitude decreases.

5. THE KINETIC POWER THEOREM AS APPLIED TO TWT

Let us examine the processes that take place in a traveling wave tube [32,35,36].

The physical picture of the processes can be well illustrated with the aid of the waveguide model.

Let us examine a cylindrical waveguide of rectangular cross section with sides a and b; the axes, x, y, and z are directed as shown in Figure 5. The waveguide walls are assumed perfectly conducting. The waveguide is filled with a dielectric having permittivity $\varepsilon = \varepsilon_0 \varepsilon'$, where $\varepsilon' \gg 1$; $\varepsilon_0 = 8.86 \cdot 10^{-12}$ farad/meter.

The dielectric reduces the phase velocity of the electromagnetic wave to a value $v_{ph0} \ll c$, where $c = 3 \cdot 10^8$ m/sec.

Let an electron beam with average current density j_0 and average velocity $v_0 \simeq v_{ph0}$ pass through the waveguide.

It is known [37] that such a system can maintain waves of the form $e^{i(\omega t - \beta z)}$, where ω is the angular frequency, assumed henceforth to be known; β is the propagation constant, determined by the dispersion equation

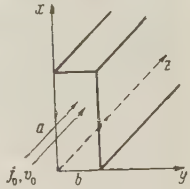

Figure 5. Waveguide model of traveling wave tube.

$$y_1(\beta) = y_2(\beta); \tag{56}$$

$$y_1(\beta) = \frac{k^2_{mn}}{k^2 - \beta^2}; \tag{57}$$

$$y_2(\beta) = 1 - \frac{\omega_0^2}{(\omega - \beta v_0)^2}; \tag{58}$$

$$k^2_{mn} = \left(\frac{m\pi}{a}\right)^2 + \left(\frac{n\pi}{b}\right)^2; \; m, n = 1, 2, \ldots; \; \omega_0^2 = \frac{e\rho_0}{m\varepsilon_0}.$$

Figures 6a, b, c show the course of the curves $y_1(\beta)$ and $y_2(\beta)$ for three cases with different values of ω_0. On going from Figure 6a to Figure 6b and Figure 6c, ω_0 increases and we are considering the case $k > \beta_e > k_{mn}$, which is of practical interest. In Figure 6a all the values of β are real, the values of β_1 and β_4 being close to those for waveguide modes in the absence of the electron beam, while β_2 and β_3 are close to the values of the slow and fast waves in the electron beam. In Figure 6b, the roots β_1 and β_2 coalesce, that is, the wave of the system and the slow wave of the electron beam become synchronized. Fig. 6c shows a case when the roots β_1 and β_2 become complex, so that $\beta_1 = \gamma + i\alpha$, $\beta_2 = \gamma - i\alpha$, where $\alpha > 0$, $\gamma > 0$.

We note that an analogous effect, wherein complex-conjugate solutions appear, can be obtained by varying β_e for fixed ω_0, that is, by varying the average velocity of the electron beam.

Reasoning that the solution has the form $e^{-i\beta z}$, we conclude that the wave β_1 increases as $e^{\alpha z}$ while the wave β_2 attenuates as $e^{-\alpha z}$. The phase velocities of these waves are determined by the value of γ. As shown by calculations, γ is equal to the values $\beta_1 = \beta_2$ in the case shown in Figure 6b. Thus, exponentially growing and attenuating solutions appear as a result of interaction between the decelerating-system wave and the slow wave component of the electron beam. In the region where the waves vary exponentially, they are synchronized in velocity.

The fast wave of the beam, whose propagation constant is $\beta_3 < \beta_e$, does not give rise to expanding solutions.

It will be shown later that the wave β_2, which is slow relative to the electron beam, is characterized by a negative flux of kinetic power, while the wave β_3, which propagates more rapidly than the beam, carries positive kinetic power. These waves behave with respect to power transfer as the slow and fast waves in a one-dimensional electron beam.

The complete expression for the field is given in each of the three cases considered above, Figures 6a, b, and c, by a superposition of four waves

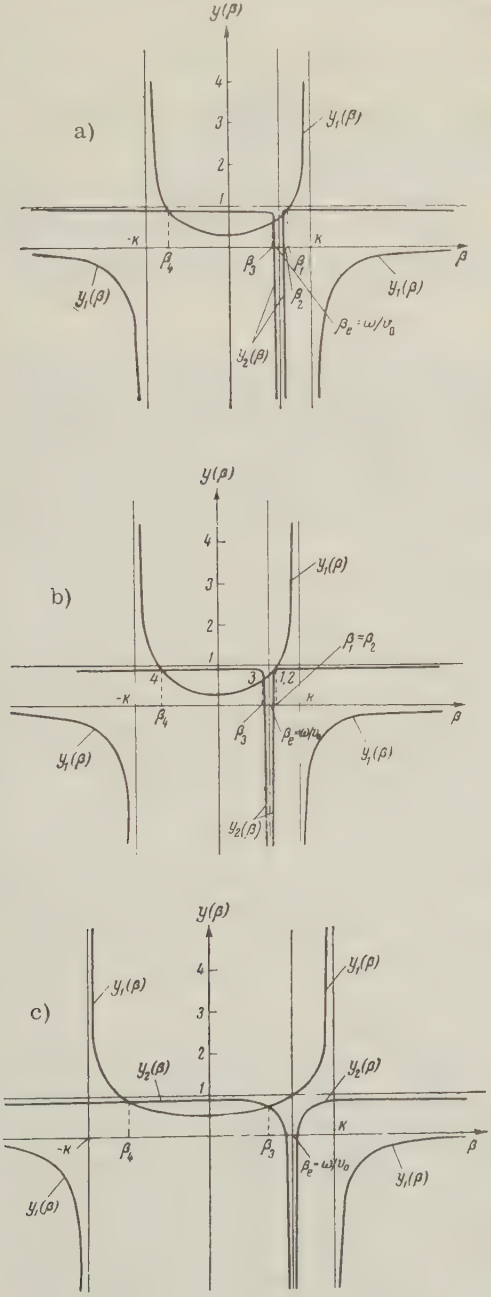

$$E = \sum_{n=1}^{4} E_n e^{-i\beta_n z}, \tag{59}$$

where β_n is determined by the dispersion relation (56), while the amplitudes of the waves E depend on the boundary conditions at the entrance and exit to the tube. If the output of the traveling wave tube is well matched, the backward wave whose wave number is β_4, practically vanishes ($E_4 = 0$) and the field can be represented as a sum of three waves with propagation constants β_1, β_2. and β_3.

The expressions for the velocity of the electrons and for the current density can be represented as a sum of the three waves β_1, β_2, and β_3.

$$v = \sum_{n=1}^{3} v_n e^{-i\beta_n z}, \tag{60}$$

$$j = \sum_{n=1}^{3} j_n e^{-i\beta_n z}, \tag{61}$$

and in the linear theory we have [11,35]

$$v_n = \frac{e}{im} \frac{E_n}{(\omega - \beta_n v_0)}, \tag{62}$$

$$j_n = -i\omega\varepsilon \frac{\omega_0^2 E_n}{(\omega - \beta_n v_0)^2}. \tag{63}$$

We note that as ω_0 is increased, β_3 goes through zero and becomes negative; it then becomes possible to synchronize the wave numbers β_3 and β_4, which again leads to the appearance of waves that attenuate and rise exponentially in the z direction.

It will be shown later, however, that these solutions are characterized by $\{P_k\} > 0$, that is, they do not lead to radiation of electromagnetic energy from the system.

Let us apply the kinetic-power theorem to traveling wave tubes. The greatest interest attaches to exponentially rising waves, which determine the values of the field and the energy effects at considerable distances from the input to the system.

Figure 6. Curves of $y_1(\beta)$ and $y_2(\beta)$ for three cases:
a) — all three values of β real; b — roots β_1 and β_2 coincide; c — roots β_1 and β_2 are complex-conjugate.

Let us enclose the electron beam traveling through the slow-wave system in a closed surface S, which contains a volume V, and let $S = S_1 + S_2 + S_3$, where S_1 and S_2 are the sections of the waveguide in the planes $z = 0$ and $z = l$, and S_3 is the lateral surface of the waveguide. Let us assume that the thermal losses in the volume V are equal to zero. We recall that the kinetic-power theorem can be formulated in this case in the following fashion:

$$\{P_{\text{rad}}\} + \{P_{\text{к}}\} = 0,$$

where $\{P_{\text{rad}}\}$ is the average power radiated through the surface S, and $\{P_k\}$ is the average kinetic power.

In the present case, assuming the surface S_3 to be perfectly conducting, we have

$$\{P_{\text{rad}}\} = \frac{1}{2}\,\text{Re}\int_{S_2} [\vec{E}\vec{H}^*]_z dS - \frac{1}{2}\,\text{Re}\int_{S_1} [\vec{E}\vec{H}^*]_z dS, \tag{64}$$

that is, $\{P_{\text{rad}}\}$ is determined by the difference in the radiation power at the output and input of the waveguide.

In the present case, where the electron trajectories are straight, the expression for $\{P_k\}$ is [see formula (20)]

$$\{P_{\text{к}}\} = \frac{1}{2}\,\text{Re}\,[I^*(l)V_{\text{к}}(l) - I^*(0)V_{\text{к}}(0)], \tag{65}$$

where $I(0),\ V_{\text{к}}(0),\ I(l),\ V_{\text{к}}(l)$ are the values of the convection current and the kinetic potential at the sections $z = 0$ and $z = l$, corresponding to the input and output of the traveling wave tube.

Let us calculate $\{P_k\}$. In the general case, the values of I, and V_k in the TWT are each a sum of three waves. Using (60) — (63) and carrying out simple algebraic transformations, we obtain

$$\frac{1}{2}\,\text{Re}\,I(z)V_{\text{к}}(z) = \frac{1}{2}\,\text{Re}\sum_{n=1}^{3}\sum_{n'=1}^{3} A_{nn'}(z), \tag{66}$$

where

$$A_{nn'} = \frac{\beta_p}{Z_0\beta_e^3}\,\frac{E_n^* E_{n'}}{a}\left(1 - \frac{\beta_n}{\beta_e}\right) e^{i(\beta_n^* - \beta_{n'})z};$$

$$Z_0 = (\omega\varepsilon\beta_p S_0)^{-1};\ \beta_e = \frac{\omega}{v_0};\ a = \left(1 - \frac{\beta_n^*}{\beta_e}\right)^2\left(1 - \frac{\beta_n}{\beta_e}\right)\left(1 - \frac{\beta_{n'}}{\beta_e}\right),$$

β_n are the roots of the dispersion equation, corresponding to the direct waves.

To analyze (66), let us examine several cases.

1) All β_n are real and there are no increasing solutions.

a) $n \neq n'$.

1/2 Re $A_{nn'}$ is a periodic function of z, varying with a period $2\pi(\beta_n - \beta_{n'})^{-1}$.

b) $n = n'$

$$\frac{1}{2}\,\text{Re}\,A_{nn'} = \frac{1}{2}\,\frac{E_n^* E_n}{Z_0\beta_e^2 a}\,\frac{\beta_p}{\beta_e}\left(1 - \frac{\beta_n}{\beta_e}\right),$$

$$a = \left(1 - \frac{\beta_n^*}{\beta_e}\right)^2\left(1 - \frac{\beta_n}{\beta_e}\right)^2 = \left(1 - \frac{\beta_n}{\beta_e}\right)^4 > 0.$$

Thus, 1/2 Re A_{nn} is independent of the coordinate z. When $\beta_n < \beta_e$, which corresponds to fast electron waves, we have $v_0 < v_n$, and 1/2 Re $A_{nn} > 0$, that is, the kinetic - power flux of this wave is positive. On the other hand, if $\beta_n > \beta_e$, corresponding to slow electron waves, we have $v_0 > v_n$, $\frac{1}{2}\,\text{Re}\,A_{nn} < 0$, that is, the kinetic power flux of this wave is negative.

We note, however, that $\frac{d}{dz}\,\text{Re}\,A_{nn} = 0$, and consequently these waves drop out when the kinetic-power theorem is used.

2. β_1 and β_2 are complex-conjugate quantities while β_3 is real. Let $\beta_1 = \gamma + i\alpha$, $\beta_2 = \gamma - i\alpha$ where $\gamma = 0$ and $\alpha > 0$; $\beta_1^* = \gamma - i\alpha$.

Substituting these values for β in the right half of (66) we see that terms proportional to $e^{2\alpha z}$, $e^{\alpha z}$, 1, $e^{-\alpha z}$, $e^{-2\alpha z}$ appear in the calculation of $\frac{1}{2}\,\text{Re}\,I(z)V_{\text{к}}(z)$ For sufficiently large $z = l$, such that $e^{2\alpha l} \gg 1$, the term with largest value is 1/2 Re A_{11}, which is proportional to $e^{2\alpha z}$.

In this case

$$\frac{1}{2}\operatorname{Re} I(l)V_{\text{к}}(l) = (2Z_0\beta_e^2)^{-1}\frac{\beta_p}{\beta_e}\frac{E_1E_1^*}{a}\left(1-\frac{\gamma}{\beta_e}\right)e^{2\alpha l}\,[1+O(e^{-\alpha l})], \qquad (67)$$

(67)

where $a = \left(1-\frac{\beta_1^*}{\beta_e}\right)^2\left(1-\frac{\beta_1}{\beta_e}\right)^2 > 0$; $O(e^{-\alpha l})$ are the residual terms of order $e^{-\alpha l} \ll 1$.

a) $\operatorname{Re}\beta_1 = \gamma > \beta_e$.

In the investigation of the dispersion equation for the TWT we have seen that the slow electron wave, for which $\operatorname{Re}\beta_1 = \gamma > \beta_e$, increased exponentially, and consequently we have $\frac{1}{2}\operatorname{Re} I^* V_{\text{к}} < 0$ for this wave. Recognizing that the value of $\hat{P}(0)$ can be neglected when $\exp \alpha l \gg 1$, compared with c $\hat{P}(l)$, we write the expression for the average kinetic power $\{P_k\}$ in the form

$$\{P_{\text{к}}\} = (2Z_0\beta_e^2)^{-1}\frac{\beta_p}{\beta_e}\frac{E_1E_1^*}{a}\left(1-\frac{\gamma}{\beta_e}\right)e^{2\alpha l}\,[1+O(e^{-\alpha l})]. \qquad (68)$$

Thus, the slow electron wave in a TWT, with an exponentially increasing amplitude, transfers negative kinetic power $\{P_k\} < 0$ through the surface S. It follows from the kinetic-power theorem that in this case $\{P_{rad}\} > 0$ is accompanied by an exponential rise in the kinetic power $\{P_k\} < 0$, connected with the slow electron wave $v_{ph1} < v_0$, $\gamma > \beta_e$ and consequently with the slow electrons. The rise in the amplitude of the slow wave with increasing z denotes that the electrons are retarded more and more as they propagate along the z-axis. This is the reason for the frequently made statement that the slow electron wave is amplified in the TWT.

Figure 7 shows a plot of $1/2 \operatorname{Re}A_{11}(z)$ [see formula (66)] for the slow electron wave.

b) $\operatorname{Re}\beta_1 = \gamma < \beta_e$, $\{P_{\text{к}}\} > 0$. In this case the fast electron wave carries positive kinetic power. The kinetic-power theorem leads to the conclusion that $\{P_{rad}\} < 0$, that is, the system absorbs power and the slow-wave system is not excited by the electron beam. Consequently the rapid growing waves with $v_1 > v_0$, $\gamma < \beta_e$, $\alpha > 0$, which appear, for example, in some cases in the solution of the dispersion equation for the TWT have no physical meanings, since they do not lead to the appearance of radiation of electromagnetic waves. These fast waves, which increase with the coordinate, have a physical meaning in the case when the system contains additional power sources, characterized with a flux which is negative when averaged over the time. Such a situation arises in parametric excitation of the electron beam, when the power is supplied to the electron beam by a pumping source with frequency ω_p, with $\omega_p \neq \omega$.

We have confined ourselves above to an examination of only the principal term, proportional to $e^{2\alpha l}$, in the expression $\frac{1}{2}\operatorname{Re} I^* V_{\text{к}}$, for the power, given by (66).

An estimate of the terms of order $e^{\alpha l}$, in this expression discloses that they are periodic functions of z with period $2\pi(\gamma-\beta_3)^{-1}$. The signs of these terms vary, depending on the values of the argument $(\gamma-\beta_3)z$, and also on the ratio of the quantities γ, β_e, and β_3. An account of these terms complicates the picture of the enrgy flow in the TWT, but is obligatory if processes occurring close to the input to the TWT are investigated. Many terms in (66) are independent of the coordinate z. These terms drop out of the kinetic theorem when the difference between the power fluxes at the section z = 0 and $z = l$ is evaluated.

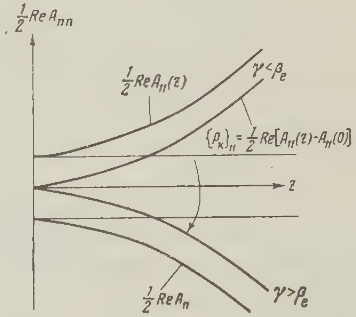

Figure 7. Value of Re $A_{11}(z)$ for a slow electron wave

The expression (66) includes also exponentially damped terms, proportional to $e^{-\alpha l}$ and $e^{-2\alpha l}$, which can be neglected when $\alpha l > 3$; these terms must be takin into account if processes near the input to the TWT are considered.

Terms of order $e^{-\alpha l}$ are periodic functions of z with period $2\pi(\gamma-\beta_3)^{-1}$. The term proportional to $e^{-2\alpha l}$ is aperiodic.

6. KINETIC POWER THEOREM AND THE TWO-BEAM TUBE

Let us apply the kinetic power theorem to the theory of a two-beam tube. To be specific, we consider the waveguide model of the two-beam tube. Let two electron beams with average electron velocities v_{01} and v_{02}, and current densities j_{01} and j_{02}, intermixed over the cross section, flow through a cylindrical waveguide filled with a dielectric. For the sake of being definite, the waveguide section will be assumed rectangular with sides a and b. We assume that the electrons can move only along the z-axis and the small-amplitude theory is valid. We assume the expressions for the ac components of the current, velocity, and charge density to be proportional to $e^{i(\omega t-\beta z)}$. The greatest interest in attached to the case of waveguide beyond cutoff, when $k=\omega\sqrt{\varepsilon\mu}<\left[\left(\frac{m\pi}{a}\right)^2+\left(\frac{n\pi}{b}\right)^2\right]^{\frac{1}{2}}$, $m, n=1,2,\ldots$; let, in addition, the condition $k\ll\beta_{e2}<\beta_{e1}$, $k\ll\beta_{e2}=\omega/v_{02}<\beta_{e1}=\omega/v_{01}$ be satisfied, that is, $v_{\mathrm{ph}0}=(\varepsilon\mu)^{-\frac{1}{2}}\gg v_{02}>v_{01}$. In this case the dispersion equation of the two-beam tube has the form

$$y(\beta)=0, \tag{69}$$

where

$$y(\beta)=1-\frac{\hat{\omega}_{p1}^2}{(\omega-\beta v_{01})^2}-\frac{\hat{\omega}_{p2}^2}{(\omega-\beta v_{02})^2};$$

$$\hat{\omega}_{p1}^2=\omega_{p1}^2(1+k_{mn}^2\gamma^{-2})^{-1};\quad \hat{\omega}_{p2}^2=\omega_{p2}^2(1+k_{mn}^2\gamma^{-2})^{-1};$$

ω_{p1} and ω_{p2} are the plasma frequencies of the first and second beam, respectively; $\gamma=\omega/v_0$; $v_0=\frac{1}{2}(v_{01}+v_{02})$. Equation (69) corresponds to a one-dimensional two-beam tube with plasma frequency $\hat{\omega}_{p1}$ and $\hat{\omega}_{p2}$. The factor $(1+k_{mn}^2\gamma^{-2})^{-1}$ takes into account the fact that the waveguide cross section is finite.

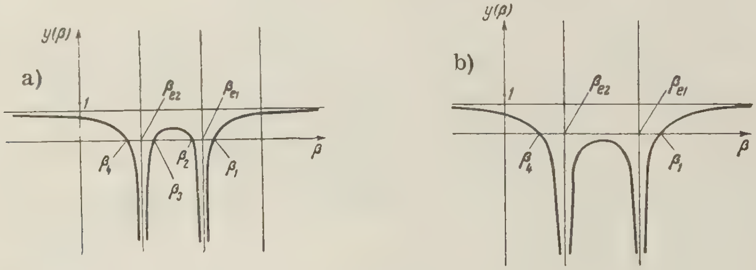

Figure 8

a) — Curves of $y_2(\beta)$ for the case $k=\omega\sqrt{\varepsilon\mu}<\beta_{e2}=\omega/v_{02}<\beta_{e1}=\omega/v_{01}$. b) — Curves of $y_2(\beta)$ for the case when two-beam amplification is in effect. The roots β_2 and β_3 are complex-conjugate.

Figure 8 shows a graphic solution of equation (69) without (a) and with (b) amplification.

It follows from Figure 8a that four natural waves of natural amplitude can propagate through the system, with propagation constants β_1, β_2, β_3 and β_4. The two waves β_1 and β_2 are close in velocity to v_{01}, since $\beta_1\simeq\beta_2\simeq\beta_{e1}=\omega/v_{01}$, and $\beta_1>\beta_{e1}$ and $\beta_2<\beta_{e2}$, that is, β_1 characterizes the slow wave of the slow beam, while β_2 characterizes the fast wave of the slow beam. The two other waves, with propagation constants β_3 and β_4, are nearly equal to v_{02}, and it follows from the inequality $\beta_3>\beta_{e2}$ and $\beta_4<\beta_{e2}$ that β_3 characterizes the slow wave of the fast beam, and β_4 characterizes the fast wave of the fast beam.

Now let the beam velocity v_{01} approach v_{02}. Then β_{e1} tends to β_{e2} and the roots

β_2 and β_3 move toward each other and coalesce at a certain ratio of the parameters. At the instant when the roots coalesce, the fast wave of the slow beam (β_2) is synchronized in velocity with the slow wave of the fast beam (β_3). A further approach to β_{e1} to β_{e2} causes the roots β_2 and β_3 to become complex-conjugate (see Figure 8b). Taking into account the fact that the solution is proportional to the factor $e^{i(\omega t-\beta_z)}$, we conclude that the wave for which $\mathrm{Im}\,\beta < 0$ is damped.

Let us make up the energy balance of the two-beam amplifier. The expression for the kinetic power of the two-beam tube will be obtained by putting N = 2 in (20). The current and the kinetic potential in every beam are each a sum of six waves.

We consider the case when two-beam amplification is present. Now the roots β_2 and β_3 are complex conjugates and can be represented in the form $\beta_2 = \gamma + i\alpha$, $\beta_3 = \gamma - i\alpha$ where $\gamma > 0$ and $\alpha > 0$. The growing wave is characterized by the root β_2.

Confining ourselves to the growing wave in the expression for the current and the kinetic potential, we can write for $\{P_k\}$ approximately

$$\{P_{\text{к}}\} = \{P_{\text{к}1}\} + \{P_{\text{к}2}\}, \tag{70}$$

where

$$\{P_{\text{к}1}\} = (2Z_1\beta_{e1}^2)^{-1}\frac{\beta_{p1}}{\beta_{e1}}\,\frac{E_2(0)\,E_2^*(0)\left(1-\frac{\gamma}{\beta_{e1}}\right)e^{2\alpha l}}{\left(1-\frac{\beta_2^*}{\beta_{e1}}\right)^2\left(1-\frac{\beta_2}{\beta_{e1}}\right)^2}\,(1+O_1); \tag{71}$$

$$\{P_{\text{к}2}\} = (2Z_2\beta_{e2}^2)^{-1}\frac{\beta_{p2}}{\beta_{e2}}\,\frac{E_2(0)\,E_2^*(0)\left(1-\frac{\gamma}{\beta_{e2}}\right)}{\left(1-\frac{\beta_2^*}{\beta_{e2}}\right)^2\left(1-\frac{\beta_2}{\beta_{e2}}\right)^2}\,e^{2\alpha l}(1+O_2); \tag{72}$$

O_1 and O_2 are remainder terms, of order $e^{-\alpha l} \ll 1$; $E_2(0)$ is the initial value of the field of the growing wave.

We have seen in the investigation of the dispersion equation of the two-beam tube that the two-beam interaction mechanism causes an exponential growth of the wave with wave number $\beta_2 = \gamma + i\alpha$, $\gamma > 0$ $\alpha > 0$, $\beta_{e2} < \gamma < \beta_{e1}$. $\{P_{k1}\}$ in (71) characterizes formally the interaction between the exponentially growing wave of the field with phase velocity ω/γ and a slow electron beam with velocity $v_{01} = \omega/\beta_{e1}$, and it follows from the inequality $\gamma < \beta_{e1}$ that $\{P_{k1}\} > 0$. The term $\{P_{k2}\}$ characterizes formally the interaction between the exponentially growing wave of the field, with phase velocity ω/γ, and a fast electron beam with velocity $v_{02} = \omega/\beta_{e2}$, and it follows from the inequality $\beta_{e2} < \gamma$, that $\{P_{k2}\} < 0$. Thus, under the approximations made (linear theory, $e^{-\alpha l} \ll 1$) the kinetic-power flux in a two-beam tube is the sum of the kinetic-power fluxes due to the interaction between the slow and fast electron beams and the resultant exponentially growing field. Although this treatment is formal, it does allow us to conclude that the slow electron beam plays in the two-beam tube the role of an active load, leading to the loss of energy. The source of the electron power is the fast electron beam. Analogous conclusions were drawn by the author of [38], where the nonlinear mode of the two-beam tube is investigated.

Assuming $\{P_{rad}\} = 0$ in the beyond-cutoff waveguide of the two-beam tube under consideration, we obtain with the aid of the kinetic-power theory $\{P_k\} = 0$, and consequently it follows from (70) that for $e^{-\alpha l} \ll 1$ we have asymptotically $\{P_{\text{к}1}\} \simeq -\{P_{\text{к}2}\}$. This equation can be verified by direct calculation.

Thus, in the case under consideration, when the waveguide is beyond cutoff and two-beam amplification is in effect, the flow of energy in the two-beam tube is analogous to the flow of energy in the drift space of a two-cavity klystron. At each given cross section (provided $e^{\alpha l} \gg 1$) the positive and negative power fluxes cancel each other. The coupling element (such as a cavity or a short helix), placed at the end of the drift space, can reduce the positive flow of kinetic power or increase (in absolute magnitude) the negative flow of kinetic power.

The advantage of the two-beam TWT over the klystron lies in the exponential growth of this positive kinetic power with tube length l, so that a large output signal can be obtained. At the same time, the negative kinetic-power wave, connected with the slow electrons remaining in the beam, even past the coupling element, rises exponentially.

7. PARAMETRIC ELECTRON BEAMS AND THE KINETIC POWER THEOREM

It was shown above that with the aid of special coupling elements it is possible to decrease the amplitude of the fast noise wave of the electron beam, but a signal in the form of a fast electron wave cannot be amplified in an ordinary TWT, the operation of which is connected with an increase in the amplitude of the slow wave.

Parametric amplifiers have been proposed for the amplification of the fast wave.

Assume that the electron beam receives not only the signal of frequency ω, but power from a pumping generator, of frequency ω_H. The nonlinear effects will then give rise in the beam to an infinite sequence of waves with combination frequencies $m\omega_H \pm n\omega$, so that the expressions for the charge density, electron current density, and electron velocity can be represented in the form

$$\rho_H = \sum_{-\infty}^{\infty} \rho_m \exp im\omega_H t, \tag{73}$$

$$v_H = \sum_{-\infty}^{\infty} v_m e^{im\omega_H t}, \tag{74}$$

$$j = \sum_{m=-\infty}^{\infty} \sum_{n=\pm 1} j_{m,n} e^{i(m\omega_H + n\omega)t}, \tag{75}$$

$$\rho = \sum_{m=-\infty}^{\infty} \sum_{n=\pm 1} \rho_{m,n} e^{i(m\omega_H + n\omega)t}, \tag{76}$$

$$v = \sum_{m=-\infty}^{\infty} \sum_{n=\pm 1} v_{m,n} e^{i(m\omega_H + n\omega)t}, \tag{77}$$

where ρ_m and v_m are the amplitudes of the corresponding Fourier coefficients, pertaining to the pumping; j_{mn}, ρ_{mn}, and v_{mn} are the amplitudes of the combination signal frequencies. Expressions (75) — (77) have been written under the assumption that the most important role is played only by the closest (higher and lower) combination frequencies so that n assumes only two values ($n = \pm 1$).

Using further Maxwell's equations, the equation of motion of the electrons, and the small amplitude condition we can arrive, in full analogy with the conclusions drawn for the single-frequency case in Section 1, at the following equation [29]:

$$\mathrm{Re} \sum_{m=-\infty}^{\infty} \oint_S \left(\frac{[\vec{E}_m \vec{H}^*_m]}{m\omega_H + \omega} + \frac{V_m \vec{j}^*_m}{m\omega_H + \omega} \right) d\vec{S} = 0, \tag{78}$$

where $\vec{E}_m$ and $\vec{H}_m$ are the electric and magnetic field intensities at the combination frequency $m\omega_H + \omega$; j_m is the current density, $V_m = mv_0 v_m/e$ is the kinetic potential at the same combination frequency; S is the surface bounding the closed volume through which the electron beam passes.

Equation (78) is equivalent to the theorem on the kinetic potential, given in Section 1, extended to include the case of a parametric beam. By setting $\omega_H = 0$ in (78) we arrive at equation (20) (when $N = 1$, since single-beam parametric flow is considered).

Equation (78) takes account of the possibility of radiating electromagnetic waves from the system not only at the fundamental frequency, $m = 0$, but also at combination frequencies.

The terms $V_m I^*_m$ are connected with the power of interaction between the electrons and the field at the frequency $m\omega_H + \omega$ ($m = 0, \pm 1, \pm 2, \ldots$).

Assume that the positive kinetic power in the fast wave of the signal ($m = 0$) is compensated by the negative kinetic power at the combination frequencies ($m \neq 0$). It then follows from (78) that electromagnetic waves can be radiated from this volume, since

$\{P_{rad}\} > 0$. If the kinetic power at the combination frequencies is negative and furthermore its modulus increases with the coordinate z, then the fast electron wave at the signal frequency can also increase with the coordinate. The energy for the signal amplification is obtained in this case from the pumping energy and from the energy of the combination frequencies.

It follows also from (78) that it is possible, in principle, to reduce the noise power at the frequency ω, noise present in the slow wave of the parametric electron beam, by using passive coupling elements. In this case the increase in the kinetic power in the beam at the frequency ω should be compensated by a reduction in the kinetic power at the combination frequencies.

Analogous conclusions are drawn in [39], where the processes that occur in parametric amplifiers are explained on the basis of the energy and the laws of conservation of angular momentum in the electron beam.

During the interaction between electromagnetic waves of different frequencies, noise power can be pumped from the combination-frequency waves to the signal wave. Consequently, to reduce the noise amplitude at the frequency ω it is essential to decrease the amplitude of the noise wave at the neighboring combination frequencies $\omega_H \pm \omega$. too Therefore, it is very experimentally difficult to obtain low noise with the aid of a tube with longitudinal interaction. As already mentioned above, greater promise of obtaining a low noise factor is offered by parametric tubes with transverse interaction [21 — 24]. These tubes make use of so-called cyclotron waves in the electron beam.

Let the cathode be placed perpendicular to a constant magnetic field of intensity H_0. The electrons will move in spiral trajectories around the z-axis; in the cross sections z = const the electrons describe circles with frequency $\omega_c = eH_0 \mu_0 / m$, where μ_0 is the permeability of a vacuum. The radius of the circle is related to the magnitude of the transverse signal. This excites in the beam a slow and fast cyclotron wave, the phase velocities of which are $v_{ph} = v_0 (1 \mp \frac{\omega_c}{\omega})^{-1}$ where v_0 is the average velocity of the electron beam, ω is the signal frequency, and ω_c is the electron cyclotron frequency.

It can be shown [26] that the fast cyclotron wave is due to the predominance of fast electrons; it is characterized by a positive power flux. To the contrary, the slow cyclotron wave is connected with predominance of the slow electrons, and carries a negative power flux. The total power flux through the section z = const is 0.

Thus, the fast and slow cyclotron waves are characterized by the same power fluxes as the longitudinal waves in an electron beam. Consequently, the fast cyclotron wave, unlike the slow one, can be extracted from the electron beam with the aid of a passive slow-wave structure.

In non parametric devices with transverse interaction (for example, in a TWT with transverse field), the amplitude of the slow cyclotron wave increases exponentially, and this is accompanied by an increase in the radiation field. The amplitude of the fast wave remains unchanged.

To increase the amplitude of the fast cyclotron wave with increasing coordinates, pumping is resorted to with the aid of a rotating azimuthal field E_φ of frequency $\omega_H = 2\omega_c$. This pumping is best effected with a quadrupole capacitor. The azimuthal field E_φ of such a capacitor is proportional to the distance from the axis. It can be shown that the signal builds up here exponentially with increasing coordinate z.

The elements used to couple to the electron beam in transverse-wave parametric tubes are usually of the capacitive type. These devices interact with the fast cyclotron wave, whose phase velocity tends to infinity when $\omega \simeq \omega_c$, and do not interact with the slow wave.

Reference [40] describes an experimental parametric tube with transverse field, designed for a frequency $\nu = 4140$ Mc, with a tube gain 24 db, a noise coefficient 2.5 db, and a bandwidth between half-power points of 67 Mc.

Cavities are used as input and output devices. In tubes with capacitive or cavity inputs, the phase velocity of the pumping wave is infinite. The author of [41] describes a tube where this velocity is finite, and in addition, there is no pumping generator. The alternating transverse high-frequency field of double frequency, acting on the electron beam, is the result of motion of the beam in a periodic electrostatic field with a transverse component. The interaction between the circular motions of the electron in the beam and the transverse components of the periodic electrostatic field causes unwinding (increase in radius) of the electron trajectories, the same as in a quadrupole capacitor. The experimental tube has a beam gain coefficient of 14 db at a frequency of 3.25 gigacycles. The coupling elements used at the input and output of the tube were π-section cavities with bandwidth $\Delta\nu \simeq 2\%$...

The fundamental component of the electron-beam noise is due to the random nature of the longitudinal displacements of the electrons, which do not interact with the transverse fields. Consequently, noise connected with the longitudinal motion of the electrons does not influence noticeable the noise properties of the devices with transverse fields. This also leads us to expect a lower noise factor in devices with transverse interaction.

Reference [43] discusses possible noise sources in parametric tubes with transverse interaction. The main cause of noise is thermal random motion of electrons in the transverse cross section, induced by the fluctuating potential at the input plates. Some of these induced currents average out, because one can almost always find for an electron moving, say, from the lower to the upper plate, a "paired" electron moving from the upper plate to the lower one. All the factors that upset the electron balance lead to noise. These include inhomogeneity of the electric field between the plates, the spread in the axial velocities of the electrons in the beam, collisions with ions, etc.

The theory of parametric amplifiers with transverse deflection of the beam is not yet complete. Thus, the existing theories do not take into account the Coulomb forces, or the interaction between the transverse and longitudinal displacements of the electrons; nor is the role of harmonics in an electron beam excited by transverse fields completely clear.

REFERENCES

1. A.S. Tagar, Investigation of Noise Properties of Traveling Wave Tube, Radiotekhnika i elektronika (Radio Engineering and Electronic Physics) 1957, 2, 2, 222.
2. A.A. Zyuzin-Zinchenko, V.M. Lopukhin, V.M. Vasil'ev. Effect of Electrostatic Field of the Gun on the Noise Factor of a TWT, Izv. Vuzov, MVO SSSR (Radiotekhnika) (News of the Colleges, Ministry of Higher Education USSR, Radio Engineering), 1959, 2, 5, 589.
3. M. R. Currie, D.C. Forster, Low noise preamplifiers for microwave receivers, Proc. I.R.E., 1958, 46, 3, 570.
4. M. Currie, A new type low noise electron gun for microwave tubes, Proc. I.R.E. 1958, 46, 5, 911.
5. M. Caulton, S-band TWT with F below 4 db, Proc I.R.E., 1958, 46, 5, 911.
6. M.R. Currie, D.C. Forster, New mechanism of noise reduction in electron beams, J. Appl. Phys., 1959,30, 1, 95.
7. J. R. Pierce, W.E. Danielson, Minimum noise figure of traveling wave tubes, J. Appl. Phys., 1954, 25, 9, 1163.
8. G. Wade, K. Amo, D.A. Watkins, Noise in transverse field TWT, J. Appl. Phys. 1954, 25, 12, 1514.
9. R. Adler, O. M. Kromhout, P. A. Clavier, Transverse field TWT with periodic electrostatic focusing, Proc, I.R.E., 1956, 44, 1, 82.
10. J. R. Pierce, The wave picture of microwave tubes, Bell System Techn. J., 1954, 33, 11, 1343.
11. V.N. Shevchik, G.N. Shvedov, Space-Charge Waves in Electron Beams. Izv. Vuzov, MVO SSSR (Radiotekhnika), 1959, 2, 5, 511.
12. W. Louisell, C. Quate, Parametric amplification of space charge waves, Proc. I.R.E., 1958, 46, 4, 707.
13. W. Louisell, Three frequency parametric beam amplifier, J. Electronics and Control, 1959, 6, 1, 1.
14. I.S. Cook, W.H. Louisell, TWT equations including the effects of parametric pumping, Proc. I.R.E., 1959, 47, 11, 2016.
15. T.J. Bridges, A parametric electron beam amplifier, Proc. I.R.E., 1958, 46, 2, 494.
16. A.Ashkin, Parametric amplification of space charge waves, J. Appl. Phys., 1958, 29, 17, 1646.
17. V.M. Lopukhin, B.D. Charkin, N.G. Zeveke, Experimental detection of parametric amplification in backward-wave tube, Radiotekhnika i elektronika, 1959, 4, 10, 1747
18. D.K. Akulina, S.A. Akhmanov, S.D. Gvozdover, A.S.Gorshkov, I.T. Trofimenko. Parametric phenomena in wave systems with long electron beams, Radiotekhnika i elektronika, 1960, 5, 10, 1736.
19. R.W. Gould, Traveling wave couplers for beam type amplifier, Proc. I.R.E., 1959, 47, 3, 419.

20. A. Ashkin, W. H. Louisell, C.F. Quate, Fast wave couplers for longitudinal beam parametric amplifiers, J. Electronics and Control, First series, 1959, 7, 1, 1.
21. R. Adler, Parametric amplification of the fast electron wave, Proc, I.R.E., 1958 46, 6, 1300.
22. R. Adler, G. Hrbek, G.Wade, A low noise electron beam parametric amplifier, Proc. I.R.E., 1958, 46, 10, 1756.
23. R. Adler, The quadripole amplifier, a low noise parametric device, Proc. I.R.E., 1959, 47, 10, 1713.
24. C.B. Crumly, R.Adler, Electron beam parametric amplifiers, Electron Industries, 1959, 47, 10, 1713.
25. A.E. Siegman, Waves in a filamentary electron beam in a transverse field slow wave circuit. J. Appl. Phys, 1960, 31, 1, 17.
26. Curtic C. Johnson, Theory of fast wave parametric amplification, J. Appl, Phys, 1960, 31, 2, 338.
27. L. J. Chu, A kinetic power theorem, IRE PGED Electron Tube Research Conference Durham, New Hampshire, June 1951.
28. H. A. Haus, A kinetic power theorem, URSE, Boulder, August, 1957.
29. H. A. Haus, The kinetic power theorem for parametric longitudinal electron -beam amplifiers, IRE, Trans. Electron Devices, 1958, 5, 4, 225
30. J.M. Manly, H.E. Row Power relations in nonlinear reactances, Proc, I.R.E., 1956, 44, 7, 904.
31. W.H. Louisell, J.R. Pierce, Power flow in electron beam devices, Proc. IRE, 1955, 43, 4, 425.
32. S.D. Gvozdover, Teoriya elektronnykh priborov, SVCh, GTI, (Theory of Microwave Electron Devices), 1956.
33. D.A. Watkins, TWT Noise figure, Proc, I.R.E., 1952, 40, 1, 65.
34. G.M. Branch, T.G. Mihran, Plasma frequency reduction factors in electron beams IRE, Trans. Electrom Devices, 1955, 2, 2, 3.
35. V.M. Lopukhin, Vozbuzhdeniye kolebaniy i voln elektronnymi potokami, (Excitation of Oscillations and Waves by Electron Beams), GITTL, 1953.
36. V.N. Shevchik, Ocnovy teorii SVCh, (Principles of microwave theory) Soviet Radio Press, 1958.
37. L.N. Loshakov, On the Theory of Propagation of Waves in an Electron Beam, ZhTF (Journal of Technical Physics), 1952, 22, 2, 193.
38. G.F. Filimonov, Nonlinear Theory of Two-Beam Tube, Parts I and II, Radiotekhnika i elektronika, 1959, 4, 3, 5, 489, 832.
39. J.R. Pierce, Use of the principles of conservation of energy and momentum in connection with the operation of wave type parametric amplifiers, J. Appl Phys., 1959, 30, 9, 1341.
40. T.J. Bridges, A.Ashkin, Adler's tube at microwaves, Proc, I.R.E. 1960, 48, 381.
41. E.I. Gordon, TWT with transverse field and cyclotron, Proc, I.R.E., 1960, 48, 6, 1158.
42. B.J. Udelson, Parametric amplifier with electrostatic focusing, Proc, I.R.E., 1960, 48, 6, 1485.
43. C.P. Lea Wilson, Possible reasons of noise in Adler's tubes. Proc, I.R.E. 1960, 48, 2, 255.

Physics Faculty
M.V. Lomonosov State University
Moscow

Submitted to the editor, September 9, 1960

INTERFERENCE IMMUNITY OF TWO METHODS OF RECEPTION OF PULSE SIGNALS

B.H. Mityashev

We consider the effect of noise in the reception of pulse signals with a synchronous receiver with modulated input and with a quadrature receiver with modulus summation of channel outputs. The detection characteristics are calculated for signals with random initial phase and random amplitude. A receiver circuit is described, and certain experimental results are cited.

INTRODUCTION

It has recently been the practice to receive weak pulsed signals by means of a quadrature circuitry, which gets around the difficulties connected with realization of optimum filtering directly at the high frequency. In such a receiver (see, for example [1]), filtering at high frequency is replaced by synchronous reception in two channels with subsequent filtering at low frequency. In particular, in quadrature reception it is easier to realize matched filters that are optimal in the case of white noise [2,3]. The advantages of the receiver are particularly noticeable when the signals are of long duration or are in the form of a group of pulses with coherent high frequency carrier [4,5]. The voltage developed at the output of the quadrature receiver is proportional to the envelope of the oscillation produced at the output of the corresponding high frequency matched filter . Thus, if the input to the high-frequency filter is an amplitude-modulated signal together with white noise having spectral density N_0, then the filter output is a signal in the form $U_{m\,c0}(t)\sin(\omega_0 t+\varphi)$ and a Gaussian noise with a correlation coefficient of the form $R(\tau)=\rho(\tau)\cos\omega_0\tau$ and a dispersion $\sigma_0^2=N_0\Delta f_0$ (Δf_0 is the effective bandwidth of the filter). The envelope of the filter output voltage can be represented as [6]

$$U=\sqrt{[A(t)+U_{mc0}(t)\sin\varphi]^2+[B(t)+U_{mc0}(t)\cos\varphi]^2},$$

where A(t) and B(t) are independent Gaussian functions, with a correlation coefficient $\rho(\tau)$ and a dispersion σ_0^2. This representation of the envelope is indeed used in quadrature reception. The first term under the square root is formed with the aid of a synchronous detector under the assumption that the phase of the signal is zero, while the second is formed under the assumption that the phase is $\pi/2$.

If we introduce the notation

$$x=\frac{U}{\sigma_0};\quad a=\frac{A(t)}{\sigma_0};\quad b=\frac{B(t)}{\sigma_0};\quad q=\frac{U_{mc0}(t)}{\sqrt{2}\,\sigma_0},$$

then the voltage at the output of the quadrature receiver will be

$$x=\sqrt{(a+\sqrt{2}\,q\sin\varphi)^2+(b+\sqrt{2}\,q\cos\varphi)^2}. \tag{1}$$

An exact performance of operation (1) is a complicated technical matter. We shall consider in this paper two different, simpler operations.

The receiving apparatus is particularly simple if only one quadrature receiver channel is used. In this case it is proposed to shape the signal in the form

$$x_1=|\,a+\sqrt{2}\,q\sin\varphi\,|. \tag{2}$$

The operation (2) describes a single-channel synchronous receiver with modulus output.

A certain simplification in the receiver circuit is found also if the operation (1) is replaced by the operation

$$x_2=|\,a+\sqrt{2}\,q\sin\varphi\,|+|\,b+\sqrt{2}\,q\cos\varphi\,| \tag{3}$$

The purpose of the present paper is to calculate the losses in interference immunity of reception, due to replacement of operation (1) by operations (2) and (3). We consider reception of signals with random initial phase, and also of signals with fluctuating amplitude.

1. EFFECT OF NOISE IN THE RECEPTION OF PULSES BY A SYNCHRONOUS RECEIVER WITH MODULUS INPUT

If the initial phase of the signal φ is a random quantity uniformly distributed in the interval $(0, 2\pi)$, then a receiver performing operation (1) is optimal. In this case the probability distribution density of the value of x obeys the Rayleigh-Rice law

$$w(x) = x e^{-\left(\frac{x^2}{2} + q^2\right)} I_0(\sqrt{2}\, q x), \tag{4}$$

where I_0 is the modified Bessel function of order zero. The maximum value of the quantity q contained in (1) — (4) is equal to the ratio of the peak value of the filtered signal to the effective value of the noise. In the case of a matched filter, this maximum value is $q = \sqrt{E/N_0}$ (E is the signal energy) [2,3]. We shall henceforth take q to mean its maximum value.

The quantity x_1, defined by expression (2), is the modulus of the sum of a normal random quantity, with zero average value and unity dispersion, and a sinusoidal quantity, the two being taken at random. Therefore, the probability distribution density of x_1 is

$$w_1(x_1) = \frac{2}{\pi\sqrt{2\pi}} \int_{-\pi/2}^{\pi/2} e^{-\frac{(x_1 - \sqrt{2}q \sin\varphi)^2}{2}} d\varphi. \tag{5}$$

Expression (5) can be represented in series from [7]

$$w_1(x_1) = \frac{2}{\sqrt{2\pi}} e^{\frac{(x_1^2 + q^2)}{2}} \left[I_0\left(\frac{q^2}{2}\right) I_0(\sqrt{2}\, q x_1) + \right.$$
$$\left. + 2 \sum_{k=1}^{\infty} (-1)^k I_k\left(\frac{q^2}{2}\right) I_{2k}(\sqrt{2}\, q x_1) \right], \tag{6}$$

where I_k is the modified Bessel function of the first kind and of the order k.

The distribution curves $w_1(x_1)$, calculated for several values of q, are shown in Figure 1. Formula (6) was used for small values of q and x_1 ($\sqrt{2}qx_1 \leqslant 6$), while the remaining data were obtained by numerical integration of equation (5).

The properties of the receiver necessary to detect weak signals by means of a system having a single threshold can be characterized by the probability of false alarm F and the probability of true detection D, which are equal to [3].

$$F = \int_{x_0}^{\infty} w_n(x)\, dx, \quad D = \int_{x_0}^{\infty} w(x)\, dx, \tag{7}$$

where x_0 is the normalized value of the threshold; w_n is the probability distribution density of the noise in the absence of a signal ($q = 0$).

Figure 2 shows the operating characteristics of a detection receiver [3], showing curves of F vs. D for different q. The curves of Figure 2a (solid lines) are the working characteristics of an ideal receiver of signals with random initial phase [3]. These curves have been obtained on the basis of expressions (4) and (7). The operating characteristics of our single-channel receiver, calculated on the basis of (5), (6), and (7) for the same values of q, are shown in Figure 2b. Figure 3 shows the dependence of D_1 on q for values of F_1 ranging from 10^{-1} to 10^{-10}. The curves for the optimal receiver are shown dotted.

It is clear from Figure 1 that at low values of q the distribution $w_1(x_1)$ is almost uniform. Therefore at large values of D_1 ($D_1 \geqslant 0.7$) we can use the approximation

$$D_1 \simeq 1 - x_0 w_1(0) = 1 - x_0 \sqrt{\frac{2}{\pi}} e^{-\frac{q^2}{2}} I_0\left(\frac{q^2}{2}\right). \tag{8}$$

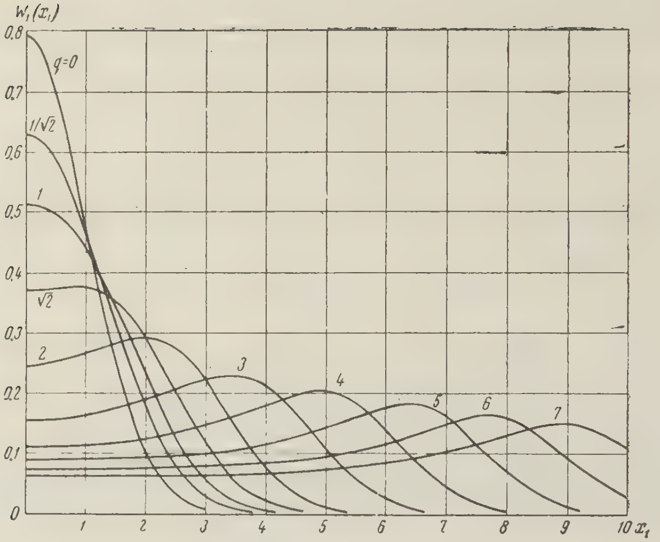

Figure 1. Probability distribution density of the voltage at the output of a synchronous receiver with modulus output, in the reception of signals with random initial phase.

If q $\geqslant 3$, then by using the approximation $I_0(z) \simeq e^z/\sqrt{2\pi z}$ $(z \gg 1)$, we obtain

$$D_1 \simeq 1 - \frac{\sqrt{2}\, x_0}{\pi q}. \tag{9}$$

In the calculation of the curves of Figure 3, the magnitude of the threshold x_0 in expressions (8) and (9) is determined by the specified probability of false alarm

$$F_1 = 1 - \Phi\left(\frac{x_0}{\sqrt{2}}\right), \tag{10}$$

where the probability integral is

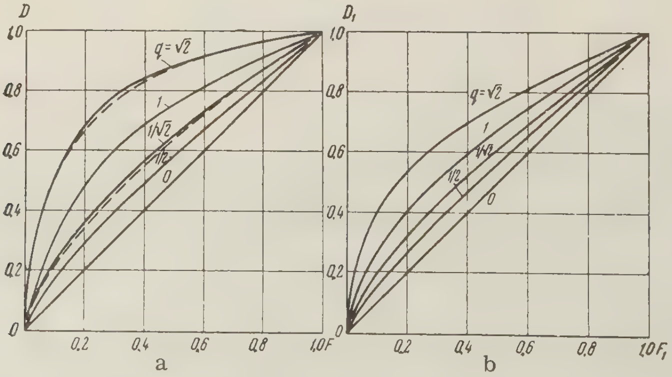

Figure 2. Working characteristics of an ideal receiver (a) and of a synchronous receiver with modulus output (b) in the reception of signals with random initial phase.

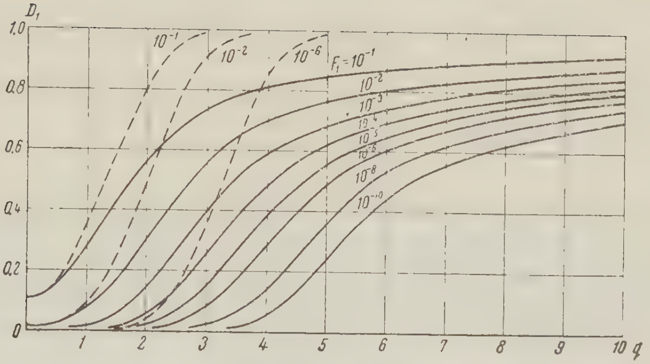

Figure 3. Characteristics of detection of signals with random initial phase received by a synchronous receiver with modulus output.

The data obtained indicate, as expected, that a single channel receiver has a reduced interference immunity. The greatest difference is observed in regions of large D. This is connected with the fact that the signal x_1 is fluctuating in character even in the absence of noise. It is remarkable, however, that the difference in the behavior of the curves decreases with decreasing q and D. Thus, when $D = D_1 = 0.5$ and $F = F_1 = 10^{-6}$ the necessary value of q in the case of single-channel synchronous reception is 1.55 times greater than in the case of ideal reception. When $D = D_1 = 0.2$, this excess drops to 1.35. If $D = D_1 = 0.2$ and $F = F_1 = 10^{-2}$, the necessary increase in q amounts to 15%. It follows, therefore, that at small D a near-ideal reception of signals can be effected by using only one channel of the quadrature receiver. The probability of signal reception can be increased by using their recurrence. In the reception of n pulses, the probability that at least one signal will exceed the threshold is $D_n = 1 - (1 - D)^n$. If $D = 0.2$ and $n = 10$, then $D \simeq 0.9$.

Let us consider a case where the received signal is the result of superposition of a very large number of signals of approximately the same intensity. In this case the quantity x has a Rayleigh distribution

$$w(x) = \frac{x}{1 + q_0^2} e^{-\frac{x^2}{2\left(1 + q_0^2\right)}}, \tag{11}$$

where $q_0^2 = \sigma_{c'}^2 \sigma_0^2$ is the excess of the signal dispersion over the noise dispersion at the output of the matched filter.

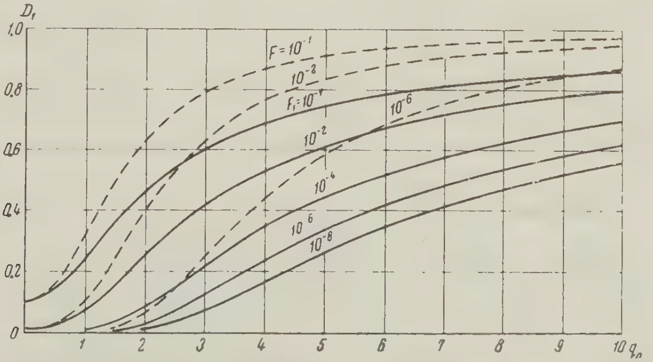

Figure 4. Characteristics of detection of fluctuating signals received by a synchronous receiver with modulus output.

In this case x_1 represents the modulus of the sum of two independent quantities with normal distribution. Therefore,

$$w_1(x_1) = \frac{2}{\sqrt{2\pi\left(1+q_0^2\right)}} e^{-\frac{x_1^2}{2\left(1+q_0^2\right)}} \tag{12}$$

In ideal reception the probabilities F and D are equal to

$$F = e^{-\frac{x_0^2}{2}}, \tag{13}$$

$$D = e^{-\frac{x_0^2}{2\left(1+q_0^2\right)}}. \tag{14}$$

In the case of reception with a synchronous receiver with a modulus output, the probability of correction detection is

$$D_1 = 1 - \Phi\left[\frac{x_0}{\sqrt{2\left(1+q_0^2\right)}}\right]. \tag{15}$$

The detection characteristics, calculated by formulas (10) and (15), are given in Figure 4. For comparison, the dotted curve shows the characteristics of an ideal receiver, calculated by formulas (13) and (14). At large values of D, the losses due to substitution of operation (2) for operation (1) are less here than in the case of reception of signals with constant amplitude. The point is that the signals at the outputs of receivers are fluctuating even in the absence of noise. In this connection, the reception of fluctuating signals with a synchronous receiver having a modulus output is more promising.

2. EFFECT OF NOISE IN THE RECEPTION OF PULSES BY A QUADRATURE RECEIVER WITH MODULUS SUMMATION

Let us estimate the properties of a receiver that performs operation (3). If only the initial phase of the signal φ is a random quantity, then by using the usual procedure (with fixed φ) to find the probability distribution density of a sum of two independent random quantities, and integrating the resultant expression over all possible values of φ, we obtain after some transformations

$$w_2(x_2) = \frac{1}{2\pi\sqrt{\pi}} \int_0^{2\pi} e^{-\left[\frac{x_2 - \sqrt{2}q(\sin\varphi+\cos\varphi)}{2}\right]^2} \left(\frac{2}{\sqrt{\pi}} \int_{z_1}^{z_2} e^{-t^2}\,dt\right) d\varphi, \tag{16}$$

where

$$z_1 = \frac{1}{2}\left[\sqrt{2}q(\sin\varphi - \cos\varphi) + x_2\right], \qquad z_2 = \frac{1}{2}\left[\sqrt{2}q(\sin\varphi - \cos\varphi) - x_2\right].$$

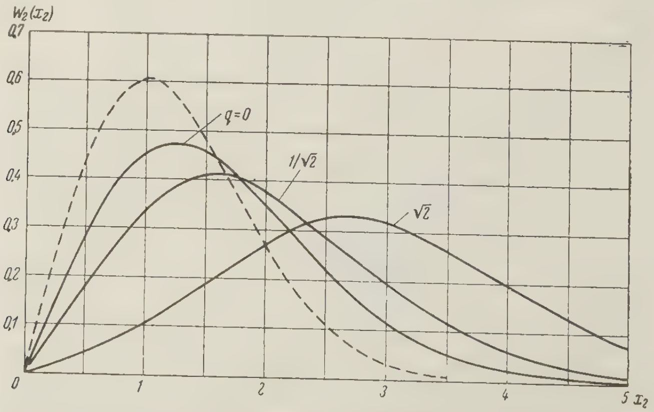

Figure 5. Probability distribution density of the voltage at the output of a quadrature receiver with modulus summation in the reception of signals with random initial phase.

It is convenient to represent the integral contained in the integrand in the following form:

$$\frac{2}{\sqrt{\pi}}\int_{z_1}^{z_2} e^{-t^2}\,dt = \begin{cases}\Phi(z_1)+\Phi(z_2), & \frac{z_1}{z_2}<0,\\ |\Phi(z_1)-\Phi(z_2)|, & \frac{z_1}{z_2}>0.\end{cases}$$

In the absence of a signal ($q = 0$) we have

$$w_2(x_2) = \frac{2}{\sqrt{\pi}} e^{-\frac{x_2^2}{4}}\Phi\left(\frac{x_2}{2}\right). \tag{17}$$

Figure 5 shows the distribution curves $w_2(x_2)$, obtained by integrating numerically equation (16) for $q = 1/\sqrt{2}$ and $\sqrt{2}$. The curve for $q = 0$ has been calculated from (17). The dotted curve is the Rayleigh distribution. It is clear from Figure 5 that the distribution (7) is very similar to a Rayleigh curve in form. The difference in the scales of the two curves is due to the nonequivalence of the normalization of the quantities x_1 and x_2. The curves for $q = 1/\sqrt{2}$ and $\sqrt{2}$ differ from the corresponding distribution curves of the envelope (4) in that they have a blunter maximum [6, 8].

The operating characteristics of a receiver, calculated from the data of Figure 5 and formula (17), are shown dotted in Figure 2. A slight difference between these curves and the ideal curves is observed in the region of medium values of D. This difference decreases with increasing signal-to-noise ratio.

In the case of a signal with fluctuating amplitude, x_2 is the sum of the moduli of two independent normal quantities, with dispersion $1 + q_0^2$ Therefore the probability distribution density of x_2 has a form analogous to (17):

$$v_2(x_2) = \frac{2}{\sqrt{\pi(1+q_0^2)}} e^{-\frac{x_2^2}{4(1+q_0^2)}}\,\Phi\left(\frac{x_1}{2\sqrt{1+q_0^2}}\right). \tag{18}$$

Substituting (18) in (7) we obtain

$$F_2 = 1-\Phi^2\left(\frac{x_0}{2}\right), \tag{19}$$

$$D_2 = 1-\Phi^2\left(\frac{x_0}{2\sqrt{1+q_0^2}}\right). \tag{20}$$

Calculations based on (19) and (20) are very simple, since the probability integral has been tabulated in detail. The table lists the threshold values of q_0 necessary to ensure specified probability ratios $F = F_2$ and $D = D_2$. The calculations were based on formulas (13) and (14) (value of q_{00}) or on (19) and (20) (the value of q_{02}). The data in the table show that substitution of operation (3) for operation (1) calls for a slight increase in the threshold value q_0 (by 2 — 8.5%).

F	$D = 0,2$			$D = 0,5$			$D = 0,9$		
	q_{02}	q_{00}	q_{02}/q_{00}	q_{02}	q_{00}	q_{02}/q_{00}	q_{02}	q_{00}	q_{02}/q_{00}
10^{-1}	0,679	0,656	1,033	1,571	1,524	1,030	4,706	4,620	1,020
10^{-2}	1,414	1,364	1,037	2,473	2,376	1,041	6,820	6,531	1,045
10^{-3}	1,900	1,814	1,048	3,153	2,994	1,051	8,486	8,030	1,055
10^{-4}	2,294	2,173	1,055	3,723	3,505	1,061	9,908	9,292	1,066
10^{-5}	2,634	2,480	1,061	4,223	3,951	1,070	11,17	10,40	1,074
10^{-6}	2,935	2,754	1,066	4,670	4,351	1,073	12,30	11,40	1,078
10^{-7}	3,211	3,002	1,070	5,083	4,717	1,077	13,35	12,33	1,082
10^{-8}	3,466	3,232	1,073	5,467	5,058	1,080	14,32	13,18	1,085

Note: Comma designates decimal point.

An effective means of separating weak signals from noise is to accumulate the signals after optimal filtering and detection. Let us find some evaluation of such receivers from this point of view. The main parameters characterizing the accumulation of a signal are a regular rise in the output voltage, due to the appearance of the output noise. These data are sufficient, if normal approximation of the output fluctuations can be used. The possibility of normal approximation of the distribution of a sum of n realizations of random quantities, with exponential and Rayleigh distributions, has been considered in sufficient detail [9]. These data can serve also as an estimate for our case, since the asymmetry in the distribution (5) when $q = 0$ is less than the exponential one, and the distribution (17) is very close to a Rayleigh distribution. One can, therefore, use the normal approximation for the distribution of a sum of n realizations of x_1 and x_2 at least for $n \geqslant 100$.

In the case of a weak signal ($q \ll 1$), by using $I_0(z) \simeq 1 + \frac{z^2}{4}$ ($z \ll 1$), we obtain on the basis of (4) and (6) the following results. For the quantity x, the increment in the statistical mean, due to the signal is $\overline{\Delta x} = \sqrt{\pi/8}\,q^2$ and the dispersion in the absence of a signal is ($q = 0$) $\sigma^2 = (4-\pi)/2$. The analogous quantities for x_1 are

Figure 6. Block diagram of the receiver. 1 — Heterodyne, 2 - summing device, 3 — linear amplitude detector, 4 — matched video filter, 5 — push-pull rectifier.

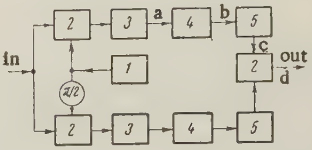

$\overline{\Delta x_1} = q^2/\sqrt{2\pi}$ and $\sigma_1^2 = (\pi - 2)/\pi$. For x_2 we have x_2 $\overline{\Delta x_2} = 2\overline{\Delta x_1}$ and $\sigma_2^2 = 2\sigma_1^2$. The increments in the statistical mean values, referred to the actual value of the fluctuations, are

$$\Delta = \frac{\overline{\Delta x}}{\sigma} = \sqrt{\frac{\pi}{4(4-\pi)}}\,q^2,$$

$$\Delta_1 = \frac{\overline{\Delta x_1}}{\sigma_1} = \sqrt{\frac{1}{2(\pi-2)}}\,q^2,$$

$$\Delta_2 = \frac{\overline{\Delta x_2}}{\sigma_2} = \sqrt{\frac{1}{\pi-2}}\,q^2.$$

The ratios of the normalized increments are

$$\frac{\Delta_1}{\Delta} = \sqrt{\frac{2(4-\pi)}{\pi(\pi-2)}} \simeq 0{,}69, \quad \frac{\Delta_2}{\Delta} = \sqrt{\frac{4(4-\pi)}{\pi(\pi-2)}} \simeq 0.98.$$

Two receivers used for the detection of signals ensure identical results if the increments Δ are identically normalized. Therefore, in the accumulation of a large number of realizations, the replacement of operation (1) by operation (2) calls for an increase in the threshold value q by a factor $\sqrt{\Delta/\Delta_1} \approx 1.20$, while the use of operation (3) necessitates an increase of $\sqrt{\Delta/\Delta_2} \approx 1.01$ times, that is, merely 1%. The data obtained are valid also for a signal with fluctuating amplitude. It is merely necessary to substitute q_0 for q. These data and the data in the table show that as the number of summed realizations decreases (from n = 100 to n = 1) the losses in the two-channel scheme with modulus summation increase from 1% to 2 – 8.5%.

3. EXPERIMENTAL RESULTS

To estimate the realizability of the relations obtained, we constructed a two-channel receiver in accordance with the block diagram shown in Figure 6. The input of the system is a signal from the output of a broadband amplifier of an ordinary radar receiver. The synchronous detection is effected by combining the signal with heterodyne oscillations tuned to the signal carrier frequency, and subsequent separation of the envelope by means of a linear amplitude detector. The heterodyne oscillations, separated 90° in phase, are fed to the receiver channels. The amplitude of these oscillations should exceed both the signal and the noise. The signals are fed from the outputs of the detectors to video filters and then, to carry out operations (2) and (3), to push-pull rectifier elements. The output signal is equal to the sum of the voltages picked off the output of the push-pull rectifiers.

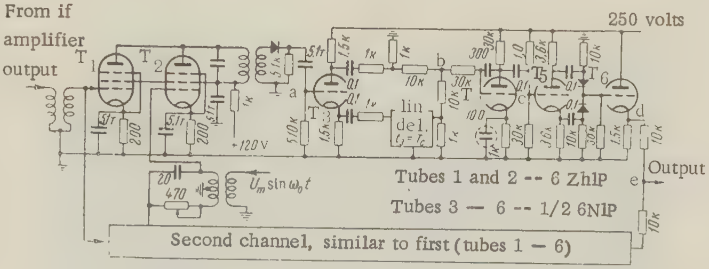

Figure 7. Circuit diagram of the receiver.

Figure 7 shows the wiring diagram of the receiver whose block diagram is shown in Figure 6. for reception of rectangular pulses whose initial phases are random and independent of each other. The operation of the receiver in the absence of noise is illustrated by the oscillograms of Figure 8. The oscillograms and the corresponding points on the wiring and block diagrams are denoted by identical letters.

In the circuit of Figure 7, the signal and the heterodyne oscillations are combined in two pentodes, 1 and 2, which have a common load. The output of the amplitude detector is a sequence of rectangular pulses whose amplitudes and polarities are random (Figure 8a). Part of the circuitry associated with tubes 3 and 4 serves as a matched video filter for the rectangular signal pulse. The signal is delayed here by its own duration, is subtracted from the undelayed signal, and the resultant difference (Figure 8b) is integrated (Figure 8c). It is well known [10,11] that the frequency characteristic of such a circuit has the form $K(f) = \sin \pi f\, T_s / \pi f T_s$, which coincides with the spectrum of a rectangular pulse of duration T_s. All the pulses assume the same polarity at the output of the push-pull rectifier (tube 5 and germanium diodes DGTs-7) (see Figure 8d). The channel terminates in a cathode follower (tube 6), thereby completing operation (2). The same processes take place also in the second channel. Inasmuch as the heterodyne voltage is applied to this channel with a phase shift of 90°, triangular pulses are obtained at the output of the circuit after summation; these pulses have slight amplitude fluctuations (Figure 8e). The presence of these fluctuations is indeed the result of replacement of operation (1) by operation (3).

The operation of the receiver in the presence of noise ($q \simeq 3$) is illustrated by the oscillograms of Figure 9. The oscillogram of Figure 9d illustrates the character of the distribution (5), while that of Figure 9e illustrates the distribution (16), The signal pulses used in the experiments were of 10 microsecond duration, the front duration was 1 microsecond, and the repetition rate was 2.5 milliseconds. The carrier (if) was 30 Mc, and the bandwidth of the if amplifier 1.5 Mc, sufficient to avoid noticeable signal distortion.

If signals of different wave form or duration are received, principal changes must be made in the parts of the circuitry involving tubes 3 and 4. These should be replaced by a video filter matched to the signal of the specified waveform. An increase in signal duration calls for an increase in the heterodyne frequency stability, a factor which is particularly important if groups of pulses with a coherent high-frequency carrier is to be received [5]. The permissible frequency deviation between the signal and the heterodyne should tentatively satisfy the condition $\Delta f_h \leq 0.3/T_{sc}$ (T_{sc} is the total duration of the coherent part of the signal.)

It was found during the experiments that it is difficult to ensure in a sensitive receiver an exact 90° phase shift between the heterodyne oscillations fed to the channels, since the heterodyne voltage had to pass through the first common stages of the receiver. The heterodyne and the power-supply filters must be carefully shielded. A single-channel system performing operation (2) needs no such heterodyne shielding.

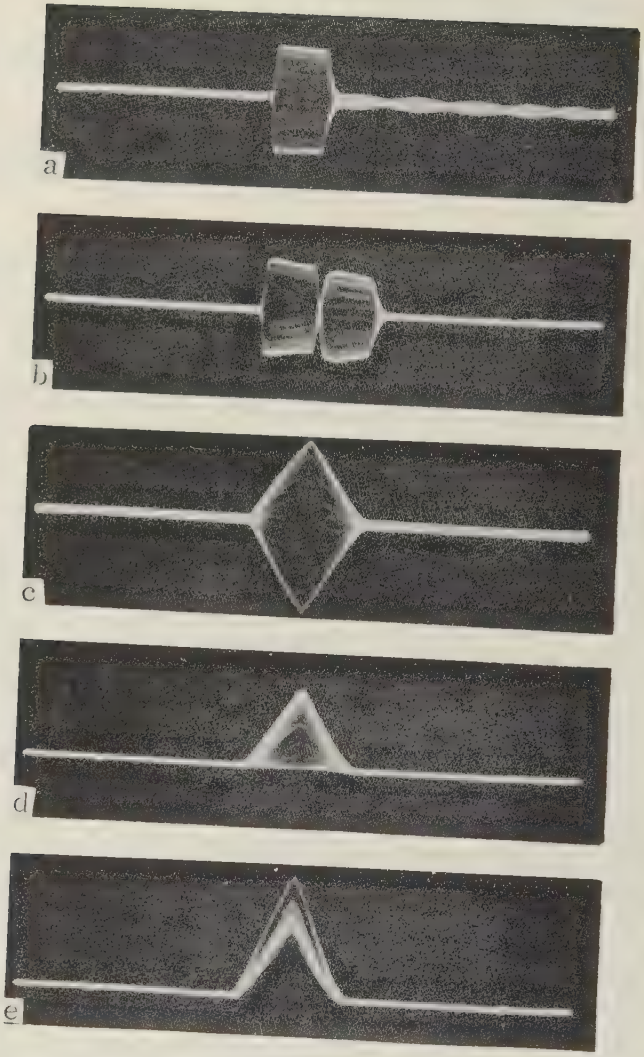

Figure 8. Voltage oscillograms in the receiver in the absence of noise.

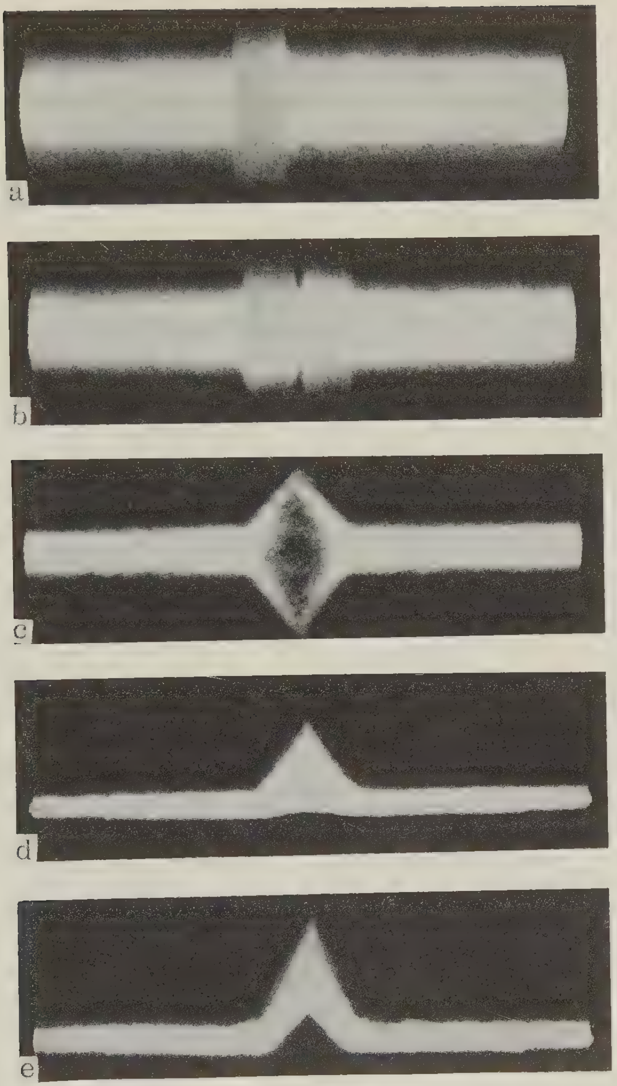

Figure 9. Voltage oscillograms in receiver in the presence of noise.

It is important that the pulses at the receiver output (Figures 8d and 8e) fluctuate only in magnitude and that their form remains constant. Consequently, the two receivers make it possible to determine the time position of pulses of relatively large curation.

CONCLUSION

A quadrature receiver with modulus summation ensures a reception which is very close to optimal. Repeated signals with random initial phase, as well as signals with random amplitude and phase, can be received with low loss by a synchronous receiver with modulus output. This receiver is exceedingly simple to realize: all that needs to be done is to apply to the input of the amplitude detector of an ordinary broadband receiver, in addition to the signal, oscillations from a stable heterodyne, tuned to the intermediate frequency, and to carry out the necessary filtering and accumulation past the detector.

REFERENCES

1. V.D. Zubakov, Optimal Detection in Correlated Noise, Radiotekhnika i elektronika, 1958, 3, 12, 1441.
2. P.M. Woodward, Probability and Information Theory with Applications to Radar, Pergamon Press, London, 1953.
3. W.W. Peterson, T.G. Birdsall, W.C. Fox, The theory of signal detectability, IRE Trans., 1954, PGIT-4, 4, 171.
4. W. Siebert, Certain Applications of Detection Theory in Radar, Radiotekhnika i elektronika za rubezhom, 1959, 1, 26.
5. H. Sherman, Some optimal signals for time measurement, IRE Trans., 1956, PGIT--2, 1, 24.
6. V.I. Bunimovich, Fluctuating Processes in Radio Receivers, Soviet Radio Press, 1951.
7. B.R. Levin, Theory of Random Processes and Its Application in Radio, Soviet Radio Press, 1957.
8. S.O. Rice, Theory of Fluctuating Noise. Collected translations on "Theory of transmission of electric signals in the presence of noise", IL, 1953.
9. Yu.V. Polyak, V.S. Kel'zon, On the Theory of Detection of Periodic Pulse Signals in Gaussian Noise with Incoherent Accumulation. Radiotekhnika i elektronika 1958, 3, 6, 764.
10. M.H. Nichols and L.L. Rauch, Radiotelemetry, Russ. Transl, IL, 1958, page 431.
11. Yu.S. Lezin, On the Synthesis of Filters which are Optimal for Pulses of Defined Waveform, NDVSh — Radiotekhnika i elektronika (Scientific Notes of the Universities, Radio Engineering and Electronic Physics), 1958, 1, 2, 23.
12. B.N. Mityashev, On an Optimal Method of Determining the Time Position of Pulses, Radiotekhnika i elektronika, 1960, 5, 2, 206.

Submitted to the editors, 7 December 1959

SUPPLY OF SPARE PARTS FOR ELECTRONIC CIRCUITS ON THE BASIS OF THE LOAD

G.V. Druzhinin

We consider the possibility and advisability of using one of the practical methods of increasing the reliability of electronic circuits by using spare (redundant) elements.

INTRODUCTION

The increasing complexity of electronic circuits, that is, the increasing number of elements used in such circuits (capacitors, resistors, vacuum tubes, etc.) has by now far overtaken the improvement in quality of these elements. The problem of increasing reliability of electronic circuits by using spare (redundant) elements has therefore become of prime importance. In the overwhelming majority of published papers, abstract mathematical models of circuits equipped with spare elements are considered. Here, as correctly noted in [1], the practical realization of systems provided with spare parts entails many difficulties, not discussed in the published papers. In particular, practical methods of providing spares for individual circuit elements have been but little developed. What papers exist [2 —5] are few in number and cover only a small part of the problem. Yet the development of practical methods of providing spare elements is the next problem to be solved if highly reliable systems provided with spare elements are to be produced. Provision of spare elements is a relatively easy matter but one can hardly expect a rapid practical realization of basic principles concerning reliable logical structure of complicated systems.

Provision with spare parts usually implies the use of duplicate elements, wherein failure of one or several parts (elements) of the circuit does not result in failure of the entire circuit. The remaining elements perform the same function as the circuit (element) without redundancy, and have the same parameters. The operating elements, the component blocks, and the other parts of the circuit remain under the same electrical conditions before and after the failure of any of these elements. The use of duplicate elements in this form can be called functional redundancy. In practice, functional redundancy with duplication of individual elements is difficult. Yet in some cases it becomes possible to effect functional duplication of blocks of single elements. For example, two vacuum tube amplifiers with a sufficient AGC range can sometimes be connected in parallel.

The foregoing universal definition of redundancy is not the only one possible. Circuit reliability can be increased by provision with spare elements on the basis of the load.

1. ESSENTIALS OF PROVISION WITH SPARE ELEMENTS

The provision of spare elements is almost always passive [6], that is, no circuit modification takes place when failure sets in. It is necessary to take into account here the various consequences that may result from a failure of an element in the spare circuit. A spare circuit, used to replace one unduplicated element, can be constructed in such a way, that when one of its elements fails the entire circuit goes out of order, and the electric load which should be supplied by one unduplicated element is distributed among all the elements of the circuit. Figure 1 shows the simplest examples of such spare provision based on load, in circuits comprised of capacitors and wire-wound resistors. Instead of one wire-wound resistor of R ohms or one capacitor of C microfarads, we use two units rated 2R and 2C (Figures 1a and 1b). Any failure (open or short circuit) of one of the circuit elements causes the entire circuit to go out of order, since the change in resistance or capacitance exceeds the tolerance.

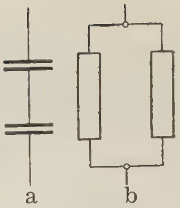

Figure 1. Simplest examples of spare provision of capacitors (a) and resistors (b) based on load.

When spare provision based on load is used, the extent of disturbance to each element of the spare-provided unit is greatly increased by the reduction in the electric load, which is distributed among all the circuit elements. For example, each of the capacitors of Figure 1a is at half voltage; each of the resistors of Figure 1b dissipates half the power with which an element not provided with a spare would be loaded. On the other hand, the rate of failure of the spare-provided circuit is equal to the sum of the failure rates of the elements.

In formula (1), $P_0(t)$ is the probability of survival of the spare circuit during a time t;

$$P_0(t) = \prod_{j=1}^{k} p_j(t) = \exp\left[-\sum_{j=1}^{k} \lambda_j(t)\right] = \exp[-\Lambda t]. \tag{1}$$

$p_j(t)$ is the probability of survival of the j-th element of the spare circuit during the time t; λ_j is the intensity of failure of the j-th element of the circuit; Λ is the intensity of failure of the entire spare circuit, and k is the number of elements in the spare circuit. When the spare-circuit consists of identical elements, as usually is the case in practice, we have

$$\Lambda = k\lambda. \tag{2}$$

Spare provision based on load is useful if the intensity of failure of the spare circuit is reduced as a result of the reduction in load to a greater extent than it is increased by increasing the number of operating elements. Here, as in any investigation of element reliability, we disregard the influence of the rating (capacitance, resistance, etc.) of the element on the intensity of its failure.

The experimental data published in numerous papers, for example [7,8], usually describe the dependence of the intensity of failure of an element on the electric load and on the ambient temperature θ. The electric load is usually power in the case of resistances, working voltage in the case of capacitors, etc. The electric load X is specified as a fraction of the nominal load X_n:

$$\gamma = \frac{X}{X_n}.$$

The experimental relationships

$$\lambda_1 = \varphi(\gamma, \theta) \tag{3}$$

are usually given in the form of curves. Figure 2 shows a relationship of the form (3), plotted for ceramic capacitors on the basis of the data in reference [8].

The rate of failure of a duplicate circuit, in which the load γ is distributed among k elements, is

$$\lambda_2 = k\varphi\left(\frac{\gamma}{k}, \theta\right). \tag{4}$$

Let us examine by way of an example the spare provision of ceramic capacitors based on load, by connecting the capacitors in series. The duplicate circuit goes out of order whenever one of the elements fails. Figure 2b shows the ratio of rate of failure of a capacitor not provided with a spare (λ_1) to that of the spare circuit (λ_2) for different numbers of elements in the spare circuit, determined with the aid of the cirves of Figure 2a. The curves of Figure 2b correspond to an ambient temperature $\theta = 60°$. When θ changes, the curves of Figure 2b are shifted slightly. In this case it is explained by the fact that the curves of Figure 2a are approximatly equidistant. The character of the curves of Figure 2b shows that for the number of elements used here in the spare circuit, the greatest gain in reliability is reached for different values of γ with different numbers k of series-connected capacitors.

We can formulate and solve an extremal problem on the determination of the optimal value of k necessary to ensure greatest gain in reliability (in the presence of a limiting factor as well). Such an investigation will however be of little practical use, since it is assumed here that the main problem of the advisability of using spare provision based on load has already been solved.

Spare provision of elements based on load increases the reliability for given values of γ and θ, if the following condition is satisfied:

$$\lambda_1 - \lambda_2 > 0 \tag{5}$$

or, taking (3) and (4) into account

$$\varphi(\gamma, \theta) - k\varphi\left(\frac{\gamma}{k}, \theta\right) > 0. \tag{6}$$

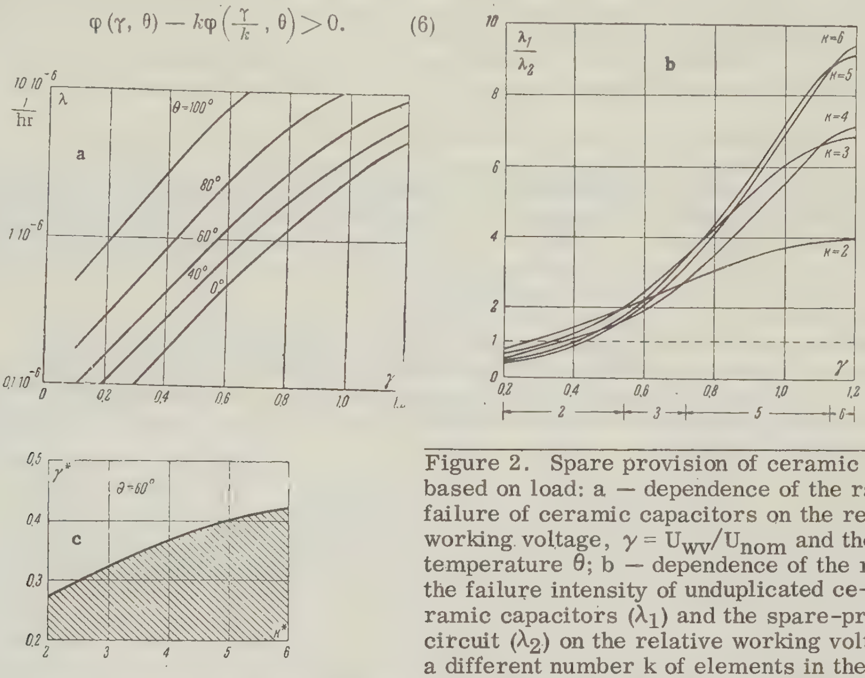

Figure 2. Spare provision of ceramic capacitors based on load: a — dependence of the rate of failure of ceramic capacitors on the relative working voltage, $\gamma = U_{wv}/U_{nom}$ and the ambient temperature θ; b — dependence of the ratio of the failure intensity of unduplicated ceramic capacitors (λ_1) and the spare-providing circuit (λ_2) on the relative working voltage γ for a different number k of elements in the circuit and for an ambient temperature θ = 60°C; the numbers under the plots indicate the number of elements in the spare-providing circuits, which ensure at a given value of γ the maximum gain in reliability; c — boundary of useful application of spare provision by load; in the shaded zone the spare provision by load reduces the reliability.

It is assumed here that the ambient temperature is the same for all elements of the given type and does not change when the number of elements in the spare circuit is changed. The latter assumption is important only for thermally active elements (resistances, vacuum tubes, etc.). Differentiating inequality (6) with respect to γ, we obtain the necessary (but not sufficient) condition under which spare provision by load is beneficial

$$\left(\frac{\partial\varphi}{\partial\gamma}\right)_{\frac{\gamma_1}{k}} k < \left(\frac{\partial\varphi}{\partial\gamma}\right)_{\gamma_1}, \tag{7}$$

where $\left(\frac{\partial\varphi}{\partial\gamma}\right)_{\gamma_1}$ is the partial derivative $\frac{\partial}{\partial\gamma}[\varphi, (\gamma, \theta)]$ at a relative electric load γ_1, and $\left(\frac{\partial\varphi}{\partial\gamma}\right)_{\gamma_1}$ is the same for a relative electric load γ_1/k.

It follows from (5) — (7) that the reliability of elements can be increased through spare provision by load only when the dependence of the intensity of failure of an element on the relative electric load is nonlinear and concave upward. In practice, usually $\gamma\ \partial\varphi/\partial\gamma > 0$, $\partial^2\varphi/\partial\gamma^2 > 0$ for all values of γ, and a spare provision by load is beneficial for all values of γ encountered in practice.

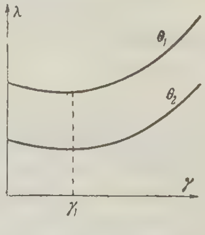

Figure 3. One of the possible cases when spare provision by load is harmful no matter what the number of elements in the spare circuit.

Cases are possible, however, however, when the use of spare provision by load leads to a reduction in reliability (Figure 3).

Inequalities (5) and (6) are not satisfied for all values of k and γ. Inasmuch as in increase in the number of employed elements leads, for fixed γ and θ, on the one hand to a reduction in the rate of failure of the spare-provided circuit owing to the reduction in the load of each of the elements, and on the other hand leads to an increase in the rate of failure of the spare circuit is greater than that of an element not provided with a spare. For the example considered above, where ceramic capacitors are spare-provided by load, the influence of a change in the ambient temperature is small. Therefore Figure 2 shows only one curve $\gamma^* = \psi_1(k^*)$, which delineates the shaded region in which the reliability of ceramic capacitors cannot be increased by spare provision by load. When $\gamma > 0.275$, spare provision by load of ceramic capacitors always reduces their reliability.

Thus, spare provision by load can serve as a means of increasing the reliability of heavily loaded elements or elements of poor quality, which have low nominal loads.

2. ADVANTAGES OF USING SPARE PROVISION OF ELEMENTS BY LOAD

This question is unavoidably faced by an engineer choosing one of the two simplest ways of reaching high reliability of elements: should he use high grade elements with increased nominal load without spares, or should he use elements that are spare-provided in accordance with the load? The use of elements unprovided with spares with increased values of nomina X_l and a constant working load X, corresponds to a reduction in the rate of failure of the elements. For example, if capacitors designed for a high working voltage are used in low-voltage circuits, they rarely fail. Spare provision by load makes it possible, under certain conditions, to increase reliability by increasing the number of lower-quality elements employed. In choosing ways to ensure high element reliability, it is usually necessary to take into account some limiting factor (cost, weight, volume, etc.). One can thereupon carry out two types of calculations.

a) Calculation minimizing the limiting factor C for a specified limiting value of failure rate λ_{lim}. This calls for calculation and comparison of the values of the limiting factor C corresponding to two ways of ensuring the required reliability for definite values of X and θ. In order for the failure rate not to exceed a specified value λ_{lim}, it is necessary that the nominal electric load of the element employed be greater than the maximum value, determined by the formula

$$X_{l\,\mathrm{lim}} = \frac{X}{\gamma_{\mathrm{lim}}}. \tag{9}$$

Quantities pertaining to elements unprovided with spares with increased values of nominal loads will be denoted by the subscript 3; those pertaining to spare-provision by load will be designated by the subscript 4.

If elements unprovided with spares are used with increased nominal ratings, the plot of $\lambda = \varphi(\gamma, \theta)$ is used to determine the value of $\lambda_{3\mathrm{lim}}$ corresponding to the specified limiting value λ_{lim} and to the fixed θ. This is followed by calculation of $X_{3n\mathrm{lim}}$ by means of formula (9). One then finds in the catalogue the commercial elements with the next highest rating corresponding to this value of $X_{3n\,\mathrm{lim}}$. From among these elements, one chooses the one with the minimum value of the limiting factor C_s.

In using spare provision by load, the relative electric load on each element of the spare system should be less than the limiting value $\lambda_{4\,\mathrm{lim}}$, which is determined from the relation

$$\lambda_{\mathrm{lim}} = k\varphi\left(\frac{\gamma_{4\mathrm{lim}}}{k}, \theta\right). \tag{10}$$

The calculation is by means of a plot of $\gamma = \varphi(\gamma, \theta)$. For this purpose we rewrite (10) in the form

$$\frac{\lambda_{\mathrm{lim}}}{k} = \varphi\left(\frac{\gamma_{4\mathrm{lim}}}{k}, \theta_1\right). \tag{11}$$

According to (11) we can determine from the plot of $\lambda = \varphi(\gamma, \theta)$ the value of $\lambda_{4\,\mathrm{lim}}/k$, corresponding to λ_{lim}/k for a fixed temperature θ and for k elements in the spare circuit. We then use formula (9) to calculate $X_{4l\,\mathrm{lim}}$ and then determine from the catalogue the closest minimal value of C'_4, corresponding to $X_{4l\,\mathrm{lim}}$ and to the k-dependent value of the element parameter (capacitance, resistance, transconductance, etc.). Similar calculations are carried out for several real values of k. By comparing C_3 and $C_4 = kC'_4$ we can decide which of the ways considered for increasing the element reliability is the more advantageous.

b) Calculation for maximum reliability for a specified limiting value of the limiting factor C_{lim} and for operating conditions X and θ.

If elements with increased nominal load are used, one chooses the element whose limiting factor C_3 is closest to C_{lim}, subject to the condition $C_3 < C_{\text{lim}}$. From the value of the nominal electric load X_{3l} of this element, and from the operating conditions X_3 and θ, we determine the value of λ_3 from the plot of $\lambda = \varphi(\gamma, \theta)$.

In spare-providing the element by load, we choose from the catalogue a spare-circuit element with a limiting-factor value C_4, and specify the spare-provision multiplicity k such that it satisfies the inequality

$$kC_4 \leqslant C_{\text{lim}}, \tag{12}$$

thus determining the rate of failure of the spare circuit under the defined operating conditions X and θ. For this purpose we determine by means of the plot of $\lambda = \varphi(\gamma, \theta)$ the value of λ'_5 corresponding to the nominal load X_{4l} of the chosen element and to the values of γ, θ, and k; we then calculate the quantity

$$\lambda_5 = k\lambda_5^{\cdot} = k\varphi\left(\frac{X}{X_{4l}k}, \theta\right). \tag{13}$$

The value of λ_5 is compared with λ_3 to determine which way of attaining reliability is the more advantageous. By choosing different values of k and C_4 satisfying condition (12), we can choose the optimal version of spare provision, ensuring the highest reliability. When the number of possible spare-provision versions is large, it is advantageous to prepare, during the process of calculation, a plot or a table of $X_{4l} = f_1(k)$, and to plot after the end of the calculation the curve $\lambda_5 = f_2(k)$.

3. MIXED SPARE PROVISION OF ELEMENTS

Spare provision by load and functional spare provision are the limiting cases of general or mixed spare provision, when the spare circuit still continues to operate but under changed conditions as when one or several elements fail. In other words, in mixed spare provision the reliability of the spare circuit is increased, both because on failure of one or several elements the functions of the elements out of order are assumed by the remaining elements, and because the electric load acting on the spare circuits is distributed among all the elements of the circuit, which in turn operate under lighter conditions. For most elements it is easier to effect mixed spare provision than functional spare provision.

Like all classifications, the division between spare provision by load and mixed spare provision is arbitrary, depending on the requirements imposed on the element. For example, if it is required that a capacitor unprovided with a spare should have a constant capacitance value within ± 5%, a capacitor circuit such as shown in Figure 4 can, under certain conditions, ensure only spare provision by load. When the capacitance can fluctuate by ± 70% from the nominal value, the same circuit ensures mixed spare provision.

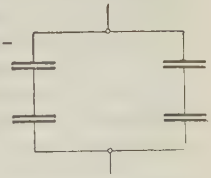

Figure 4. Spare circuit.

In the case of mixed spare provision, account must be taken of different variations in the structure of the circuit, caused by the failure of each of its elements, that is, the types of element failures must by considered. Failure elements may have entirely different manifestations, that is, different degrees of influence on neighboring circuits. For most elements, however, we can separate limiting cases of possible external manifestations of failures, namely open and short circuits. It is possible to reduce to these two limiting cases various external manifestations of failures of almost all elements. Consequently, for an approximate investigation of mixed-spare-provision networks, one can use the procedures developed for the investigation of the spare provision for contact elements [3,5].

The character of the redistribution of the electric load among the elements of the spare circuit in the case of failure of one or several elements is determined by the type of specific spare circuit for the specific element. The features of mixed spare provision of elements of a definite type can therefore be disclosed only after examining many specific spare circuits made up of these elements.

REFERENCES

1. N.G. Bruevich, On the Reliability and Accuracy of Automatic Production. Izv. AN SSSR, Otd. tekhn. n., Energetika i avtomatika, 1959, 4.

2. C.J. Creveling, Increasing the reliability of of electronic equipment by the use of redundant circuits, Proc. I.R.E., 1956, April.
3. G.V. Druzhinin, Spare Provision for Circuits with Contact Elements, Izv. AN SSSR. Otd. tekhn. n. 1958, 6, 96.
4. G.V. Druzhinin, Spare Provision of Capacitors, Radiotekhnika i elektronika 1959, 4, 3, 463.
5. G.V. Druzhinin, Use of Spare Parts in the Construction of Contact Elements. Collection of Articles, Reliability of Electronic Apparatus, Izd. Sovyetskoye radio, 1960.
6. G.V. Druzhinin, Classification of Spare-Provided Systems, Elektrosvyaz', 1959, 7, 72.
7. J. Connor, Calculation of Risk in the Use of Circuit Elements, Russian Translation, Vopr. radiolokatsionnoi tekhniki, 1957, 4, 15.
8. A. Wulfsberg, The price of reliability in airborne electronic equipment, IRE Trans. Reliabil. and Qual. Control, 1957, PGRQC-9, 1, 9

Submitted to the editors 14 October 1960

EFFECT OF EARTH IN UHF TROPOSPHERIC-SCATTER PROPAGATION

A.I. Kalinin

A solution is found for determining the average magnitude of the field intensity in tropospheric-scatter propagation of UHF waves, based on the hypothesis of coherent scattering from inhomogeneities of the troposphere, exponential variation of the permittivity of air with altitude above the earth's surface and diffraction around the earth's surface.

1. It was shown in reference [1] that the experimentally observed laws governing UHF tropospheric scatter propagation can be attributed to reflection of radio waves from an upper half-space in which the permittivity of air ϵ varies exponentially with the height h above the earth's surface.

The boundary between the upper and lower half-spaces is brought about by the screening influence of the earth, and has been assumed to be of zero thickness in reference [1], for the sake of simplicity. The height h_1 of this boundary is determined by the intersection of the tangents to the earth's surface drawn at the transmission and reception points (Figure 1a), and for zero heights of the transmitting and receiving antennas its value is

$$h_1 = \frac{R^2}{8a_{eq}}, \tag{1}$$

where R is the distance between the transmission and reception points and a_{eq} is the equivalent radius of the earth.

Reflection from the earth's surface and from the troposphere layer located at heights $h < h_1$ were neglected in [1], and consequently the distribution of the amplitude of the field intensity of the incident wave in the vertical plane have the form shown in Figure 1b, where E_0 is the field in free space.

Owing to diffraction around the earth's surface, the boundary between the upper and lower half-space becomes "diffuse." The purpose of the present investigation is to account for the effect of this diffuseness of the boundary on the average field intensity in UHF tropospthereic scatter propagation.

2. As in reference [1], we shall assume that the real dependence of the permittivity

of air ϵ on height h can be approximated in the mean by the exponential dependence

$$\varepsilon(h) = 1 + \Delta\varepsilon_0 \exp\Big(\frac{g}{\Delta\varepsilon_0}\, h, \tag{2}$$

where $\Delta\epsilon_0$ is the deviation of ϵ from unity at the earth's surface and $g < 0$ is the value of the vertical gradient of the permittivity of air near the earth's surface.

The exponential dependence $\epsilon(h)$ given by equation (2) has been recently confirmed by extensive experimental material [2] and adopted by the International Radio Consultative Committee (IRCC) as the basic model of the troposphere [3].

By splitting up the troposphere into thin spherical layers of thickness Δh, we can determine the field at the reception point as being the result of the interference of waves reflected from all the interfaces between the layers. Assuming the coefficient of reflection from each boundary to be equal to the Fresnel coefficient and in the limit, as $\Delta h \to 0$, we can obtain the following general formula for the attenuation coefficient of the free-space field V:

$$V = -\frac{gh_0}{4}\int_0^\infty \frac{\exp\left(\frac{g}{\Delta\varepsilon_0} h_0 y\right)}{\sin^2\Theta(y)}\, U^2(y) F^2(y)\, dy\,, \tag{3}$$

where y is the height h in dimensionless units:

$$y = \frac{h}{h_0}\,; \tag{4}$$

h_0 is the "standard" height

$$h_0 = \sqrt[3]{\frac{a_{\mathrm{eq}}\lambda^2}{8\pi^2}}\,; \tag{5}$$

λ is the wavelength, $\theta(y)$ is the glancing angle for the interface located at a height y; U(y) is the attenuation function that accounts for the variation in the amplitude and phase of the waves due to the influence of the earth in the paths from the transmission point to the reflection point and from the reflection point to the reception point; $F^2(y)$ is a factor that accounts for the directivities of the transmitting and receiving antennas, assumed to be equal.

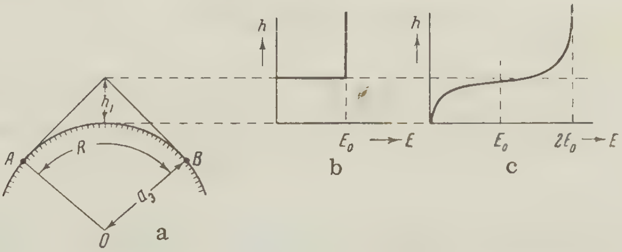

Figure 1.

We shall disregard henceforth the directivity of the antennas (that is, we shall assume $F^2(y) = 1$), since it is shown in [1] that this influence is negligible.

3. We shall seek the solution of this problem for the case when a vertical electric dipole is placed on the surface of a perfectly conducting earth. The field distribution of the incident wave in the vertical plane will have the form shown in Figure 1c. In the case when the transmitting and receiving antennas are raised above the earth's surface and $h > h_1$, the interference structure of the incident-wave field will be observed.

The solution for this case is of interest in itself, and is not considered here.

4. On the basis of the papers of V. A. Fok [4] for the case of a vertical electric dipole located on a perfectly conducting earth and for the case of $y >> 1$, the attenuation function can be represented in the form

$$U(y) = \sqrt[4]{\frac{x^2}{4y}} \exp\left(i\,\frac{2}{3}\, y^{3/2}\right) V_1'(z), \tag{6}$$

where x is the distance in dimensionless units

$$x = \frac{R}{R_0}; \tag{7}$$

R_0 is the "standard" distance

$$R_0 = \sqrt[3]{\frac{a^2_{\mathrm{eq}}\lambda}{\pi}}, \tag{8}$$

$$z = \frac{x}{2} - \sqrt{y}; \tag{9}$$

$V_1(z)$ is the attenuation function of the plane wave; the absolute magnitude and the phase of this function, taken from [5], are shown in Figures 2a and 2b respectively.

Changing in (3) from the integration variable y to the variable z as given by (9) and taking (6) into account, we get

$$V = \frac{g h_0 x}{4} \exp\left(\frac{g h_0 x^2}{4\Delta\varepsilon_0}\right) \int_{x/2}^{-\infty} \frac{\exp\left[\frac{g}{\Delta\varepsilon_0} h_0 (z^2 - xz) + i\,\frac{4}{3}\left(\frac{x}{2} - z\right)^3\right]}{\sin^2\Theta(z)} V_1^2(z)\,dz. \tag{10}$$

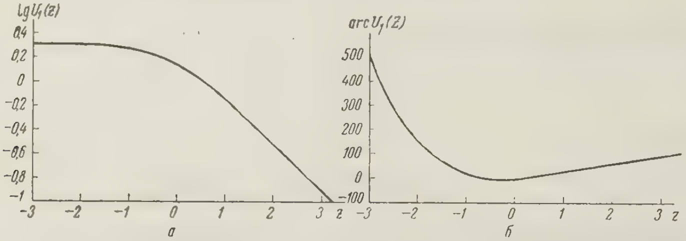

Figure 2.

From geometrical considerations, taking (7) and (9) into account, we find that

$$\sin\Theta(z) = \frac{R}{2a_{\text{э}}}\left(1 - \frac{2z}{x}\right) \tag{11}$$

and consequently

$$V = \frac{a^2\mathrm{eq}^{g h_0}}{R_0^2 x} \exp\left(\frac{g h_0 x^2}{4\Delta\varepsilon_0}\right) \int_{x/2}^{-\infty} \frac{\exp\left[\frac{g}{\Delta\varepsilon_0} h_0 (z^2 - xz) + i\,\frac{4}{3}\left(\frac{x}{2} - z\right)^2\right]}{\left(1 - \frac{2z}{x}\right)^2} V_1^2(z)\,dz. \tag{12}$$

It is obvious that the essential region of integration will be of those values of z, satisfying the inequality

$$|z| \ll \frac{x}{2}, \tag{13}$$

and therefore approximately

$$V = \frac{a^2\mathrm{eq}^{g h_0}}{R_0^2 x} \exp\left(\frac{g h_0 x^2}{4\Delta\varepsilon_0} + i\,\frac{x^3}{6}\right) \int_{x/2}^{-\infty} \exp\left[-\left(\frac{g}{\Delta\varepsilon_0} h_0 + i x^2\right) z\right] V_1^2(z)\,dz. \tag{14}$$

To calculate the integral (14) we must know the analytic expression for the function $V_1(z)$. On the basis of the work of V.A. Fok [4], $V_1(z)$ can be represented in series form

$$V_1(z) = \frac{4}{3} + \sum_{n=1}^{\infty} a_n z^n, \tag{15}$$

which converges for any finite z. The coefficients a_n are determined by the formula

$$a_n = \frac{2}{3}\,\frac{1}{3^{\frac{n}{3}}\,\Gamma\left(1 + \frac{n}{3}\right)}\left[\exp\left(-i\,\frac{5n\pi}{6}\right) + \exp\left(i\,\frac{n\pi}{2}\right)\right]. \tag{16}$$

The series (15) converges sufficiently rapidly for small values of $|z|$. For large $|z|$ we can use asymptotic expressions for the function $V_1(z)$. On the basis of the same papers [4], the following formula can be used for large negative values of z:

$$V_1(z) = 2\exp\left(-\frac{i}{3}z^3\right). \tag{17}$$

For positive z, $V_1(z)$ can be expressed as a series of residues

$$V_1(z) = i2\sqrt{\pi}\sum_{s=1}^{\infty}\frac{\exp(it'_s z)}{t'_s w(t'_s)}, \tag{18}$$

where t'_s are the roots of the equation

$$w'(t'_s) = 0, \tag{19}$$

and w(t) is the complex Airy function.

At sufficiently large positive values of z, we can confine ourselves to the first term of the sum (18), corresponding to the first root of equation (19)

$$t'_1 = 1.01879\exp\left(i\frac{\pi}{3}\right). \tag{20}$$

A comparison of the results of the calculations of $V_1(z)$ by formula (17) and the value obtained from the first term of (18) with the exact values of $V_1(z)$, cited in [5], shows that when $z > 1$ we can use with sufficient degree of accuracy formula (18) with but one term, while asymptotic formula (17) is applicable when $z < -1$.

Breaking up the path of integration in (14) into three parts, namely $\frac{x}{2} > z > 1$, $1 > z > -1$, and $-\infty > z > -1$, and using the corresponding expressions for $V_1(z)$ in each part, we obtain

$$V = \frac{a^2\mathbf{eq}gh_0}{R_0^2 x}\exp\left(\frac{gh_0x^2}{4\Delta\varepsilon_0} + i\frac{x^3}{6}\right)L, \tag{21}$$

where

$$\begin{aligned} L = 3.35\int_{x/2}^{1}\exp\left\{-\left[\frac{g}{\Delta\varepsilon_0}h_0x + i(x^2 - 2t'_1)\right]z\right\}dz + \\ + \int_{1}^{-1}\left[1{,}78 + 2{,}66\sum_{n=1}^{\infty}a_nz^n + \left(\sum_{n=1}^{\infty}a_nz^n\right)^2\right]\exp\left[-\left(\frac{g}{\Delta\varepsilon_0}h_0x + ix^2\right)z\right]dz + \\ + 4\int_{-1}^{-\infty}\exp\left[-\left(\frac{g}{\Delta\varepsilon_0}h_0x + ix^2\right)z - i\frac{2}{3}z^3\right]dz. \end{aligned} \tag{22}$$

In tropospheric-scatter propagation of UHF waves, the following inequalities are always satisfied

$$x^2 \gg 1; \quad x^2 \gg |2t'_1 \text{ and} x \gg \frac{g}{\Delta\varepsilon_0}h_0. \tag{23}$$

In addition, by virtue of the first inequality of (23), we have

$$\int_{1}^{-1}z^n\exp(-ix^2z)\,dz \cong \frac{i}{x^2}[(-1)^n\exp(ix^2) - \exp(-ix^2)]. \tag{24}$$

Taking (13), (23), (20), and (24) into account and carrying out the integration in (22), we obtain

$$\begin{aligned} L = \Bigg\{\left[-1.21 - 2.66\sum_{n=1}^{\infty}a_n - \sum_{n=1}^{\infty}a_n^2 - 2\sum_{n\neq k}a_na_k\right]\exp(-ix^2) + \\ + \left[-2.22 + 2.66\sum_{n=1}^{\infty}(-1)^na_n + \sum_{n=1}^{\infty}a_n^2 + 2\sum_{n\neq k}a_na_k(-1)^{n+k}\right]\exp(ix^2)\Bigg\}. \end{aligned} \tag{25}$$

The series in (25) converge rather rapidly, and consequently we can confine ourselves in the calculations to the first several terms. Calculation with account of the first three terms yields

$$L = \frac{i}{x^2}\left[(0.084 - i\,0.171)\exp(-ix^2) + (-1.59 + i\,1.57)\exp(ix^2)\right] \simeq$$
$$\simeq \frac{i}{x^2}(-1.59 + i\,1.57)\exp(ix^2). \tag{26}$$

Substituting this value of L in (21) and taking (5) and (8) into account, we get

$$|V| = 2.24\,\frac{1}{2\pi}\,\frac{a^2\mathbf{eq}^{gh_0}}{R^3}\exp\left(\frac{R^2\mathbf{eq}}{8a_{\text{э}}\Delta\varepsilon_0}\right). \tag{27}$$

The absolute value of the attenuation factor in (27) differs from the corresponding value of $|V|$ in [1] only in the constant multiplier 2.24. If we assume the boundary between the half-spaces to have zero thickness in this case, this constant factor should be equal to 4. Consequently, the diffusion of the boundary leads to a slight decrease in the field intensity, owing to the compensating action of the lower half-space. Thus, the diffuseness of the boundary between the upper and lower half spaces, caused by diffraction, does not change in practice the results obtained in [1], under the assumption that this boundary is ideally sharp.

REFERENCES

1. A.I. Kalinin, Coherent Theory of Tropospheric-Scatter UHF Propagation, Elektrosvyaz' (Electric Communication), 1959, 6, 41.
2. B.R. Been, G.D. Thayer, A model radio refractivity atmosphere, NBS Report No 5576, June 9, 1958.
3. Recommendation No. 309, adopted by the Ninth Plenary Session of the IRCC Assembly (Los Angeles, 1959).
4. V.A. Fok, Diffraction of Radio Waves around the Earth's Surface, Izd. AN SSSR, 1946.
5. P.A. Azrilyant, M.G. Belkina, Numerical Results of the Theory of Diffraction of Radio Waves around the Earth's Surface, Izd. Sovetskoe Radio, 1957.

Submitted to the editors 14 November, 1960

PROPAGATION OF PULSED SIGNALS OVER A HOMOGENEOUS FLAT EARTH

V.V. Novikov and G.I. Makarov

We consider the problem of nonstationary propagation of radio waves from a vertical electric dipole, over a flat homogeneous earth with allowance for the displacement current in the earth. The solution of the problem reduces either to elementary functions, depending on the type of current in the dipole. The main laws governing nonstationary phenomena occurring during the propagation of radio waves are clarified.

INTRODUCTION

Nonstationary propagation of radio waves has attracted much attention recently. White and Johler [1 — 3] developed a theory of the propagation of pulsed signals over a flat earth with the displacement current in the earth neglected. This neglect, however, is permissible only for signals with a sufficient low-frequency spectrum propagating over an earth that has high or medium conductivity. Consequently, the theory developed by White does not encompass all the cases encountered in practice.

In the present paper we discuss nonstationary propagation of radio waves over a flat homogeneous earth with allowance for the displacement currents in the earth, and obtain a sufficiently simple approximate formula for the solution of this problem. We also discuss the results of numerical calculations and elucidate the main lows governing nonstationary phenomena occurring during the propagationof radio waves.

1. CONSTRUCTION OF THE SOLUTION

Consider the problem of the radiation field of a vertical electric diploe, located on a flat homogeneous earth of conductivity σ and relative dielectric constant ϵ_m and excited current $I(t)$ $[I(t) = t < 0]$. Its solution can be obtained with the aid of the inverse Fourier transform from the well known expression for a field produced by a dipole, whose current varies sinusoidally with time [as $\exp(-i\omega t)$]. The vertical component of the electric field of such a dipole on the surface of the earth is determined by the following expression (in the MKS system)

$$E = \frac{i\omega\mu dh}{2\pi r} I w\left(\sqrt{sr}\right) e^{ikr},$$

where $\mu = 4\pi \cdot 10^{-7}$ henry/meter; I is the amplitude of the current in the dipole; dh is the height of the dipole; $sr = ikr/2(\epsilon'_m + 1)$ is the numerical distance; $\epsilon'_m = \epsilon_m + i\frac{\sigma}{\omega\epsilon_0}$ is the relative complex dielectric constant of the earth;

$$w(x) = 1 + 2xe^{-x^2} \int_x^{i\infty} e^{z^2} dz \tag{2}$$

is the Sommerfeld attenuation function.

If we take I in equation (1) to mean the spectrum of the current in the dipole

$$I = I(\omega) = \int_0^\infty I(t) e^{i\omega t} dt,$$

then this quantity is the spectrum of the vertical component of the electric field (radiation field), and the integral of this quantity with respect to the frequency yields the solution of the nonstationary problem for this component

$$E(t') = \frac{i\mu dh}{4\pi^2 r} \int_{-\infty+i\varepsilon}^{\infty+i\varepsilon} \omega w\left(\sqrt{sr}\right) I(\omega) e^{-i\omega t'} d\omega; \quad t' = t - \frac{r}{c}. \tag{3}$$

It must be noted that (1) is an approximate formula, describing the field spectrum with a relative accuracy on the order of $1/|\epsilon'_m|$ (for more details see reference [4]). It is difficult to say what error in the field is brought about by such an error in the spectrum. But it is quite obvious that the relative error in the field coincides in order of magnitude to the error in the spectrum at that frequency for which the spectral density has a maximum, and in any case does not exceed the maximum relative error in the spectrum at very high frequencies — an order of $1/\epsilon_m$. Thus, the results given in the present paper are applicable for signals with arbitrary spectrum, propagating over earths with sufficiently high relative dielectric constant ($\epsilon_m \gg 10$, takes place in many practical cases).

Expression (3) for the radiation field is a rather complicated double integral, since the attenuation function under the integral sign is in turn expressed in terms of the integral (2). Our problem consists in finding a simple analytic function for the radiation field (3).

Let us note briefly the following general properties of the integral (3). The field vanishes when $t' < 0$ and the equation $t' = 0$ is the equation of the front. The front of the disturbance propagates at the velocity of light in the upper medium. The value of the field on the front is determined by the behavior of the integrand $\omega w(\sqrt{sr})I(\omega)$ at infinity. Using the well known asymptotic representation of the attenuation function, we can readily verify that the function $\omega w(\sqrt{sr})$ tends at infinity either to zero, if the displacement currents are neglected

$$\omega w\left(\sqrt{sr}\right) \sim -\frac{\sigma c}{\varepsilon_0 r}\frac{1}{\omega}$$

or to a constant value, if the displacement currents are taken into account

$$\omega w\left(\sqrt{sr}\right) \to i\frac{(\varepsilon_m+1)c}{r}.$$

The presence of the displacement currents changes the decrease of the integrand at infinity by one order of magnitude. If the displacement currents are taken into account, the field on the front has the same singularity as the current in the dipole at t = 0: thus, the jump in current at t = 0 causes the field to experience a discontinuity of the first kind on the fronts. On the other hand, if the displacement currents are not taken into account, then the singularity of the field on the front is found to be one order of magnitude lower than the singularity of the current at t = 0: a jump in the current becomes a jump in the first derivative of the field, while the field itself is described by a continuous function and vanishes on the front. The displacement currents appreciably affect the behavior of the field in the vicinity of the front.

2. QUALITATIVE EXAMINATION OF THE PRINCIPAL LAWS GOVERNING NONSTATIONARY PHENOMENA

Before we proceed to calculating the integral (3), it is desirable to elucidate qualitatively the main laws that govern nonstationary phenomena in this case. We start from spectral representations. The factor ω in the integrand of expression (3) for the radiation field is due to the radiating properties of the dipole, and makes the field above a perfectly reflecting plane proportional to the derivative of the current in the dipole (the dipole has differentiating properties). On the other hand, the effect of the propagation path consists, first, in delaying the pulse, a fact accounted for by the quantity t', and second, in the case of a path of finite conductivity, in distortion of the pulse due to the dispersion, which is described by the attenuation function. The attenuation function is essentially the complex transfer function of the propagation path (disregarding the delay of the signal, which is separately treated)

$$K(\omega) = w\left(\sqrt{sr}\right).$$

Starting from the amplitude and phase characteristics of the propagation path

$$A(\omega) = \left|w\left(\sqrt{sr}\right)\right|, \qquad \Phi(\omega) = \arg w\left(\sqrt{sr}\right),$$

we can estimate the transient time and determine how it depends on the distance and on the conductivity of the path, and how the displacement currents affect the transients.

In the analysis of the frequency characteristics as functions of the attenuation, it is expedient to change from the circular frequency ω to the dimensionless parameters $\alpha\omega$, where,

$$\alpha = \sqrt{\frac{\varepsilon_0 r}{2\sigma c}}. \tag{4}$$

Then the numerical distance can be represented as follows:

$$sr = \frac{(\alpha\omega)^2}{1 - i\gamma\alpha\omega}, \qquad \gamma = \frac{\varepsilon_m + 1}{\sqrt{60\pi\sigma r}}. \tag{5}$$

If the displacements currents are neglected, $\gamma = 0$. The amplitude and phase characteristics corresponding to this case are shown in Figure 1.

The absolute value of the transfer function of the path has a maximum at zero frequency, and then decreases monotonically with increasing frequency. The bandwidth of the propagation path at the 0.7 level by

$$\Delta\nu \simeq \frac{1{,}15}{\alpha} = 0.15\sqrt{\frac{2\sigma c}{\varepsilon_0 r}}.$$

The duration of the transient is inversely proportional to the bandwidth [5]:

$$t_{\text{уст}} \approx a_1 \sqrt{\frac{\varepsilon_0 r}{2\sigma c}}; \tag{6}$$

where a_1 is a certain constant on the order of several times one. From expression (6) it follows that the duration of the transient is inversely proportional to $\sqrt{\sigma}$ and increases with the distance as $\sqrt{r}$.

Let us investigate the effect of displacement currents on the frequency characteristics. When these are taken into account, the value of γ as given by (5) differs from zero and becomes smaller than unity for real earths, at distances greater than 5 or 10 km. The numerical calculations show that in those cases when $\gamma < 1$, an account of the displacement currents reduces the bandwidth of the path (Figure 1) $\gamma = 0.2$, and consequently increases the duration of the transient and reduces its amplitude. It must be noted, however, that the effect of the displacement currents on the nonstationary phenomena depends on the distance.

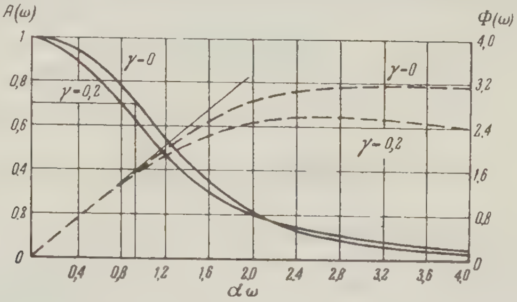

Figure 1. Amplitude and phase characteristics of propagation path.

This is perfectly understandable, for with increasing distance from the source, the low frefrequencies , for which the displacement currents are much less than the conduction currents assume a major role.

3. INVESTIGATION OF THE SOLUTION OF THE PROBLEM

Let us proceed now to evaluate the integral (3). It is expedient to use an integration variable such as to make the phase of the attenuation function sufficiently simple. We put

$$u = \sqrt{sr} = \frac{\alpha\omega}{\sqrt{1 - \frac{i\omega}{\zeta}}}, \quad \zeta = \frac{\sigma}{\varepsilon_0 (\varepsilon_m + 1)}, \tag{7}$$

then

$$E(t') = \frac{i\mu\, dh}{4\pi^2 r\alpha^2} \int_l \vartheta(u)\,\vartheta'(u)\,w(u)\,I\left[\frac{\vartheta(u)}{\alpha}\right] e^{-2i\vartheta(u)T}\,du, \tag{8}$$

where

$$T = \frac{t'}{2\alpha}; \quad \vartheta(u) = u\left(\sqrt{1 - \frac{\gamma^2 u^2}{4}} - \frac{i\gamma u}{2}\right), \tag{9}$$

and we choose that branch of the root $\sqrt{1 - \frac{\gamma^2 u^2}{4}}$, for which $\operatorname{Re}\sqrt{1 - \frac{\gamma^2 u^2}{4}} > 0$. The integration contour l in the integral (8) is shown in Figure 2.

We begin the analysis of the integral (8) with the case when the dipole current is described by the units that function

$$I_1(t) = I_a \cdot 1(t) = \begin{cases} 0 & t < 0, \\ I_a & t > 0 \end{cases}$$

and

$$E_1(t') = -\frac{\mu I_a\, dh}{4\pi^2 r\alpha} \int_l \vartheta'(u)\, w(u)\, e^{-2i\vartheta(u)T}\, du. \tag{10}$$

When t' > 0 the integration contour can be made congruent with the real axis. The attenuation function w(u) contained in the integrand of (10) has a singularity at infinity in the lower half-plane. This singularity can be separated by representing the function w(u) in the form of a sum

$$w(u) = v(u) + 2i\sqrt{\pi}ue^{-u^2}, \quad v(u) = 1 + 2ue^{-u^2} \int_u^{-i\infty} e^{z^2}\, dz,$$

where v(u) is regular in the lower half-plane. The integral (10) then breaks up into two parts:

$$E_1(t') = E_{11}(t') + E_{12}(t'),$$

$$E_{11}(t') = -\frac{i\mu I_a\, dh}{2\pi\sqrt{\pi}\alpha r} \int_{-\infty}^{+\infty} u\vartheta'^{+}(u)\, e^{-u^2-2i\vartheta^{+}(u)T}\, du,$$

$$E_{12}(t') = -\frac{\mu I_a\, dh}{4\pi^2 r\alpha} \int_{-\infty}^{-\infty} \vartheta'^{+}(u)\, v(u)\, e^{-2i\vartheta^{+}(u)T} du, \tag{11}$$

where the superscript plus of the functions $\vartheta(u)$ and $\vartheta'(u)$ denotes that the values of these functions corresponding to the upper edges of the cuts are taken. The integrand of (11) rapidly decreases in the lower half plane as $|u| \to \infty$, and its only singularities below the integration contour are the branch points. As a result of this, the integral (11) can be reduced to integrals along the cuts, and after some simple transformations, using the relation

$$v(u) - v(-u) = -2i\sqrt{\pi}ue^{-u^2},$$

we find that (see [4])

$$E_{12}(t') = -\frac{i\mu I_a\, dh}{2\pi\sqrt{\pi}\alpha r} \int_{2/\gamma}^{\infty} \{-u\vartheta'^{+}(u)\, e^{-u^2-2i\vartheta^{+}(u)T} + u\vartheta'^{-}(u)\, e^{-u^2-2i\vartheta^{-}(u)T}\}\, du.$$

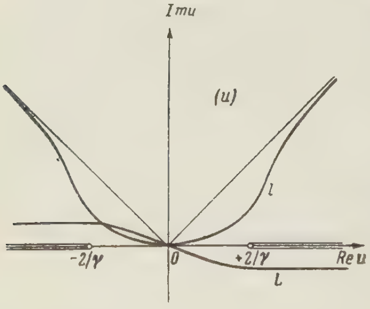

Figure 2. Plane of the complex variable u.

Rejoining E_{11} with E_{12} we obtain ultimately for the radiation field a rather simple expression in the form of a single integral

$$E_1(t') = -\frac{i\mu I_a\, dh}{2\pi\sqrt{\pi}\alpha r} \int_L u\vartheta'(u)\, e^{-u^2-2i\vartheta(u)T}\, du, \tag{12}$$

the integration contour of which is shown in Figure 2.

Analogous transformations can be carried out also when the current in the dipole is a unit step envelope of a sinusoidal carrier

$$I_2(t) = I_a e^{-i\omega_0 t} \cdot 1(t),$$

where

$$E_2(t') = E_{2\,\mathrm{st}}(t') + E_{2\,\mathrm{non}}(t'),$$

$$E_{2\,\mathrm{st}}(t') = \frac{i\omega_0\mu I_a\, dh}{2\pi r}\, w\left(\sqrt{s_0 r}\right) e^{-i\omega_0 t'} \tag{13}$$

is the stationary part of the field (s_0r is the numerical distance at the carrier frequency ω_0) and

$$E_{2\,\mathrm{non}}(t') = -\frac{i\mu I_a\, dh}{2\pi\sqrt{\pi}\alpha r} \int_L \frac{u\vartheta(u)\,\vartheta'(u)}{\vartheta(u) - \alpha\omega_0}\, e^{-u^2-2i\vartheta(u)T}\, du \tag{14}$$

is the nonstationary part of the field, describing the transients.

It is convenient to introduce in the integrals (12) to (14) an integration variable $p - \sqrt{u}/2$ which yields

$$E_1(t') = -\frac{\mu I_a\, dh}{2\pi r}\,\frac{4i\zeta^2\alpha}{\sqrt{\pi}} \int\limits_{\widetilde{L}} p u'(p) \exp\left[-2\frac{\zeta}{\beta} f(p)\right] dp, \tag{15}$$

$$E_{2\,\text{нест}}(t') = -\frac{\mu I_a\, dh}{2\pi r}\,\frac{4i\zeta^2\alpha}{\sqrt{\pi}} \int\limits_{\widetilde{L}} \frac{pu(p)\,u'(p)}{u(p) - a} \exp\left[-2\frac{\zeta}{\beta} f(p)\right] dp, \tag{16}$$

where

$$u(p) = p\left(\sqrt{1-p^2} - ip\right); \quad f(p) = p^2 + i\tau u(p); \quad a = \frac{\omega_0}{2\zeta};$$

$$\tau = \beta t'; \quad \beta = \frac{(\varepsilon_m + 1)\, c}{r}. \tag{17}$$

We evaluate the integrals (15) and (16) by the stationary-phase method. The large parameter necessary for the application of this method is the quantity $2\zeta/\beta$, which depends on the distance and on the electric properties of the earth, and assumes a value much greater than unity even at small distances from the dipole. As a result we obtain

$$E_1(t') = -\frac{\mu I_a\, dh}{2\pi r}\,\zeta F(\tau) \exp\left[-\frac{\zeta}{\beta} f(\tau)\right]\left\{\tau + \frac{\beta}{\zeta} u(\tau)\right\}, \tag{18}$$

$$E_{2\,\text{non}}(t') = -\frac{\mu I_a\, dh}{2\pi r} F(\tau) \exp\left[-\frac{\zeta}{\beta} f(t)\right]\Big\{\zeta\tau + \beta u(\tau) +$$

$$+ i\omega_0\varphi(\tau)\left[1 + \psi(\omega_0, \zeta, \tau)\, 2z_0 e^{-z_0^2} \int\limits_{z_0}^{i\infty} e^{z^2} dz\right]\Big\}, \tag{19}$$

where we use the notation

$$F(\tau) = \frac{2}{(1+2\tau)(1+\sqrt{1+2\tau})}, \quad u(\tau) = \frac{1+\sqrt{1+2\tau}}{2\sqrt{1+2\tau}},$$

$$f(\tau) = \frac{\tau^2}{1+\tau+\sqrt{1+2\tau}}, \quad \varphi(\tau) = \frac{1}{2}\left[1 + 2\tau + \sqrt{1+2\tau}\right], \tag{20}$$

$$\psi(\omega_0, \zeta, \tau) = \left[1 + i\frac{\zeta}{\omega_0}\,\frac{\tau}{\varphi(\tau)}\right]^{-1}, \quad z_0^2 = s_0 r + i\omega_0 t' - \frac{\zeta}{\beta} f(\tau).$$

The condition for applicability of the resultant expressions (18) and (19) is the fulfillment of the inequality

$$2\frac{\zeta}{\beta} \gg 1. \tag{21}$$

In the most unfavorable case $\epsilon_m = 5$ and $\sigma = 10^{-4}$ mho/m; this inequality is fulfilled at distances on the order of 5 km up.

We note that if we neglect the displacement current in expressions (18) and (19) for the radiation fields, these expressions coincide with the results obtained by Wait [1].

4. ANALYSIS OF RESULTS AND NUMERICAL DATA

Let us analyze the radiation field (18), produced by a dipole excited by a unit step function. We represent (18) in the form

$$E_1(t') = -\frac{\mu I_a\, d\, h}{2\pi\, r\, \alpha} A(\gamma, T),$$

$$A(\gamma, T) = F(\gamma T)\{T +$$

$$+ \frac{1}{2}\gamma u(\gamma T)\} \exp\left[-\chi(\gamma T) T^2\right].$$

where the functions F(γT) and u(γT) are determined by the formulas in (20), γ and T are given by (5) and (9) respectively, and

$$\chi(x) = \frac{2}{1 + x + \sqrt{1+2x}}.$$

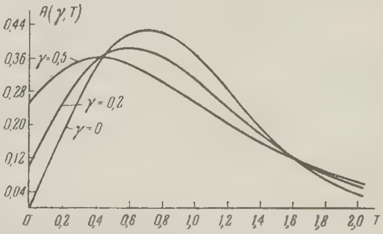

Figure 3. Plots of the function A(γ, T)

Plots of the function $A(\gamma, T)$ vs. T are shown for different values of γ in Figure 3. Were the conductivity of the earth to be infinite, the radiation field would have the form of a δ-function propagating with the velocity of light. The finite conductivity and the displacement currents in the earth, however, bring about propagation transients that distort the signal. The attenuation of the transients is described by the exponential factor $\exp[-\chi(\gamma T)T^2]$. Neglecting the displacement currents, the value of the function χ is unity. Let us define the duration of the transient to mean the time during which the exponential factor is reduced to one-tenth its value. Then if the displacement currents are neglected,

$$t_{\text{stable}}\ 2\sqrt{\frac{\varepsilon_0 r}{2\sigma c}} \simeq 10^{-2}\sqrt{\frac{r(\text{km})}{\sigma(\text{mho/m})}}\ \mu\text{SEC}$$

For dry soil ($\sigma = 10^{-4}$ mho/m) and the large distances ($r \simeq 100$ km), the duration of the transients can reach large values, on the order of 10 microseconds. Owing to the displacement currents, a function $\chi(\gamma, T)$ appears in the exponent; its value is unity when $t' = 0$ and decreases monotonically, thus increasing the duration of the transient.

It is clear from Figure 3 that at short distances, which amounts to several tenths, the displacement currents greatly influence the form of the signal and reduce its amplitude. In addition, they prescribe the behavior of the field in the vicinity of the front. If, neglecting the displacement currents, the initial conditions for the field due to excitation of the dipole by a unit-step current have zero values, then including the displacement currents makes the field on the front experience a finite jump, the magnitude of which depends on the dielectric constant of the earth but not on the conductivity; the value of the jump is

$$E_1(0) = -\frac{\mu I_a\, dhc}{2\pi r^2}(\varepsilon_m + 1).$$

The field jump on the front is inversely proportional to the square of the distance. The front of the signal is made up of high frequencies, characterized by such a dependence of the field on the distance. As to the amplitude of the signal, the maximum of the function $A(\gamma, T)$ is approximately 0.4 and depends very little on the distance. Consequently, the amplitude of the field is inversely proportional to the distance raised to the 3/2 power.

The front of the pulse propagates with the velocity of light c, but the rate of propagation of its maximum is less than the velocity of light, and the maximum of the signal lags the front more and more as the distance is increased, the pulse itself becoming diffused. The delay time of the signal maximum relative to the front is given by the expression

$$\Delta t = 1.4\,\alpha \simeq 0.6\cdot 10^{-2}\sqrt{\frac{r(\text{km})}{\sigma(\text{mho/m})}}\ \mu\text{SEC}$$

We proceed now to examine the field of a dipole excited by a pulse consisting of a sinusoidal or cosinusoidal carrier with a unit-step envelope. The attenuation of the transient (19) is again described by an exponential factor $\exp\left[-\frac{\zeta}{\beta}f(\tau)\right] = \exp\left[-\chi\left(\gamma T\right)T^2\right]$. . It must be pointed out that the attenuation depends only on the propagation path and is independent of the spectrum of the signal. Formulas (13) and (19) show that the field is a function of the five variables t', r, σ, ϵ_m, and ω_0. In order to simplify the calculations with these formulas, it is advisable to change to the dimensionless variables

$$\tau_1 = \omega_0 t', \quad \varkappa = \frac{(\varepsilon_m + 1)\,\varepsilon_0\omega_0}{\sigma}, \quad \rho = \alpha^2\omega_0^2.$$

Then

$$E_2(t') = -\frac{i\omega_0\mu I_a\, dh}{2\pi r}\,|w(\sqrt{s_0 r})|\,V(\rho, \varkappa, \tau_1),$$
$$V(\rho, \varkappa, \tau_1) = -e^{i\varphi_{\text{sup}} - i\tau_1} + W(\rho, \varkappa, \tau_1). \qquad (22)$$

where $w(\sqrt{s_0 r})$ is the Sommerfeld attenuation function, φ_{sup} is its argument or the so-called supplementary phase at the carrier frequency ω_0:

$$
\begin{gathered}
W(\rho, \varkappa, \tau_1) = \frac{F(x)}{w(\sqrt{s_0 r})} \exp\left[-\chi(x)\frac{\tau_1^2}{4\rho}\right]\left\{-i\left[\frac{\tau_1}{2\rho} + \frac{\varkappa}{2\rho}u(x)\right]\right. \\
\left.\varphi(x)\left[1 + \psi(\rho, \varkappa, \tau_1)\, 2z_0 e^{-z_0^2}\int_{z_0}^{i\infty} e^{z^2}\,dz\right]\right\}; \\
x = \frac{\varkappa}{2\rho}\tau_1; \quad s_0 r = \frac{\rho}{1 - i\varkappa}; \quad \psi(\rho, \varkappa, \tau_1) = \left[1 + i\frac{\tau_1}{2\rho}K(x)\right]^{-1}; \\
K(x) = \frac{2}{\sqrt{1+2x}\,(1+\sqrt{1+2x})}; \quad z_0^2 = s_0 r + i\tau_1 - \chi(x)\frac{\tau_1^2}{4\rho}.
\end{gathered} \tag{23}
$$

Expression (23) for the nonstationary part of the field is valid if the inequality

$$\frac{\varkappa^2}{4\rho} \ll 1,$$

which is the consequence of inequality (21), is satisfied.

The real part of the function W (23) describes the nonstationary part of the radiation field, while the real part of the function V (22) describes the total field when the dipole is excited by a current of the form

$$I(t) = I_a \sin\omega_0 t \cdot 1(t). \tag{24}$$

The functions ImW and ImV describe the nonstationary part and the total radiation field, respectively, for a dipole current in the form

$$I(t) = I_a \cos\omega_0 t \cdot 1(t).$$

Plots of ReW and ImW for two values of $\varkappa$ ($\varkappa = 0$ and $\varkappa = 1$) are shown in Figures 4 and 5. It is seen from these plots that an account of the displacement currents reduces the amplitude of the nonstationary part of the field. Furthermore, the magnitude of the transient depends on the spectrum of the current and the dipole. The amplitude of the nonstationary part at large numerical distance for a sinusoidal current in the dipole, is much greater than the amplitude of the nonstationary part for a cosinusoidal current. Moreover, it can be shown that in the latter case the amplitude of the transients tends to zero as the numerical distance increases. The explanation for this is that at large numerical distances the transients are caused by the low-frequency part of the spectrum, while a cosinusoidal excitation is much poorer in low-frequency components than a sinusoidal one.

Plots of the function ReV, to which the total radiation field is proportional when the exciting current in the dipole is given by (24,) are shown in Figure 6 ($\varkappa = 0$). We see that the transients during the propagation lead to noticable distortion in the signal form.

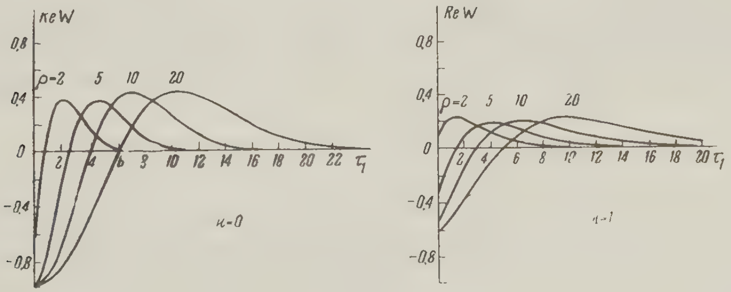

Figure 4. Plot of the function ReW.

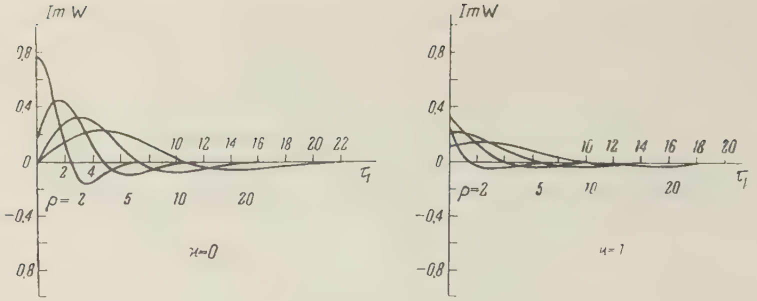

Figure 5. Plot of the function ImW.

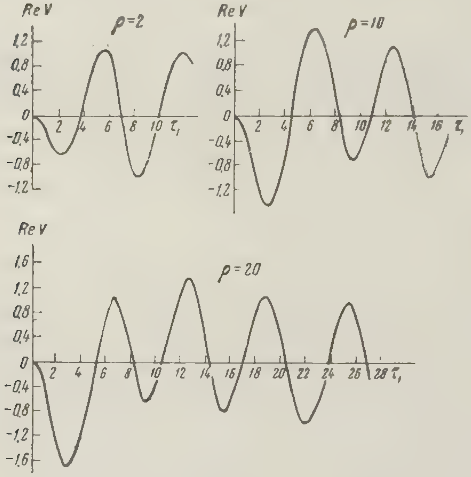

Figure 6. Plots of the function ReV.

CONCLUSION

The problem of propagation of pused signals over the earth's surface is not only of theoretical interest, but also of practical significance. For example, the question of the distortion of the wave form of propagating radio signals plays an important role in the study of atmospheric discharges. The results obtained can be used to solve the inverse diffraction problem (determination of the properties of the underlying surface from known distortions of a pulsed signal). Thus, by meansuring the delay time (relative to the front) of the maximum of a signal radiated by a diploe excited by a step function, we can determine the conductivity of the path from distance values determined by other measurements.

REFERENCES

1. J.R. Wait, Canad, J. Phys, 1956, 34, 27.
2. J.R. Johler, Geofis, pura e appl. 1957, 37, 116.
3. J.R. Johler, J. Res. Nat. Bur. Standards, 1958, 60, 281.
4. V.V Novikov, Propagation of a Radio Pulse Over a Flat Homogeneous Earth, Vestn. Leningr. univ, 1960, No.2, No. 10.
5. A.A. Kharkevich, Spectra and Analysis, GITTL, 1957.

A.A. Zhdanov Leningrad State University
Geophysics Department

Submitted to the editors 24 March 1960

INVESTIGATION OF A MODEL OF LARGE-SCALE IONOSPHERIC INHOMOGENEITIES BY A RADIO ASTRONOMICAL METHOD

Yu.L. Kokurin, A.N. Sukhanovskiy and Yu.I. Alekseyev

Results are reported of simultaneous measurements of irregular refraction of radio waves in the ionosphere at two zenith angles, $z \simeq 0 - 30°$ and $z \simeq 85°$. It is concluded that the irregular refraction is due to the presence of wavelike inhomogeneities in the ionosphere. The horizontal and vertical dimensions of the inhomogeneities are estimated.

INTRODUCTION

We have shown in an earlier paper [1] that oscillations in the refraction of radio waves passing through the entire thickness of the ionosphere are due to the presence in the ionosphere of inhomogeneities whose horizontal dimensions are on the order of hundreds of kilometers. One cannot draw any conclusion regarding the structure of the inhomogeneities (regarding their vertical cross section) from the results of this investigation, in which the irregular refraction was measured at one value of the zenith angle, $z \simeq 80°$. It was shown, however, that the data of the measurements can be fitted to two different models of inhomogeneities in the layer. According to one model, quasi-periodic variations of the optical thickness of the layer take place along the layer (model I, Figure 1a). In the second model the inhomogeneities have a wave-like structure (model II, Figure 1b).

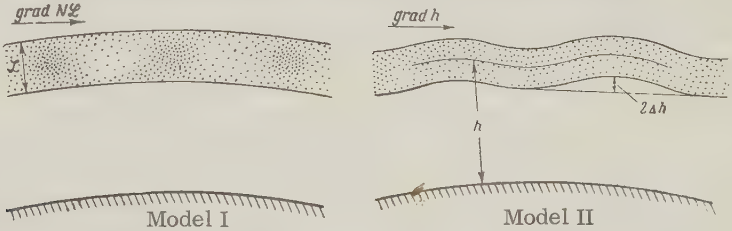

Model I
a

Model II
b

Figure 1. Two possible models of inhomogeneities of the ionosphere.

The data on the refraction oscillations at $z \simeq 80°$ were used to estimate the parameters of the inhomogeneities for these two models. In another paper [2] we gave approximate calculations of the dependence of the average refraction oscillation amplitude $\overline{(R_i)}_{max}$ on the zenith angle z, and have shown that the dependence is quite different for each of the two models. In particular, for the first model the amplitudes of the refraction oscillations at the zenith ($z \simeq 0 - 30°$) amounted to 15 — 20% of the corresponding value on the horizon ($z \simeq 80°$), whereas for the second model the amplitude of the oscillations at the zenith is close to zero (Figure 2).

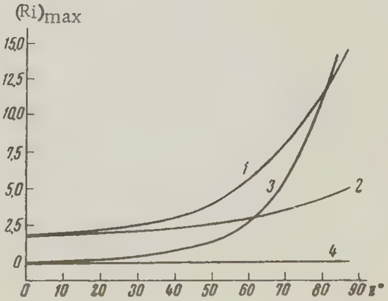

Figure 2. Dependence of irregular ionospheric refraction on the zenith angle, $\overline{(R_i)}_{max} = f(z)$:
1 — vertical refraction for Model I; 2 — horizontal refraction for Model I; 3 — radical refraction for Model II; 4 — horizontal refraction for Model II.

We can thus propose that the variation of the refraction oscillations with the zenith angle be used as a method for the investigation of the model of the ionospheric inhomogeneities, and that the first step in this direction be the measurement of the amplitudes of the refraction oscillations near the zenith, where the very presence or absence of oscillations can lead to definite conclusions.

In the present paper we report the results of measurements of the irregular ionospheric refraction made simultaneously at two zenith angles, $z \simeq 0 - 30°$ and $z \simeq 85°$.

1. MEASUREMENT OF OSCILLATIONS OF VERTICAL REFRACTION NEAR THE HORIZON

In the investigation of the vertical refraction, the radiation sources used were sunspots. The measurements were carried out by means of a vertical marine interferometer. The procedure used in such measurements is described in [1]. The main parameters of the interferometer were as follows: operating frequency $f = 207$ Mc ($\lambda = 1.45$ m); the height of the antenna above the surface of the sea was $H = 268.3$ m.

The antenna position at sea was such that when the elevation angle exceeded 12 — 13° the ray was reflected from the shore rather than from the surface of the sea. The interference pattern therefore covers the zenith-angle $z \simeq 77 - 90°$. The annual motion of the sun in the sky limits the period of observations, because in the summer months (unlike the winter months) the sun rises not from behind the sea, but from behind the land.

Thus, the interference curves could be plotted only approximately one hour after sunrise, or else an hour before sunset, and only in the winter months.

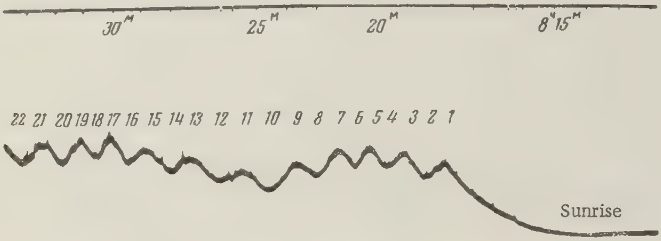

Figure 3. Specimen of interference record of the sunrise on 29 December 1958.

Figure 3 shows a sample recording of the sunrise on 29 December 1958. A simplified method, which does not call for knowledge of the coordinates of the radio-emitting sunspots, was used to plot the dependence of the vertical refraction on the zenith angle on the basis of such recordings. During the instants corresponding to the minima of the interference plot, the positions of which (z_m) were calculated from the well-known formulas of the diagram of the vertical interferometer (see reference [1]), we determined the directions to the source z'_m. The value of z'_m was taken to be the zenith angle of the center of the sun, the motion of which over this angle was assumed to be approximately uniform, with a velocity equal to the average velocity during the first hour after sunrise (or the last hour before sunset). The curves $R^r(z)$ obtained in this fashion differ from the exact curves in that they contain a term that varies smoothly along the z-axis and has a single extremum during the observation session. This excludes the possibility of determining the regular ionospheric refraction, but in practice it does not distort its oscillations. The period of the oscillation is much less than the duration of the session, so that the oscillations are observed as deviations from the course described above. This course is determined by averaging the plotted curves over a large number of observation sessions.

An investigation of the quiet sun as a whole does not yield an interference pattern, inasmu as its angular dimensions (about 30') are much greater than the angular width of the interferometer-diagram lobe, which is equal to about 8.7'. The only useful observations are therefore those made when radio-emitting spots of sufficiently small dimensions exist on the sun.

We have carried out a cycle of observations at 44° N latitude (Crimea) from 8 September 1958, through 20 April 1959 at sunrise and from 24 October 1958 through 1 March 1959 at sunset. A total of 213 sunrise records and 122 sunset records was obtained, of which 106 sunrise and 61 sunset records were suitable for processing. The remainder were cases when there were no radio-emitting sunspots. Typical curves of R^r vs. z for sunrises are shown in Figure 4. The sunset curves differ from the sunrise curves in having much smaller oscillation amplitudes and a lower probability of occurrence.

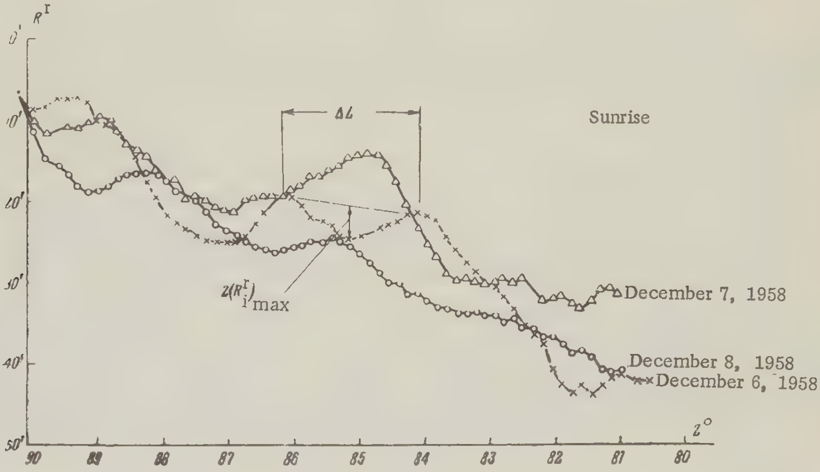

Figure 4. Specimens of curves of irregular vertical refraction $R_i^r(z)$ for sunrise hours.

Only the sunrise curves were subjected to further detailed processing. They were used to determine the principal parameters of large ionospheric inhomogeneities, by measuring the periods and amplitudes of the refraction oscillations. For each wave (cycle) of oscillations tangents were drawn to the curve $R^r(z)$ at two crests (or troughs) corresponding to the start and end of the cycle (see Figure 4) The distance between the tangency points was taken to be the period of the oscillations or the angular dimension of the inhomogeneity Δz (under the assumption that the inhomogeneity is stationary), and the half-height of the maximal rise (or drop) of the curve $R^r(z)$ above (below) the tangent was taken to be the amplitude of the refraction oscillations $(R_i^r)_{max}$. The angular dimensions of the inhomogeneities were then recalculated into linear dimensions d under the assumption that the inhomogeneities are located at a height $h_0 = 300$ km (see [1]). The values of d fluctuated from 100 to 500 km. The most probable value was $\overline{d} \simeq 200 - 220$ km. The amplitudes of the refraction oscillations, $(R_i^r)_{max}$, averaged over each session of observations, range essentially from 0.5 to 5.0' and have a most probable value $\overline{(R_i^r)}_{max} = 2.5 - 3.0'$.

Let us estimate, on the basis of these data, the parameters of the inhomogeneities in accordance with the above-described models of the inhomogeneous layer.

Model I. Assuming the linear dimension of the inhomogeneity to be $\overline{d} = 200$ km, the effective thickness of the inhomogenity $\mathscr{L} = 50$ km* and the refractive index to be $n = 0.9983$ ($N = 1.8 \times 10^6$ cm $^{-3}$), we obtain for the difference between the geometric and optical thickness of the inhomogeneity a value $L \simeq 80$m.

On the basis of equation (6) of reference [2], the variation of this difference is

$$\Delta L = \overline{(R_i^r)}_{max}\, d\, \frac{\left(1 - \frac{r_0}{r_0 + h_0} \sin z\right)^2}{2\pi} = 2{,}7 - 3{,}5\ \text{м} \qquad (1)$$

(r_0 is the radius of the earth). Hence $\Delta L/L = 3.3 - 4.4\%$

Thus, if the irregularities of the refraction are due to the presence of a horizontal gradient in the F layer, then the horizontal variation (with an average period of about 200 km) in the optical thickness of the large inhomogeneities and of the total number of electrons in them amounts to 3.3 —3.4%.

---

*See Section 3 concerning the choice of the effective-layer thickness.

Model II. Using the same inhomogeneity parameters ($\overline{d}$ = 200 km, l = 50 km, n = 0.9983) we obtain for the wavelike model, on the basis of equation (10) of reference [2],

$$\overline{\Delta h} = \frac{\overline{(R_i^r)}_{\max}\bar{d}^2\left[1-\left(\frac{r_0}{r_0+h_0}\sin z\right)^2\right]^{3/2}}{L(2\pi)^2\frac{r_0}{r_0+h_0}\sin z} = 0{,}45 - 0{,}54 \text{ km}, \tag{2}$$

Consequently, the observed oscillations of refraction can be ascribed to a wavelike structure of ionospheric inhomogeneities with a period $\overline{d} \simeq 200$ km and a wave amplitude (see Figure 1b) $\Delta h \simeq 0.5$ km.

2. MEASUREMENT OF OSCILLATIONS OF REFRACTION NEAR THE ZENITH

Measurement of the irregular refraction near the zenith was carried out with the aid of a horizontal interferometer. Since this was the first attempt at such measurements, and the method has many distinguishing features compared with the preceding method, we shall describe it in greater detail.

Large ionospheric irregularities are detected with the aid of a vertical interferometer because of the angular displacement of the radiating source. Actually, the zenith angle subtended during the time of one observation session amounts to 10 — 15° (from z = 90 to z = = 89 — 75°), corresponding to a linear distance of 800 — 1200 km along the layer. This means that if the average linear dimension of the inhomogeneities is about 200 km, some 4 — 6 refraction cycles are registered during one session. Consequently the vertical interferometer makes it possible to register stationary inhomogeneities in the ionosphere. When the inhomogeneities move at a velocity that is customary in the ionosphere, about 100 m/sec [3 — 5], the apparent changes in their linear dimensions are only about ± 30%, since these velocities are small compared with the rate of motion of the point of intersection of the beam with the layer (about 300 m/sec) due to the motion of the source. On the contrary, when extraterrestrial sources are observed near the zenith with the aid of a horizontal interferometer, the linear dimensions of the region of ionosphere subtended by the antenna directivity patterns (usually not more than 15 — 20°) do not exceed 100 — 130 km, that is, they are less than the average scales of the inhomogeneity of the layer. Thus, less than one cycle of refraction oscillation is recorded during one observation session, so that the amplitudes of these oscillations cannot be measured in the overwhelming majority of cases. The observation of large-scale ionospheric inhomogeneities with the aid of a horizontal interferometer is therefore possible only if these inhomogeneities move with sufficiently high speed.

It is known that the F-layer of the ionosphere is subject to drifts whose speeds, measured in many investigations (see, for example, [3 — 5]) by observation of small ionospheric inhomogeneities, average about 100m/sec. Information on the motion of large inhomogeneities is less plentiful. According to references [6 — 8], large-scale inhomogeneities observed by the method of pulsed sounding from the earth, move with velocities of 80 — 160 m/sec. However, it is not quite obvious that these are the same inhomogeneities responsible for the refraction oscillations. The rates of motion of large inhomogeneities were determined by radioastronomic methods only in one work [9]; there were found to be 150 — 300 m/sec.

To detect ionospheric inhomogeneities by their motion it is necessary to catch at least two or three cycles of refraction oscillations. At the inhomogeneity velocities indicated above, the necessary time required is 1.0 — 1.5 hours. The angular velocity of motion of the source near the zenith at our latitude (Crimea, 44° N) is about 15° per hour. This means that at a minimum possible session duration (one hour) the width of the diagram of each of the interferometer antennas, should not be less than 15°. We used for the measurements two parabolic antennas, with an east-west separation of about D = 520 m. The eastern antenna had a rectangular aperture 18 by 22 m, while the western one had a round aperture 30 m in diameter. Thus, the envelope of the interference pattern is determined by the western antenna. The angular dimension of its diagram is determined by the relation

$$\Theta = \frac{1{,}22\lambda}{d},$$

where d is the antenna diameter. Putting $\theta \simeq 15°$, we obtain for the minimum wavelength $\lambda \simeq 6$ m. Since an increase in wavelength reduces the accuracy with which the refraction curves are plotted (increases the period of the interference pattern), we used a working wavelength $\lambda = 5.8$ m.

Four cosmic sources with declinations $\delta = 12 - 58°$ were used for the observations. This interval is much greater than the aperture of the antenna diagrams. We therefore placed on each focal surface of the antenna two diploe-reflector arrays for the reception of signals from all four sources. The diagrams of these arrays were aimed at declinations $\delta_1 = 49°$ and $\delta_2 = 17°$ in such a way that each array received signals from two sources.

We have already mentioned that in measurements with a horizontal interferometer, the angular velocities of the sources are much less than the rate of angular displacement of the inhomogeneities due to the drift. One can, therefore, roughly assume the source to be stationary and the irregular refraction regarded not as a function of the zenith angle but as a function of the time.

To plot the time dependence of the irregular refraction R_i on the interference recordings, the positions of the interferometer diagram lobes were determined in time units, the reference point being the instant of culmination of each source.

The effect of irregular refraction on the interference curve manifests itself in a deviation of its lobes from their calculated positions. To simplify the processing, we took the calculated positions to be those determined by averaging over many sessions of observations of a given source. Then the irregular refraction at the instant of time t_n, expressed in time units, is defined as $\Delta t_n = t_n - \bar{t}_n$, where t_n is the instant corresponding to the n-th maximum of the recording; $\bar{t}_n$ is the averaged position of the n-th maximum of the interference recording. The angular magnitude of the irregular refraction is determined by simple recalculation for each source from the time magnitude

$$(R_i)_n = \Delta t_n k_\delta,$$

where k_δ is the conversion coefficient, which depends on the declination of the source.

This processing method, as in the determination of vertical refraction, does not permit investigation of the regular refraction, but only of the irregular components.

The observations were carried out during the period from 12 December 1958 through 1 June 1959 in Crimea (latitude of 44° N) using the cosmic sources listed in the table.

Source	Intensity at f = 52 mc in $w \cdot m^{-2}\ 10^{-23}$ cps	Coordinates		Period of Observation		Total number of sessions	Number of reduced recordings
		Declination	Direct ascension				
Cassiopeia - A	32	58°32′	$23^h21^m12^s$	27 IV 1959	— 1 VI 1959	25	17
Cygnus - A	20	40°36′	$19^h58^m13^s$	19 III 1959	— 1 VI 1959	65	50
Taurus - A	1,85	22°01′	$05^h31^m30^s$	12 XII 1958	— 1 VI 1959	151	60
Virgo - A	2,5	12°41′	$12^h28^m06^s$	16 XII 1958	— 1 VI 1959	145	67

For each analyzed session of observations, we plotted $R_i = f(t)$. Typical curves are shown in Figure 5. The time references chosen were the instants of culmination of the sources (indicated for each curve). The values of R_i are marked on the ordinates in angular minutes. A characteristic feature of all the curves is their irregular variation.

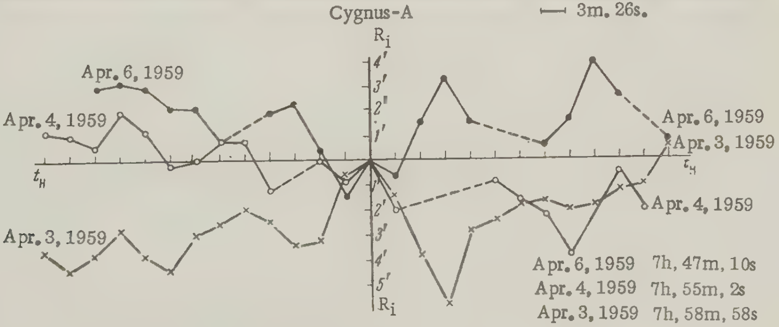

Figure 5. Specimens of curves of irregular refraction $R_i(t)$ for $z \simeq 0 - 30°$.

The irregularities can be grouped in two types: short-period and long-period. The irregularities of the former type are present in practically all curves and manifest themselves as random deviations in the values of R_i relative to the neighboring values. Consequently, the period of these deviations is less that $\overline{t_{n+1} - t_n}$. Their amplitude, averaged over all recordings, is approximately ±1.1. These deviations are not related to the large-scale ionospheric inhomogeneities. Analysis has shown that they may be due to the following factors: subjective errors in the determination of t_1 and $\overline{t}_n$ approximately ± 30"); distortion in the interference curve due to slight industrial and atmospheric interference (approximately ± 30"); small-scale inhomogeneities in the ionosphere (during the time of strong ionospheric disturbances, the angular deviations may reach several minutes of angle [10]).

In the presence of irregular refraction one observes during the time of one session, as a rule, several periods of oscillation (from 2 to 5) so that their average duration and amplitude over the session can be determined. The duration or the period of oscillation fluctuates from 5 to 37 minutes, and has a probable value of about 15 minutes. It is impossible to calculate the dimensions of large ionospheric inhomogeneities directly from this value, since this would necessitate simultaneous measurement of their velocities.

We use results of references [6 — 8] ($v = 80 - 160$ m/sec) to estimate the dimensions. Then the dimensions of the inhomogeneities in the direction of their motion amounts to $\overline{d}_v \simeq 70 - 140$ km. If we use the results of reference [9] ($v = 150 - 300$ m/sec), we get accordingly $\overline{d}_v \simeq 135 - 270$ km. Thus, it can be concluded that the dimensions of the observed inhomogeneities are 100 — 250 km.

The amplitude of the oscillations was determined in the same manner as in the measuremen of vertical refraction (Section 1). The most probable value of the amplitude of the oscillations in (R_i) max amounts to about 1.0', with a corresponding slight spread about this value.

3. COMPARISON OF MEASUREMENTS OF THE IRREGULAR REFRACTION NEAR THE ZENITH AND THE HORIZON

In the comparison of the results of measurement of the irregular refraction near the zenith and at the horizon, it is necessary to take into account the following circumstances. In view of the probable anisometry of the ionospheric inhomogeneities in the horizontal direction (see [11]) we can compare only parameters, such as scale and others, measured in the same direction relative to the four cardinal points. A horizontal interferometer with a base running from east to west and a vertical interferometer oriented to the sunrise or to the sunset make it possible to measure the oscillations of one and the same angular coordinate of the source, corresponding to the direction along the ionosphere approximately parallel to the east-west line. In this relation, the results of our measurements near the zenith are comparable with those made at the horizon.

Certain doubts can be raised concerning the fact that the regions of the ionosphere observed with our two interferometers are different, and are spaced some 1500 — 2000 km in the indicated direction along the F-layer. This circumstance is immaterial in a statistical comparison of the results, but must be taken into account in a detailed comparison of the individual observation sessions. In the last case the comparison was carried out in two ways; a) for simultaneous sessions and b) for sessions spaced by the time required for the earth to turn an angle corresponding to a distance of 1500 — 2000 km along the F-layer.

As shown in Section 1, the magnitude of the irregular refraction at $z \simeq 85°$ and $\lambda = 1.45$ m amounts to $(\overline{R_i^f})_{max}$ 2.5 — 3.0'. This value pertains to the morning hours. The value of $(R_i^f)_{max}$ corresponding to this magnitude, for $\lambda = 5.8$ m and $z \simeq 85°$, calculated from the quadratic dependence of the irregular refraction on the wavelength ($R_i \simeq \lambda^2$) is $(\overline{R_i^f})_{max} \sim$ 40 — 48'. Furthermore, using the curves of Figure 2 we obtain for $\lambda = 5.8$ m at $z \simeq 0 - 30°$ the values $(\overline{R_i})_{max} = 6.7 - 8.0'$ for model I and $(\overline{R_i})_{max} \simeq 0$ for model II. To compare these expected values with the experimental value of the irregular refraction at $z \simeq 0 - 30°$ and $\lambda = 5.8$ m, the latter was determined also for the morning hours. It was found to be $(\overline{R_i})$ max $\simeq 0.9'$. This value differs greatly from that expected for model I, but is close to that expected for model II.

An analogous comparison of the irregular refraction at the horizon and in the zenith was made for individual observation sessions by the two methods described above. It was found that the ratios of the values of the irregular refraction at the horizon to those in the zenith were in most cases the same as the ratios of their probably values. In many cases the presence of irregular refraction at the horizon was accompanied by an absence of refraction in the zenith. On the basis of the foregoing, it is natural to conclude that the large-scale irregularities of the ionosphere have a wavelike structure (model II) and there are no considerable gradients in the total number of electrons along the layer.

It must be emphasized that the calculation of the curves of Figure 2, which serve as the basis for the comparison of the results, was made under the assumption that the inhomogeneities are not thick ($\mathscr{L} \leqslant 100$ km). Let us present some ideas concerning the value of $\mathscr{L}$. To estimate $\overline{\Delta h}$, we chose an effective inhomogeneity thickness $\mathscr{L} = 50$ km and an effective electron concentration $N = 1.8 \times 10^6$ cm^{-3}. Then the total number of electrons in a vertical inhomogeneity column of 1 cm^2 cross section is $\int N dh = N\mathscr{L} = 9 \times 10^{12}$. This corresponds to $\overline{\Delta h} \simeq 0.5$ km, which is approximately in agreement with data of other investigations, in which periodic variations of the height of the signal-reflection level associated with large ionospheric irregularities were measured (by soundings from the earth): according to [7 — 8], $\overline{\Delta h} \simeq 0.25 - 5.0$ km; according to [6,12] the value of $\overline{\Delta h}$, calculated from the angles of inclination of the reflection level (1 — 2°) and from the horizontal scale of the inhomogeneities amounts to 1 — 2 km. Thus, the value which we obtained may be somewhat underestimated, and we must therefore assume $\overline{\Delta h} \gtrsim 0.5$ km. According to equation (2) we have $\Delta h \sim 1/L$, where $L = \mathscr{L}\, Ne^2/2\pi m f^2$ is the difference between the geometrical and optical thicknesses of the inhomogeneity. Since the quantity $N\mathscr{L}$ is connected with $\overline{\Delta h}$ by the reciprocal relationship $N\mathscr{L} \sim 1/\overline{\Delta h}$, we must, taking the foregoing estimate of $\overline{\Delta h}$ into account, assume that $N\mathscr{L} \lesssim 9 \cdot 10^{12}$. Results of rocket investigations give for $N\mathscr{L}$, taken over the entire ionosphere, a value similar to $\gtrsim 5 \cdot 10^{13}$. According to reference [13], $N \simeq 1.8 \cdot 10^6$ cm^{-3} and $\mathscr{L} \geqslant 350$ km; reference [14] cites $N \simeq 1.8 \cdot 10^6$ cm^{-3} and $\mathscr{L} \simeq 400$ km.

It is seen from the foregoing data that the value of $N\mathscr{L}$ for the inhomogeneities is one-fifth that for the entire layer or less. It must be assumed that the wavelike part of the layer is the one with the highest density, near the ionization maximum, since wavelike inhomogeneities have been observed from sounding from the earth.* In this case, the effective thickness $\mathscr{L} = 50$ km which we have assumed for the inhomogeneities may be somewhat too high, but is apparently close to the actual value.

Thus, the results obtained in the present investigation allow us to make the following basic conclusions. The large-scale ionospheric inhomogeneities are wavelike formations (Figure 1d, model II) with average horizontal scale ("period") $d \simeq 250$ km and a wave amplitude $\Delta h \geqslant 0.5$ km. Only a portion of the layer with insignificant effective thickness. less than 20% of the total effective thickness, is wavelike . Apparently this part is located near the region of maximum electron concentration and a geometric thickness $\sim \leqslant 50$ км

REFERENCES

1. V.V. Vitkevich, Yu.L. Kokurin, Radiotekhnika i elektronika, 1957, 2, 7, 826.
2. Yu.L. Kokurin, Radiotekhnika i elektronika, 1959, 4, 12, 1985.
3. Yu. L. Kokurin, Drifts and Inhomogeneities in the Ionosphere. Article collection No. 1 on Section V of the IGY Program, Published by the Academy of Sciences, USSR, 1959, page 60.
4. A. Hewish, Proc. Roy. Soc., 1952, 214A, 494.
5. J.P. Wild, J.A. Roberts, J. Atmos. and Terr. Phys, 1956, 8, 55.
6. V.D. Gusev, L.A. Drachev, S.F Mirkotan, Yu.V. Berezin, M.P. Kiyanovskiy, M.V. Vinogradova, T.A. Gailit, Doklady AN SSSR, 1958, 123, 817.
7. G. N. Munro, Proc. Roy. Soc., 1950, 202, 208.
8. E.N. Bramley, Proc, Roy. Soc., 1953, 220, 39.
9. B.M. Chikhachev, Radiotekhnika i elektronika, 1960, 5, 9, 1359.
10. V.V. Vitkevich, Yu.L. Kokurin, Radiotekhnika i elektronika, 1958, 3, 11, 1373.
11. V.D. Gusev, S.F. Mirkotan, L.A. Crachev, Yu.V. Berezin, M.P. Kiyanovskiy, Drift and Inhomogeneities in the Ionosphere, Collection No. 1 of Articles on Section V of the IGY Program, Published by the Academy of Sciences USSR, 1959, page 7.
12. L.A. Drachev, Yu.V. Berezin, Radiotekhnika i elektronkia, 1957, 2, 10, 1234.
13. K.I. Gringauz, Artificial Earth Satellite , AN SSSR, 1958, 1, 62.

---

*The effective height of the inhomogeneities, determined approximately in [1], amounted to about 350 km.

14. Ya. L. Al'pert, E.F. Chudesenko, B.S. Shapiro, Preliminary Results of Scientific Researches with the Aid of the First Soviet Artificial Satellites and Rockets, Collection of Articles No. 1 on Section XI of the IGY Program, published by AN SSSR, 1959, page 40.

P.N. Lebedev Physics Institute,
Academy of Sciences, USSR

Submitted to the editor, 4 April 1960

STRUCTURE OF ELECTROMAGNETIC FIELD OF DIRECTIONAL ANTENNAS ABOVE A FLAT EARTH WITH FINITE CONDUCTIVITY

G.N. Krylov

Methods are considered for the calculation of the electromagnetic field components of a vertical electric dipole and of a vertical antenna with sinusoidal current distribution, subject to the condition that the boundary condition to be satisfied on the earth's surface is of the surface-impedance type. A rigorous solution is obtained for the Hertz vector as well as an expression for the electromagnetic field components of the dipole and of the antenna in space. For an exact calculation of the electromagnetic field components, it is necessary to evaluate two integrals, for which convergent and asymptotic expansions are given. It is pointed out that these integrals can be approximately calculated in terms of the Sommerfeld attenuation factor. To calculate the components of the electromagnetic field of the antenna, it is sufficient to determine the electromagnetic field of two dipoles with specified amplitude and phase, located on the ends of the antenna, and to add to this expression a certain term that accounts for the distribution of the current along the antenna; this term is expressed with the aid of trigonometric functions.

Antennas radiating in the direction of the earth's surface are extensively used at the present time and are of particular importance in the medium and long-wave bands, where optimum signal reception at large distance must be ensured with the aid of the direct wave, without reflection from the ionosphere. One of the main factors distorting the structure of the electromagnetic field of the direct wave, compared with the field of an analogous radiator in free space, is the finite conductivity of the earth.

It is possible to account for the finite conductivity of the earth by various methods, widely used among which are approximate methods of solution with the use of boundary conditions of the surface-impedance type. In this case the Hertz vector must satisfy the following boundary condition on the earth's surface:

$$\frac{\partial \pi_z}{\partial z} = -ik\delta\pi_z . \qquad (1)$$

The use of boundary conditions of the surface-impedance type allows us to disregard the electromagnetic field in the lower medium, and to account for it approximately by introducing the constant δ. This method can be applied both in the case of a homogeneous earth, and in the case of a stratified earth, or even in the case of an earth having arbitrary electric properties that vary with depth, provided the quantity δ is assigned suitable values. The question of the choice of the value of δ has already been considered in the literature, [1], [2] and we shall consider this quantity to be known.

We proceed to find a rigorous solution of this problem and to a derivation of the final equations, without introducing any additional restrictions whatever. We assume that the Hertz vector is the sum of the "incident" field and of the field "reflected" from the earth's surface

$$\pi_z^0 = \int\limits_{-\infty}^{\infty} H_0(\lambda\rho) e^{-n|h-z'|} \frac{\lambda d\lambda}{n}; \qquad \pi_z' = \int\limits_{-\infty}^{\infty} H_0(\lambda\rho)\, e^{-nz} R(\lambda)\, \lambda d\lambda; \qquad \pi_z = \pi_z^0 + \pi_z';$$

$$n = \sqrt{\lambda^2 - k^2}; \quad \operatorname{Re} n \geqslant 0; \quad z = z' + h, \tag{2}$$

where ρ is the distance from the dipole to the receiver along the earth's surface, h is the height of the dipole above the earth's surface, z' is the height of the point of observation above the earth's surface, and k is the wave number in air.

To determine the unknown function R(λ) it is necessary to use boundary condition

$$n[1 - nR(\lambda)] = -ik\delta[1 + nR(\lambda)], \quad R(\lambda) = \frac{n + ik\delta}{n(n - ik\delta)},$$

from which we obtain the rigorous solution of our boundary value problem in the form

$$\pi_z = \frac{e^{ikR_1}}{R_1} - \frac{e^{ikR}}{R} + 2I; \quad I = \frac{1}{2} \int\limits_{-\infty}^{\infty} \frac{H_0(\lambda\rho)\, e^{-nz}}{n - ik\delta} \lambda\, d\lambda, \tag{3}$$

where

$$R = \sqrt{\rho^2 + z^2}; \quad R_1 = \sqrt{\rho^2 + (z' - h)^2}.$$

After differentiation we can determine the components of the electromagnetic field of a vertical electric dipole

$$E_z = k^2(1 + D_z^2)\pi_z; \quad E_\rho = k^2 D_{z\rho}^2 \pi_z; \quad H_\varphi = \frac{ik^2}{\omega\mu} D_\rho \pi_z, \tag{4}$$

where

$$D_z = \frac{d}{d(kz')}; \quad D_\rho = \frac{d}{d(k\rho)}.$$

To differentiate the integral I with respect to z', we can use the following relations

$$D_z I = D_z \frac{e^{ikR}}{R} - ik\delta I; \quad U = D_\rho I, \tag{5}$$

which are obtained after differentiation under the integral sign and after carrying out an identity transformation.

Let us proceed now to a determination of the components of the electromagnetic field of a vertical antenna, located from $h = h_1$ to $h = h_2$, the current in which is sinusoidally distributed, $j = kj_0 \sin\varphi$, where $\varphi = kn + b$ (b is a certain phase constant). In this case the Hertz vector and the components of the electromagnetic field of such an antenna can be obtained in the form

$$\pi_z^a = \int\limits_{h_1}^{h_2} \pi_z \sin\varphi\, dh; \tag{6}$$

$$E_z^a = k^2(1 + D_z^2)\pi_z^a; \quad E_\rho^a = k^2 D_{z\rho}^2 \pi_z^a; \quad H_\varphi^a = \frac{ik^2}{\omega\mu} D_\rho \pi_z^a. \tag{7}$$

The Hertz vector obtained for the vertical antenna can be expressed in form of definite integrals, which are not taken in terms of elementary functions and which do not reduce to the previously derived integral I and U. However, after the differentiation required to change to the components of the electromagnetic field, we can express these components in terms of elementary functions and of the integrals I and U. For this purpose we first integrate over the height of the antenna and change over to the components of the electromagnetic field in the terms outside the integrals in the expression (3) for the Hertz vector.

If we change to the vertical component of the electric field E_z^a in the terms under the integral sign, carry out differentiation under the integral sign, and then integrate twice by parts, the integrals cancel out, and we obtain

$$k(1 + D_z^2) \int\limits_{h_1}^{h_2} \sin\varphi \frac{e^{ikR_1}}{R_1} dh = -\left[\cos\varphi - \sin\varphi \frac{d}{kdh}\right] \frac{e^{ikR_1}}{R_1} \Bigg|_{h_1}^{h_2}, \tag{8}$$

$$k(1 + D_z^2) \int_{h_1}^{h_2} \sin\varphi \frac{e^{ikR}}{R} dh = -\left[\cos\varphi - \sin\varphi \frac{d}{kdh}\right] \frac{e^{ikR}}{R} \Bigg|_{h_1}^{h_2}. \tag{9}$$

On going to the horizontal component of the electric and magnetic fields, it is necessary to make a change of variable in these integrals [$R \pm (z' + h) = \mu$ or $R_1 \pm (z' - h) = \mu$], after which the parameter ρ will enter only into the integration limits and the differentiation with respect to ρ will give an expression in terms of elementary functions:

$$kD_\rho \int_{h_1}^{h_2} \sin\varphi \frac{e^{ikR_1}}{R_1} dh = -i\left[\cos\varphi - \sin\varphi \frac{d}{kdh}\right] \frac{e^{ikR_1}}{\rho} \Bigg|_{h_1}^{h_2}, \tag{10}$$

$$kD_\rho \int_{h_1}^{h_2} \sin\varphi \frac{e^{ikR}}{R} dh = -i\left[\cos\varphi - \sin\varphi \frac{d}{kdh}\right] \frac{e^{ikR}}{\rho} \Bigg|_{h_1}^{h_2}. \tag{11}$$

Let us now proceed to a determination of that part of the components of the electromagnetic field, which correspond to integration of the integral I over the height of the antenna, and let us carry out the integration under the integral sign. If we then carry out the operation $1 + D_z^2$, also under the integral sign, we arrive at the sought-after representation for the determination of the vertical component of the electric field of the antenna:

$$k(1 + D_z^2) \int_{h_1}^{h_2} I \sin\varphi \, dh = -\left[\cos\varphi - \sin\varphi \frac{d}{kdh}\right] I \Big|_{h_1}^{h_2}. \tag{12}$$

To determine the horizontal component of the electric and magnetic field, it is necessary, after integrating over the height of the antenna, to transform the integrand and to expand it into simple fractions, and then use the identity

$$kD_\rho \int_{-\infty}^{\infty} \frac{H_0(\lambda\rho)}{\lambda^2} e^{-nz} \lambda \, d\lambda = -2iD_z \frac{e^{ikR}}{\rho}, \tag{13}$$

Hence

$$\begin{aligned} kD_\rho \int_{h_1}^{h_2} \sin\varphi I \, dh = -\delta' \Big\{ &(\cos\varphi + i\delta \sin\varphi) U - \\ &- i[\sin\varphi (1 + i\delta D_z) + \cos\varphi (D_z - i\delta)] D_z \frac{e^{ikR}}{\rho} \Big\} \Bigg|_{h_1}^{h_2} \end{aligned} \tag{14}$$

and

$$\begin{aligned} kD_{\rho z}^2 \int_{h_1}^{h_2} \sin\varphi I \, dh = \delta' \Big\{ &(\cos\varphi + i\delta \sin\varphi) i\delta U + \\ &+ i[\sin\varphi (D_z - i\delta) - \cos\varphi (1 + i\delta D_z)] D_z \frac{e^{ikR}}{\rho} \Big\} \Bigg|_{h_1}^{h_2}, \end{aligned} \tag{15}$$

where $\delta' = 1/(1 - \delta^2)$.

We have obtained all the expressions necessary to represent the components of the electromagnetic field of the dipole and the antenna. To calculate the components of the electromagnetic field of the dipole we can use the following expressions:

$$E_z = k^2 \left\{ (1 + D_z^2) \frac{e^{ikR_1}}{R_1} - (1 - D_z^2 + 2i\delta D_z) \frac{e^{ikR}}{R} + (1 - \delta^2) 2I \right\}, \tag{16}$$

$$E_\rho = k^2 \left\{ D_{z\rho}^2 \left[\frac{e^{ikR_1}}{R_1} + \frac{e^{ikR}}{R} \right] - 2i\delta U \right\}, \tag{17}$$

$$H_\varphi = \frac{ik^2}{\omega\mu}\left\{D_\rho\left[\frac{e^{ikR_1}}{R_1} - \frac{e^{ikR}}{R}\right] + 2U\right\}. \tag{18}$$

Analogous expressions are obtained also for the components of the electromagnetic field of a vertical antenna:

$$E_z^a = k^2 j_0\left\{(\cos\varphi + \sin\varphi D_z)\left[\frac{e^{ikR}}{R} - \frac{e^{ikR_1}}{R_1}\right] - (\cos\varphi + i\delta\sin\varphi)\,2I\right\}\Bigg|_{h_1}^{h_2}, \tag{19}$$

$$\begin{aligned} E_\rho^a = k^2 j_0 \Big\{ &- i(\cos\varphi + \sin\varphi\, D_z) D_z \frac{e^{ikR_1}}{\rho} + \delta_0'(\cos\varphi + i\delta\sin\varphi)U + \\ &+ i[\sin\varphi(\delta_0 D_z - \delta_0') - \cos\varphi(\delta_0 + \delta_0' D_z)]\, D_z \frac{e^{ikR}}{\rho}\Big\}\Bigg|_{h_1}^{h_2}, \end{aligned} \tag{20}$$

$$\begin{aligned} H_\varphi^a = \frac{ik^2}{\omega\mu} j_0 \Big\{ &- i(\cos\varphi + \sin\varphi\, D_z)\frac{e^{ikR_1}}{\rho} - 2\delta'(\cos\varphi + i\delta\sin\varphi)U + \\ &+ i[\cos\varphi(1 - \delta_0' D_z + 2\delta' D_z^2) + \sin\varphi(\delta_0 + \delta_0' D_z)\, D_z]\frac{e^{ikR}}{\rho}\Big\}\Bigg|_{h_1}^{h_2}, \end{aligned} \tag{21}$$

where $\delta = \delta'(1 + \delta^2)$; $\delta_0' = 2i\delta\delta'$.

It is easy to note that the components of the electromagnetic field of the antenna can be directly expressed with the aid of the components of the electromagnetic field of the dipole. For this purpose it is sufficient to express the integrals I and U in expressions (16) —(18) in terms of E_z, E_ρ, and H_φ, and to substitute them in lieu of I and U in the expressions (19) — (21). After making these substitutions, we obtain

$$\begin{aligned} E_z^a &= j_0(A_1E_z + B_1)\big|_{h_1}^{h_2}, \\ E_\rho^a &= j_0(A_2E_\rho + B_2)\big|_{h_1}^{h_2} = j_0(A_3H_\varphi + B_3)\big|_{h_1}^{h_2}, \\ H_\varphi^a &= j_0(A_4E_\rho + B_4)\big|_{h_1}^{h_2} = j_0(A_5H_\varphi + B_5)\big|_{h}^{h_2}, \end{aligned} \tag{22}$$

where the coefficients A_i and B_i are expressed in terms of trigonometric functions.

Thus, we can reach the conclusion that in order to determine the components of the electromagnetic field of a vertical antenna it is sufficient to examine the radiation of two dipoles, located at the ends of the antenna, the amplitudes and phases of which are determined by the coefficients A_i, and to add the term corresponding to the members outside the integral signs and expressed by means of elementary functions.

The author has previously obtained convergent and asymptotic expansions for the calculation of the integrals I and U in the case of an earth with arbitrary electric properties, the argument δ can change over a broader range than in the case of a homogeneous earth, and this leads sometimes to the appearance of an additional term in the asymptotic expansion (the Stokes phenomenon). It can be shown that in the case of a homogeneous earth this additional term is always absent. Therefore it is useful to cite in the present paper (without proof) convergent and asymptotic expansions for these integrals with allowance for the notation introduced here.

To calculate the integrals I and U for "small" values of the initial parameters, we employ the convergent expansions

$$I = \frac{e^{ikR}}{R} + k\sum_{n=0}^{\infty} B_n; \quad U = D_\rho \frac{e^{ikR}}{R} + k\sum_{n=0}^{\infty} C_n. \tag{23}$$

where the coefficients B_n and C_n are conducted by the recurrence relations

$$\begin{aligned} B_{n+2} &= \frac{n\delta^2}{n+2}B_n - \frac{(k\rho\delta^2)^2}{n(n+2)}B_{n-2} + M_n[ikR(n+1) + (kz)^2], \\ C_{n+2} &= \frac{n\delta^2}{n+2}C_n - \frac{(k\rho\delta)^2}{n(n+2)}C_{n-2} - \frac{2k\rho\delta^4}{n(n+2)}B_{n-2} + \end{aligned} \tag{24}$$

$$+ i\left[(ikR+1)(n+1)+(kz)^2\right]\frac{\rho}{R} M_n,$$

$$M_n = \frac{i\delta^4 (ik\delta z)^{n-1}}{(n+2)!} e^{ikR - ik\delta z}. \tag{25}$$

The initial terms of these recurrence relations can be represented in the form

$$B_0 = i\delta\alpha(kz;\ k\rho)e^{-ik\delta z}, \quad C_0 = \left(i - \frac{1}{kR}\right)\frac{z}{\delta\rho}B_1 - \frac{2}{k\rho\delta^2}B_2,$$

$$B_1 = -i\delta^2 e^{ikR - ik\delta z}, \quad C_1 = i\frac{\rho}{R}B_1, \tag{26}$$

$$B_2 = -\frac{i\delta^3}{2}\beta(kz;\ k\rho)e^{-ik\delta z}, \quad C_2 = \frac{k\rho\delta^2}{2}B_0 - \frac{\delta k\rho z}{2R}B_1,$$

$$B_3 = -\frac{\delta^2}{6}\left[2ikR - 2 + (kz)^2\right]B_1, \quad C_3 = i\frac{\rho}{R}B_3 - \frac{i\delta^2\rho}{3R}B_1.$$

The calculation of the coefficients α and β is considered in reference [13].

For "large" values of the initial parameters, it is necessary to change over from an evaluation with the aid of asymptotic expansions, but the forms of the asymptotic expansions depend appreciably on the argument δ. The initial expression for a derivation of an asymtotic expansion is the representation of the integral I in the form

$$I = \frac{e^{ikR}}{R} + ik\delta e^{-ik\delta z}\int\limits_{k(R+\delta z)}^{i\infty}\frac{e^{iU}dU}{\sqrt{U^2 - k^2\rho^2(1-\delta^2)}},$$

and an asymptotic expansion (by the method of steepest descent) can be obtained, for example, by integration by parts. The steepest-descent path will in this case be a line drawn from the point $y_1 = k(R + \delta z)$ to $i\infty$ parallel to the imaginary axis, and the form of the asymptotic expansion depends on the position of the branch point relative to this line. Two essentially different cases are possible, depending on which of the inequalities $\operatorname{Re} k\left[R + \delta z - \rho\sqrt{1-\delta^2}\right] \gtrless 0$ is satisfied (Figure 1). It is convenient here to make the cuts on the complex plane of the variable U parallel to the imaginary axis.

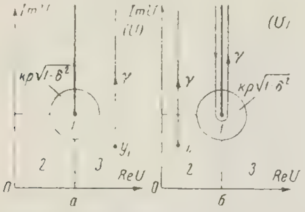

Figure 1. Position of contour of integration as a function of the magnitude of the surface impedance. 1 — region of applicability of convergent expansion; 2 — region of applicability of asymptotic expansion with separated supplementary term; 3 — region of applicability of asymptotic expansions without separation of the supplementary term.

If the inequality $\operatorname{Re} k\left[R + \delta z - \rho\sqrt{1-\delta^2}\right] > 0$ is satisfied, the steepest-descent path passes to the right of the cut, and integrating by parts we obtain for the integrals I and U the asymptotic expansions (Figure 1a).

$$I = kI', \ U = kU', \tag{27}$$

$$I' \sim e^{ikR} y_2 \left(\frac{z}{R} - \delta\sum_{n=1}^{\infty} V_n\right), \tag{28}$$

$$U' \sim (i - \delta y_2)\frac{\rho}{R}I' - \frac{\rho z y_2}{kR^3}e^{ikR} - \frac{\delta\rho y_2}{R}e^{ikR}\sum_{n=1}^{\infty} W_n, \tag{29}$$

where the coefficients V_n and W_n are connected by the recurrence relations

$$V_n = \left[-iy_1(2n-1)V_{n-1} + (n-1)^2 V_{n-2}\right]y_2^2,$$

$$W_n = \left[-iy_1(2n-1)W_{n-1} + (n-1)^2 W_{n-2} - i(2n-1)V_{n-2}\right]y_2^2 - 2\delta y_2 V_n \tag{30}$$

The initial terms of the relations are in this case equal to

$$V_1 = -iy_2^2 y_1, \quad W_1 = iy_2^2(2\delta y_2 y_1 - 1),$$

$$V_2 = 3V_1^2 + y_2^2, \quad W_2 = 6V_1W_1 - 2\delta y_2^3, \qquad y_3 = k(\delta R + z), \ y_2 = y_3^{-1}. \tag{31}$$

However, if the opposite inequality $\operatorname{Re} k[R + \delta z - \rho\sqrt{1-\delta^2}] < 0$ is satisfied, the steepest-descent path passes to the left of the cut and deformation of the initial contour of integration is therefore, necessary, as shown in Figure 1b; this leads to an additional term, corresponding to the integral along the cut. The integral along this cut can be readily calculated and is equal exactly to the surface wave obtained by Sommerfeld

$$\begin{aligned} I &= kI' - 2k\delta\pi e^{-ik\delta z} H_0(k\rho\sqrt{1-\delta^2}), \\ U &= kU' + 2k\delta\pi\sqrt{1-\delta^2}\, e^{-ik\delta z} H_1(k\rho\sqrt{1-\delta^2}). \end{aligned} \tag{32}$$

The question may arise of which of the foregoing asymptotic expansions can be used when $\operatorname{Re} k(R + \delta z - \rho\sqrt{1-\delta^2}) = 0$, since in this case an additional term appears in the asymptotic expansion. It is found that in this case both asymptotic expansions are valid, since $\operatorname{Im} k(R + \delta z - \rho\sqrt{1-\delta^2}) \gg 1$, that is, the exponential factor under the integral sign is sufficiently small near the branch point, and the magnitude of the additional term in the asymptotic expansion is of the same order as the error in the asymptotic expansion itself. If it is found that $\operatorname{Im} k(R + \delta z - \rho\sqrt{1-\delta^2}) \sim 1$ and the additional term is sufficiently large, corresponding to the case when the lower limit of integration is close to the branch point, we cannot use the asymptotic expansion, but must use the previously obtained convergent expansion.

Thus, if the inequality $\operatorname{Re} k(R + \delta z - \rho\sqrt{1-\delta^2}) < 0$ is satisfied, an additional term appears in the asymptotic expansion, corresponding in form to the Zenneck surface wave. The phase velocity of such a wave is always less than the velocity of light, since the inequality $\operatorname{Re}\sqrt{1-\delta^2} > 1$ is satisfied. Another important property of such a wave is that, if it exists at all, it is only in a limited region of space, since as the parameter z increases the inequality $\operatorname{Re} k(R + \delta z - \rho\sqrt{1-\delta^2}) < 0$ is no longer satisfied, , that is, such a wave "exists" only near the earth's surface. As is well known, the separation of the term corresponding to the Zennec surface wave is independent of the parameter z and, as has been shown by several authors (see, for example, [4]), this term does not satisfy the radiation condition. In our case, if the source or point of observation is raised above the earth's surface, the need for separating this term drops out, and consequently, its separation has nothing in common with the Zenneck surface wave.

To calculate the integrals I and U, we can use also the approximate expressions of the attenuation-factor type, as is done in reference [5],

$$I = \frac{e^{ikR}}{R}\left[1 + 2\sqrt{s_0}\, e^{-s}\int_{\sqrt{s}}^{i\infty} e^{x^2}\,dx\right]; \quad U = \left(i - \frac{1}{kR}\right)\frac{\rho}{R} I, \tag{33}$$

where

$$s_0 = \frac{ik\delta^2 R}{2}\left(\frac{R}{\rho}\right)^2; \quad s = s_0\left(1 + \frac{z}{\delta R}\right)^2.$$

However, using the attenuation factor, it is necessary to bear in mind that the asymptotic expansion will have a different form, depending on the sign of the imaginary part of s

$$I \sim \frac{e^{ikR}}{R}\left[1 - \sqrt{\frac{s_0}{s}}\sum_{n=0}^{\infty}\frac{(2n-1)!!}{(2s)^n}\right], \quad \operatorname{Im}\sqrt{s} > 0 \tag{34}$$

and

$$I \sim \frac{e^{ikR}}{R}\left[1 - \sqrt{\frac{s_0}{s}}\sum_{n=0}^{\infty}\frac{(2n-1)!!}{(2s)^n} + 2i\sqrt{\pi s_0}\, e^{-s}\right], \quad \operatorname{Im}\sqrt{s} < 0. \tag{35}$$

The exact expansion for this integral does not depend on the imaginary part of s; it is given in [5].

In conclusion, the author considers it his pleasant duty to thank G.I. Makarov for interest in the work and for much useful advice.

REFERENCES

1. A.D. Petrovskiy, E.L. Feynberg, On the Approximate Boundary Condition in the Theory

of Propagation of Radio Waves Along the Earth, Radiotekhnika i elektronika, 1960, 5, 3, 385.
2. J.R. Wait. Transmission and reflection of electromagnetic waves in the presence of stratified media, J.Res. Nat. Bur. Standards, 1958, 61, 3, 205.
3. G.N. Krylov, G.I. Makarov, Structure of the Electromagnetic Field of a Vertical Electric Dipole and a Vertical Antenna in Space Above a Flat Earth, Vestn. Leningr. univ. 1960, 16, 42.
4. T. Kahan, G. Eckart, On the existence of a surface wave in dipole radiation over a plane earth, Proc. I.R.E., 1950, 38, 7, 807.
5. G.N. Krylov, G.I. Makarov, Attenuation function of the electromagnetic field of a vertical dipole and a vertical antenna, Radiotekhnika i elektronika, 1960, 5, 4, 684.

A.A. Zhdanov Leningrad State University
Physics Faculty

Submitted to the editors May 30, 1960

A METHOD OF CALCULATION OF CHARACTERISTIC MODES AND DISPERSION IN STRAIGHT AND BENT WAVEGUIDES OF COMPLEX CROSS SECTION

A. Ya. Yashkin

A method permitting separation of variables is described for the integration of a wave function in a complex step region, in which the steps are formed by closely-spaced coordinate surfaces of a certain orthogonal system. It is shown that for an N-step region integration of the wave equation is reduced to a solution of a system of N-1 homogeneous integral equations. As an example, this method is applied to stepped waveguides in a circular-cylindrical coordinate system. To a first approximation, the characteristic modes and dispersion are obtained for straight and bent waveguides.

INTRODUCTION

In all problems of waveguides having a complex cross section, the main difficulties are connected with the necessity of a transition from a formal solution to a form which allows us to carry out numerical calculations. In the simplest cases, when the complex region can be represented by two simple regions, the problem is easily solved. [1,2,3]. The author proposed a method for the calculation of straight waveguides having a complex cross section in a Cartesian coordinate system [4,5], based on the representation of a complex cross section in the form of a set of N simple (rectangular) regions. A generalization of this method enables us to make a similar calculation in an arbitrary orthogonal system permitting separation of variables. Proceeding further to a calculation of the critical frequency and propagation constant, we note that the determination of these parameters is related to the calculation in a complex region of the characteristic modes of the wave equation, soluble under specific boundary conditions.

According to the perturbation method [6], insignificant deformations of the region of integration of the wave equation lead to an insignificant change in the characteristic mode of the equation. On this basis, one may always reduce the complex region by small deformations to a step form, while the values of the characteristic mode and consequently the critical wave and propagation constant, do not change noticeably. As steps we can choose coordinate surfaces, a procedure which significantly eases the transition from general to specific expressions, enabling us to carry out numerical calculations. Thus, the calculation for a waveguide of complex form is reduced to the calculation for a waveguide of step form.

In the study of straight waveguides it is natural to take the axis of the waveguide as one of the coordinate axes. Hence, there arises the necessity of choosing from the various curvilinear coordinates q_1, q_2, q_3 the generalized cylindrical coordinates with the Cartesian axis $q_1 = Z$. In this system it is also easy to give a calculation for bent waveguides. The metric coefficients for the generalized cylindrical coordinates are such:

$$h_1 = 1, \ h_2 = h_2(q_2, q_3), \ h_3 = h_3(q_2, q_3), \tag{1}$$

that they automatically ensure fulfillment of the condition of splitting the Maxwell equations into TE and TM types relative to the Cartesian axis q_1 [7].

Expressing the components of the field in terms of electric Π_E^* and the magnetic Π_H^* potential functions [8] and assuming the field to be harmonic in time, we see that each of these features must satisfy the three-dimensional Helmholtz wave equation (under the appropriate boundary conditions [8])

$$\frac{\partial^2\Pi^*}{\partial q_1^2} + \frac{1}{h_2h_3}\left[\frac{\partial}{\partial q_2}\left(\frac{h_3}{h_2}\frac{\partial\Pi^*}{\partial q_3}\right) + \frac{\partial}{\partial q_3}\left(\frac{h_2}{h_3}\frac{\partial\Pi^*}{\partial q_3}\right)\right] = \gamma_0{}^2\varepsilon\mu\Pi^* = 0, \tag{2}$$

where γ_0 is the propagation constant in free space; ϵ, μ is the dielectric constant and permeability of the medium filling the waveguide.

1. INTEGRATION OF THE WAVE EQUATION FOR A STEP REGION IN CYLINDRICAL COORDINATES

1. General part. The three-dimensional equation (2) with the substitution decomposes into two equations

$$\frac{d^2Z}{dq_1} + \gamma^2 Z = 0, \tag{3}$$

$$\frac{1}{h_2h_3}\left[\frac{\partial}{\partial q_2}\left(\frac{h_3}{h_2}\frac{\partial\Pi}{\partial q_2}\right) + \frac{\partial}{\partial q_3}\left(\frac{h_2}{h_3}\frac{\partial\Pi}{\partial q_3}\right)\right] + k^2\Pi = 0, \tag{4}$$

where

$$k^2 = \gamma_0^2\varepsilon\mu - \gamma^2 \tag{5}$$

is the characteristic mode of the two-dimensional wave equation (4); γ^2 is the separation constant of Eq. (4) can be formed in analogy with [9] in the form

$$\frac{h_2h_3}{h_i^2} = T_i f_2(q_2) f_3(q_3); \quad i = 2, 3, \tag{6}$$

where f_2, f_3 are functions depending only on a single variable; T_i is a function which is independent of coordinate q_i, but may depend on the second coordinate; although condition (6) is not general, it encompasses all the systems of practical importance, with well-known functions. Since our problem is the creation of a suitable method of numerical calculation it is not appropriate to use coordinate systems in which the functions are little known. By determining the ratios h_3/h_2, h_2/h_3, expressing the products as the half-sum

$$h_2 h_3 = \frac{h_2^2 T_2 f_2 f_3 + h_3^2 T_3 f_2 f_3}{2} = \frac{f_2 f_3}{2}\left(h_2^2 T_2 + h_3^2 T_3\right); \tag{7}$$

and assuming $\Pi(q_2, q_3) = X(q_2)\, Y(q_3)$, we transform Eq. (4) into the following form

$$\frac{1}{T_3 f_2 X}\frac{d}{dq_2}\left(f_2 \frac{dX}{dq_2}\right) + \frac{1}{T_2 f_3 Y}\frac{d}{dq_3}\left(f_3 \frac{dY}{dq_3}\right) + \frac{1}{2}\left(\frac{h_2^2}{T_3} + \frac{h_3^2}{T_2}\right) k^2 = 0. \tag{8}$$

For all systems of practical importance, the following condition is fulfilled

$$\frac{1}{2}\left(\frac{h_2^2}{T_3} - \frac{h_3^2}{T_2}\right) = g_2(q_2) - g_3(q_3). \tag{9}$$

For this condition Equation (8) decomposes into two equations (if we introduce the separation constant μ). Together with Equation (3), we obtain a system of three ordinary differential equations, resulting from the decomposition of the three-dimensional wave equation;

$$\frac{d^2 Z}{dq_1} + \gamma^2 Z = 0, \tag{3}$$

$$\frac{1}{T_3 f_2}\frac{d}{dq_2}\left(f_2 \frac{dX}{dq_2}\right) + (g_2 k^2 - \mu) X = 0, \tag{10}$$

$$\frac{1}{T_2 f_3}\frac{d}{dq_3}\left(f_3 \frac{dY}{dq_3}\right) + (\mu - g_3 k^2) Y = 0. \tag{11}$$

The general solution of Equation (3) has the form

$$Z(q_1) = C_1 e^{-j\gamma q_1} + C_2 e^{+j\gamma q_1}, \tag{12}$$

where C_1, C_2 are constants of integration. In Equations (10), (11) $K = K_m$ has discreet values, has discreet values, because it is the characteristic mode of the wave equation (4); according to the Sturm-Liouville theorem the characteristic modes constitute an infinite series

$$k_1,\ k_2, \ldots, k_m, \ldots,$$

which correspond to the characteristic function

$$\Pi_{(1)},\ \Pi_{(2)}, \ldots, \Pi_{(m)}, \ldots,$$

which form a complete set. On the other hand, the parameter μ in equation (10), (11) is the eigenvalue of these equations, and therefore also forms an infinite series of values

$$\mu_1,\ \mu_2, \ldots, \mu_n, \ldots,$$

which correspond to the characteristic functions

$X_{m1},\ X_{m2}, \ldots, X_{mn}, \ldots$ [for equation (10)]

$Y_{m1},\ Y_{m2}, \ldots, Y_{mn}, \ldots$ [for equation (11)]

It is important that the functions X_{mn} (as well as Y_{mn}) form a complete orthogonal set for a fixed m, so that an arbitrary function $F_2(q_2)$ or $F_3(q_3)$, continuous up to the second derivative over the range of definition of $X_{mn}(Y_{mn})$, can be expanded within this range in a series with respect to the characteristic function $X_{mn}(Y_{mn})$. Since equations (10), (11) are second-order linear differential equations, the characteristic functions X_{mi}, Y_{mi} are in general linear combinations of two independent solutions, i.e.,

$$X_{mi} = X_{mi}^{(1)} + B_{mi} X_{mi}^{(2)}; \quad Y_{mi} = Y_{mi}^{(1)} + C_{mi} Y_{mi}^{(2)}.$$

2. Straight waveguides with a step cross section. The arguments given below are valid for waveguides with an arbitrary number of steps N, but Figure 1 (or Figure 2), which illustrates the cross section of the waveguide, necessarily has a finite number of steps (N = 4). As mentioned above, we form the particular coordinate surfaces q_2 = const, q_3 = const.

When considering a wave propagating in the direction of positive q_1, it is necessary to set $C_2 = 0$ in (12). In this case γ is a constant of propagation along the axis of the wavelength and can be determined from Equation (5) if the magnitude of k is known.

In the critical case $\gamma = 0$ we have

$$\gamma_0^2 \varepsilon\mu = k^2,$$

hence, the cutoff wavelength is

$$\lambda_{cr} = \frac{2\pi}{k}\sqrt{\varepsilon\mu}.$$

Thus, the problem of calculating the critical wavelength is reduced to that of establishing the eigenvalue of the two dimensional equation (4), given in the stepped region. Let us consider the region depicted in Figure 1. We will separate this complex region into a number of simple regions, bounded by coordinate surfaces. The boundary conditions in each region are determined on the surfaces $q_2 = b_0$, b_i as on metallic walls with infinite conductivity. On the surfaces q_3 = const (excluding the edge regions $i = 1$, $i = N$) the boundary conditions are still undetermined.

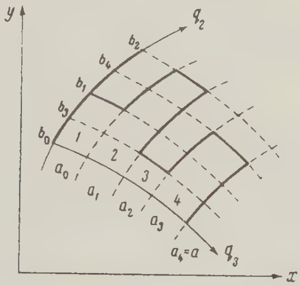

Figure 1.

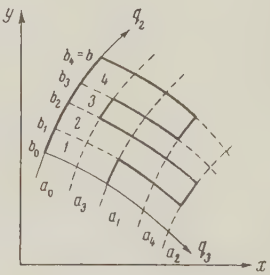

Figure 2.

The solution of wave equation (2) for the stepped region of Figure 1 is given piecewise for each "simple" region, while requiring that it satisfy the boundary conditions on a stepped contour and be continuous at the boundaries of separation of the simple regions.

The particular solution of wave equation (2) for the i-th simple region has the form

$$\Pi^{*}_{imn} = A_{imn} X_{imn} Y_{imn} e^{-j\gamma q_1}. \tag{13}$$

By applying the boundary conditions to the walls of the waveguide $q_2 = b_0$, b_i and treating k_m as a parameter, we find a discrete series of eigenvalues μ_n should also be eigenvalues of equation (10), but a certain arbitrariness exists in the determination of the characteristic function Y_{imn}, because the boundary conditions at q_3 = const are still not given. Using this, we will consider the characteristic function Y_{imn} as dependent not only on the coordinate q_3, but also on a certain parameter δ_i, which, together with the magnitude of k_m is determined from the condition of continuity of the field at the boundaries of separation of the simple regions. We note that δ_i for the first and last region can be determined from the condition at the walls $q_3 = q_0$, q_n. Thus the particular solution for the i-th region should be represented in the following form:

$$\Pi^{*}_{imn} = A_{imn} Y_{imn}(q_3, \delta_i) X_{imn}(q_2) e^{-j\gamma q_1}. \tag{14}$$

We will represent the potential function corresponding to the eigenvalue k_m (the same for the entire region) in the form of an infinite sum

$$\Pi^{*}_{im} = \sum_{n}^{\infty} A_{imn} Y_{imn}(q_3, \delta_i) X_{imn}(q_2) e^{-j\gamma q_1}, \tag{15}$$

each term of which describes a wave traveling in the direction of positive q_1; the phase velocities of all the particular waves are the same (since k_m are the same), but differ in the number of half-wavelengths laid out on the distance $b_1 - b_0$ and differ in the field distribution along the q_3 coordinate.

We now require that the functions Π^*_{im} guarantee the continuity of all the components of the field at each line of separation of the simple regions ($q_3 = a_1, a_2, \ldots, a_{N-1}$). It is not difficult to see (see Appendix) that for the TE mode (and we limit ourselves to a consideration of only this type of wave) the continuity of the field components at the boundary of separation of the i-th and i + 1-th region ($q_3 = a_i$) is guaranteed upon fulfillment of the following conditions:

$$\Pi^*_{im} = \Pi^*_{i+1,\,m}, \tag{16}$$

$$\frac{\partial \Pi^*_{im}}{\partial q_3} = \frac{\partial \Pi^*_{i+1,\,m}}{\partial q_3}, \tag{17}$$

which lead to two equations

$$\sum_n^\infty A_{imn} Y_{imn}(a_i,\ \delta_i) X_{imn}(q_2) = \sum_n^\infty A_{i+1,\,mn} Y_{i+1,\,mn}(a_i,\ \delta_{i+1}) X_{i+1,\,mn}(q_2), \tag{18}$$

$$\sum_n^\infty A_{imn} Y'_{imn}(a_i,\ \delta_i) X_{imn}(q_2) = \sum_n^\infty A_{i+1,\,mn} Y'_{i+1,\,mn}(a_i,\ \delta_{i+1}) X_{i+1,\,mn}(q_2) = \\ = \Psi_i(q_2) \sim E_{q_2}, \tag{19}$$

where the dashes in Y designate differentiaion with respect to q_3. As we see, equations (18) and (19) no longer contain a term which determines the dependence on the coordinate q_1. This was found to be possible because in each particular wave such a relation was expressed by a factor, identical for all waves.

The left and right-hand sides of equation (19) were compared with a certain function $\Psi_i(q_2)$ which was unspecified until now. The proportionality of Ψ_i to the field components E_{q2} follows from the relationships of Π^*_{im} to the field components. But because of this relation, the functions $\Psi_i(q_2)$ should become zero on the conducting branch $b_{i+1} - b_i$, which we will take into consideration hereafter.

Assuming the function $\Psi_i(q_2)$ to be continuous up to the second derivative, we can consider equation (19) as an expansion of $\Psi_i(q_2)$ in a series with respect to the characteristic functions X_{imn} over the interval b_0, b; and with respect to the characteristic functions $X_{i+1},{}_{mn}$ over the interval b_0, $b_i + 1$. These are intervals on which the functions X_{imn}, $X_{i+1,\,mn}$ respectively are defined. Since the functions X form a complete set, it is entirely possible to expand a given continuous function in terms of them. From these expansions (assuming $b_{i+1} > b_i$) it follows that

$$A_{imn} = \frac{1}{Y'_{imn}(a_i,\,\delta_i)} \int_{b_0}^{b_i} \Psi_i(\xi) X_{imn}(\xi)\, d\xi, \tag{20}$$

$$A_{i+1,\,mn} = \frac{1}{Y'_{i+1,\,mn}(a_i,\,\delta_{i+1})} \int_{b_0}^{b_{i+1}} \Psi_i(\xi) X_{i+1,\,mn}(\xi)\, d\xi = \\ = \frac{1}{Y'_{i+1,\,mn}(a_i,\,\delta_{i+1})} \int_{b_0}^{b_i} \Psi_i(\xi) X_{i+1,\,mn}(\xi)\, d\xi. \tag{21}$$

Contraction of the interval of integration in equation (21) is caused by the vanishing of $\Psi_i(\xi)$ over the entire segment $b_{i+1} - b_i$. If we assume that $b_i + 1 < b_i$, contraction of the interval of integration occurs in equation (20). Below we will indicate two values for the upper limit of the integrals; in the calculation one must abandon the small ones.

Substituting the resulting values of the coefficients in equation (18), we obtain a homogeneous integral equation with respect to the function ψ_i

$$\int_{b_0}^{b_i\,(b_{i+1})} \Psi_i(\xi)\, P_i(q_2, \xi)\, d\xi = 0 \tag{22}$$

with a symmetric kernel

$$P_i(q_2, \xi) = \sum_n^{\infty} \frac{Y_{imn}(a_i, \delta_i)}{Y'_{imn}(a_i, \delta_i)} X_{imn}(q_2)\, X_{imn}(\xi) -$$
$$- \sum_n^{\infty} \frac{Y_{i+1,\,mn}(a_i, \delta_{i+1})}{Y'_{i+1,\,mn}(a_i, \delta_{i+1})} X_{i+1,\,mn}(q_2)\, X_{i+1,\,mn}(\xi).$$

The expression $Y_{i+1,\,mn} / Y'_{i+1,\,mn} = \mathrm{ct}_{i+1,\,mn}(a_i, \delta_{i+1})$ should be called a large generalized cotangent. In the Cartesian system this expression transforms into an ordinary cotangent, in the cylindrical system — to a radial cotangent and in the spherical system — to a spherical cotangent [11] etc.

If the stepped cross section is divided into N simple regions, equation (22) denotes a system of N-1 integral equations. This system contains N-1 unknowns k_m, δ_2 . . . , δ_{N-1} occuring in the nucleus of the equation. Since the integration and differentiation in system (22) is not performed over a single one of the unknowns, each integral equation of the system can be solved independently of the other equations. As a result we obtain a system of N -1 algebraic equations in the N - 1 unknowns indicated above.

The Bubnov-Galerkitz method can be used to solve integral equations (22). In this method the unknown function $\Psi_i(\xi)$ is approximated by linear combination of the ν-th number of functions which form a complete set when $\nu \to \infty$ and satisfy the boundary conditions for the E_{q2} field components,

$$\Psi_i(\xi) = \beta_{i1}\varphi_{i1}(\xi) + \ldots + \beta_{i\nu}\varphi_{i\nu}(\xi). \tag{23}$$

The coefficients β_{ij} of this sum are determined from the system of homogeneous equations

$$\sum_{j=1}^{\nu} M_{ij\mu}\beta_{ij} = 0; \; \mu = 1, 2, \ldots, \nu, \tag{24}$$

where

$$M_{ij\mu} = M_{j\mu i} = \int_{b_0}^{b_i\,(b_{i+1})} \int_{b_0}^{b_i\,(b_{i+1})} \varphi_{i\mu}(\xi)\, P_i(q_2, \xi)\, \varphi_{ij}(q_2)\, dq_2\, d\xi. \tag{25}$$

Writing the condition for a nontrivial solution of system (24), we obtain

$$\begin{vmatrix} M_{i11} M_{i12} \ldots M_{i1\nu} \\ M_{i21} M_{i22} \ldots M_{i2\nu} \\ \ldots\ldots\ldots \\ M_{i\nu1} M_{i\nu2} \ldots M_{i\nu\nu} \end{vmatrix} = 0; \; i = 1, 2, \ldots, N-1. \tag{26}$$

Equation (26) represents the final calculated system relating the dimensions of the stepped region to the eigenvalue k_m (and to the unknowns δ_2 . . . δ_{N-1}). Since the functions X, Y are known in actual coordinate systems, calculation of (26) is possible. In a practical calculation, it is expedient to choose approximating functions which even in small numbers sufficiently reproduce the function $\Psi_i(\xi)$ and allow calculation of integral (26). One may choose as such functions the set of characteristic functions X_{imn} (or $X_{i+1,\,mn}$, if $b_{i+1} < b_i$). Such a representation is suitable because of the orthogonality of X_{imn}, X_{ims} all the integrals in (25) for which n ≠ s, vanish and the final expressions acquire the simplest form.

After solving equation (26) for the unknowns k_m, δ_i, it is easy to calculate the coefficients β_{ij} from system (24) and the functions ψ_i from (21). Furthermore, after finding the coefficients A_{imn}, $A_{i+1,\,mn}$ from relations (20) (21) one may determine the characteristic functions Π_{im} for each simple region. So we have solved the eigenvalue problem for the wave equation given in the step region (Figure 1).

The problem for the region shown in Figure 2 is solved by a method of subdivision analogous to the above, because the functions Y on which the expansion is based, as well as X, form a complete orthogonal set.

3. Bent waveguides having a stepped cross section. If we assume that in this generalized cylindrical coordinate system, the wave is propagated along the curvilinear coordinate q_2, we arrive at the problem of a bent waveguide, the bend of the waveguide being in the general case, nonuniform (i.e. having a variable curvature). By dividing the stepped cross section into simple regions, one may write out for each region a general solution of the three-dimensional wave equation (2), just as before, in the form of an infinite sum, [equation (15)] . But now each term of this sum is an individual wave with its law of propagation in terms of the q_2 coordinate. Thus, the aforementioned method of calculation of stopped waveguides, based on the concept of a field inside the waveguide in the form of an infinite number of individual waves, having a simple law of propagation, cannot be applied to the general case of a bent waveguide. The exception is a uniform bend considered in the circular-cylindrical coordinate system. This case is discussed below.

2. SEVERAL APPLICATIONS

An application of this method of calculating transverse and longitudinal waves in complex waveguides in a rectangular coordinate system [8] can be found in [4,10]. We will discuss an example of the application of the method in a circular cylindrical coordinate system.

In the cylindrical system $q_1 - Z$, $q_2 = r$, $q_3 = \varphi$, when we take into account the values of the Lamé coefficients and designating $\mu = p^2$, take the form

$$\frac{d^2Z}{dz^2} + \gamma^2 Z = 0, \tag{3}$$

$$\frac{d^2X}{dr^2} + \frac{1}{r}\frac{dX}{dr} + \left(k^2 - \frac{p^2}{r^2}\right)X = 0, \tag{27}$$

$$\frac{d^2Y}{d\varphi^2} + p^2 Y = 0. \tag{28}$$

The solutions for each equation of this system are known; therefore, the potential function $\Pi^* = XYZ$ has the form

$$\Pi^*(z, r, \varphi) = A\,[J_p(kr) + BN_p(kr)]\,[D_1 e^{-jp\varphi} + D_2 e^{+jp\varphi}] \times \\ \times [C_1 e^{-j\gamma z} + C_2 e^{+j\gamma z}], \tag{29}$$

where

$$k^2 = \gamma_0^2 \varepsilon\mu - \gamma^2.$$

1. Straight waveguides having a stepped cross section. Assuming that the wave is propagated in the direction of positive z, one must set $C_2 = 0$ in equation (29). We divide the cross section of the waveguide (Figure 3) into N = 4 simple regions in the form of segments and represent the potential function of an infinite sum, any term of which is a solution of the wave equation in the r, φ plane, corresponding to the same k value, but different p:

$$\Pi_i^*(z, r, \varphi) = \sum_{n=0}^{\infty} \Pi_{in}^*(z, r, \varphi) = \sum_{n=0}^{\infty} A_{in}'\,[J_{p_{in}}(kr) + \\ + B_{p_{in}} N_{p_{in}}(kr)]\,[B_1 \sin p_{in}\varphi + B_2 \cos p_{in}\varphi]\, e^{-j\gamma z}. \tag{30}$$

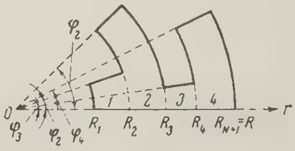

Figure 3.

Limiting ourselves to a treatment of an H type wave, we apply to Π_{in} the following boundary conditions at the infinitely conducting walls:

$$\left(\frac{\partial \Pi_{in}^*}{\partial \varphi}\right)_{\varphi=0,\,\varphi_i} = 0; \quad \left(\frac{\partial \Pi_{im}'}{\partial r}\right)_{r=R_1,\,R} = 0.$$

This gives the following values of the constants

$$B_1 = 0; \; p_{in} = \frac{n\pi}{\varphi_i}; \; n = 0, 1, 2, \ldots; \; B_{p_{1n}} = -\frac{J'_{p_{1n}}(kR_1)}{N'_{p_{1n}}(kR_1)};$$

$$B_{p_{Nn}} = -\frac{J'_{p_{Nn}}(kR)}{N'_{p_{Nn}}(kR)}. \tag{31}$$

If we denote the coefficient $B_{p_{in}}$ for an arbitrary i by the ratio

$$B_{p_{in}} = -\frac{J'_{p_{in}}(k\delta_i)}{N'_{p_{in}}(k\delta_i)},$$

according to (31) we have $\delta_1 = R_1$, $\delta_N = R_{N+1} = R$; the remaining δ_i are determined from the continuity condition on the lines $r = -R_2, R_3 \ldots R_N$.

Substituting the values of the constants into the expression for the potential function (30), we obtain

$$\Pi_i^*(z, r, \varphi) = A_{i0} Z_{p_{i0}}(kr) + \sum_{n=1}^{\infty} A_{in} Z_{p_{in}}(kr) \cos p_{in}\varphi e^{-j\gamma z}, \tag{32}$$

where

$$Z_{p_{in}}(kr) = J_{p_{in}}(kr) + B_{p_{in}} N_{p_{in}}(kr), \tag{33}$$

$J_{p_{in}}$, $N_{p_{in}}$ are the Bessel and Neumann functions of order p.

Applying to Π_i^*, Π_{i+1}^*, the conditions guaranteeing continuity of the field components at the boundary $r = R_{i+1}$:

$$\Pi_i^* = \Pi_{i+1}^* \frac{\partial \Pi_i^*}{\partial r} \frac{\partial \Pi_{i+1}^*}{\partial r}, \tag{34}$$

we obtain two equations

$$A_{i0} Z_{p_{i0}}(kR_{i+1}) + \sum_{n=1}^{\infty} B_{in} Z_{p_{in}}(kR_{i+1}) \cos p_{in}\varphi =$$

$$= A_{i+1,0} Z_{p_{i+1,0}}(kR_{i+1}) + \sum_{n=1}^{\infty} A_{i+1,n} Z_{p_{i+1,n}}(kR_{i+1}) \cos p_{i+1,n}\varphi, \tag{35}$$

$$A_{i0} Z'_{p_{i0}}(kR_{i+1}) + \sum_{n=1}^{\infty} A_{in} Z'_{p_{in}}(kR_{i+1}) \cos p_{in}\varphi =$$

$$= A_{i+1,0} Z'_{p_{i+1,0}}(kR_{i+1}) + \sum_{n=1}^{\infty} A_{i+1,n} Z'_{p_{i+1,n}}(kR_{i+1}) \cos p_{i+1,n}\varphi = F_i(\varphi) \sim E_\varphi. \tag{36}$$

Determining the coefficients A_{in}, $A_{i+1,n}$ from (36) and substituting them into (35), we obtain the integral equations

$$\int_0^{\varphi_i (\varphi_{i+1})} F_i(\xi) \left[Q_i(\xi, \varphi) + Q_{i0} \right] d\xi = 0, \tag{37}$$

in which only the larger of the two values may serve as the upper limit. The nucleus of equation (37) has the form

$$Q_i(\xi, \varphi) = \sum_{n=1}^{\infty} \frac{2\,\mathrm{ct}_{p_{in}}(kR_{i+1}, k\delta_i)}{\varphi_i} \cos p_{in}\xi \cos p_{in}\varphi -$$

$$- \sum_{n-1}^{\infty} \frac{2\,\mathrm{ct}_{p_{i+1,\,n}}(kR_{i+1}, k\delta_{i+1})}{\varphi_{i+1}} \cos p_{i+1,\,n}\xi \cos p_{i+1,\,n}\varphi,$$

$$Q_{i0} = \frac{\mathrm{ct}_{p_{i0}}(kR_{i+1}, k\delta_i)}{\varphi_i} - \frac{\mathrm{ct}_{p_{i+1,\,0}}(kR_{i+1}, k\delta_{i+1})}{\varphi_{i+1}},$$

where

$$\mathrm{ct}_{p_{jn}}(kR_{i+1}, k\delta_j) = \frac{Z_{p_{jn}}(kR_{i+1})}{Z'_{p_{jn}}(kR_{i+1})} =$$

$$= \frac{J_{p_{jn}}(kR_{i+1})\,N'_{p_{jn}}(k\delta_j) - N_{p_{jn}}(kR_{i+1})\,J'_{p_{jn}}(k\delta_j)}{J'_{p_{jn}}(kR_{i+1})\,N'_{p_{jn}}(k\delta_j) - N'_{p_{jn}}(kR_{i+1})\,J'_{p_{jn}}(k\delta_j)}, \tag{38}$$

in analogy with [11], we designate the larger radial cotangent by the index p_{in}.

Applying the Bubnov-Galerkin method to solution of equation (37), we obtain a system of N - 1 equations which relate the dimensions of the stepped cross section to the unknowns $k_m = k, \delta_2, \delta_3 \ldots \delta_{N-1}$,

$$\begin{vmatrix} G_{i11} & G_{i12} & \ldots & G_{i1\nu} \\ \cdot & \cdot & \cdot & \cdot \\ G_{i\nu 1} & G_{i\nu 2} & \ldots & G_{i\nu\nu} \end{vmatrix} = 0; \; i = 1, 2, \ldots, N-1, \tag{39}$$

where

$$G_{ij\sigma} = \int\limits_0^{\varphi_i\,(\varphi_{i+1})} \int\limits_0^{\varphi_i\,(\varphi_{i+1})} \psi_j\,[Q_i(\xi, \varphi) + Q_{i0}]\,\psi_\sigma\,d\xi\,d\varphi; \; j = 1, 2, \ldots, \nu;$$

$$\sigma = 1, 2, \ldots, \nu;$$

ψ_j, ψ_σ are the approximating functions.

To a first approximation ($\psi_1 = 1$) the calculated system (39) will consist of two forms of equations corresponding to the two possibilities ($\varphi_{i+1} > \varphi_i$, $\varphi_{i+1} < \varphi_i$):

When $\varphi_{i+1} > \varphi_i$

$$\mathrm{ct}_{p_{i0}}(kR_{i+1}, k\delta_i) = \frac{\varphi_i}{\varphi_{i+1}} \Bigg\{ \mathrm{ct}_{p_{i+1,0}}(kR_{i+1}, k\delta_{i+1}) +$$

$$+ 2 \sum_{n=1}^{\infty} \mathrm{ct}_{p_{i+1,\,n}}(kR_{i+1}, k\delta_{i+1}) \left(\frac{\sin p_{i+1,\,n}\varphi_i}{p_{i+1,\,n}\varphi_i} \right)^2 \Bigg\}, \tag{40}$$

when $\varphi_{i+1} < \varphi_i$

$$\mathrm{ct}_{p_{i+1,\,0}}(kR_{i+1}, k\delta_{i+1}) = \frac{\varphi_{i+1}}{\varphi_i} \Bigg\{ \mathrm{ct}_{p_{i0}}(kR_{i+1}, k\delta_i) +$$

$$2 \sum_{n=1}^{\infty} \mathrm{ct}_{p_{in}}(kR_{i+1}, k\delta_i) \left(\frac{\sin p_{in}\varphi_{i+1}}{p_{in}\varphi_{i+1}} \right)^2 \Bigg\}; \; i = 1, 2, \ldots, N-1; \tag{41}$$

the system of equations (40), (41) is characteristic, because it relates the dimensions of the cross section to the critical wavelength ($k = 2\pi/\lambda_{cr}$).

It is easy to show, by using the asymptotic expressions for the Bessel and Neumann functions with large indices, that the radial cotangents in equations (40), (41) decrease sufficiently rapidly, so that the terms in the sum decrease with a rise in n no slower than $1/n^2$. This fact is of great value in numerical calculations.

2. Bent waveguides. Let the cross section of a bent waveguide have the form shown in Figure 4. Let the bend occur in the H plane (electric type wave $E_z \neq 0$, $H_z = 0$), the wave in the waveguide is propagated in the direction of positive φ [$D_2 = 0$, see equation (29)]. We

divide stepped cross section into N = 4 simple regions and represent for each region (taking into account boundary conditions at the walls of the waveguide) the potential function in the form

$$\Pi_i^* = A_{i0} Z_p(k_0 r) + \sum_{n=1}^{\infty} A_{in} \cos s_{in} z Z_p(\varkappa_{in} r) e^{-jp\varphi}; \; i = 1, 2, \ldots, N, \tag{42}$$

where

$$Z_p(\varkappa_{in} r) = J_p(\varkappa_{in} r) + B_{in} N_p(\varkappa_{in} r);$$

p is the constant of propagation of the wave inside the waveguide on an arc of radius r;

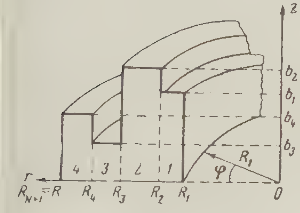

Figure 4.

$$s_{in} = \frac{n\pi}{b_i}; \; n = 1, 2, \ldots; \; \varkappa_{in} = \sqrt{k_0^2 - s_{in}^2} \quad (k_0^2 = \gamma_0^2 \varepsilon\mu); \tag{43}$$

$$B_{in} = -\frac{J_p(\varkappa_{in}\delta_i)}{N_p(\varkappa_{in}\delta_i)}, \tag{44}$$

wherein from the boundary conditions for the first and last region, it follows that $\delta_1 = R_1$, $\delta_N = R_{N+1}$. All the remaining δ_i are determined from the continuity condition on the lines r = R_2, R_3 . . . . . . R_N. Applying to Π_i^*, Π_{i+1}^* conditions guaranteeing continuity of the field components on the line r = R_{i+1}

$$\left(\frac{\partial^2}{\partial z^2} + k_0^2\right) \Pi_i^* = \left(\frac{\partial^2}{\partial z^2} + k_0^2\right) \Pi_{i+1}^* = \Phi_i(z) \sim E_z, \tag{45}$$

$$\frac{\partial \Pi_i^*}{\partial r} = \frac{\partial \Pi_{i+1}^*}{\partial r}, \tag{46}$$

we obtain two equations, from which we obtain in the usual manner the integral equation

$$\int_0^{b_i (b_{i+1})} \Phi_i(\xi) [P_i(\xi, z) + P_{i0}] \, d\xi = 0, \tag{47}$$

in which one must use only the larger of the two indicated values as the upper limit. The nucleus of the integral equation (47) has the form

$$P_i(\xi, z) = \sum_{n=1}^{\infty} \frac{2 \operatorname{ct}_p(\varkappa_{in} R_{i+1}, \varkappa_{in}\delta_i)}{b_i \varkappa_{in}} \cos s_{in}\xi \cos s_{in} z -$$

$$- \sum_{n=1}^{\infty} \frac{2 \operatorname{ct}_p(\varkappa_{i+1,\,n} R_{i+1} \varkappa_{i+1,\,n} \delta_{i+1})}{b_{i+1} \varkappa_{i+1,\,n}} \cos s_{i+1,\,n}\xi \cos r_{i+1,n} z,$$

$$P_{i0} = \frac{\operatorname{ct}_p(k_0 R_{i+1}, k_0 \delta_i)}{k_0 b_i} - \frac{\operatorname{ct}_p(k_0 R_{i+1}, k_0 \delta_{i+1})}{k_0 b_{i+1}},$$

where

$$\operatorname{ct}_p(x, y) = \frac{Z_p'(x, y)}{Z_p(x, y)} \frac{J_p'(x) N_p(y) - N_p'(x) J_p(y)}{J_p(x) N_p(y) - N_p(x) J_p(y)}$$

is the radial cotangent of indices p.

Applying the Bubnov-Galerkin method for solving integral equation (47) and limiting ourselves to the first approximation, we obtain the calculated system (i = 1, 2 . . . . N -1) which relates the cross-sectional dimensions of the waveguide to the unknowns k_0, δ_2 . . . . . . δ_{N-1} (it is treated as a parameter). This system consists of two forms of equations, corresponding to the two possibilities ($b_i > b_{i+1} > b_i < b_{i+1}$)

When $b_i > b_{i+1}$

$$\operatorname{ct}_p(k_0 R_{i+1}, k_0 \delta_{i+1}) =$$

$$= \frac{b_{i+1}}{b_i} \left\{ \operatorname{ct}_p(k_0 R_{i+1}, k_0 \delta_i) + 2k_0 \sum_{n=1}^{\infty} \frac{\operatorname{ct}_p(\varkappa_{in} R_{i+1}, \varkappa_{in}\delta_i)}{\varkappa_{in}} \left(\frac{\sin s_{in} b_{i+1}}{s_{in} b_{i+1}} \right)^2 \right\}, \tag{48}$$

When $b_i < b_{i+1}$

$$\mathrm{ct}_p(k_0,\ R_{i+1},\ k_0\delta_i) =$$

$$= \frac{b_i}{b_{i+1}}\left\{\mathrm{ct}_p(k_0 R_{i+1},\ k_0\delta_{i+1}) + 2k_0 \sum_{n=1}^{\infty} \frac{\mathrm{ct}_p(\varkappa_{i+1,\,n} R_{i+1} \varkappa_{i+1,\,n} \delta_{i+1})}{\varkappa_{i+1,\,n}} \left(\frac{\sin s_{i+1,\,n} b_i}{s_{i+1,\,n} b_i}\right)^2\right\}. \tag{49}$$

By determining from the calculated system (48), (49) the number k_0 at different values of the parameter p, one may plot the graphical relation $p = f(k_0)$, from which knowing the effective wavelength $\lambda = 2\pi/k_0$, it is easy to determine the propagation constant inside the waveguide. Thus the system of equations (48), (49) should be called dispersive, because it determines the variation of the propagation constant as a function of the effective frequency (for a given form of the waveguide cross section).

The characteristic system, i.e., the system used to calculate the critical wavelength is obtained from (48), (49) when $p = 0$.

It is easy to show, using the asymptotic formulas for the Bessel functions, that the sum terms in equations (48), (49) decrease with an increase of integer which is not slower than $1/n^2$.

CONCLUSION

The method described above for the calculation of complex waveguides in generalized cylindrical coordinates can be applied also to the calculation of cavity resonators of complex shape. We note that uniform bent waveguides in complex cavity resonators can be calculated by the indicated methods not only in generalized cylindrical coordinates, but also in other orthogonal systems permitting a separation of variables (for instance, in spherical coordinates).

APPENDIX

In orthogonal coordinates, the field components of transverse electric waves are related to the magnetic potential function Π^* by means of the following relations:

$$\begin{gathered} E_1 = 0, \quad E_2 = -\frac{j\gamma_0\mu}{h_3}\frac{\partial \Pi^*}{\partial q_3}, \quad E_3 = \frac{j\gamma_0\mu}{h_2}\frac{\partial \Pi^*}{\partial q_2}, \\ H_1 = \frac{\partial^2 \Pi^*}{\partial q_1^2} + \gamma_0^2 \varepsilon\mu \Pi^*, \ H_2 = \frac{1}{h_2}\frac{\partial^2 \Pi^*}{\partial q_1 \partial q_2}, \ H_3 = \frac{1}{h_3}\frac{\partial^2 \Pi^*}{\partial q_1 \partial q_3}. \end{gathered} \tag{I}$$

The continuity of the field at the boundary $q_3 = a_i$ of separation of two simple regions is guaranteed upon fulfilling the following two conditions:

$$\left(\frac{\partial^2}{\partial q_1^2} + \gamma_0^2 \varepsilon\mu\right)\Pi_i^* = \left(\frac{\partial^2}{\partial q_1^2} + \gamma_0^2 \varepsilon\mu\right)\Pi_{i+1}^*, \tag{II}$$

$$\frac{\partial \Pi_i^*}{\partial q_3} = \frac{\partial \Pi_{i+1}^*}{\partial q_3}, \tag{III}$$

a fact easy to substantiate. Actually, condition (II) guarantees the equation for the $H_{1\,i}$, $H_{1\,,i+1}$, components; condition (III) guarantees the equation for the $E_{2\,,i}$, $E_{2\,,i+1}$ components. The equation at the boundary of separation of the other field components follows from condition (II). Rewriting it in the form

$$\frac{\partial^2}{\partial q_1^2}(\Pi_i - \Pi_{i+1}) + \gamma_0^2 \varepsilon\mu(\Pi_i^* - \Pi_{i+1}^*) = 0, \tag{IV}$$

we see that the integral of the resulting equation

$$\Pi_i^* - \Pi_{i+1}^* = A\cos\gamma_0\sqrt{\varepsilon\mu}\,q_1 + B\sin\gamma_0\sqrt{\varepsilon\mu}\,q_1 \tag{V}$$

shows such a relation between the functions Π_i, Π_{i+1} (A, B are constants of integration), which causes the equality of derivatives with respect to q_2 and mixed respect to q_1, q_2 and with respect to q_1, q_3, i.e. the equality of components (respectively $E_{3i} - E_{3\,i+1}$, $H_{2i} = H_{2,i+1}$. The conditions of the continuity of field in the form (II), (III) have the most general form, suitable for a study of straight and bent waveguides in an arbitrary orthogonal system permitting a separation of varibles. For straight waveguides however, with the conditions one may give a simpler form. Taking into consideration that $\Pi_i^* = e^{j\gamma q_1}\Pi_i(q_2, q_3)$, and $k^2 = \omega^2\varepsilon\mu - \gamma^2$ for straight waveguides and for all regions we represent equations (II), (III) in the form

$$\Pi_i = \Pi_{i+1}, \qquad \text{(VI)}$$

$$\frac{\partial\Pi_i}{\partial q_3} = \frac{\partial\Pi_{i+1}}{\partial q_3}. \qquad \text{(VII)}$$

From equations (I) we find

$$\Pi_i = \frac{H_{1i}}{k^2} e^{j\gamma q_1}, \quad \Pi_{i+1} = \frac{H_{1,\,i+1}}{k^2} e^{j\gamma q_1},$$

where H_{1i}, $H_{1,i+1}$ are the axial field components.

Substituting the values of the functions Π_i, Π_{i+1} into (VI), (VII), we obtain a final form of the continuity condition for straight waveguides (and for magnetic waves)

$$H_{1i} = H_{1,\,i+1}, \qquad \text{(VIII)}$$

$$\frac{\partial H_{1i}}{\partial q_3} = \frac{\partial H_{1,\,i+1}}{\partial q_3}. \qquad \text{(IX)}$$

The conditions in the form of (VIII), (IX) were used by the author in [4].

REFERENCES

1. E. Mayer, Resonant frequencies of the nosed-in cavity, J. Appl Phys., 1046, 17, 12, 1046.
2. L.N. Deryugin, Calculation of critical frequency of II and H waveguides, Radiotekhnika, Vol. 17, No. 12, 1046, 1948.
3. N.N. Malov, Approximate calculation of the critical wavelength of a T-shaped waveguide. Uch, Zap. Mosk. Gor. Ped. Inst. im. V.L. Lenin, Vol. 88, 33, (1954).
4. A. Ya. Yashkin, New method of approximate calculation of waveguides with a complicated tranverse cross-sectional shape. Radiotekhnika i elektronika, Vol. 3, No. 6, 831, 1958.
5. A.Ya. Yashkin, On a single method of calculation of waveguides of triangular and trapezoidal cross sections, Radiotekhnika, Vol. 13, No. 10, 3, 1958.
6. A.G. Gurevich, Hollow Resonators and Waveguides. Izd. Sovetskoye radio, 1952.
7. G.V. Kisunko, Electrodynamics of Hollow Systems, Izd. VKAS, 1959.
8. B.A. Vvedenskii, A.G. Arenberg, Radio Waveguides, GTI, 1946.
9. D.A. Stratton, Theory of Electromagnetism, transl. from English, GTI, 1948.
10. A. Ya. Yashken, Longitudinal waves in stepped, straight waveguides, Izv. vuzov, MVO, SSSR, (Radiotekhnika) 1961, 2.
11. Spravochnik po volnovodam, Waveguide Manual, Izd. Sovyetskoye Radio, 1952.

Submitted to the editors 19 May, 1960

COUPLING COEFFICIENT BETWEEN ELECTRON BEAM AND TRANSVERSE ELECTROMAGNETIC FIELD IN A MICROWAVE WAVEGUIDE

L.N. Loshakov

An explanation is given of the interaction of an electron beam with the transverse electromagnetic field in a microwave waveguide. This discussion, supplements the theory expounded in a previous paper by the author [1].

Reference [1] described the process of interaction of an electron beam with the transverse field of an electromagnetic wave(electron motion in a direction perpendicular to the power flux in a microwave waveguide.)

Because of the newness of the subject and the provisional character of the calculation, it is of interest to examine the problem in greater detail, and in particular, to compare the coupling coefficient introduced in [1] with the known coupling coefficient of a conventional traveling-wave tube with longitudinal interaction.

Hereafter, the device under study will be called a transverse interaction tube.

In [11] we obtained the following expression for the coupling coefficient K_c between the electron beam and the wave in the transverse interaction tube

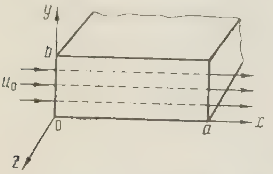

$$K_c = \frac{k^2 - \frac{m^2\pi^2}{a^2}}{\frac{m^2\pi^2}{a^2}}, \tag{1}$$

where $k = \omega\sqrt{\epsilon\mu}$ is the phase constant of the medium (ϵ, μ are parameters of the medium, ω is the angular frequency) and $m\pi/a$ is the phase constant of a wave excited by the beam in the decelerating system, traveling in the direction of possible electron motion along the axis. See figure.

Taking into account the fact that the transmitting wave in the waveguide model of a transverse interaction tube is a LM_{mn} - type wave, in which no component of magnetic field exists in the direction of electron motion (H_{0x}), we may describe the waveguide field in the absence of an electron beam with the aid of known expressions (2):

$$E_{0x} = A\cos\frac{m\pi}{a}x\sin\frac{n\pi}{b}y\,e^{j(\omega t-\beta_0 z)}, \tag{2}$$

$$E_{0y} = -\frac{\frac{m\pi}{a}\frac{n\pi}{b}}{k^2-\frac{m^2\pi^2}{a^2}}A\sin\frac{m\pi}{a}x\cos\frac{n\pi}{b}y\,e^{j(\omega t-\beta_0 z)}, \tag{3}$$

$$E_{0z} = \frac{j\beta_0\frac{m\pi}{a}}{k^2-\frac{m^2\pi^2}{a^2}}A\sin\frac{m\pi}{a}x\sin\frac{n\pi}{b}y\,e^{j(\omega t-\beta_0 z)}, \tag{4}$$

$$H_{0y} = \frac{\omega\varepsilon\beta_0}{k^2-\frac{m^2\pi^2}{a^2}}A\cos\frac{m\pi}{a}x\sin\frac{n\pi}{b}y\,e^{j(\omega t-\beta_0 z)}, \tag{5}$$

$$H_{0z} = -j\frac{\omega\varepsilon\frac{n\pi}{b}}{k^2-\frac{m^2\pi^2}{a^2}}A\cos\frac{m\pi}{a}x\cos\frac{n\pi}{b}y\,e^{j(\omega t-\beta_0 z)}, \tag{6}$$

$$m = 1, 2, 3, \ldots;\ n = 1, 2, 3, \ldots.$$

The following notation is used in equations (2-6): a, b - transverse waveguide dimensions; β_0 is the phase constant along the longitudinal (z) axis, i.e., in the direction of the power flux. This phase constant is related to the phase constants along the x- and y-axes by the well-known relations

$$\beta_0^2 = k^2 \quad \frac{m^2\pi^2}{a^2} - \frac{n^2\pi^2}{b^2}. \tag{7}$$

According to Brillouin, the LM_{mn} waveguide mode is formed as a result of the superposition of homogeneous transverse waves propagating along four intersecting directions.

The transverse wave, propagating in the direction of increase of coordinate x, y, z, which may interact with the electron beam directed along the z-axis, contains the field components determined by the formulas

$$E_{01x} = j\frac{A}{4}e^{j\omega t - jk(x\cos\alpha + y\cos\beta + z\cos\gamma)}, \tag{8}$$

$$E_{01y} = -j\frac{\frac{m\pi}{a}\frac{n\pi}{b}}{k^2 - \frac{m^2\pi^2}{a^2}}\frac{A}{4}e^{j\omega t - jk(x\cos\alpha + y\cos\beta + z\cos\gamma)}, \tag{9}$$

$$E_{01z} = -j\frac{\beta_0\frac{m\pi}{a}}{k^2 - \frac{m^2\pi^2}{a^2}}\frac{A}{4}e^{j\omega t - jk(x\cos\alpha + y\cos\beta + z\cos\gamma)}, \tag{10}$$

$$H_{01y} = j\frac{\omega\varepsilon\beta_0}{k^2 - \frac{m^2\pi^2}{a^2}}\frac{A}{4}e^{j\omega t - jk(x\cos\alpha + y\cos\beta + z\cos\gamma)}, \tag{11}$$

$$H_{01z} = -j\frac{\omega\varepsilon\frac{n\pi}{b}}{k^2 - \frac{m^2\pi^2}{a^2}}\frac{A}{4}e^{j\omega t - jk(x\cos\alpha + y\cos\beta + z\cos\gamma)}, \tag{12}$$

where the directional cosines of the propagation vector equal

$$\cos\alpha = \frac{m\pi}{ak}; \quad \cos\beta = \frac{n\pi}{bk}; \quad \cos\gamma = \frac{\sqrt{k^2 - \frac{m^2\pi^2}{a^2} - \frac{n^2\pi^2}{b^2}}}{k} = \frac{\beta_0}{k}. \tag{13}$$

For this transverse wave, the ratio of the electric field E_{01} to the magnetic field H_{01} equals the wave impedance of the medium:

$$\frac{|E_{01}|}{|H_{01}|} = \frac{\sqrt{|E_{01x}|^2 + |E_{01y}|^2 + |E_{01z}|^2}}{\sqrt{|H_{01y}|^2 + |H_{01z}|^2}} = \sqrt{\frac{\mu}{\varepsilon}} \tag{14}$$

and the magnitude of the Umov-Poynting vector equals

$$\Pi_{01} = \frac{1}{2}\sqrt{\frac{\varepsilon}{\mu}}|E_{01}|^2. \tag{15}$$

In addition, the angle α, formed by the $\vec{E}_{01}$ vector with the x-axis, is defined by

$$\cos^2\alpha_1 = \frac{|E_{01x}|^2}{|E_{01}|^2} = \sin^2\alpha. \tag{16}$$

On the basis of equations (1), (7), (13), (15) and (16), one may obtain the following expression for the coupling coefficient of a transverse interaction tube

$$K_c = \frac{k^2}{\frac{m^2\pi^2}{a^2}}\sin^2\alpha = \frac{\omega\varepsilon|E_{01}|^2\cos^2\alpha_1}{2\frac{m\pi}{a}\Pi_{01}\cos\alpha}, \tag{17}$$

where

Equation (17) enables us to describe the physical picture of the tube operation and to establish an analogy between the transverse interaction tube and the traveling-wave tube.

It follows that (17) the amplification of the field in the transverse interaction tube can be considered as a consequence of the interaction of the electron beam with the (Brillouin) partial wave, which is propagated at a certain angle from the direction of electron motion.

With the aid of a calculation similar to the above, it can be easily shown [3] that for the coupling coefficient of the usual traveling-wave tube with longitudinal interaction (electron beam in the direction of power flux in the waveguide), the following expression is valid:

$$K_c\mathrm{TWT} = \frac{k^2 - \beta_0^2}{\beta_0^2} = \frac{\omega\varepsilon\,|E_{01}|^2\cos^2\gamma_1}{2\beta_0\Pi_{01}\cos\gamma}. \tag{18}$$

In the derivation of equation (18) we retain the notation adopted above and by γ_1 we denote the angle between the direction of the electric field vector ($\vec{E}_{01}$) of the Brillouin wave and the z-axis.

Acomparison of Equation (17) and (18) shows the generality of the mechanism of interaction in the transverse interaction and traveling-wave tubes.

The result expounded in this paper can also be treated as a generalization of the expression for K_c in the case of interaction of the electron beam and traveling wave moving in different directions.

In conclusion we note that in the case of a waveguide of a transverse interaction tube, adopted in [1], the value of the deceleration coefficient of the space field charge Γ equaling unity, can be based on the agreement of the wave equations for the total field E_x, the circuital vector part of this field E_x^c and the variable component of the current i_1. We point out that the values of η_{opt} given in [1] are obtained when MK_c = const.

REFERENCES

1. L.N. Loshakov, Theory of a micjowave electron device with transverse interaction, Radiotekhnika i elektronika, 1960, 5, 9, 1448.

2. B.A. Vvedenskiy, A.G. Arenberg, Radio Waveguides, Pt.1, OGIZ, 1946, 60-61.
3. L.N. Loshakov, Approximate calculation of propagation constants in transmission lines in the presence of an electron beam. Zh. Tekh. Fiz. 1956, 26, 4, 809.

Submitted to the editors 17 October 1960

PLASMA MOTION IN CROSSED ELECTRIC AND MAGNETIC FIELDS*

A.K. Musin

We consider several special cases of plasma motion in crossed electric and magnetic fields in stationary and nonstationary regimes with viscosity. Formulae suitable for analysis and calculations are obtained, and graphs are plotted of the velocity as a function of the magnitude of the external magnetic field. The "induced saturation" of the velocity in a strong magnetic field is discussed.

INTRODUCTION

The subject of plasma motion in external fields has been given a great deal of attention recently in connection with various problems of theoretical and experimental physics [1]. In particular the possibility is repeatedly discussed of using the "cold" (T ≃ 10°K) of a moving plasma to build thermoelectric energy converters, magnetohydrodynamic generators, microwave devices — oscillators, phase-inverting and phase-shifting apparatus [2].

We will discuss the motion of a viscous conductive medium in a magnetic field in the presence of a flat current layer created by an external electric field, and we will explain several features of its motion in the stationary and nonstationary cases. In addition, we will assume that the physical properties of the moving medium remain constant during the entire motion and that the conditions for the applicability of the equations of magnetohydrodynamics are fulfilled.**

We will write the equations of momentum and magnetic induction in symmetrical form:

$$\vec{u}_t + w_\alpha \vec{u}_{x_\alpha} + \vec{e}_\alpha \Phi_{x_\alpha} = (a\vec{u} + b\vec{w})_{x_\alpha x_\alpha}, \qquad (1)$$

$$\vec{w}_t + u_\alpha \vec{w}_{x_\alpha} + \vec{e}_\alpha \Phi_{x_\alpha} = (a\vec{w} + b\vec{u})_{x_\alpha x_\alpha},$$

where we introduce the notation [3]

$$\vec{u} = \vec{v} + \frac{\vec{H}}{\sqrt{4\pi\rho}}; \qquad \Phi = \frac{p}{\rho} + (\vec{u} - \vec{w})^2/8;$$

$$\vec{w} = \vec{v} - \frac{\vec{H}}{\sqrt{4\pi\rho}}; \qquad 2a = \nu + \nu_m; \qquad 2b = \nu - \nu_m; \qquad (2)$$

$\vec{e}_\alpha$ are unit vector along the axes x_α; $\alpha = 1, 2, 3$; the remaining notation in equations (1) and

---

*A portion of the results of this paper was reported in the Second All-Union Conference of Theoretical and Applied Magnetohydrodynamics, (Riga, June, 1960).

**As we know, the condition of the applicability of the hydrodynamic approximation is the requirement $\lambda \ll R$, i.e., the length of the mean free path of the particles must be many times smaller than the characteristic dimensions of the problem R. For a plasma in a strong magnetic field there exists a second characteristic length r_L the Larmor radius. At $r_L \ll R$ the magnetohydrodynamical equations are valid, if the frequency of external fields is substantially less than the characteristic frequencies (the plasma frequency $\omega_0 = \sqrt{4\pi e_0^2 n/M}$ and the Larmor frequency $\omega_L = e_0 H/Mc_0$.

(2) are conventional.*The physical meaning of the functions $\vec{u}\,(t, x_\alpha)$ and $\vec{w}\,(t, x_\alpha)$ may be seen by introducing two magnetohydrodynamic waves which are propagated in opposite directions with different speeds $\vec{v}_A = \pm \vec{H} / \sqrt{4\pi\rho}$. Since the excitations in the conducting medium with constant physical properties are propagated with speeds not exceeding $2\vec{v}_A$, these waves do not interact with one another. In the stationary case, this leads to the fact that the problem of integration of a joint system of equations reduces to an integration of several independent equations. In the nonstationary case, with certain peculiar assumptions, the problem may also be simplified.

1. STEADY-STATE MOTION WITH A TRANSVERSE CURRENT LAYER.

Suppose a viscous conducting gas moves along the x_1 axis between the nonconducting planes $x_3 = \pm R$; the external uniform magnetic field is directed along the x_3 axis; the direction of the external electric field coincides with the x_2 axis, so that in the x_2 direction a constant current flows in the current layer with a linear current density $\vec{j}_0$. The lines of force of the transverse magnetic field are carried along by the motion of the conducting gas, and consequently there emerges a longitudinal magnetic field $H_1 \parallel x_1$. In addition, all the quantities, except for the possible exception of the total pressure $p^* = \rho\Phi = p + (H_3^2 + H_1^2)/8\pi$, do not depend on x_1, and the following conditions are fulfilled:

$$u_2 = w_2 = 0,\ u_3 = -w_3 = H_3/\sqrt{4\pi\rho},$$
$$u_1 = u_1(x_3),\ w_1 = w_1(x_3),\ w_3 = w_3(x_3),\ u_3 = u_3(x_3),\ \Phi_{x_1} = \Phi_{x_1}(x_1). \tag{3}$$

From the equation of continuity $(\rho v_\alpha)x\alpha = 0$, the equation of state for an ideal gas $p = R\rho T$ and the solenoidal condition for the magnetic field $H_\alpha x_\alpha = 0$, we find

$$\rho = \text{const},\ \Phi_{x_1} = \text{const},\ u_3 = \text{const},\ w_3 = \text{const}. \tag{4}$$

From the general equations (1) and conditions (3) for the problem, we obtain

$$\alpha u_{1x_3x_3} + H_3 u_{1x_3} = \Phi_{x_1}\beta,$$
$$\alpha w_{1x_3x_3} - H_3 w_{1x_3} = \Phi_{x_1}\beta. \tag{5}$$

For convenience we use a notation somewhat different from (2):

$$u_1 = v_1 + H_1\sqrt{\nu_m/4\pi\rho\nu};\ \alpha = \sqrt{4\pi\rho\nu\nu_m};$$
$$w_1 = v_1 - H_1\sqrt{\nu_m/4\pi\rho\nu};\ \beta = \sqrt{4\pi\rho\nu_m/\nu}. \tag{6}$$

By virtue of the continuity of the tangential components of the magnetic field in the absence of surface currents and because of adhesion of the viscous gas to the surface boundaries, we hav

$$u_1|_{x_3=R} = -u_1|_{x_3=-R} = -w_1|_{x_3=R} = w_1|_{x_3=-R} = \frac{2\pi j_0\sqrt{4\pi\rho\nu}}{c_0\sqrt{\nu_m}}. \tag{7}$$

Adapting the solution of system (5) to conditions (7) and changing to the quantities $v_1(x_3)$ and $H_1(x_3)$, we obtain

$$v_1(x_3) = \sqrt{\frac{4\pi\nu_m}{\rho\nu}}\left(\frac{j_0}{c_0} - \frac{2Rp^*_{x_1}}{H_3}\right)\frac{\operatorname{sh} L(R+x_3)\operatorname{sh} L(R-x_3)}{\operatorname{sh} L_1},$$
$$H_1(x_3) = \frac{2j_0\pi}{c_0}\left(1 - \frac{\operatorname{sh} L(R-x_3)\operatorname{ch} L(R+x_3)}{\operatorname{sh} L_1}\right) -$$
$$-\frac{4\pi p^*_{x_1}}{H_3}\left(1 - \frac{\operatorname{sh} L(R-x_3)\operatorname{ch} L(R+x_3)}{\operatorname{sh} L_1} - \frac{x_3}{R}\right). \tag{8}$$

---

*Hereafter, the notation is made compact by denoting the variables by the corresponding indices and by repeating indices for summations (for example, $u_\alpha \vec{w}_{x_\alpha} = \sum_{\alpha=1}^{3} u_\alpha\,(\partial\vec{w}/\partial x_\alpha)$).

Here

We will consider two special cases: (p) is the external electric field $\vec{E}_2 = 0$, $p^*_{x_1} \neq \neq 0$, (m) is the gas pressure is constant everywhere, i.e., $p^*_{x_1} = 0$, but $\vec{E}_2 \neq 0$.

In case (p) the total current in the direction of the x_2 axis is found to be equal to zero, and the first terms in (8) disappear. In this case the motion of the gas is due to a gradient of the total pressure $p^*_{x_1}$, and the expressions for the speed $v_1^{(p)}(x_3)$ and magnetic field $H_1^{(p)}(x_3)$, obtained from (8), are solutions of the problem [4].

In case (m) the total pressure $p^* = p + (H_3^2 + H_1^2)/8\pi = \text{const}$, in (8) the last terms vanish, and for velocity $v_1^{(m)}(x_3)$ and magnetic field $H_1^{(m)}(x_3)$ we have

$$v_1^{(m)}(x_3) = \sqrt{\frac{\pi\nu_m}{\rho\nu}} \frac{j_0}{c_0 \operatorname{sh} L_1} \left(\operatorname{ch} L_1 - \operatorname{ch} L_1 \frac{x_3}{R} \right),$$
$$H_1^{(m)}(x_3) = \frac{2\pi j_0}{c_0} \left(1 - \frac{\operatorname{sh} L(R - x_3) \operatorname{ch} L(R + x_3)}{\operatorname{sh} L_1} \right). \tag{9}$$

In this case the gas motion is wholly determined for the current density in the current layer. For the rate of movement of gas in the plane $x_3 = 0$ $(v_{10}^{(m)})$ and the velocity averaged over the cross-section $\bar{v}_1^{(m)}$ respectively, we obtain

$$v_{10}^{(m)} = \sqrt{\frac{\pi\nu_m}{\rho\nu}} \frac{j_0}{c_0} \operatorname{th} \frac{L_1}{2}, \quad \bar{v}_1^{(m)} = \frac{2\pi\nu_m j_0}{c_0 H_3 R} (L_1 \operatorname{cth} L_1 - 1). \tag{10}$$

The criterion of the degree of influence of the external magnetic field on the movement of the gas is the number $L_1 = H_3 R / \sqrt{4\pi\nu_m \nu\rho}$. When $L_1 \ll 1$ (weak magnetic fields and heavy viscous gases with low conductivity) the rates of movement in cases (m) and (p) have the form

$$v_1^{(m)} \simeq \frac{H_3 j_0 R}{4\nu\rho c_0} \left(1 - \frac{x_3^2}{R^2} \right), \quad \bar{v}_1^{(m)} \simeq \frac{j_0 H_3 R}{6\rho\nu c_0} = \frac{3}{2} v_{10}^{(m)},$$
$$v_1^{(p)} \simeq \frac{R^2 p^*_{x_1}}{2\rho\nu} \left(\frac{x_3^2}{R^2} - 1 \right), \quad \bar{v}_1^{(p)} \simeq -\frac{R^2 p^*_{x_1}}{3\rho\nu} = \frac{3}{2} v_{10}^{(p)}. \tag{11}$$

Here the dynamical viscosity prevails over the induction drag, and the streamlines, just as in nonmagnetohycrodynamics, are parabolic. The quantity $v_1^{(m)}$ is proportional to the external magnetic field intensity H_3, but $v_1^{(p)}$ does not depend on the magnetic field. at $L_1 \gg 1$ (large magnetic field and strongly ionized gases), for $v_1^{(m)}$ and $v_1^{(p)}$ we have

$$v_1^{(m)} \simeq j_0 \sqrt{\frac{\pi\nu_m}{\rho\nu c_0^2}} \left\{ 1 - \exp\left[L_1 \left(\frac{|x_3|}{R} - 1 \right) \right] \right\}, \quad \bar{v}_1^{(m)} \simeq \frac{2\pi\nu_m j_0 (L_1 - 1)}{c_0 R H_3} \simeq v_{10}^{(m)},$$
$$v_1^{(p)} \simeq -\frac{R p^*_{x_1}}{H_3} \sqrt{\frac{4\pi\nu_m}{\rho\nu}} \left\{ 1 - \exp\left[L_1 \left(\frac{|x_3|}{R} - 1 \right) \right] \right\}, \quad \bar{v}_1^{(p)} \simeq -\frac{4\pi\nu_m p^*_{x_1} (L_1 - 1)}{H_3^2} \simeq v_{10}^{(p)}, \tag{12}$$

i.e., $v_1^{(p)}$ decreases as we increase the external magnetic field $\vec{H}_3$, but $v_1^{(m)}$ ceases to depend on $\vec{H}_3$ and reaches saturation. In this case viscosity does not play a significant role, except at a thin layer at the walls, and the stream line is greatly smoothed due to induction drag. Instead of the usual parabolic stream line, this streamline has an almost flat central part and exhibits a sharp decrease in velocity close to the boundary surfaces. This phenomenon is related to the fact that the electromagnetic force $\vec{f}_H$ of the interaction of induction currents with the external magnetic field turns out to be proportional to the magnitude of $\bar{v}_1 - v_1$ and at $v_1 < \bar{v}_1$ $\vec{f}_H > 0$, but at $v_1 > \bar{v}_1$ $\vec{f}_H < 0$. Consequently, the force a $\vec{f}_H$ accelerates the particles of the gas, moving with velocity $v_1 < \bar{v}_1$, and retards those particles for which $v_1 > \bar{v}_1$. Figures 1 and 2 depict the functions $v_1(x_3)$ and $\vec{H}_1(x_3)$ for the cases (m) and (p).

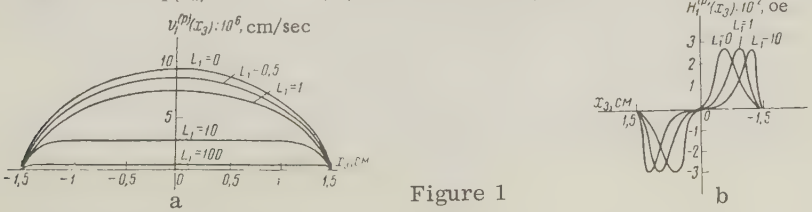

a Figure 1 b

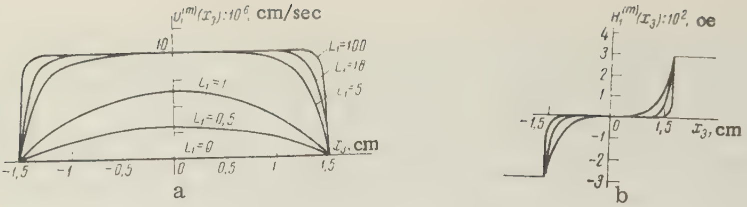

Figure 2

2. NONSTATIONARY MOTION WITH AN ALTERNATING CURRENT LAYER

Suppose the alternating electric field $\vec{E}(t)$ acts parallel to the x_2 axis, so that in the space under consideration an alternating current flows in a flat current layer with a magnitude of current per unit length in the direction of the x_1 axis of

$$\vec{j}(t) = \vec{j}_0 \exp i(\omega t + \varphi). \tag{13}$$

As before, the magnetic field is parallel to the x_3 axis; the motion takes place along the x_1 axis and is constrained by the planes $x_3 = \pm R$.

Projecting equations (1) on the x_1 axis, we obtain a fundamental system of equations for the nonstationary problem:

$$\begin{gathered} u_{1t} + w_3 u_{1x_3} + \Phi_{x_1} = a u_{1x_3x_3} + b w_{1x_3x_3}, \\ w_{1t} + u_3 w_{1x_3} + \Phi_{x_1} = a w_{1x_3x_3} + b u_{1x_3x_3}. \end{gathered} \tag{14}$$

At $t \leq 0$ suppose the electric field is absent and motion takes place under the influence of a constant pressure gradient $\partial p^*/\partial x_1 = \text{const} \neq 0$, i.e.,

$$u_1(t, x_3)|_{t=0} = \tilde{u}_1(x_3), \quad w_1(t, x_3)|_{t=0} = \tilde{w}_1(x_3). \tag{15}$$

Here $\tilde{u}_1(x_3)$ and $\tilde{w}_1(x_3)$ are stationary solutions of equation (14) in the absence of a current layer and are obtained from equation (8) when $j_0 = 0$. As boundary conditions analogous to (7) write

$$\begin{gathered} u_1(t, x_3)|_{x_3=R} = -u_1(t, x_3)|_{x_3=-R} = -w_1(t, x_3)|_{x_3=R} = \\ = w_1(t, x_3)|_{x_3=-R} = \frac{h_0(t)}{\sqrt{4\pi\rho}}, \end{gathered} \tag{16}$$

where $h_0(t) = (2\pi/c_0)\, j_0 \exp i(\omega t + \varphi)$. With the aid of the operator equation (15)

$$s^n u - \{u^{(n)}(\lambda)\} = \sum_{m-1}^{n} s^{m-1}\{u^{(n-m)}(0)\}; \quad m = 1, \ldots, n, \tag{17}$$

where s is the operator of differentiation with respect to the variable λ, equations (14) can be reduced to an algebraic system

$$\begin{gathered} u(k + w_3 s - as^2) + wbs^2 = \Phi_1(s, k), \\ ubs^2 + w(k + u_3 s - as^2) = \Phi_2(s, k), \\ \Phi_1(s, k) = -\frac{\Phi_{x_1}}{sk} + u_0 + u^0(w_3 - as) - au^0_{x_3} - w^0 bs - bw^0_{x_3}, \\ \Phi_2(s, k) = -\frac{\Phi_{x_1}}{sk} + w_0 + w^0(u_3 - as) - aw^0_{x_3} - bsu^0 - bu^0_{x_3}. \end{gathered} \tag{18}$$

Here k and s are differentiation operators with respect to the variables t and x_3; the values of u_0 and w_0 designate the initial operator values of the functions $u_1(t_1 x_3)$ and $w_1(t_1 x_3)$ with respect to the variable t, and the quantities u^0, w^0, $u^0_{x_3}$, $w^0_{x_3}$ play the role of initial operator values of the corresponding functions with respect to variable x_3. After a single application of equation (17) subject to conditions (16) there results

$$u(x_3)|_{x_3=R} = -u(x_3)|_{x_3=-R} = -w(x_3)|_{x_3=R} = w(x_3)|_{x_3=-R} = \frac{h(k)}{\sqrt{4\pi\rho}}, \tag{19}$$

where $h(k) = 2\pi j_0 \exp i(\varphi + \operatorname{arc\,tg} \omega/k) / c_0 (\omega^2 + k^2)^{1/2}$. It is convenient to introduce, for simplicity of calculation, the additional relations resulting by virtue of well-known theorems of analysis from the symmetry of the problems and conditions (19):

$$(u_{x_3} + w_{x_3})|_{x_3=0} = (u - w)|_{x_3=0} = 0. \tag{20}$$

representing the solution of system (18) in the form of a fractional rational function relative to operator s. Expanding equation (18) into simple fractions, with the aid of a formula from [15]

$$\frac{s-p}{(s-p)^2 - b^2} = \{e^{px_3} \operatorname{ch} bx_3\}, \quad \frac{1}{s-p} = \{e^{px_3}\} \tag{21}$$

we obtain a solution of system (14), expressed in terms of the operator function $u(x_3) = \{u_1(t, x_3)\}$ and $w(x_3) = \{w_1(t, x_3)$. Adapting this solution to conditions (19) and (20), after simple transformations we obtain an expression for the operator functions $v(x_3, k)$ and $H(x_3, k)$:

$$\begin{gathered} v(x_3, k) = M_2 + M_1 \operatorname{ch} 2Lx_3 + (p_1 G_3 \operatorname{ch} p_1 x_3 - p_3 G_1 \operatorname{ch} p_3 x_3)/A p_1 p_3 B(k), \\ H(x_3, k) = \{[(k - \nu p_1^2) G_3 \operatorname{sh} p_1 x_3 - (k - \nu p_3^2) G_1 \operatorname{sh} p_3 x_3]/A^2 p_1 p_3 B(k)\} + \\ + (v_A^2/\lambda \sqrt{4\pi\rho}) \left[M_3 + M_1 \left(k - \frac{v_A^2}{\nu_m} \right) \right] \operatorname{sh} 2Lx_3 + (M_4 + kM_2)(x_3/A). \end{gathered} \tag{22}$$

Here we adopt the notation

$$\begin{gathered} G_i(k) = Ap_i(b_0 + h(k)) \operatorname{ch} Rp_i + (k - \nu p_i^2)(M_2 + M_1 \operatorname{ch} L_1) \operatorname{sh} Rp_i; \; i = 1, 3; \\ p_{1,3}(k) = (\sqrt{2ak + v_A^2 + 2|k|\lambda} \pm \sqrt{2ak + v_A^2 - 2|k|\lambda})/\lambda; \\ b_0(k) = (v_A^2/\lambda \sqrt{4\pi\rho}) \left[M_3 + M_1 \left(k - \frac{v_A^2}{\nu_m} \right) \right] \operatorname{sh} L_1 - [R(M_4 + kM_2)/A]; \\ B(k) = [(k - \nu p_1^2) \operatorname{sh} Rp_1 \operatorname{ch} Rp_3/Ap_1] - (k - \nu p_3^2) \operatorname{sh} Rp_3 \operatorname{ch} Rp_1/Ap_3; \\ M_1 = p_{x_1}^* \left[(L/\lambda^2 \rho) + \alpha_3 \left(k - \frac{v_A^2}{\nu_m} \right) / \lambda^2 \right] / [(2L)^4 + \alpha_1 (2L)^2 + \alpha_2]; \\ M_2 = (-p_{x_1}^* \alpha_3 \operatorname{ch} L_1)/\alpha_2; \; M_3 = -p_{x_1}^* \alpha_3; \; M_4 = (p_{x_1 0}^*/\rho k) + p_{x_1}^* \alpha_3 \operatorname{ch} L_1; \\ \alpha_1 = -(2ak + v_A^2)/\lambda^2; \; \alpha_2 = (k/\lambda)^2; \; \alpha_3 = 2R \sqrt{\pi \nu_m}/H_3 \sqrt{\rho\nu} \operatorname{sh} L_1; \\ A = H_3/4\pi\rho; \; \lambda^2 = \nu\nu_m; \; v_A^2 = H_3^2/4\pi\rho; \; 2a = \nu + \nu_m. \end{gathered}$$

From a representation of the solution in the form of operator functions $v(x_3, k)$, $H(x_3 k)$ we may now change to a solution in the symbols of classical analysis in the form of initial functions $v_1(t, x_3)$ $H_1(t, x_3)$, which use formulae similar to (21). In the general case, however, the formulae obtained are rather complex, and during analysis it is best to use directly the simple operator solution (22). Depending on the character of the active driving forces and the condition of motion from the general solution (22), we may visualize certain special cases. Below we will consider the motion in the case of two special assumptions. The remaining cases can be treated in an analogous fashion.

a) Suppose the external field equals zero; no current layer exists. At the moment $t = 0$ there arises a constant and uniform pressure gradient $p^*x_1 0$, equal to zero when $t < 0$ ($p^*x_1 = 0$). In this case active electromagnetic forces are absent, and the motion occurs only under the influence of hydrodynamical pressure forces. * Under these conditions

$$\begin{gathered} M_1 = M_2 = M_3 = 0, \; M_4 = p_{x_1 0}^*/\rho k, \; b_0(k) = -Rp_{x_1 0}^*/A\rho k, \; h(k) = 0, \; G_i = \\ = Ap_i b_0 \operatorname{ch} Rp_i, \; i = 1.3. \end{gathered}$$

---

*Such a problem is considered in [6] and, taking into account induction currents at the boundary surfaces, in [7].

Expressions (22) are simplified and are brought into the form

$$v(x_3, k) = N_1(k)\, p_1 p_3 (\mathrm{ch} p_3 R \mathrm{ch} p_1 x_3 - \mathrm{ch} R p_1 \mathrm{ch} p_3 x_3) / D_1(k), \tag{23}$$

$$H(x_3, k) = (N_2(k) / D_1(k)) \Big[p_3 (k - \nu p_1^2) \mathrm{ch} R p_3 \mathrm{sh} p_1 x_3 - p_1 (k - \nu p_3^2) \mathrm{ch} R p_1 \mathrm{sh} p_3 x_3 - D_1(k) \frac{x_3}{R} \Big],$$

where

$$D_1(k) = p_3 (k - \nu p_1^2) \mathrm{sh} R p_1 \mathrm{ch} R p_3 - p_1 (k - \nu p_3^2) \mathrm{sh} p_3 R \mathrm{ch} R p_1;$$

$$N_1(k) = -R p^*_{x_1 0} / \rho k; \qquad N_2(k) = -4\pi R p^*_{x_1 0} / k H_3.$$

Formulae (23) are operator solutions of the stated problem. In this case the role of the external magnetic field is to create induction currents in the moving conductive medium. As a result of induction drag, the velocity in the external magnetic field is less than in the absence of a magnetic field, so that with a rise in the magnetic field strength the velocity decreases. The magnetic field in this case smooths the streamline just as it does in the case of stationary motion (see Figure 1)

b) Now suppose the gradient of the total pressure equals zero and in (19) $\varphi = \pi/2$. In this case the motion takes place only under the influence of electromagnetic forces of interaction between the external magnetic field and the current layer, due to the external alternating electric field. In this case $M_j = b_0 = 0$ ($j = 1,2,3,4$), $G_i = Ap_i\, h(k)\, \mathrm{ch}\, Rp_i$ ($i = 1,3$), $h(k) = 2\pi j_0 \cdot \omega / c_0 (k^2 + \omega^2)\ 1/2$, and from the general solution of (22), we obtain an operator solution in the form

$$v(x_3) = F_1 p_1 p_3 (\mathrm{ch}\, R p_1\, \mathrm{ch}\, p_3 x_3 - \mathrm{ch}\, R p_3\, \mathrm{ch}\, p_1 x_3) / D_2(k); \tag{24}$$

$$H(x_3) = F_2 [p_1 (k - \nu p_3^2)\, \mathrm{ch}\, R p_1\, \mathrm{sh}\, p_3 x_3 - p_3 (k - \nu p_1^2)\, \mathrm{ch}\, R p_3\, \mathrm{sh}\, p_1 x_3] / D_2(k),$$

where

$$D_2(k) = D_1(k)(k^2 + \omega^2); \quad F_1 = j_0 \omega H_3 / 2 c_0 \rho; \quad F_2 = 2\pi j_0 \omega / c_0.$$

From the operator functions $v(x_3)$ and $H(x_3)$ with the aid of well-known theorems of contour integration (see, for example [8]), we go over to the initial functions $v_1(t, x_3)$ and $H_1(t, x_3)$

$$v_1(t, x_3) = \left\{ \frac{F_1 \exp(kt)\, p_1 p_3}{\partial D_2 / \partial k} (\mathrm{ch}\, p_1 R\, \mathrm{ch}\, p_3 x_3 - \mathrm{ch}\, p_3 R\, \mathrm{ch}\, p_1 x_3) \right\}_{k = k_i}, \tag{25}$$

$$H_1(t, x_3) = \left\{ \frac{F_2 \exp(kt)}{\partial D_2 / \partial k} [p_1 (k - \nu p_3^2)\, \mathrm{ch}\, p_1 R\, \mathrm{sh}\, p_3 x_3 - p_3 (k - \nu p_1^2)\, \mathrm{ch}\, p_3 R\, \mathrm{sh}\, p_1 x_3] \right\}_{k = k_i}.$$

Here k_1 are the roots of the equation $D_2(k) = 0$; the summation is carried out over i.

Formulae (25), which give an accurate solution of the stated problem, are rather complex With certain assumptions with respect to the flow parameters they can be simplified. Suppose for example, inequality $\sigma\nu \ll c_0^2 / 4\pi\mu$, is fulfilled, i.e., the viscosity and conductivity of the medium are not too large and that the magnetic viscosity is considerably greater than the kinematic viscosity. Then, after appropriate simplifications and excluding the real part, the formula for the velocity at the axis of flow $v_{10}(t)$ can be presented in analytic form:

$$v_{10}(t) = G \frac{[\gamma_1 \mathrm{sh} \gamma_2 + \gamma_2 \sin(R\gamma_2 / \sqrt{2}\lambda)] \sin\omega t + [\gamma_1 \sin(R\gamma_2 / \lambda\sqrt{2}) - \gamma_2 \mathrm{sh} \gamma_1] \cos\omega t}{\mathrm{ch} \gamma_1 + \cos(R\gamma_2 / \lambda\sqrt{2})}, \tag{26}$$

where

$$\gamma_{1,2} = [(H_3^4 + (4\pi\rho\omega\nu_m)^2)^{1/2} \pm H_3^2]^{1/2} / \sqrt{4\pi\rho};$$

$$G = j_0 H_3 \sqrt{2\nu_m / \nu} / 4\rho c_0 (v_A^4 + (\omega\nu_m)^2)^{1/2}.$$

Equation (26) is convenient for calculations and retains sufficient generality, being correct for arbitrary values of magnetic field and the density of the medium at which the equations of magnetic hydrodynamics are still applicable.

A further simplification is possible, if we require that $(\omega\nu_m/v^2_A)^2 \ll 1$ and in (26) neglect the value of $(\omega\nu_m/v^2_A)^2$ in comparison with unity. This can be done at a rather large external magnetic field and at small densities. Then for the maximum velocity on the flow axis, achievable at the moment $t \simeq \varphi\omega = \pi\omega/2$, we observe a simple formula convenient for analysis and calculation and correct for rather large external magnetic fields:

$$v_0 = \frac{j_0\sqrt{\pi\nu_m}\,(\mathrm{sh}\,2\delta_1\cos\delta_2 + \sin\delta_2\sin 2\delta_3)}{2c_0\sqrt{\rho\nu}\,(\mathrm{sh}^2\delta_1\sin^2\delta_3 + \mathrm{ch}^2\delta_1\cos^2\delta_3)}, \tag{27}$$

where

$$\delta_1 = Rv_A/2\lambda\,; \qquad \delta_2 = \omega\nu_m/2v_A^2\,; \qquad \delta_3 = R\omega\nu_m/4\lambda v_A\,.$$

Figure 3 shows curves calculated from equation (27) for a single value of current layer in the current layer $j_0 = 430$ amp/cm and at different values of density of the medium ρ (here ρ plays the role of a parameter). The behavior of these curves is easy to understand, if in (27) we neglect the value of $\omega\nu_m/v_A^2$ in comparison with unity. which can be done for magnetic field such that the inequality $\omega\nu_m/v_A^2 \ll 1$ is fulfilled. Then from (27) we obtain for the maximum velocity

$$v_0 = \frac{j_0\sqrt{\pi\nu_m}[\exp(RH_3/2\lambda\sqrt{\pi\rho}) - 1]}{c_0\sqrt{\rho\nu}[\exp(RH_3/2\lambda\sqrt{\pi\rho}) + 1]} = \frac{j_0\sqrt{\pi\nu_m}}{c_0\sqrt{\rho\nu}}\,\mathrm{th}\,\frac{RH_3}{4\lambda\sqrt{\pi\rho}}\,. \tag{28}$$

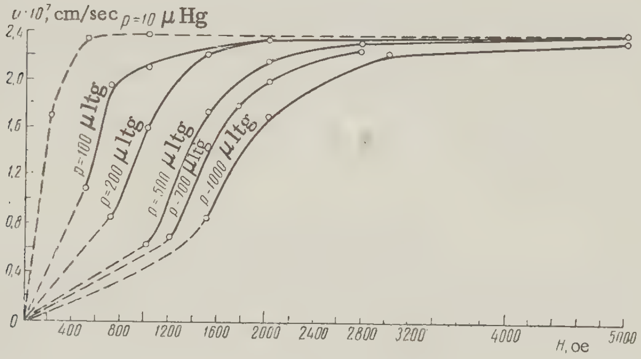

Figure 3

From this it is apparent that the velocity tends asymptotically with increasing magnetic field to a certain limiting value

$$v_{\lim} = j_0\sqrt{\pi\nu_m}/c_0\sqrt{\rho\nu}\,, \tag{29}$$

i.e., at large magnetic fields, the velocity ceases to depend on the magnetic field and saturation sets in. The smaller the density of the medium the smaller the value of the magnetic field at which saturation sets in. Physically, the meaning of this phenomenon is that as the field increases its accelerating action is counteracted gradually by induction drag as a result of the interaction between it and increasing induction currents.

At sufficiently small densities and slow variations of the electric current $\vec{j}(t)$, the velocity ceases to depend on the density of the medium. This is explained by the smallness of the inertial terms under these conditions, and resistance to motion is determined by the viscous dissipation. The limiting velocity v_{lim} depends only on the amplitude of j_0 the electric current flowing through the medium, the conductivity of the medium σ, and the dynamic viscosity of the gas $\rho\nu$ and does not depend on the density of the medium ρ.

At those densities of the medium at which the variation of the velocity with density does not vanish, this relation is rather complex, but the velocity of the movement changes approximately proportional to $\rho^{-1/2}$. The increase of linear current density in the current layer, other conditions being the same, increases the velocity.

It is apparent from (28) and Figure 3 that the limiting velocity is attained later (i.e., in stronger magnetic fields, the greater the density of the medium ρ. From this it is clear that an increase of the magnetic field beyond values at which saturation sets in. although not allowing an increase of velocity at constant j_0, does permit a larger mass to be set in motion.

In order to verify the results experimentally, the theory of plasma motion accelerated in crossed electric and magnetic fields was investigated experimentally [9]. It was established that the velocity of the plasma motion increases with magnetic field intensity only up to a certain limit. The other results of the experiment were found to be in qualitative agreement with the theoretical conclusions [9].

CONCLUSION

1. In the absence of an external field, the mean velocity of a plasma increases with a decrease in the external magnetic field $(\vec{H})$ and reaches a maximum at $\vec{H} = 0$.

2. In the presence of a current layer, created by an external electric field, the velocity of the plasma increases with a rise in the external magnetic field and tends asymptotically to a limiting value determinable by: 1) linear current density j in a current layer 2) the conductivity σ, and 3) the dynamic viscosity of the plasma ν (the phenomenon of induction saturation.

3. With slow changes in the external electric field, the limiting value of velocity is independent of plasma density ρ and reaches larger magnetic fields, the greater ρ.

4. At high magnetic field intensities, a velocity equal to the limiting value can be transmitted to a large body of the gas. The basic conclusions of the theory are confirmed by experiment.

In conclusion the author expresses profound gratitude to V. L. Granovska for his guidance and valuable discussions.

REFERENCES

1. Works of the Second International Conference on the Peaceful Uses of Atomic Energy (Geneva, 1958), Moscow, 1959, Trudy 2-y Vsesoyuznoy konferentsii po teoreticheskoy i prikladnoy magnitnoy gidrodinamike, (Works of the Second All-Union Conference on Theoretical and Applied Magnetohydrodynamics (Riga, 1960), (Riga, 1961.
2. Foreign Radio Engineering, 1960, Vol. 3,4, (Materials of the Session of the Radio Engineering Institute (Boston, USA), 1959); J. L. Neuringer, J. Fluid Mechanics 1960, 7, 287.
3. W.M. Elsasser, Phys, Rev., 1950, 79, 183.
4. J. Hartmann, Def. Kgl. Danske Vidensk. Selskass, 1937, 15, 6.
5. Ya. Mikusinskiy ,Operational Calculus, IL, 1956.
6. S.A. Regirer,Inzhenerno-fiz, zh., 1959, 8, 43.
7. I.B. Chekmarev, ZhTF, 1960, 3, 338.
8. A.I. Markushevich, Theory of Analytic Functions, GTI, 1950.
9. L.S. Lomonosova, V.I. Servin, G.G. Timofeyeva,A.K. Musin and V. L. Granovskii, Investigation of the motion of a plasma accelerated in a crossed electric and magnetic field, Tr. 2-y Vsesoyuznoy konferentsii po teoreticheskoy i prikladnoy magnitnoy girodinamike, (Riga, 1960) Riga, 1961.

Submitted to the editors 15 August 1960

INFLUENCE OF PARASITIC PARAMETERS OF A SEMICONDUCTOR DIODE UPON THE OPERATION OF A PARAMETRIC AMPLIFIER

M.D. Karasev

General equations are found for a two-tank circuit parametric amplifier taking into account all the parasitic parameters, including parasitic inductance. In the case of small diode losses and a low percentage modulation of the time-varying capacitance, an analysis is given of the gain and noise figure. It is shown that in addition to losses introduced in the diode at the operating frequencies, additional coupling is formed, which, in the case of resonance caused by parasitic parameters of the diode, can greatly alter the operating conditions of the amplifier.

INTRODUCTION

In an account of parametric amplifiers having a nonlinear reactance, it is usually assumed that the reactive element does not have parasitic parameters [1,2,3]; as a last resort only its losses are taken into account [4]. At the same time, a real nonlinear reactive element has a complex structure which cannot always be replaced by a pure capacitance or inductance.

The diodes used at the present time are prepared in the fittings of a standard socket of a microwave mixer diode (Figure 1a). For frequencies not exceeding 10 Mc the design of Figure 1a can be presented in the form of an equivalent circuit with lumped parameters, as is done in Figure 1b [5]. With a sufficient pumping power supplied to the diode, which considerably exceeds the signal, one may assume the system to be linear with a time-varying capacitance. This assumption lies at the basis of subsequent calculations. We will assume that capacitance C changes sinusoidally in time with a pumping frequency of ω_0 i.e.,

$$C = C_0(1 + m\cos\omega_0 t) \equiv C_0 + \frac{\Delta C}{2}(e^{j\omega_0 t} + e^{-j\omega_0 t}), \tag{1}$$

where C_0 is the average capacitance; m is the percentage modulation $\Delta C = mC_0$ is the amplitude of the capacitance pulsation of the p-n junction.

Usually we know C_{max} the initial capacitance of the parametric diode at zero bias and C_{min} the capacitance of the highest permissible back bias.

In this case the parameters occuring in (1) will be expressed as

$$\left.\begin{aligned} C_0 &= \frac{C_{\max} + C_{\min}}{2}, \\ \Delta C &= \frac{C_{\max} - C_{\min}}{2}, \\ m &= \frac{C_{\max} - C_{\min}}{C_{\max} - C_{\min}}. \end{aligned}\right\} \tag{2}$$

In the equivalent circuit (Figure 1b), the inductance $L = 3(10)^{-3}$ μh at a frequency of 10^4 Mc has an inductive impedance of $\omega L \simeq 190$ ohms, and at an average capacitance of $C_0 = 0.2$ μμf the capacitive impedance of the p - n junction at the same frequency 10^4 Mc will be $(1/\omega C_0) \simeq 80$ ohms. From this, it is clear that it is impossible to neglect parasitic inductance at these frequencies, since its impedance is of the same order of magnitude as the capacitive impedance of the junction.

In linear electrical circuits with constant coefficients the RC circuit of series-connected capacitance C and resistance R (Figure 2a) can be replaced by a shunt capacitance C_1 and conductance g (Figure 2b). With sinusoidal frequency in one or more circuits, the complex impedance will be the same, if:

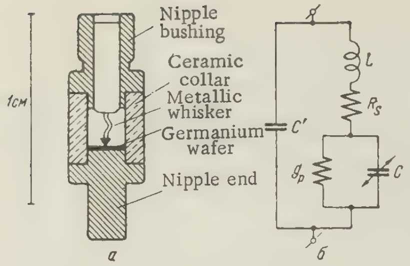

Figure 1

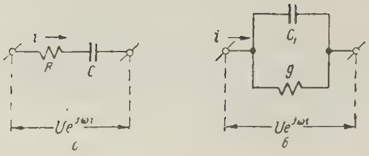

Figure 2

$$g = \frac{R}{R^2 + (1/\omega C)^2}, \qquad \omega C_1 = \frac{1/\omega C}{R^2 + (1/\omega C)^2}.$$

If the same linear circuit contains a time-varying element, however, this substitution is impossible in the general case, since the character of the processes in the circuits presented in Figures 2a and 2b is qualitatively different even with a pure sinusoidal frequency, Actually, in circuit Figure 2b under the action of the harmonic voltage Ue^{jwt} the following current flows:

$$i = Ie^{j\omega t} + I_+ e^{j(\omega+\omega_0)t} + I_- e^{j(\omega-\omega_0)t}, \tag{3}$$

which contains only three harmonic components; frequency of the voltage source ω and its combination frequencies $\omega \pm \omega_0$ with the frequency of the capacitance pulsation, the latter varies according to equation (1). The amplitude of the current components will equal, respectively,

$$I = (g + j\omega C_0)U, \quad I_+ = j(\omega + \omega_0)\frac{1}{2}\Delta CU,$$
$$I_- = j(\omega - \omega_0)\frac{1}{2}\Delta CU. \tag{4}$$

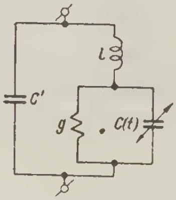

Figure 3

The same voltage Ue^{jwt} generates in the RC network of Figure 2a an infinite number of harmonic components with combination frequencies which contain harmonics of the frequency ω_0. Only in the case of sufficiently small losses and a low percentage modulation which satisfy the inequalities

$$\left.\begin{array}{l} R_s \ll \dfrac{1}{\omega C_0}, \\ g_p \ll \omega C_0, \\ m \ll 1, \end{array}\right\} \tag{5}$$

can one approximately represent a series RC circuit by an equivalent parallel circuit, as in the case of linear circuits with constant elements. When inequality (5) is fulfilled, the equivalent circuit represented by Figure 1b can be replaced approximately by the circuit shown in Figure 3 where

$$g = g_p + R_s(\omega C_0)^2. \tag{6}$$

There is tendency to assume that the conductance g_p in the circuit of Figure 1b may be neglected at high frequencies if we introduce a sufficiently large back bias on the diode. In that case, however, the diode losses are accounted for only by the series base resistance R_s, and, apparently, the effect of neglecting g_p is not entirely proportional to that of R_s. At high frequencies the base resistance R_s and capacitance of the p-n junction change little with frequency, whereas, according to experiment, p-n junction losses do change appreciably with frequency. Therefore, in order to approximate them merely by the resistance R_S one would have to assume that R_S varies with the frequency. But at high frequencies, losses in the dielectric semiconductor are added to the losses in the base conductivity and these losses change with frequency and are localized where the varying field is most intensive i.e., in the dielectric of the depletion layer of the p-n junction. Consequently, they must represent a conductivity which depends on the frequency and shunting capacitance of the junction. This is important for calculations, if the inequalities (5) are not fulfilled, and also in the determination of numerical values from equation (6), taking into account (5), where g_p depends on frequency.

1. BASIC RELATIONS

We will consider the equivalent circuit (Figure 4) of a two-tank circuit parametric amplifier, in which the coupling element is a semiconductor diode with parasitic parameters as in Figure 1b. In this circuit g_c designates the conductance of the harmonic signal source

$$i_c = I_c e^{j\omega_1 t}. \tag{7}$$

The equivalent conductance g_{k1}, takes into account the losses, and L_1, C_1 are the reactive conductance of the input circuit. g_{k_2}, L_2 and C_2 play the corresponding role in the output circuit. The load conductance is g_H. The capacitance C(t) varies with time according to equation (1)

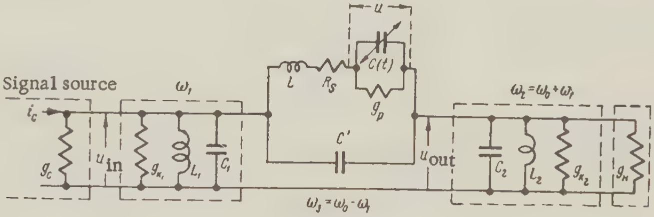

Figure 4

We will assume that the input circuit possesses a finite conductance only for currents with a frequency close to ω_1, for currents of all the remaining frequencies, including ω_0, ω_2, ω_3, it represents a short-circuit. Then in the case of signal (7), the voltage u_{in} will be harmonic

$$u_{in} = U_{in} e^{j\omega_1 t}. \tag{8}$$

If analogously the output circuit resonates only at the frequency ω_2, u_{out} will also be harmonic:

$$u_{out} = U_{out} e^{j\omega_2 t}. \tag{9}$$

At inductance L and resistance R_S, a voltage drop is created by currents of all frequencies, which are due to the presence of a pulsating capacitance. Thus, even under the assumption of an ideal circuit filter, we obtain by capacitance C(t) a complex spectrum of the combination frequencies. We introduce one more simplification. We assume that at the frequencies $2\omega_0$, $3\omega_0$, and above, the inductive impedance is so large and the capacitive impedance C_0 so small, that the voltages and currents at these frequencies, as well as the energies associated with them are negligibly small. Then assuming that

$$\omega_0 \gg \omega_1, \tag{10}$$

we may confine ourselves to currents of only three frequencies: ω_1, $\omega_2 = \omega_0 + \omega_1$ and $\omega_3 = \omega_0 - \omega_1$. The voltage u at the capacitance C(t) of the p-n junction can be approximated by a sum of only three components:

$$u = U_1 e^{j\omega_1 t} + U_2 e^{j\omega_2 t} + U_3 e^{j\omega_3 t}. \tag{11}$$

Furthermore, we will consider a summing amplifier. But the equations obtained below can be transformed simply into equations for a circuit with the difference frequency of the second circuit.

For a steady-state regime, by the total resistance method expounded in [6] , we may obtain a system of three equations

$$\left.\begin{aligned} & Y_1 U_1 + j\omega_1 \frac{\Delta C}{2} U_2 + j\omega_1 \frac{\Delta C}{2} U_3^* = I, \\ & j\omega_2 \frac{\Delta C}{2} U_1 + Y_2 U_2 + O = 0, \\ & - j\omega_3 \frac{\Delta C}{2} U_1 + O + Y_3^* U_3^* = 0. \end{aligned}\right\} \tag{12}$$

In equation (12) the following notation is adopted in accordance with Figure 4 just as for equations (7) and (9):

$$Y_1 = g_p(\omega_1) + j\omega_1 C_0 + \cfrac{1}{R_s(\omega_1) + \omega_1 L + \cfrac{1}{g_{\text{c}} + g_{\text{K}1} + j\left[\omega_1 (C_1 + C') - \cfrac{1}{\omega_1 L_1}\right]}},$$

$$Y_2 = g_p(\omega_2) + j\omega_2 C_0 + \cfrac{1}{R_s(\omega_2) + j\omega_2 L + \cfrac{1}{g_{\text{H}} + g_{\text{K}2} + j\left[\omega_2 (C_2 + C') - \cfrac{1}{\omega_2 L_2}\right]}},$$

$$Y_3 = g_p(\omega_3) + j\omega_3 C_0 + \frac{1}{R_s(\omega_3) + j\omega_3 L},$$

$$I = \frac{1}{1 + [R_s(\omega_1) + j\omega_1 L]\left\{g_{\text{c}} + g_{\text{K}1} + j\left[\omega_1 (C_1 + C') - \frac{1}{\omega_1 L_1}\right]\right\}} I_{\text{c}}.$$

In equations (12) the possibility of a different value of diode loss at various frequencies is considered, because the values of the shunt conductance g_p and the series resistance R_s are assumed to be frequency-dependent.

In analogy with the conventional electron-tube amplifier, the parametric amplifier can be represented by a small signal equivalent circuit suitable for calculations. The main difference in the case of a parametric amplifier lies in the necessity of using several equivalent circuits, because each frequency will have its own circuit.

Figure 5 shows three equivalent circuits for the parametric amplifier under consideration at the input frequency ω_1 (Figure 5a) ; at the output frequency ω_2 (Figure 5b) ; and at the difference frequency of the parasitic coupling ω_3 (Figure 5c).

In the equivalent circuit of Figure 5a, admittances Y_{12} and Y_{13} are complex, induced through parametric coupling from the output circuit and the circuit of the difference frequency on the parasitic parameters, respectively. They are expressed by the following relations

$$Y_{12} = \frac{\omega_1 \omega_2 \left(\frac{\Delta C}{2}\right)^2}{Y_2}, \tag{13}$$

$$Y_{13} = - \frac{\omega_1 \omega_3 \left(\frac{\Delta C}{2}\right)^2}{Y_3^*}. \tag{14}$$

According to the equivalent circuit of Figure 5a, it is easy to find the input impedance of the amplifier Z_{in}, which equals

$$Z_{\text{in}} = \frac{R_s(\omega_1) + j\omega_1 L +}{1 + [R_s(\omega_1) + j\omega_1 L]\left\{g_{\text{c}} + g_{\text{K}1} + j\left[\omega_1 (C_1 + C') - \frac{1}{\omega_1 L_1}\right]\right\}} \longrightarrow \ldots$$

$$\ldots \frac{+ \dfrac{1}{Y_{1\,\text{eq}}\left\{1 + [R_s(\omega_1) + j\omega_1 L]\left\{g_{\text{c}} + g_{\text{K}1} + j\left[\omega_1 (C_1 + C') - \frac{1}{\omega_1 L_1}\right]\right\}\right\}}}{1 + [R_s(\omega_1) + j\omega_1 L]\left\{g_{\text{c}} + g_{\text{K}1} + j\left[\omega_1 (C_1 + C') - \frac{1}{\omega_1 L_1}\right]\right\}}, \tag{15}$$

where

$$Y_{1\,\mathbf{eq}} = Y_1 + Y_{12} + Y_{13}.$$

In the equivalent circuit of Figure 5b, the input current equals

$$I_2 = -j\omega_3 \frac{\Delta C}{2} U_1. \tag{16}$$

The input voltage U_{out} equals

$$U_{\text{out}} = \frac{I_2}{Y_2} \frac{1}{1 + [R_s(\omega_2) + j\omega_2 L] \left\{ g_n + g_{K2} + j \left[\omega_2 (C_2 + C') - \frac{1}{\omega_2 L_2} \right] \right\}} \tag{17}$$

In the equivalent circuit of Figure 5c the input current I_3^* equals

$$I_3^* = -j\omega_3 \frac{\Delta C}{2} U_1. \tag{18}$$

The power amplification of the amplifier is defined as the ratio of the output power Pout at the frequency ω_2 to the input power P_{in} at the signal frequency ω_1. The input

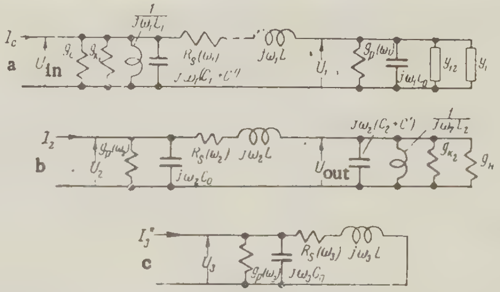

Figure 5

circuit power equals the ratio $\frac{P_{\text{in}}}{|I_c|^2/4g_c}$. The resulting gain in accordance with (15) and (18) will equal

$$G = \frac{P_{\text{out}}}{|I_c|^2/4g_c} =$$

$$= \frac{\omega_2}{\omega_1} \frac{4g_c g_H \omega_1 \omega_2 \left(\frac{\Delta C}{2}\right)^2}{|Y_{1\,\mathbf{eq}}|^2 |Y_2|^2 \left| 1 + [R_s(\omega_2) + j\omega_2 L] \left\{ g_H + g_{K2} + j \left[\omega_2 (C_2 + C') - \frac{1}{\omega_2 L_2} \right] \right\} \right|}. \tag{19}$$

If we introduce the thermal noise of the generator, due to conductances g_c, g_p, g_{k_1}, g_{k_2} and resistance R_S, we can also find in this fashion the noise factor of the amplifier under consideration.

2. SAMPLE CALCULATION

We will consider, as an example, an amplifier with signal frequency $\nu_0 = \omega_0/2\pi = 10^4$ Mc and a pumping frequency of $\nu_1 = \omega_1/2\pi = 10^3$ Mc. We will assume that inequalities (5) are

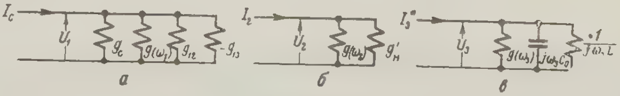

Figure 6

fulfilled. In addition we will neglect conductances g_{k_1} and g_{k_2}, assuming the unloaded amplifier resonators to be of sufficiently good quality. The inductive diode impedance $(1/\omega_1 C_0) \simeq 800$ ohms; consequently, in the equivalent circuit of Figure 5a, L can be neglected.

Resistance R_S is transformed into a shunt conductance according to equation (6). With these assumptions, the entire calculation for the amplifier is greatly simplified.

The input and output circuits provide two degrees of freedom for tuning the amplifier. With the selection of a reactive input circuit we obtain

$$\operatorname{Im} Y_{1\,\mathbf{eq}} = \operatorname{Im}(Y_1 + Y_{12} + Y_{13}) = 0. \tag{20}$$

Then the equivalent circuit of Figure 5a changes to the circuit of Figure 6a wherein

$$g(\omega_1) = g_p(\omega_1) + R_s(\omega_1)(\omega_1 C_0)^2; \tag{21}$$

$$g_{12} = \operatorname{Re} Y_{12}, \tag{22}$$

$$-g_{13} = \operatorname{Re} Y_{13}. \tag{23}$$

with the selection of a reactive output circuit, we obtain

$$\operatorname{Im} Y_2 = 0. \tag{24}$$

In addition, the equivalent circuit of Figure 5b simplifies to that of Figure 6b, where

$$g(\omega_2) = g_p(\omega_2) + R_s(\omega_2)(\omega_2 C_0)^2, \tag{25}$$

and g'_H is the transformed load conductance. Insofar as (24) is complied with

$$Y_2 = g(\omega_2) + g'_H,$$

then in accordance with (13)

$$g_{12} = \frac{\omega_1 \omega_2 (\Delta C/2)^2}{g(\omega_2) + g'_H}. \tag{22'}$$

The difference frequency ω_3 circuit will in general possess a complex conductance (Figure 6c Therefore, in accordance with (14)

$$-g_{13} = \frac{\omega_1 \omega_3 (\Delta C/2)^2}{|Y_3|^2} g(\omega_3). \tag{26}$$

In addition

$$g(\omega_3) = g_p(\omega_3) + R_s(\omega_3)(\omega_3 C_0)^2. \tag{27}$$

Introducing the following notation:

$$x = \operatorname{tg} \delta_p \sqrt{\frac{g(\omega_1)\, g(\omega_2)}{\omega_1 \omega_2 (\Delta C/2)^2}}, \tag{28}$$

$$\xi_1 = \frac{g_C}{g(\omega_1)}, \qquad \xi_2 = \frac{g'_H}{g(\omega_2)}, \qquad \eta = \frac{g(\omega_1) - g_{13}}{g(\omega_1)}, \tag{29}$$

we obtain in accordance with (19) an expression for the gain

$$C = \frac{\omega_2}{\omega_1} \frac{4\xi_1 \xi_2}{x^2 \left[(\xi_1 + \eta)(\xi_2 + 1) + \frac{1}{x^2}\right]^2}. \tag{30}$$

The magnitude $x = \tan \delta_p$, determined from (28), can be called the parametric loss tangent of a time-varying diode capacitor. In the absence of parasitic coupling at the differen frequency ($\eta = 1$) and in the case of perfect matching $\xi_1 = \xi_2 = \sqrt{1 + 1/x^2}$ the frequency ratio ω_2/ω_1 and x determine the gain

$$G = \frac{\omega_2}{\omega_1} \frac{1}{(x + \sqrt{1 + x^2})^2}. \tag{31}$$

Equation (31) agrees with the expression of the maximum amplifier gain, taking into account diode losses [4].

Thermal noise of the amplifier is calculated in an analogous manner. On the right-hand sides of equations (12) we write out the noise currents, generated conductances g_C and $g(\omega_1)$ at frequency ω_1; $g(\omega_2)$ at frequency ω_2; and $g(\omega_3)$ at frequency ω_3 and taking into account these simplifications, the equations are then solved. The input noise is assumed to be merely the conductance noise g_C at frequency ω_1 at standard temperature T_0.

All the remaining noise currents at the diode temperature T at the frequencies ω_1, ω_2, ω_3 are created in the amplifier. The noise factor F obtained in this manner is

$$F = 1 + \left[\frac{1}{\xi_1} + \frac{\omega_1}{\omega_2}\frac{(\xi_1 + \eta)^2}{\xi_1}x^2 + \frac{\omega_1}{\omega_3}\frac{1-\eta}{\xi_1}\right]\frac{T}{T_0}, \tag{32}$$

where T is the diode temperature; $T_0 = 290°$ K.

For concrete values of the diode parameters

$$C_{max} = 0.25 \ \mu\mu f$$
$$C_{min} = 0.11 \ \mu\mu f \qquad R_s = 10 \text{ ohms} \quad g_p = 0, \ L = 3\cdot 10^{-3} \text{ мкгн}$$

in our examples, based on equations (2), (6) and (28), x = 0.2. If we do not take into account the coupling constant at the resonant frequency due to aprasitic diode parameters, in accordance with equations (31) and (23) we obtain (at $T = T_0$)

$$\left.\begin{aligned} C &= \frac{\omega_2}{\omega_1}0.67 = 7.4\,(8.7 \text{ db}), \\ F &= 1.22\,(0.86 \text{ db}). \end{aligned}\right\} \tag{33}$$

Because of parametric coupling at the difference frequency $\eta < 1$, a negative resistance is introduced into the input circuit. But while $\eta > 0$, the gain G remains smaller than ω_2/ω_1. If $\eta < 0$, the gain may become larger than ω_2/ω_1; in this case it is impossible to match perfectly the amplifier with the signal generator and load.

If no resonance occurs at the difference frequency in the circuit of Figure 6c,

$$|Y_3| \gg g(\omega_3)$$

we may neglect the very small negative resistance introduced into the input circuit by coupling at the resonance frequency. At resonance however when

$$|Y_3| \simeq g(\omega_3),$$

g_{13} becomes comparable with $g(\omega_1) + g_{12}$ and the resulting input circuit conductance

$$Y_{1\,eq} = g_c + g(\omega_1) + g_{12} - g_{13}$$

can become a suitably small quantity. Consequently, in the case of resonance of the diode's parasitic parameters at the difference frequency, the amplifier can acquire a gain (greater than ω_2/ω_1) and even a loss of stability, in spite of the fact that at this frequency no special resonator is provided in the amplifier.

With a change in diode bias, one may vary C_0 over wide limits and in this way control the gain. For definiteness, we assume that matching of the input and output is realized in the absence of positive feedback coupling at the difference frequency. Then, as a result of the approach to resonance on the part of the parasitic parameters, we increase the gain when we decrease η, when ξ and ξ_2 are constant. In this case we can determine from (32) the noise factor corresponding to a prescribed gain, since ξ_1, ξ_2 remain definite. In this example we have

$$\text{at} \quad G = 10^2\,(20 \text{ db}) \qquad F = 1.36\,(1.32 \text{ db}), \tag{34}$$
$$\text{at} \quad G = 10^3\,(30 \text{ db}) \qquad F = 1.41\,(1.48 \text{ db}). \tag{35}$$

Comparison of equations (34) and (35) gives a basis for the assumption that, although positive feedback increases amplifier noise, this increase is insignificant in comparison with the rise in the gain. The general noise factor

$$F_{gen} = F + \frac{F_1 - 1}{G}$$

of equipment containing sucessive stages of amplification with a large noise factor F_1 decreases during regeneration.

A.A. Brandt and I.V. Ivanov conducted the following experiment. In a two-circuit parametric amplifier with a sum output frequency, schematically shown in Figure 7, the gain was measured at various diode biases and pumping powers. The output meter was tuned on the sum frequency and connected to the mixer chamber through a terminal waveguide, which introduced an attenuation of no less than 80 db at the pumping frequency and the difference frequency, but at the same time, it freely transmitted the sum frequency wave. In the experiment we succeeded in obtaining a stable gain exceeding ω_2/ω_1, and even in driving the amplifier by suitably matching the bias and the pumping power for several specimens of germanium diodes.

This analysis of the effect of the parasitic parameters of a semiconductor diode parametric amplifier shows that in addition to the introduction of losses at the operating frequencies, the parasitic parameters can still form additional resonant tank circuits for frequencies at which the parametric amplifier was not examined. This can lead to a great change in mode of operation. One may, however, specially introduce an additional tank circuit, forming a three-tank parametric amplifier. For example, in a two-tank parametric amplifier having the total output frequency of the third tank circuit, by using the additional resonator at the difference frequency, one may increase the gain to the required value by mear of positive feedback. The general relations (12) are entirely applicable to calculation of the three-tank circuit amplifier. At the same time, a third independent degree of freedom for tuning appears.

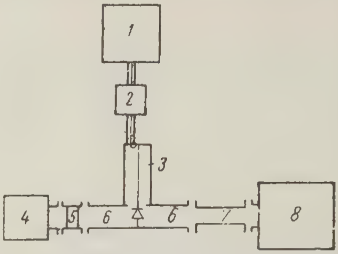

Figure 7. 1 — Signal generator, λ = 30 cm; 2 — input attenuator; 3 — input resonator; 4 — pumping oscillator λ = 3.4 cm; 5 — unidirectional valve; 6 — mixer chamber; 7 — terminal waveguide; 8 — resonant power meter λ, 3.1 cm.

Table 1

	Type	
	Double-frequency	Triple-frequency
G, db	12.4±0.5	~20
F, db	~0.9	~ 1.0

Table 2

	Type	
	Double-frequency	Triple-frequency
G, db	12.4	20
F, db	0.6	0.9

In [7], a three-tank circuit is described, in which the input frequency equals 410 Mc and the output frequency 9227 Mc. The results of the experimental measurements obtained in [7] are given in Table 1.

Assuming that, in the two-frequency type amplifier, a gain of 12.4 db is obtained in the case of perfect matching of the input and output, one may determine from (31) the paramet loss tangent of the diode: for the amplifier described in [7], it equals 0.14. Incidentally, at these frequencies ($\nu_1 = 0.4\ (10)^3$ Mc, $\nu_1 = 9.23\ (10)^4$ Mc) the diode in out example has the same value of x. Carrying out a calculation of the noise factor for the indicated value of $x = \tan \delta_p = 0.14$, we obtain the following results (Table 2). By comparing Tables 1 and 2, we see that good agreement is obtained between calculation and experiment.

As shown in Section 1, one may calculate by a similar method the effect of parasitic parameters in a two-tank circuit positive feedback amplifier with a difference frequency. In this case, parasitic coupling may occur initially at the sum frequency and will be highly noticeable at resonance of the parasitic parameters, which correspond to the frequency. Its influence, on the contrary, leads to a decrease of the gain and consequently to an increase of amplifier stability.

CONCLUSION

An analysis was made of the effect of the diode parasitic parameters on the operation of a two tank circuit parametric amplifier in the case of a small signal.

It was found that as a consequence of the parasitic parameters, in addition to losses caused by the diode at the operating frequency, additional feedback is produced. In the case of resonance at the parasitic parameters, this feedback can greatly alter the amplifier operation and, in particular, even lead to a loss in stability for an amplifier with a sum output frequency.

In the case of small diode loss and a low modulation factor of a time-varying capacitance, expressions are found for the gain and noise factor of the amplifier with a sum output frequency and additional positive feedback coupling at the difference frequency. A comparison was made of the calculated and experimental results, and qualititive and quantitative agreement was established. The author is grateful to V.V. Mifulin for valuable discussions on all the subjects treated in this paper.

REFERENCES

1. H.E. Rose, Proc. I.R.E., 1958, 46, 850.
2. S. Bloom, K. Chang, RCA Rev., 1957, 18, 4, 578.
3. H. Heffner, G. Wade, J. Appl. Phys. 1958, 29, 9, 1321.
4. D. Leenov, Bell System Techn. J., 1958, 37, 4, 989.
5. N.Ye. Skvortsova, Radiotekhnika i elektronika, 1957, 2, 3, 296.
6. M.D. Karasev, Uspekhi fiz, nauk, 1959, LXIX, 2, 217.
7. E.M.T. Jones, J.S. Honda, IRE WESCON Convention Record, part I, 1959.

Physics Department.
M.V. Lomonosov Chair
of Theory of Oscillations
Moscow State University

Submitted to the editors, 5 January, 1960

INTERACTION OF MAGNETOSTATIC OSCILLATIONS IN A FERRITE SAMPLE IN THE CASE OF REGENERATION. PART II—CONDITIONS OF EXCITATION OF OSCILLATIONS IN GENERAL

A.L. Mikaelyan and A.A. Vasil'yev

On the basis of the method expounded in [1], the interaction of higher types of natural oscillations in a ferrite sample in the case of regeneration is investigated at microwave frequencies. A general formula is given for calculation of the threshold of oscillation.

1. INTERACTION OF POTENTIALS $3,0,1 - 3,\overline{1},0$

It was shown in [1] that the action on a ferrite by high-frequency magnetic fields, between frequencies satisfying the following relation

$$\omega_1 + \omega_2 = \omega_p, \tag{1}$$

leads to an interaction between the natural magnetostatic oscillations in the sample. In this case, the indices of the interacting oscillations are determined from the following formula

$$n_2 = n_1, \quad m_2 = -(m_1 + 1). \tag{2}$$

This condition was illustrated by a consideration of the indicated interaction between the simplest magnetostatic oscillations $2,0,1$ - $2,\bar{1},0$.

We will now proceed to an investigation of interaction potentials with higher indices - the pairs $3,0,1$ - $3,1,0$. As was pointed out in [1], the excitation of this pair reduces to the fact that at the frequencies ω_1 and ω_2 the following potential spectrum exists

$$\omega_1:\ 3,0,1;\ \ 1,0,0;$$

$$\omega_2:\ 3,\bar{1},0;\ \ 1,\bar{1},0.$$

Taking into account that the fundamental potentials have a structure of the form [2]:

$$\begin{aligned} \psi_1 &= A_1 \cdot 30\, z\left[-\frac{x^2+y^2}{2} + \frac{1}{3}\mu_1 z^2 + \frac{a^2(1-\mu_1)}{5}\right], \\ \psi_2 &= A_2 \cdot 20\,(x - jy)\left[-\frac{x^2+y^2}{4} + \mu_2 z^2 + \frac{a^2(1-\mu_2)}{5}\right], \end{aligned} \tag{3}$$

we determine φ_1 and φ_2 in the following form:

$$\begin{aligned} \varphi_1 &= \frac{40}{3}(\tau_1 + \overset{*}{\tau}_2)\,\overset{*}{\mu}_2 z^3 \overset{*}{A}_2, \\ \varphi_2 &= -15\,(\tau_2 + \overset{*}{\tau}_1)(x - jy)\, z^2 \overset{*}{A}_1. \end{aligned} \tag{4}$$

In this case, we take into consideration that the potentials $1,\bar{1},0$ and $1,0,0$ do not influence φ_1 and φ_2. The total potentials inside and outside the ferrite are now determined in this manner

$$\begin{aligned} \Psi_1^i &= E_1 z + 30 z A_1\left[-\frac{x^3+y^2}{2} + \frac{1}{3}\mu_1 z^2 + \frac{a^3(1-\mu_1)}{5}\right] + \frac{40}{3}(\tau_1 + \overset{*}{\tau})\,\overset{*}{\mu}_2 \overset{*}{A}_2 z^3, \\ \Psi_1^e &= D_1 \frac{1}{r^4} P_3^0(\cos\theta) + F_1 \frac{1}{r^2} P_1^0(\cos\theta), \\ \Psi_2^i &= E_2(x - jy) + 20\,(x - jy)\,A_2\left[-\frac{x^2+y^3}{4} + \mu_2 z^2 + \frac{a^2(1-\mu_2)}{5}\right] - \\ &\quad - 15\,(\overset{*}{\tau}_1 + \tau_2)\,\overset{*}{A}_1 (x - jy)\, z^2, \\ \Psi_2^e &= D_2 \frac{1}{r^4} P_3'(\cos\theta)\, e^{-j\varphi} + F_2 \frac{1}{r^2} P_1'(\cos\theta)\, e^{-j\varphi}. \end{aligned} \tag{5}$$

In these expressions E_1, E_2 and F_1, F_2 are respectively the inner and outer amplitudes of the potentials $1,0,0$, and $1,\bar{1},0$.

From the continuity conditions of the potentials and normal components of induction at the frequencies ω_1 and ω_2, we obtain the following system of equations:

$$\begin{aligned} &1)\ \left[\mu_1 + \frac{3}{4} + 0{,}3\,(\overset{*}{\tau}{}_2^{2} - \tau_1^2)\right] A_1 = \left[0{,}2\overset{*}{\tau}_2 - 0{,}8\tau_1\overset{*}{\mu}_2 - \frac{4}{15}(\tau_1 + \overset{*}{\tau}_2)\,\overset{*}{\mu}_2\right]\overset{*}{A}_2, \\ &2)\ [4\overset{*}{\mu}_2\overset{*}{k}_2 - 4\overset{*}{\mu}{}_2^{2} + \overset{*}{k}_2 - 27\overset{*}{\mu}_2 - 4 + 8\overset{*}{\tau}_2\overset{*}{\mu}_2(\tau_1 + \overset{*}{\tau}_2)]\,\overset{*}{A}_2 = \\ &\qquad = -[21\overset{*}{\tau}_2 + 12\tau_1 + 6\overset{*}{\tau}_2\overset{*}{\mu}_1 + 3\,(\overset{*}{\mu}_2 - \overset{*}{k}_2)(\tau_1 + \overset{*}{\tau}_2)]\,A_1, \\ &3)\ \frac{1}{a^2}[(\overset{*}{\mu}_2 - \overset{*}{k}_2 + 2)\,\overset{*}{E}_2 - \overset{*}{\tau}_2 E_1] + [16 + 104\,\overset{*}{\mu}_2 + 16\,\overset{*}{\mu}_2(\overset{*}{\mu}_2 - \overset{*}{k}_2) + \\ &\qquad + 8\,(\overset{*}{\mu}_2 - \overset{*}{k}_2) - 40\,\overset{*}{\mu}_2\overset{*}{\tau}_2(\tau_1 + \overset{*}{\tau}_2)]\,\overset{*}{A}_2 - [90\overset{*}{\tau}_2 - 54\tau_1 + \\ &\qquad + 24\,\mu_1\overset{*}{\tau}_2 - 15\,(\overset{*}{\mu}_2 - \overset{*}{k}_2)(\tau_1 + \overset{*}{\tau}_2)]\,A_1 = 0, \\ &4)\ \frac{1}{a^2}[3E_1 - 2\overset{*}{\tau}_2\overset{*}{E}_2] + [30\,\tau_1(\tau_1 + \overset{*}{\tau}_2) - 60\,\mu_1 - 45]\,A_1 + \\ &\qquad + [12 - 8\,\overset{*}{\mu}_2\overset{*}{\tau}_2 - 36\,\overset{*}{\mu}_2\tau_1]\,\overset{*}{A}_2 = 0. \end{aligned} \tag{6}$$

In the absence of a pumping field ($m_0 = 0$), system (6) decomposes into independent equations characterizing the resonant oscillations in the ferrite [2]:

$$\begin{aligned} &1)\ \mu_1 = -\frac{3}{4}, \\ &2)\ \overset{*}{k}_2 - 27\,\overset{*}{\mu}_2 - 4\,\overset{*}{\mu}_2 + 4\,\overset{*}{\mu}_2\overset{*}{k}_2 - 4 = 0, \\ &3)\ \overset{*}{\mu}_2 - \overset{*}{k}_2 + 2 = 0. \end{aligned} \tag{7}$$

equation (4) of system (6) in the absence of a pumping field does not give a characteristic equation, because the potential 1, 0, 0 is not resonant.

As we see, the action of the pumping field is almost manifest in the fact that the independent oscillations become coupled to one another, and in each of the considered cases at each operating frequency ω_1 and ω_2 there emerges a spectrum consisting of two potentials. In this case the additional potentials caused by the action of the pumping field may be nonresonant. As equations 1 and 2 of system (6) show, the basic potentials 3, 0, 1 - 3, $\bar{1}$, 0 are not connected with the additional potentials (1, 0, 0 and 1, $\bar{1}$, 0) and independently of the latter they can interact among themselves. Eliminating amplitudes A_1 and A_2 from equations 1 and 2, we obtain

$$\left[\mu_1 + \frac{1}{4} + 0,3\,(\tau_2^{*2} - \tau_1^2)\right]\left[4\mu_2^* k_2^* - 4\,\mu_2^{*2} + k_2^* - 27\,\mu_2^* - 4 + 8\tau_2^*\mu_2^*(\tau_1 + \tau_2^*)\right] = \left[0,8\tau_1\mu_2^* - 0.2\tau_2^* + \frac{4}{15}\,\mu_2^*(\tau_1 + \tau_2^*)\right][21\tau_2^* + 12\tau_1 + 6\tau_2^*\mu_1^* + 3\,(\mu_2^* - k_2^*)(\tau_1 + \tau_2^*)]. \tag{8}$$

The critical value of the percentage modulation of a ferrite medium, corresponding to the total loss compensation, is determined from (8) and is of the form

$$m_0 = \frac{2\sqrt{\mu_1''\,[\mu_2'' + 0,1\,(\mu_2'' - k_2'')\,(4\mu_2 + 1)^2]}}{2\mu_2\,(\mu_1 - k_1 - 1) + (0,8\mu_2 - 0,3)\,(\mu_2 - k_2 - 1)}. \tag{9}$$

Figure 1 presents a graph exhibiting the dependence of the operating frequency, the pumping frequency and external threshold pumping field on the magnitude of the dc magnetic field. A graph for small values of the magnetic field is given in Figure 2. We see here, just as for the potentials 2, 0, 1 - 2, $\bar{1}$, 0, the case of resonant pumping is possible, characterized by a sharply lowered threshold. The internal magnetic field then equals (0.07) $4\pi M$.

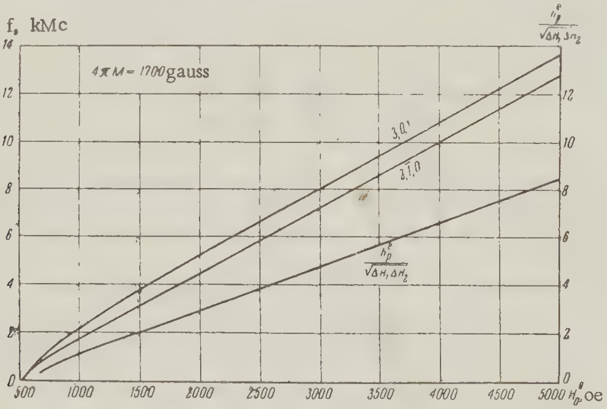

Figure 1

Substituting the indicated value of the field into the formula (1) of the first part of paper [1], we obtain, taking into account (7), the following value of the threshold field of resonant pumping:

$$h_p^e \simeq 5\,\frac{\sqrt{\Delta H_1 \Delta H_2}}{4\,\pi M}\,\Delta H_p. \tag{10}$$

As is well-known, certain high order potentials in the same resonant structure can have different resonant frequencies. This "degeneracy" is reflected in the notation of Walker by the third index of the potential. Thus, among the natural oscillations of a magnetized ferrite, in addition to the 3, $\bar{1}$, 0 oscillations, there are 3, $\bar{1}$, 1 oscillations with an analogous structure. In this case the interaction of the pair 3, 0, 1 - 3, $\bar{1}$, 1 does not differ qualitatively from the interaction of the potentials 3, 0, 1 - 3, $\bar{1}$, 0. The dependence of the threshold value of the pumping field and the values of the operating frequencies for the oscillations 3, 0, 1 - 3, $\bar{1}$, 1 are given in Figure 3.

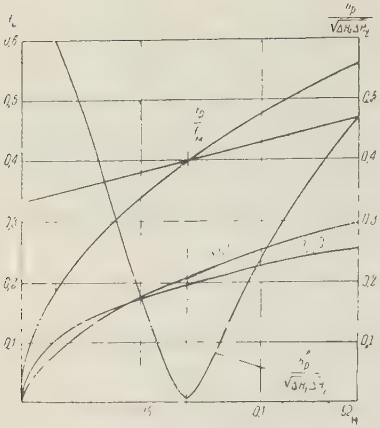

Figure 2

2. GENERAL METHOD OF CALCULATION OF THE THRESHOLD OF OSCILLATION

The determination of the threshold values of the external pumping field with the aid of a solution of the boundary problem in the case of high index potentials is rather complex. Therefore it is of interest to examine a method of determining the threshold, which is based on perturbation theory.

Let the "unperturbed" medium be a magnetized ferrite with characteristic functions in the form of magnetostatic potentials. For simplicity, in future formal operations we will assume that the initial medium has no losses. The perturbing action will be regarded as both the loss in the system and the modulation of the ferrite properties caused by the pumping field. The frequencies of the perturbation oscillations $\omega_{1,2}$ will be complex, the imaginary parts of these frequencies $\omega_{1,2}''$ describing the attenuation of the natural oscillations of the system caused by the presence of losses. In a regenerated ferrite, on account of the pumping field energy, compensation of the losses in the system will occur. In the mode of operation corresponding to the generation of oscillations at the frequencies $\omega_{1,2}$, attenuation of the system is absent, i.e., the imaginary parts of the "perturbed" frequencies must vanish.

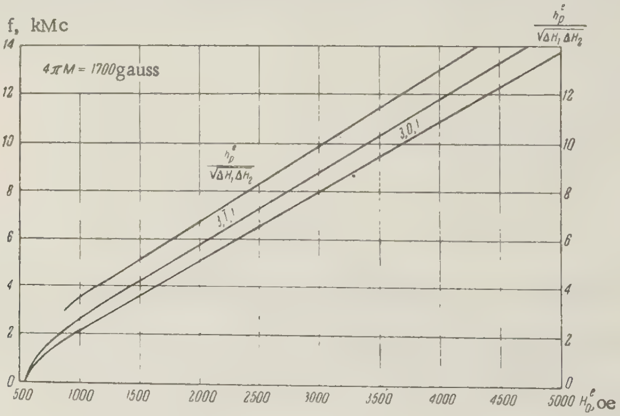

Figure 3

From the Maxwell equation, it is easy to obtain the equation

$$\frac{\Delta\omega_1}{\omega_1} = -2\pi \frac{\int (\vec{M}_1 \vec{H}_1^{0*} - \vec{M}_1^{0*} \vec{H}_1)\, dv}{\int\limits_{V_0} \vec{H}_1 \vec{H}_1^{0*}\, dv + 4\pi \int\limits_{V_1} \vec{M}_1^{0*} \vec{H}_1\, dv}, \tag{11}$$

where $\vec{M}_1^{0*}$, $\vec{H}_1^{0*}$ are the initial magnetization and field; $\vec{M}_1$, $\vec{H}_1$ are the magnetization and field, disturbed by losses and pumping; V_1, V_0 are the volume of the ferrite and the total volume, respectively;

$$\Delta\omega_1 = \dot{\omega}_1 - \omega_1 = \omega_1' - \omega_1 + j\omega_1''; \tag{12}$$

$_1$ is the initial frequency $\dot{\omega}_1$ is the complex perturbed frequency.

Assuming that $\operatorname{Im} \frac{\Delta\omega_1}{\omega_1} = 0$ and after eliminating the amplitude, we obtain

$$m_0 \geqslant \frac{2\sqrt{(\mu_1'' I_1 - k_1'' N_1)(\mu_2'' I_2 - k_2'' N_2)}}{|(\mu_1 - k_1 - 1) Z_1 + (\mu_2 - k_2 - 1) Z_2|}. \tag{13}$$

In this equation I, N, Z are the following integral relations:

$$I_1 = \int\limits_{V_1} \left(\frac{\partial\psi_1}{\partial x} \frac{\partial\psi_1^*}{\partial x} + \frac{\partial\psi_1}{\partial y} \frac{\partial\psi_1^*}{\partial y} \right) dv,$$

$$N_1 = \left| \int\limits_{V_1} \left(\frac{\partial\psi_1}{\partial x} \frac{\partial\psi_1^*}{\partial y} - \frac{\partial\psi_1}{\partial y} \frac{\partial\psi_1^*}{\partial x} \right) dv \right|, \tag{14}$$

$$Z_1 = \int\limits_{V_1} \frac{\partial\psi_2^*}{\partial z} \left(\frac{\partial\psi_1^*}{\partial x} - j \frac{\partial\psi_1^*}{\partial y} \right) dv.$$

For the other frequency, these relations are written with the variable indices 1 and 2. The type φ potentials drop out of (13), because they are connected with terms which are negligibly small.

In expressions (14) I_1 and N_1 represent orthogonal relations for magnetostatic potentials, and the integral Z_1 characterizes the relation between the oscillations and the regenerated ferrite. Direct verification can convince us that this integral is nonvanishing only in the case of interacting potentials whose indices are determined by relation (2). If relation (2) is not fulfilled for the chosen potentials, the integrals $Z_{1,2}$ equal zero and $m_0 = \infty$, which also means that no interaction is present. Equation (13) allows us to determine rather simply the threshold value of m_0 both in the case of higher type potentials and in the case of oscillations, the frequencies of which differ from the natural resonant values, when an application of the method expounded in the preceding paragraph will be hampered because of the cumbersomeness of the calculations.

In the case of potentials $2, 0, 1$ (ω_1) and $2, \overline{1}, 0$ (ω_2), from (14) we determine

$$I_1 = I_2 = N_2 = Z_2 = \frac{8\pi}{3\cdot 5} a, \quad Z_1 = -2\mu_1 \frac{8\pi}{3\cdot 5} a, \quad N_1 = 0. \tag{15}$$

Substituting (15) into (13) and taking into account equation (28) from [1], we obtain (30) from [1].

In the case of potentials $3, 0, 1$ (ω_1) and $3, -\overline{1}, 0$ (ω_2) from expression (14) we find, taking into account (7),

$$I_1 = \frac{4\pi a}{3\cdot 5\cdot 7} 16\cdot 5 \left(\frac{42}{2}\right), \quad N_1 = 0, \quad Z_1 = -\frac{4\pi a}{3\cdot 5\cdot 7} (30\mu_2),$$

$$I_2 = \frac{4\pi a}{3\cdot 5\cdot 7} 16\cdot 5 (16\mu_2^2 + 8\mu_2 + 11), \quad N_2 = \frac{4\pi a}{3\cdot 5\cdot 7} 16\cdot 5 (16\mu_2^2 + 8\mu_2 + 1), \tag{16}$$

$$Z_2 = \frac{4\pi a}{3\cdot 5\cdot 7} 16\cdot 5 [15 (0{,}8\mu_2 - 0{,}3)].$$

Substituting (16) into (13), we obtain an equation agreeing with (9)*.

By means of this method, we will investigate one more pair of potentials: $3, \overline{2}, 0$ - $3, 1, 0$. The structure of these potentials is of the form [2]:

$$3, 1, 0\ (\omega_1): \quad \psi_1 = (x + jy) [20 \mu_1 z^2 - 5 (x^2 + y^2) - 4a^2 (\mu_1 - 1)],$$

$$3, \overline{2}, 0\ (\omega_2): \quad \psi_2 = z (x - jy)^2. \tag{17}$$

---

*A similar check was made for other pairs of oscillations.

Integrating equations (14), we obtain

$$I_1 = \frac{4\pi a}{3\cdot5\cdot7}\,16\cdot5\,(16\mu_1^2 + 8\,\mu_1 + 11), \quad N_1 = \frac{4\pi a}{3\cdot5\cdot7}\,16\cdot5\,(16\,\mu_1^2 + 8\,\mu_1 + 1),$$

$$Z_1 = -\frac{4\pi a}{3\cdot5\cdot7}\,16\cdot5, \quad I_2 = N_2 = \frac{4\pi a}{3\cdot5\cdot7}\,16\cdot5\left(\frac{1}{5}\right), \quad Z_2 = \frac{4\pi a}{3\cdot5\cdot7}\,16\cdot5\,(4\,\mu_1). \qquad (18$$

Substituting these expressions into equation (13) and taking into consideration that the resonant frequency of the potential $3, \overline{2}, 0$ is characterized by the relation $\omega_2 - \omega_0 = \frac{2}{7}\,\omega_M$ [2], we determine the threshold m_0 in the following form:

$$m_0 \geqslant \frac{2\sqrt{[2\,\mu_1'' + 0{,}2\,(\mu_1'' - k_1'')\,(4\,\mu_1 + 1)^2]\,(\mu_2'' - k_2'')}}{k_1 - 15\,\mu_1 + 1}\,. \qquad (19$$

The results of the calculation of the threshold value of the external pumping magnetic field, carried out with the aid of equation (19), are shown in Figure 4, analogous to the previous treatment.

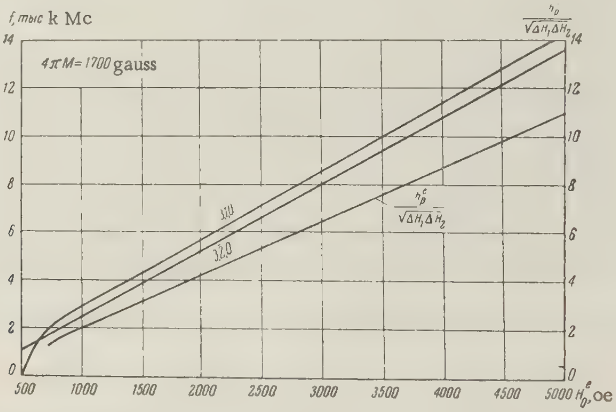

Figure 4

CONCLUSION

This investigation enabled us to draw the following conclusions.

1. Interaction of magnetostatic type oscillations, which are the result of a regeneration of the system, is possible only between oscillations with a definite field structure {see equation (19) in [1]}.

2. In the presence of the action of the pumping field in the case of interaction of higher type of oscillations at frequencies ω_1 and ω_2, an entire spectrum of simpler oscillations arise the indices of which are determined by equations (15) and (17) from [1].

3. The threshold value of the external pumping field, corresponding to the regime of gene tion of oscillations, in the region 5000-8000 Mc, amounts to several oersteds and increases as we raise the frequency of generated oscillations.

In conclusion we mention the papers of G. Suhl [3] and Ya.A. Monosov [4], referred to in the introduction of [1].

Suhl obtained a formula for the threshold value of m_0, similar to equation (13) of the present paper. A type Z integral, contained in [4] [equation (39)], correctly reflects the law of interaction between the oscillations. The approximations in writing the induction (30) lead however to a lowering of the quantitative results of the threshold value of m_0. Thus, in the case of potentials $2, 0, 1 - 2, \overline{1}, 0$, the value of m_0 in [4] is reduced by a factor of $\sqrt{(\omega_0^2 + \omega_1^2)/\omega_0\omega_1}$, where ω_1 is the frequency of oscillation of 2,0,1, i.e., at the frequency $f_1 = 5000$ Mc ($4\pi M = 1700$ gauss) the factor is approximately two.

The principal error of [5] is connected with the assertion of the impossibility of interaction of types of oscillations, one of which has an index m differing from n by more than two (for instance, 3, 0, and $3, \bar{1}$, 4, 0 and $4, \bar{1}$ etc.). Consequently, only one group of mutually interacting oscillations is considered. In this connection, an error also arises in equation (10), leading to a twofold reduction in the threshold value. In addition, the particular solution used in [5] is not entirely successful, because it rejects the case of the degenerate mode of operation.

The authors express their gratitude to the student V.V. D'yachenko of the MFTI, who participated in the derivation of a number of formulae and in the performance of the numerical calculations.

REFERENCES

1. A.L. Mikaelyan, and A.A. Vasilyev, Interaction of magnetostatic oscillations in a ferrite sample during regeneration. Pt. I. Interaction of the simplest type of oscillations. Radiotekhnika and elektronika, 1961, 6, 4, 623.
2. P.S. Fletcher, and R.O. Bell, Ferrimagnetic resonance modes in spheres, J. Appl. Phys. 1959, 30, 5, 687.
3. H. Suhl, Theory of the ferromagnetic microwave amplifier, J. Appl. Phys., 1957, 28, 11, 1225.
4. Ya.A. Monosov, On the theory of nonlinear phenomena in ferrites at UHF, Pt. I–II, Radiotekhnika and electronika, 1960, 5, 1, 2, 59, 278.

Submitted to editors 21 April 1960

INVESTIGATION OF MASER FREQUENCY DEPENDENCE UPON DIFFERENT PARAMETERS

PART I—(THEORY, LINE J=3, K=2)

N.G. Basov, V.V. Nikitin and A.N. Orayevskiy

We calculated the frequency of oscillation of a maser as a function of the pressure in the molecular beam source and of the voltage on the sorting system both for a maser using the $J = K = 3$, $N^{14}H_3$ line and for a maser operating on the inversion transition $J = 3$, $K = 2$, $N^{14}H_3$. An experimental investigation was made of a maser operating on the $J = 3$, $K = 2$, $N^{14}H_3$ line and having two head-on beams. Good agreement was found between the results of calculation and experiment. It was shown that the frequency of two different masers (with two identical head-on beams), operating on line with hyperfine structure, can be tuned with an accuracy of $\sim 10^{-10}$ by means of a change of pressure.

INTRODUCTION

This work was undertaken for the purpose of explaining the possibility of using a molecular generator as an absolute frequency standard with a frequency of $\sim 10^{-10}$. In order to choose a maser design and mode of operation suitable for the solution of the given problem, a detailed clarification is required of the variation of the maser frequency of oscillation with various parameters. For this purpose it is necessary to carry out both an experimental and theoretical investigation of the subject in order to check the correctness of our concepts concerning the operation of a maser.

In a number of papers the effect of various factors on the frequency of oscillation of a maser was evaluated. In [1, 2] the dependence of the frequency of oscillation of a maser on the natural frequency of the cavity resonator is clarified; in [2] it was shown that the nonuniformity of the radiation of molecules along the cavity resonator leads to a shift of the frequency of oscillation; the influence of the unresolved satellites of the hyperfine structure was pointed out in [3]; [4] explains the dependence of the shift in the frequency of oscillation of the maser caused by the hyperfine structure on the voltage in the sorting system and the intensity of the molecular beam.

However the analysis given in these papers cannot possibly be considered final, because it does not take into account the real velocity distribution of the molecules.

In this paper we undertake the task of calculating the frequency of oscillation of the maser, taking into account the different factors noted in [1-4] and assuming a velocity distribution of the molecules sufficiently close to the real one. We studied experimentally the effect on the frequency of the maser of the various parameters (pressure in the molecular beam source, voltage in the molecular beam source, voltage in the separating system, and the tuning of the cavity resonator). A comparison was made of the experimental and theoretical results. On the basis of the characteristics obtained in this manner we investigated the possibility of tuning the frequency of the maser operating on the inversion line J = 3, K = 2 of ammonia $N^{14}H_3$. The maser had two head-on beams. The investigations showed that by means of modulating the ammonia pressure in the molecular beam we could tune the frequency of the maser to the frequency of the spectral line to an accuracy of the order 10^{-10}.

1. DEPENDENCE OF THE FREQUENCY OF OSCILLATION OF THE MASER ON THE VARIOUS PARAMETERS (THEORETICAL CONSIDERATION)

The effects which influence the frequency of oscillation of the maser to 10^{-10} of the frequency of the radiation line are discussed at length in [4]. Therefore we will merely enumera them.

I. The dependence of the frequency of oscillation of the maser on the natural frequency o the cavity resonator.

II. The shift of the peak of the spectral line due to the presence of unresolved component of the hyperfine structure and the dependence of this shift on the voltage of the sorting system and the intensity of the molecular beam.

III. The effect of nonuniformity of molecular emission on the resonator, leading to a Doppler shift of the frequency of oscillation of the maser. As was shown in [2, 4], this effect can be compensated to a considerable extent by passage through the cavity resonator of two head-on molecular beams of the same intensity.

IV. The dependence of the frequency of oscillation of the maser on the intensity of the molecular beam and on the voltage of the sorting system by virtue of the difference between th real distribution of the molecules according to the time of flight and the distribution $\frac{1}{\tau}e^{-\theta/\tau}$, used to carry out the calculation in [1, 4]. The deviation of the frequency of oscillation of the maser from spectral line frequency by virtue of effect IV is proportional to separation betwee the natural frequency of the cavity resonator and the peak of the spectral line and can be eliminated by accurate tuning of the cavity resonator at the spectral line frequency.

In order to calculate the oscillatory frequency of the molecular generator, we may use the equation, [1]

$$\frac{\bar{\varkappa}'}{\bar{\varkappa}''} = 2Q\frac{\omega_0 - \omega}{\omega}, \qquad (1$$

where $\bar{\varkappa} = \bar{\varkappa}' + i\bar{\varkappa}''$ is the average complex polarizability of the molecular beam; ω_0 the desire oscillatory frequency of the molecular generator, ω_0, is the natural frequency of the cavity re nator and Q is its quality factor.

This equation in the case of a suitable calculation of $\bar{\varkappa}$, includes all the above-mentioned effects. Nevertheless, we will assume in the future, that effect III (nonuniformity of the molecular emission along the resonator) is compensated for by two head-on beams of the same intensity and is thus not involved.

In [1] a calculation was made of $\varkappa$ for a single molecule, if the latter has two isolated energy levels. For the two levels

$$\varkappa'_m = \frac{\delta_m}{\gamma_m^2}\frac{|d_m|^2}{\hbar}(1 - \cos\gamma_m\theta),$$
$$\varkappa''_m = -\frac{|d_m|^2}{\hbar\gamma_m}\sin\gamma_m\theta, \tag{2}$$

$\delta_m = \omega_m - \omega$; ω_m is the frequency of the molecular transition; d_m is the matrix element of the dipole moment, which can be presented in the form $d_m = d_0\lambda_m$ where d_0 is the value of the dipole moment, depending on the structure of the molecule, and λ_m describes the dependence of d_m on the quantum numbers characterizing the given transition; $\gamma_m = \gamma\frac{\lambda_m^2}{\bar{\theta}^2}$; $\gamma = \frac{d\mathscr{E}}{\hbar}\bar{\theta}$; $\mathscr{E}$ is the amplitude of the field in the resonator; $\bar{\theta}$ is the time of flight of the molecule through the resonator (see below). If the same line consists of several pairs of independent energy transitions,

$$\varkappa' = \sum_m \varkappa'_m, \quad \varkappa'' = \sum_m \varkappa''_m, \tag{3}$$

the summation is carried out over all the transitions. In order to obtain $\bar{\varkappa}$, it is necessary to average (2) over the length of the resonator. For this purpose note that $t = \frac{z}{l}\theta$, where Z is a running coordinate along the resonator, l is its length; $\theta = l/v$, v is the velocity of the molecule. In such a case

$$\varkappa_m = \int_0^\infty F(\theta)\,d\theta\int_0^l \varkappa_m\frac{1}{l}\,dz, \tag{4}$$

where $F(\theta)$ is the distribution of molecules with respect to the time of flight through the resonator.

If we designate

$$J_m^s = \int_0^\infty F(\theta)\left(1 - \frac{\sin\gamma_m\theta}{\gamma_m\theta}\right)d\theta,$$
$$J_m^c = \int_0^\infty F(\theta)\frac{1 - \cos\gamma_m\theta}{\gamma_m\theta}\,d\theta \tag{5}$$

and introduce a certain average line frequency ω_l such that $\omega_m = \omega_l + \eta_m$, the solution of equation (1) with respect to ω, close to ω_l, can be presented in the form

$$\omega = \omega_l\left[1 + \frac{\omega_0 - \omega_\text{л}}{\omega_\text{л}}\frac{Q}{Q_\text{л}}G + \Delta\right], \tag{6}$$

where

$$G = \frac{\sum\limits_m |d_m|^2\gamma_m^{-1}J_m^c}{\sum\limits_m |d_m|^2\gamma_m^{-2}J_m^s}; \quad \Delta = \frac{\sum\limits_m \eta_m|d_m|^2\gamma_m^{-1}J_m^s}{\sum\limits_m |d_m|^2\gamma_m^{-1}J_m^s}. \tag{7}$$

In order to make a concrete calculation of the values of G and Δ, it is necessary to know the molecular distribution $F(\theta)$. This distribution depends substantially on the character of the molecular emission from the molecular beam source.

If the aperture diameter d of the grating in the molecular beam source is much less than the foil thickness a, from which the grating is prepared, the emission of gas from the source has the character of a molecular (Knudsen) source. In the grating customarily used, a ≃ d, so that at sufficiently high pressures the emission has an intermediate character between molecular and viscous. But, evidently, it is closest of all to molecular, and in order to deriv the molecular distribution of molecules F(θ) with respect to the time of flight, we will use the Maxwellian velocity distribution of molecules

$$\Phi(v,\ \vartheta,\ \varphi)\,dv\,d\Omega \sim e^{-\frac{Mv^2}{2kT}}\,v^3\,dv \sin\vartheta \cos\vartheta\, d\vartheta\, d\varphi. \qquad (8$$

If the angle of flight of molecules in the quadrupole capacitor is less than or equal to the angle at which the output aperture of the capacitor is apparent from the molecular beam source, i.e

$$\operatorname{tg}\vartheta \leqslant \frac{R}{L}, \qquad (9$$

where R is the radius of the quadrupole capacitor, and L is its length, then all such molecules fall into the cavity. If, however, the angle of flight is such that tan ϑ >R/L, the following relat must be fulfilled:

$$v^2 \sin^2\vartheta \leqslant \frac{2W_{\max}}{M}, \qquad (10$$

$W_{\max}$ is the maximum interaction energy of the molecules with the field of the sorting system M is the mass of the molecule. From this is obtained the following distribution of molecules with respect to time of flight through the cavity:

$$F(\theta)\,d\theta \sim \begin{cases} e^{-\bar{\theta}^2/\theta^2}\left(1 - e^{-\frac{R^2}{L^2}\frac{\bar{\theta}^2}{\theta^2_{\min}}}\right)\dfrac{1}{\theta^3}\,d\theta, & \theta_{\min} \leqslant \theta < \infty, \qquad (11\\ -e^{-\bar{\theta}^2/\theta^2}\left(e^{-\frac{R^2}{L^2}\frac{\bar{\theta}^2}{\theta^2_{\min}}} - e^{-\frac{R^2}{L^2}\frac{\bar{\theta}^2}{\theta^2}}\right)\dfrac{1}{\theta^3}\,d\theta, & 0 < \theta < \theta_{\min}, \qquad (12 \end{cases}$$

where

$$\bar{\theta}^2 = \frac{Ml^2}{2kT}; \quad \theta = \frac{l}{v\cos\vartheta}; \quad \theta_{\min} = R\frac{l}{L}\sqrt{\frac{M}{2W_{\max}}},$$

$W_{\max}$ depends on the voltage on the separating system. Therefore, F(θ), and more importan G and Δ, depend not only on γ, i.e., in the final reckoning on the number of active molecules entering the cavity, but also on the voltage U, i.e., $G \equiv G(\gamma,\ U)$, $\Delta = \Delta(\gamma, U)$.

In addition, $W_{\max}$ depends on the quantum numbers of the molecular transition m, which leads to a corresponding dependence of F(θ) on these numbers. But the characteristic quantu numbers of the energy levels of the molecules in the quadrupole capacitor may differ from the corresponding quantum numbers in the cavity. Thus, for example, for a cavity operating in t TE_{010} mode, the electric field in the cavity is perpendicular to the electric field in the quadru capacitor, by virtue of which the projection of the total molecular moment in the direction of the electric field is one of the quantum numbers characterizing the energy transition and is different for the quadrupole capacitor in the cavity. Therefore, the distribution with respect to the time of flight in the cavity $F_m(\theta)$ will have the form

---

*For inversion levels of the ammonia molecule

$$W_{\max} = \frac{\hbar\omega_{\text{inv}}}{2}\left[\left(1 + 2\frac{(\vec{d}\vec{E})^2}{\hbar\omega_{\text{inv}}}\right)^{1/2} - 1\right],$$

where E is the field intensity in the separating system; ω_{inv} is the frequency of the inversion transition.

where m is the index characterizing the energy transition in the cavity; m' is the corresponding index for the quadrupole focussing device, and $a_{mm'}$ is the probability of a molecule having the index m in the cavity if in the quadrupole focussing device it has the index m'.

Using the distribution (13), where $F_{m'}(\theta)$ is given by (11)-(12), we can calculate J_m^s and J_m^c.

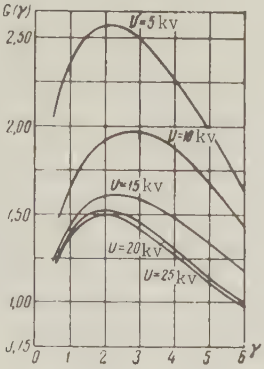

Figure 1. Graph of the function G(γ , U)

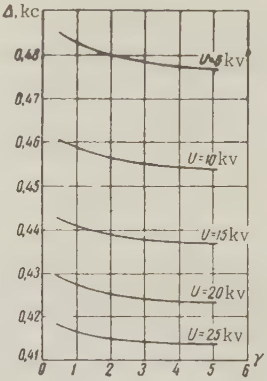

Figure 2. Dependence of the shift of the top of the ammonia spectral line $N^{14}H_3$ J = 3, K = 3 on the saturation parameter and the voltage on the sorting system U. The shift is caused by the presence of unresolved components of the quadrupole hyperfine structure.

$$F_m(\theta) = \sum_{m'} a_{mm'} F_{m'}(\theta), \tag{13}$$

Further calculation depends on the concrete emission line, used in the molecular generator. Usually the inversion line of ammonia J = 3, K = 3, which is used in the maser, consists of three* components due to the quadrupole hyperfine structure [3, 4, 6], which are characterized by the quantum number F_1, corresponding to the total spin of the nitrogen nucleus I_N and the angular momentum $\vec{J}$ ($\vec{F}_1 = \vec{I}_N + \vec{J}$) and the projection M_{F1} of the total moment $\vec{F}_1$ in the direction of the external field. In ammonia, F_1 runs through the values 2, 3, 4. Consequently, for the line J = 3, K = 3, the index m signifies the quantum numbers of F_1, M_{F1}. The values $\eta_m \equiv \eta_{F^1 M_{F_1}}$ do not depend on the number M_{F1}, and can be calculated on the basis of [6]: $\eta_2 = 1.00$ kc, $\eta_3 = -1.25$ kc, $\eta_4 = 0.4$ kc. The coefficients $a_{mm'} \equiv a^{F_1}_{M_{F_1} M'_{F_1}}$ are given in [4]. Therefore, the calculation of functions G and Δ can be carried to a conclusion. However, such a calculation in analytic form is impossible and was performed with the aid of a computer. The results of the calculation are given in the graphs of Figures 1 and 2.

Using the values of G(λ , U) and Δ(λ , U), we can calculate the dependence of the oscillatory frequency of the maser on pressure and voltage, if the dependence of γ on these parameters is known. Knowing the number of molecules, emitted per unit time from the molecular beam source, γ can be calculated from the equation [1]

$$\bar{\varkappa}'' = \frac{1}{4\pi Q}. \tag{14}$$

Unfortunately, it is difficult to calculate the flux of molecules from the molecular beam source, because it differs from both the viscous and molecular type and is of an intermediate character which was not investigated. The deterioration of the vacuum at large molecular beam intensities, leading to the disruption of regeneration at sufficiently large source pressures (0.3 - 1 mm Hg), complicates even more the pressure dependence of γ. Therefore, in order to calculate the oscillatory frequency of the maser as a function of the parameters, it is convenient to use the experimental graph of the dependence of the maser power on the parameters of the apparatus We used the results of [5], where relative measurements were made of maser power as a function of the pressure in the molecular beam source and the separating system voltage.

---

*Actually the J = 3, K = 3 line of ammonia $N^{14}H_3$ consists of 12 components, since each of the 3 quadrupole components is split into 4 more components due to the magnetic interaction. But the magnetic interaction is weak, and the correction caused by taking into account the magnetic splitting amounts to $\sim 10^{-11}$.

The results of the calculation of frequency of the 3, 3 line are given in Figure 3 and 4. For a generator operating on the 3, 2 line, the dependence of frequency on the parameters (voltages and pressures) is simpler than for 3, 3 line. This, evidently is explained by the fact that the 3, 2 line does not possess quadrupole hyperfine structure and for this line we must set $\Delta = 0$.* Secondly, line 3, 2 is ~12 times weaker than the 3, 3 line, so that at the maximum possible pressures p the parameter γ does not exceed ~1.5. The results of the calculation of the frequency fo the 3, 2 line are given in Figures 5 and 6.

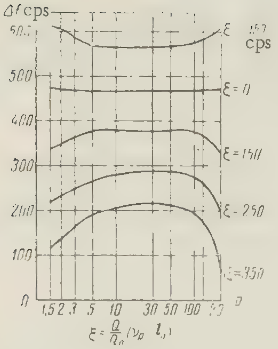

Figure 3. Dependence of the oscillatory frequency of the maser on the pressure in the molecular beam source when effect II is compensated for the J = 3, K = 3 line of $N^{14}H_3$. The pressure p is given in relative units, the p -axis scale is logarithmic.

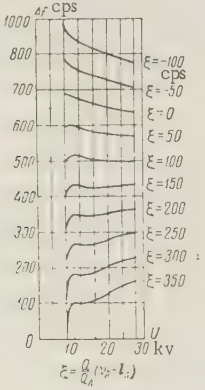

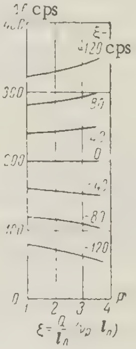

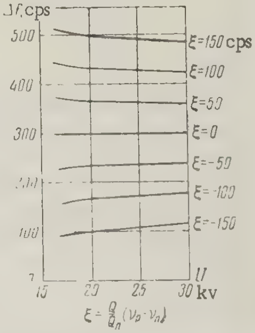

Figure 4. Dependence of the oscillatory frequency of the maser on the sorting system voltage with compensation of effect III for the J = 3, K = 3 line of $N^{14}H_3$.

Figure 5. Dependence of the oscillatory frequency of the maser on the sorting system voltage with compensation of effect III for the J = 3, K = 2 line of $N^{14}H_3$.

Figure 6. Dependence of the oscillatory frequency of the maser on the sorti system voltage with compensation of effect III for the J = 3, K = 2 line of N^{14}

2. EXPERIMENTAL INVESTIGATION OF THE MASER OPERATING ON THE 3, 2 LINE WITH TWO HEAD-ON BEAMS

The experimental investigations were carried out in a maser, which uses the inversion transition line J = 3, K = 2 of ammonia $N^{14}H_3$ and which does not possess quadrupole hyperfine structure. The feature of our design was the presence of two head-on beams (Figure 7)

---

*Actually, the 3, 2 line consists of 6 components caused by the hyperfine structure. The frequency separation between these components, however, is extremely small, and as a result their presence does not lead to a noticeable dependence of the peak of the line (to an accuracy of 10^{-11}) on the pressure and voltage.

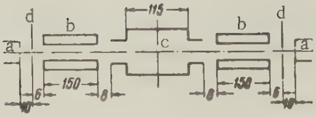

Figure 7. Schematic diagram of the maser with two head-on beams operating on the J = 3, K = 2 line of $N^{14}H_3$;
a - molecular beam source; b - quadrupole focussing device; c - cavity; d - diaphragm cooled by liquid nitrogen.

of ammonia molecules, which improved the self-excitation condition of the maser, and more importantly, allowed us to compensate partially for the nonuniformity of emission of molecules along the cavity resonator, a condition which leads to a shift in the frequency of oscillation of the maser [2,4]. In order to diminish this effect, we effected a power tap of the emission in the middle of the cavity resonator. The cavity resonator was made of invar; its parameters were selected in such a manner that the maser was excited in the TE_{010} mode. The cavity length was 11.2 cm, which ensured transit line width of the order of 1 kc. The cavity resonator was tuned with the aid of a screw dipped into the cavity resonator in its median plane. The frequency of the cavity resonator could be changed by several megacycles, without substantially lowering its quality ($Q \simeq 9000$). Sorting of the molecules according to energy levels was accomplished with the aid of quadrupole focussing devices 15 cm in length. In order to improve the beam intensity, we placed between the beam source and the sorting system a diaphragm with an aperture diameter 0.6 cm, cooled by liquid nitrogen. The beam of molecules was obtained with the aid of a lattice with square apertures 0.05 × 0.05 mm ; the distance between the apertures also equaled 0.05 mm.

This design of a maser was used to study its frequency of oscillation as a function of various parameters (pressure in the molecular beam source, voltage on the sorting system, and the cavity resonator frequency).

In our arrangement there were three masers of the same design. During the measurements of the dependence of the maser frequency on the parameters, the frequency of the adjustable maser was compared with the fixed frequency of another maser.*

The signal of the two masers was fed to the balanced mixer of a superheterodyne receiver, using as a heterodyne a klystron stabilized by a cavity resonator. The signal of intermediate frequency (60 Mc) was amplified by an amplifier with a 2 Mc band. At the detector output the difference frequency of the two masers was isolated and was compared with the frequency of an audio oscillator by means of Lissajous figures; a conversion circuit permitted a measurement of the frequency of the audio oscillator by means of a quartz crystal oscillator with an accuracy of 0.1-1 cps.

The pressure in the molecular beam source was measured by a manometer tube type LT-2.

For compensation of the effect related to the nonuniformity of the emission of molecules along the length of the cavity resonator, the pressure inside the source was determined with the aid of measurements of the frequency of oscillation of the maser. Two such pressures for each of the head-on beams were selected:

p_1' and p_1'' for the first beam
p_2' and p_2'' for the second beam,

at which the frequency of oscillation of the maser (which is a function of the pressure of the first and second beams) satisfied the following conditions:

$$\nu(p_1', p_2') = \nu(p_1'', p_2''). \tag{15}$$

Since the 3,2 line was used in the maser, the frequency of oscillation depends monotonically on pressure. Equation (15) ensures the equality of the beam intensity at $p_1' = p_2'$ and $p_1'' = p_2''$.

---

*The measurements showed that several hours after filling with liquid nitrogen, the relative change in the frequency of oscillation of the two masers did not exceed 1 cps after 10 min.

The measuring tube was used not as an absolute measuring device, but merely to fix a specific value of pressure. A check of the accuracy of such a method can be made from two absolute points of pressure, corresponding to the point where oscillations cease in each of the beams individually. The variation of the frequency of oscillation of the maser with pressure and voltage was recorded at various separations of the cavity resonator frequency and spectral line frequency. Then the characteristics were recorded both for a maser operating on a single beam, and for a maser operating with two identical head-on beams. The results of the measurements are given in Figures 8, 9, 10.

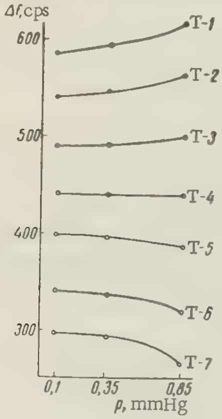

Figure 8. Dependence of the frequency of oscillation of a maser with two identical head-on beams (J = 3, K = 2, $N^{14}H_3$) on pressure in the molecular beam source (experimental curves).

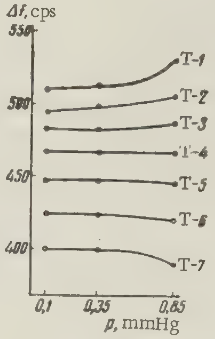

Figure 9. Dependence of the frequency of oscillation of a maser with a single beam (J = 3, K = 2, $N^{14}H_3$) on the pressure in the molecular beam source (experimental curves).

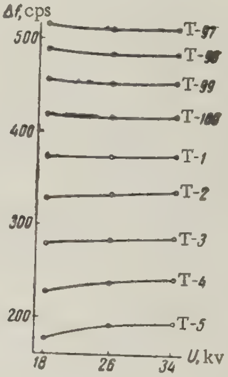

Figure 10. Dependence of the frequency of oscillation of a maser with two identical head-on beams (J = 3, K = 2, $N^{14}H_3$) on the voltage on the quadruple focusser (experimental curves).

It is apparent from the figures that for a maser with two identical head-on beams, there exists a value of cavity resonator frequency such that the frequency of oscillation of the maser does not depend on pressure. This corresponds to accurate tuning of the cavity resonator frequency to the spectral line frequency (resonance curve).

The curves of the frequency of oscillation of the maser as a function of pressure and volta recorded after equal intervals of change of cavity resonator frequency, are symmetrical relative to the resonance curve during operation of a maser with two different beams. During operation with a single beam, symmetry is violated, and the frequency of a maser with one beam differs from that of a maser with two head-on beams in the case of pressure tuning. The investigation of the possibility of tuning the frequency of the maser to the frequency of the spectral line showed that two different masers with two identical head-on beams having a symmetrical design relative to the cavity resonator (during a measurement of the difference frequency to an accuracy of 1-0.5 cps), tuning to an accuracy of 3 cps, was attained by a change in the pressure in the molecular beam source.

In the absence of symmetry in the design, together with a shift in the frequency of oscillation caused by the presence of a difference in molecular beam intensity, we observed an additional shift in the frequency of oscillation even in the case when each beam separately gave the same amplitude of oscillation: a change in the distance between the diaphragm and the molecular beam source in one half of the resonator reduced to a frequency shift in comparison with the frequency in the case of a symmetrical design by 15-20 cps, the shift being dependent on the voltage of the sorting system.

Upon decreasing the distance between the molecular beam source and the diaphragm by 8 mm in comparison with the dimensions indicated in Figure 7, we failed to obtain oscillation if the maser was operated on only one beam.

These effects are, evidently, connected with a change in the effective width of the spectral line in the cavity resonator. It is expedient to carry out a more extensive investigation of these effects in cavity resonators using $N^{14}H_3$, because in this case the parameters can be varied over wider limits.

3. DISCUSSION OF RESULTS

By comparing the calculated curves of the dependence of the frequency of oscillation of a maser for the 3,2 line on pressure and voltage with the experimental curves (Figures 5,6,8,10), we see that the calculated curves convey the functional behavior of the maser frequency. A quantitative comparison of the theoretical and experimental values requires absolute measurements of maser power, which are difficult to carry out with a sufficient degree of accuracy. It should be noted however that by means of a small change in the scale of the pressure axis, sufficiently good agreement can be obtained between the theoretical and experimental curves, which indicates the validity of the concepts prescribed in the calculation. We note that no choice of pressure scale enabled us to join the experimental curves recorded for a maser with a single molecular beam with the theoretical curves calculated for the case of compensation of effect III (nonuniformity of the emission of molecules along the cavity resonator).

A maser with two identical head-on beams, operating on a spectral line having no hyperfine structure and having a symmetrical design, can be used as an absolute frequency standard (time) to an accuracy of 10^{-10}.

REFERENCES

1. N.G. Basov, and A.M. Prokhorov, Uspekhi fiz. nauk, 1955, 1, 7, 485.
2. K. Shimoda, T.C. Wang, and C.H. Townes, Phys. Rev., 1956, 5, 102, 5, 1308.
3. K. Shimoda, J. Phys. Soc. Japan, 1957, 12, 1006; 1958, 13, 939.
4. N.G. Basov, and A.N. Orayevskiy, Radiotekhnika and elektronika, 1959, 4, 7, 1185.
5. N.G. Basov, G.M. Strakhovskiy, and I.V. Cheremiskin, Radiotekhnika and elektronika, 1961, 6, 6.
6. J.P. Gordon, Phys. Rev., 1955, 99, 4, 1253.

P.N. Lebedev Physics Institute,
Academy of Sciences, USSR

Submitted to editors 17 June 1960

Fe^{3+} SPIN LEVELS IN CORUNDUM

G.A. Siulina and G.A. Feshchenko

The eigenvalues of the spin Hamiltonian used by L.C. Kornienko and A.M. Prokhorov for the interpretation of the splitting of the spin levels of the Fe^{3+} ion in corundum are calculated and tabulated for magnetic field orientations in which both iron ions in the elementary cell are magnetically equivalent.

INTRODUCTION

The study of the electron paramagnetic resonance of the Fe^{3+} ion in corundum is of great importance for the creation of paramagnetic amplifiers.

In the Al_2O_3 crystal lattice, the Fe^{3+} ion is found in the ground state $^6S\,5/2$ and has a total electron spin $S = 5/2$. The strong electric field of the lattice splits the lower orbital singlet of the ion into three spin doublets, which are split further by an external magnetic field (Figure 1). The separations of the spin doublets equal $\Delta_1 = 0.402$ cm^{-1} and $\Delta_2 = 0.642$ cm^{-1}, and consequently even in a low magnetic field, a three level paramagnetic amplifier can be realized in the microwave region, because the mixing of states necessary for saturation of a subsidiary transition is guaranteed by both the external magnetic field and the cubic component of the crystal electric field [1, 2]. The decrease in magnitude of the magnetic field necessary for the operation of a paramagnetic amplifier is undoubtedly of practical interest.

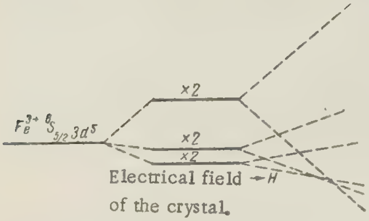

Figure 1. Splitting of the orbital singlet of the Fe^{3+} ion key.

By using the Fe^{3+} ion in the microwave region at various crystal orientations we can obtain versions of the paramagnetic amplifier two-stage use of subsidiary emission, enabling us to vary the frequency of the subsidiary emissio at a given signal frequency.

There is great interest in the use of Fe^{3+} in microwave paramagnetic amplifiers, because here the system of energy levels permits a version of the paramagnetic amplifier with two-stage use of subsidiary emission, whereas for the Cr^{3+} ion similar combined versions can be realized at waves shorter than 6 cm.

At an arbitrary orientation of the cubic axes of the magnetic field and of the trigonal axis of Fe^{3+} ion two magnetically nonequivalent systems [3, 4] are formed, each of which gives its system of lines of different intensity. Thus the complete spectrum consists of 30 lines. The richness of the spectrum creates favorable conditions for the study of cross relaxational phenomena in the paramagnetic amplifier [5], which arise with: a) matching of transitions between spin levels of the same ion; b) matching of transitions of ions of different systems; c) matching of transitions of the Fe^{3+} ion with transitions of another paramagnetic ion introduced into the same lattice.

The initial investigations of paramagnetic resonance of the Fe^{3+} ion in Al_2O_3 were made by L.C. Kornienko and A.M. Prokhorov [3], who showed that the observable spectrum of electron paramagnetic resonance can be explained with the aid of the spin Hamiltonian in the form proposed by Bleaney and Trenam [6]. Its constants were measured at room temperatures. The measurements of the constants over a wide temperature range were performed by Bogle and Symmons [4]. A calculation of the eigenvalues and wave function for a parallel orientation was made by V.M. Vinokurov, M.M. Zaripov and N.R. Yafayev [7].

In this paper a calculation is made of the energy level at an arbitrary orientation of the magnetic field relative to the trigonal axis in the planes for which all the ions are magnetically equivalent. The numerical results are given in the form of tables and graphs enabling us to find the magnitude of the magnetic field, the crystal orientation and the wavelength of the subsidiary emission, at which it is possible to create a paramagnetic amplifier of a given range, and to calculate the probability of transitions for the fundamental and subsidiary emission.

1. SPIN HAMILTONIAN AND NONEQUIVALENT SYSTEMS

The paramagnetic properties of a Fe^{3+} ion, introduced into the Al_2O_3 crystal lattice, are determined by the trigonal and cubic components of the electric field created at the site of the position of this ion by the octahedrom of oxygen ions. In this case there exist two types of octahedrons corresponding to two possible positions of the Fe^{3+} ion in the unit cell. The trigonal axes of symmetry for both types of octahedrons coincide and form the (111) direction in the cubic axis system, and the cubic axes corresponding to different octahedrons, are turned 60° relative to one another around the trigonal axis. Therefore, for an arbitrary mutual orientation of the external magnetic field the trigonal axis and cubic xes of magnetically nonequivalent ions differ in the orientation of cubic axes. Experiment nows [3, 4] that for any orientation of the magnetic field relative to the trigonal axis, the pectra of both systems can be superimposed by turning the crystal around the trigonal axis, e., by choosing the orientation of the cubic axes relative to the magnetic field. We will larify the conditions under which this occurs.

The splitting of the spin levels of the Fe^{3+} ion in corundum is interpreted with the help of the pin Hamiltonian in the form

$$\hat{\mathcal{H}} = g\beta \vec{H}\hat{\vec{S}} + \frac{a}{6}\left[\hat{S}_\xi^4 + \hat{S}_\eta^4 + \hat{S}_\zeta^4 - \frac{1}{5}S(S+1)(3S^2+3S-1)\right] +$$

$$+ D\left[\hat{S}_z^2 - \frac{1}{3}S(S+1)\right] + \frac{1}{180}F\left[35\hat{S}_z^4 - 30S(S+1)\hat{S}_z^2 +\right.$$

$$\left. + 25\hat{S}_z^2 - 6S(S+1) + 3S^2(S+1)^2\right],$$

vhere S is the effective spin (S + 5/2); $\hat{S}_x$, $\hat{S}_y$, $\hat{S}_z$ are the operators of the projection of spin on he axis of a coordinate system in which the Z axis coincides with the trigonal symmetry axis f the crystal field; $\hat{S}_\xi$, $\hat{S}_\eta$, $\hat{S}_\zeta$ are operators of the projection of spin in the cubic system of oordinates; $\vec{H}$ is the vector external magnetic field; g is the spectroscopic splitting factor; is the Bohr magneton; D, F are constants of the electric crystalline fields of trigonal ymmetry, of the second and fourth orders respectively; a is the constant of the electric field f cubic symmetry. The constants of the spin Hamiltonian depend on temperature and at .2°K have the following values: $D = 0.1719\ cm^{-1}$ $a-F - 0.339\ cm^{-1}$, $|a| = 0.0224\ cm^{-1}$, g = 2.003 [4].

For a spin Hamiltonian of the form (1), the influence of a cubic field on the angular dependence of spectrum in strong magnetic fields is determined by the magnitude of the parameter $p = l^2m^2 + l^2n^2 + m^2n^2$, where l, m, n are the directional cosines of the magnetic field in cubic axes [6]. We choose a coordinate system in which the magnetic field lies in the zox plane. If the angle between the magnetic field and trigonal axis equals α, the directional cosines of the magnetic field in the x, y, z axes equal $l_0 = \sin\alpha$, $m_0 = 0$, $n_0 = \cos\alpha$. The orientation of the cubic axes is characterized by the Euler angles θ_i, ψ_i, $\varphi_i (i = 1,2)$, wherein $\theta_1 = \theta_2$, $\varphi_1 = \varphi_2$, $\psi_2 = \psi_1 + 60°$.

For our choice of the relative location of ξ_i, η_i, ζ_i and x, y, z $\varphi_i = 225°$, $\theta_i = 125°$ and the directional cosines of the magnetic field in the cubic axes equal

$$l = -\frac{1}{\sqrt{2}}\sin\alpha\left(\cos\psi + \sqrt{\frac{1}{3}}\sin\psi\right) - \sqrt{\frac{1}{3}}\cos\alpha,$$

$$m = \frac{1}{\sqrt{2}}\sin\alpha\left(\cos\psi - \sqrt{\frac{1}{3}}\sin\psi\right) - \sqrt{\frac{1}{3}}\cos\alpha,$$

$$n = \sqrt{\frac{2}{3}}\sin\alpha\ \sin\psi - \sqrt{\frac{1}{3}}\cos\alpha.$$

For the parameter p we obtain

$$p = \frac{1}{4}\sin^3\alpha + \frac{1}{3}\cos^4\alpha + \frac{5\sqrt{2}}{3}\sin^3\alpha\cos\alpha\sin 3\psi. \quad (2)$$

In the parallel ($\alpha = 90°$) orientations p does not depend on ψ, and all the ions are magnetically equivalent. At the intermediate orientations, with a rotation of the crystal around the trigonal axis, the spectrum of each system is repeated after 120°, and the total observable spectrum after 60°. The conditions of coincidence of the spectra of the two systems can be represented in the form

$$p(\psi) = p(\psi + 60°),$$

which, taking into account (2), leads to the condition $\psi_0 = n\pi/3$, $n = 1, 2, 3, \ldots$. It is easy to convince oneself that, in this case, the zox plane containing the magnetic field vector lies at half the dihedral angle formed by planes passing through the trigonal and corresponding cubic axes of the two systems. Thus the equivalency of the ions is due to the presence of cubic axes relative to planes containing a trigonal axis and magnetic field, and consequently, the result obtained above is valid for any value of the magnetic field.

When the spectra coincide, the sign of the constants of the cubic field does not influence the results, and the experimental data are sufficient for carrying out numerical calculations.

2. SECULAR EQUATION. NUMERICAL RESULTS

We calculate the spin Hamiltonian (1) in the representation, in which the operators $\hat{S}^2$, $\hat{S}_z$ are diagonal. Using the three-dimensional rotation matrix with $\theta = 125°16'$, $\varphi = 225°$, $\psi = 0$ and transforming the components of spin in the cubic axes according to a proper transformatio of the components of the vector, one can show that in the S_z representation the energy matrix h the form

$$\mathcal{H}_{ik} = \begin{Vmatrix} \left[\frac{10-b}{3} + \frac{5}{2} h\cos\alpha\right] & \frac{\sqrt{5}}{2} h\sin\alpha & 0 & -ic & 0 & 0 \\ \frac{\sqrt{5}}{2} h\sin\alpha & \left[-\frac{2}{3} + b + \frac{3}{2} h\cos\alpha\right] & \sqrt{2}\, h\sin\alpha & 0 & 0 & 0 \\ 0 & \sqrt{2}\, h\sin\alpha & \left[-\frac{8+2b}{3} + \frac{1}{2} h\cos\alpha\right] & \frac{3}{2} h\sin\alpha & 0 & ic \\ ic & 0 & \frac{3}{2} h\sin\alpha & \left[-\frac{8+2b}{3} - \frac{h}{2}\cos\alpha\right] & \sqrt{2}\, h\sin\alpha & 0 \\ 0 & 0 & 0 & \sqrt{2}\, h\sin\alpha & \left[-\frac{2}{3} + b - \frac{3}{2} h\cos\alpha\right] & \frac{\sqrt{5}}{2} h\sin\alpha \\ 0 & 0 & -ic & 0 & \frac{\sqrt{5}}{2} h\sin\alpha & \left[\frac{10-b}{3} - \frac{5}{2} h\cos\alpha\right] \end{Vmatrix} \quad (3)$$

where the dimensionless values $h = \frac{g\beta}{D} H$, $b = \frac{a-F}{D}$, $c = \frac{2}{3}\sqrt{5}\frac{a}{D}$ are introduced.

The eigenvalues are roots of the secular equation

$$|\mathcal{H}_{ik} - \varepsilon\delta_{ik}| = 0, \quad (4)$$

where $\varepsilon = E/D$.

In the case of a parallel ($\alpha = 0$) and perpendicular ($\alpha = 90°$) orientations this equation decomposes into a number of equations of lower order. Thus, in the parallel orientation equatio (4) is decomposed into two linear and two quadratic equations, which enables us to obtain simp relations for the eigenvalues and wave functions [7]. In the perpendicular orientation, equation (4) decomposes into two cubic equations and can be written in the form

$$\begin{vmatrix} \frac{10-b}{3} - \varepsilon & \frac{\sqrt{5}}{2} h & -ic \\ \frac{\sqrt{5}}{2} h & -\frac{2}{3} + b - \varepsilon & \sqrt{2}\, h \\ ic & \sqrt{2}\, h & \frac{3}{2} h - \frac{8+2b}{3} - \varepsilon \end{vmatrix} \begin{vmatrix} \frac{10-b}{3} - \varepsilon & \frac{\sqrt{5}}{2} h & -ic \\ \frac{\sqrt{5}}{2} h & -\frac{2}{3} + b - \varepsilon & \sqrt{2}\, h \\ ic & \sqrt{2}\, h & -\frac{3}{2} h - \frac{8+2b}{3} - \varepsilon \end{vmatrix} = 0. \quad (5)$$

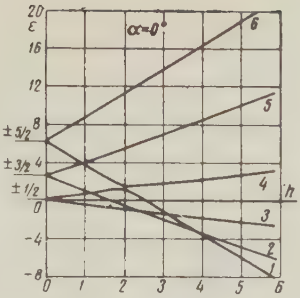

Figure 2. Energy-level diagram of Fe^{3+} ion in corundum for $\alpha = 0°$.

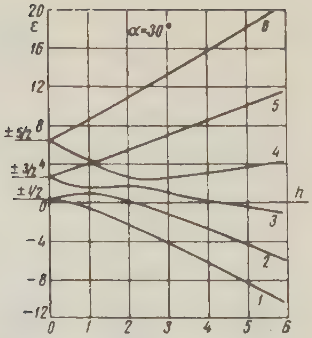

Figure 3. Energy-level diagram of Fe^{3+} ion in corundum for $\alpha = 30°$.

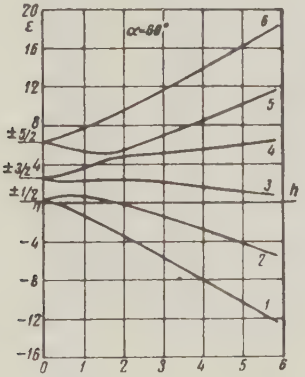

Figure 4. Energy-level diagram of Fe^{3+} ion in corundum for $\alpha = 60°$.

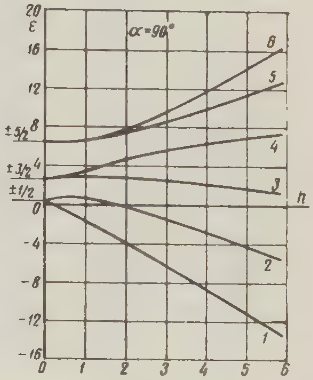

Figure 5. Energy-level diagram of Fe^{3+} ion in corundum for $\alpha = 90°$.

In the general case of an arbitrary orientation, one must obtain a numerical solution of a sixth-degree equation. Solving equation (4), we can demonstrate that its coefficients are real.

We have carried out a numerical solution of equation (4) over the interval $\alpha = 0 - 90°$, $h = 0-5.9$ with a step of $\Delta h = 0.1$, $\Delta\alpha = 5°$. The behavior of the energy levels with a change in the magnitude of the magnetic field for $\alpha = 0, 30, 60, 90°$ is illustrated in Figures 2-5. In the appendix, values are given for the energy of the spin levels ε_i of the Fe^{3+} ion in corundum for seven orientations of the external magnetic field with respect to the trigonal axis of the crystal ($\alpha = 0, 15, 30, 45, 60, 75, 90°$) with a step of $\Delta h = 0.2$ ($\Delta H = 364.5$ oe).

It is essential to note that upon diagonalizing matrix (3) the value was increased to $\frac{63}{64}\frac{a-F}{D}+\frac{35}{12} = 3.1104$. This shift of the level must be taken into account when calculating the wave functions.

The authors express their gratitude to A.M. Prokhorov and L.S. Korniyenko for their interest in the work and fruitful discussions.

Appendix

Spin Levels of the Fe^{3+} Ion in Corundum*

h	ε_1	ε_2	ε_3	ε_4	ε_5	ε_6
$\alpha = 0°$						
0.0	0,3126	0,3126	2,6413	2,6413	6,3784	6,3784
0.2	0,2070	0,4058	2,3413	2,9413	5,8853	6,8840
0.4	0,1075	0,5049	2,0413	3,2413	5,3861	7,3836
0.6	0,0078	0,6038	1,7413	3,5413	4,8872	7,8832
0.8	—0,0918	0,7024	1,4413	3,8413	4,3886	8,3828
1.0	—0,1915	0,8004	1,1413	3,8906	4,1413	8,8825
1.2	—0,2912	0,8413	0,8974	3,3936	4,4413	9,3823
1.4	—0,3910	0,5413	0,9926	2,8984	4,7413	9,8821
1.6	—0,4908	0,2413	1,0835	2,4075	5,0413	10,3819
1.8	—0,5906	—0,0587	1,1601	1,9309	5,3813	10,8817
2.0	—0,6905	—0,3587	1,1485	1,5425	5,6413	11,3815
2.2	—0,7903	—0,6587	0,8152	1,4758	5,9413	11,8814
2.4	—0,9587	—0,8902	0,3460	1,5450	6,2413	12,3812
2.6	—1,2587	—0,9901	—0,1431	1,6341	6,5413	12,8811
2.8	—1,5587	—1,0900	—0,6377	1,7287	6,8413	13,3810
3.0	—1,8587	—1,1898	—1,1344	1,8255	7,1413	13,8809
3.2	—2,1587	—1,6322	—1,2897	1,9233	7,4413	14,3808
3.4	—2,4587	—2,1307	—1,3897	2,0218	7,7413	14,8807
3.6	—2,7587	—2,6296	—1,4896	2,1206	8,0413	15,3806
3.8	—3,1287	—3,0587	—1,5895	2,2197	8,3413	15,8805
4.0	—3,6280	—3,3587	—1,6994	2,3190	8,6413	16,3805
4.2	—4,1274	—3,6587	—1,7894	2,4184	8,9413	16,8804
4.4	—4,6269	—3,9587	—1,8893	2,5179	9,2413	17,3803
4.6	—5,1265	—4,2587	—1,9892	2,6175	9,5413	17,8803
4.8	—5,6261	—4,5587	—2,0892	2,7172	9,8413	18,3802
5.0	—6,1258	—4,8587	—2,1891	2,8169	10,1413	18,8802
5.2	—6,6256	—5,1587	—2,2891	2,9166	10,4413	19,3801
5.4	—7,1253	—5,4587	—2,3890	3,0164	10,7413	19,8801
5.6	—7,6251	—5,7587	—2,4890	3,1162	11,0413	20,3800
5.8	—8,1249	—6,0587	—2,5889	3,2160	11,3413	20,8800
$\alpha = 15°$						
0.2	0,1805	0,4276	2,3531	2,9324	5,9032	6,8679
0.4	0,0492	0,5443	2,0688	3,2255	5,4241	7,3528
0.6	—0,0888	0,6562	1,7904	3,5201	4,9478	7,8391
0.8	—0,2350	0,7607	1,5217	3,8158	4,4749	8,3266
1.0	—0,3913	0,8460	1,2764	4,0012	4,1173	8,8152
1.2	—0,5600	0,8385	1,1294	3,5406	4,4115	9,3047
1.4	—0,7437	0,6589	1,1613	3,0836	4,7095	9,7951
1.6	—0,9448	0,4338	1,2451	2,6364	5,0081	10,2861
1.8	—1,1652	0,2083	1,3301	2,2066	5,3071	10,7779
2.0	—1,4061	—0,0118	1,3778	1,8283	5,6063	11,2702
2.2	—1,6676	—0,2283	1,2175	1,6742	5,9059	11,7630
2.4	—1,9490	—0,4468	0,8721	1,7264	6,2056	12,2564
2.6	—2,2491	—0,6756	0,5181	1,8158	6,5055	12,7501
2.8	—2,5670	—0,9246	0,1932	1,9134	6,8055	13,2442
3.0	—2,9015	—1,2011	—0,0907	2,0138	7,1056	13,7387
3.2	—3,2520	—1,5057	—0,3323	2,1154	7,4058	14.2335
3.4	—3,6178	—1,8321	—0,5376	2,2175	7,7060	14,7287
3.6	—3,9981	—2,1716	—0,7159	2,3200	8,0063	15,2240
3.8	—4,3921	—2,5169	—0,8750	2,4225	8,3066	15,7197
4.0	—4,7989	—2,8630	—1,0209	2,5250	8,6070	16,2155
4.2	—5,2172	—3,2071	—1,1573	2,6275	8,9074	16,7116
4.4	—5,6460	—3,5479	—1,2869	2,7299	9,2078	17,2079
4.6	—6,0839	—3,8846	—1,4114	2,8322	9,5082	17,7043
4.8	—6,5298	—4,2174	—1,5321	2,9345	9,8086	18,2009
5.0	—6,9826	—4,5464	—1,6497	3,0366	10,1091	18,6977
5.2	—7,4412	—4,8719	—1,7650	3,1387	10,4095	19,1946
5.4	—7,9049	—5,1944	—1,8783	3,2407	10,7099	19,6917
5.6	—8,3729	—5,5143	—1,9901	3,3427	11,0104	20,1889
5.8	—8,8445	—5,8318	—2,1005	3,4445	11,3108	20,6862

* In the following tables, all commas represent decimal points.

Appendix (continued)

h	ε_1	ε_2	ε_3	ε_4	ε_5	ε_6
$\alpha = 30°$						
0,2	0,1251	0,4704	2,3873	2,9059	5,9557	6,8203
0,4	—0,0730	0,6149	2,1477	3,1786	5,5346	7,2620
0,6	—0,2881	0,7343	1,9295	3,4574	5,1228	7,7088
0,8	—0,5204	0,8151	1,7469	3,7408	4,7221	8,1602
1,0	—0,7699	0,8316	1,6252	4,0244	4,3378	8,6156
1,2	—1,0366	0,7615	1,5850	3,9521	4,3281	9,0746
1,4	—1,3199	0,6185	1,6093	3,6015	4,6185	9,5369
1,6	—1,6191	0,4335	1,6613	3,2734	4,9136	10,0019
1,8	—1,9332	0,2255	1,7110	2,9811	5,2108	10,4696
2,0	—2,2614	0,0022	1,7307	2,7444	5,5093	10,9396
2,2	—2,6027	—0,2338	1,6883	2,5924	5,8088	11,4116
2,4	—2,9561	—0,4817	1,5688	2,5390	6,1092	11,8856
2,6	—3,3208	—0,7413	1,3961	2,5594	6,4102	12,3612
2,8	—3,6960	—1,0120	1,2027	2,6200	6,7116	12,8384
3,0	—4,0810	—1,2928	1,0073	2,7008	7,0134	13,3171
3,2	—4,4751	—1,5823	0,8177	2,7919	7,3155	13,7970
3,4	—4,8775	—1,8791	0,6366	2,8886	7,6178	14,2781
3,6	—5,2877	—2,1817	0,4645	2,9890	7,9202	14,7603
3,8	—5,7050	—2,4887	0,3009	3,0912	8,2228	15,2435
4,0	—6,1290	—2,7989	0,1449	3,1946	8,5254	15,7277
4,2	—6,5589	—3,1114	—0,0044	3,2987	8,8281	16,2127
4,4	—6,9944	—3,4253	—0,1480	3,4033	9,1308	16,6984
4,6	—7,4350	—3,7400	—0,2866	3,5080	9,4334	17,1849
4,8	—7,8802	—4,0552	—0,4210	3,6129	9,7361	17,6721
5,0	—8,3295	—4,3704	—0,5518	3,7177	10,0388	18,1599
5,2	—8,7827	—4,6854	—0,6794	3,8225	10,3414	18,6483
5,4	—9,2394	—5,0001	—0,8043	3,9273	10,6440	19,1372
5,6	—9,6993	—5,3143	—0,9268	4,0319	10,9465	19,6267
5,8	—10,1620	—5,6280	—1,0473	4,1364	11,2490	20,1166
$\alpha = 45°$						
0,2	0,0671	0,5113	2,4405	2,8632	6,0385	6,7442
0,4	—0,2009	0,6729	2,2673	3,1022	5,7075	7,1158
0,6	—0,4932	0,7791	2,1316	3,3554	5,3937	7,4982
0,8	—0,8062	0,8155	2,0453	3,6202	5,0996	7,8903
1,0	—1,1372	0,7759	2,0123	3,8935	4,8292	8,2911
1,2	—1,4837	0,6695	2,0203	4,1663	4,5924	8,6998
1,4	—1,8439	0,5149	2,0476	4,3014	4,5290	9,1157
1.6	—2,2160	0,3276	2,0745	4,1498	4,7909	9,5379
1,8	—2,5986	0,1176	2,0868	4,0069	5,0861	9,9660
2,0	—2,9908	—0,1092	2,0755	3,9019	5,3878	10,3995
2,2	—3,3913	—0,3493	2,0367	3,8381	5,6928	10,8377
2,4	—3,7995	—0,6003	1,9712	3,8131	5,9999	11,2803
2,6	—4,2145	—0,8605	1,8835	3,8209	6,3084	11,7270
2.8	—4,6359	—1,1284	1,7796	3,8545	6,6177	12,1772
3,0	—5,0629	—1,4029	1,6649	3,9072	6,9276	12,6308
3,2	—5,4950	—1,6829	1,5438	3,9738	7,2377	13,0874
3,4	—5,9320	—1,9675	1,4192	4,0502	7,5480	13,5468
3,6	—6,3732	—2,2561	1,2932	4,1337	7,8583	14,0088
3,8	—6,8185	—2,5478	1,1670	4,2224	8,1685	14,4731
4,0	—7,2673	—2,8421	1,0415	4,3147	8,4785	14,9395
4,2	—7,7195	—3,1386	0,9169	4,4098	8,7883	15,4079
4,4	—8,1748	—3,4368	0,7936	4,5068	9,0978	15,8782
4,6	—8,6329	—3,7365	0,6716	4,6053	9,4070	16,3501
4,8	—9,0936	—4,0372	0,5510	4,7050	9,7160	16,8236
5,0	—9,5567	—4,3389	0,4318	4,8054	10,0247	17,2985
5,2	—10,0220	—4,6413	0,3137	4,9065	10,3330	17,7747
5,4	—10,4893	—4,9443	0,1969	5,0080	10,6411	18,2522
5,6	—10,9584	—5,2477	0,0812	5,1099	10,9489	18,7309
5,8	—11,4294	—5,5514	—0,0335	5,2121	11,2564	19,2106

Appendix (continued)

h	ε_1	ε_2	ε_3	ε_4	ε_5	ε_6
$\alpha = 60°$						
0,2	0,0189	0,5422	2,5080	2,8063	6,1452	6,6441
0,4	—0,3067	0,7099	2,4126	2,9992	5,9277	6,9221
0,6	—0,6605	0,7949	2,3609	3,4181	5,7340	7,2173
0,8	—1,0356	0,7942	2,3507	3,4607	5,5664	7,5284
1,0	—1,4271	0,7195	2,3681	3,7221	5,4280	7,8541
1,2	—1,8316	0,5897	2,3951	3,9948	5,3233	8,1934
1,4	—2,2466	0,4214	2,4178	4,2665	5,2605	8,5452
1,6	—2,6704	0,2262	2,4267	4,5145	5,2580	8,9086
1,8	—3,1014	0,0114	2,4216	4,7011	5,3493	9,2827
2,0	—3,5387	—0,2180	2,3986	4,8081	5,5483	9,6666
2,2	—3,9815	—0,4590	2,3598	4,8699	5,8160	10,0595
2,4	—4,4289	—0,7092	2,3072	4,9201	6,1147	10,4608
2,6	—4,8805	—0,9669	2,2430	4,9723	6,4271	10,8697
2,8	—5,3358	—1,2308	2,1695	5,0306	6,7457	11,2856
3,0	—5,7944	—1,4999	2,0887	5,0954	7,0671	11,7078
3,2	—6,2559	—1,7733	2,0022	5,1662	7,3895	12,1360
3,4	—6,7201	—2,0505	1,9114	5,2422	7,7121	12,5695
3,6	—7,1866	—2,3307	1,8174	5,3225	8,0343	13,0079
3,8	—7,6553	—2,6137	1,7209	5,4064	8,3558	13,4507
4,0	—8,1260	—2,8989	1,6225	5,4931	8,6764	13,8976
4,2	—8,5985	—3,1861	1,5229	5,5822	8,9960	14,3483
4,4	—9,0727	—3,4749	1,4222	5,6732	9,3146	14,8023
4,6	—9,5483	—3,7652	1,3208	5,7657	9,6322	15,2595
4,8	—10,0253	—4,0568	1,2189	5,8596	9,9488	15,7195
5,0	—10,5036	—4,3494	1,1167	5,9545	10,2644	16,1821
5,2	—10,9831	—4,6429	1,0142	6,0503	10,5792	16,6471
5,4	—11,4637	—4,9373	0,9115	6,1469	10,8930	17,1143
5,6	—11,9453	—5,2324	0,8087	6,2440	11,2061	17,5835
5,8	—12,4278	—5,5281	0,7059	6,3416	11,5184	18,0546
$\alpha = 75°$						
0,2	—0,0125	0,5611	2,5838	2,7381	6,2680	6,5262
0,4	—0,3755	0,7290	2,5677	2,8743	6,1775	6,6917
0,6	—0,7683	0,7975	2,5868	3,0544	6,1141	6,8802
0,8	—1,1820	0,7742	2,6232	3,2793	6,0793	7,0907
1,0	—1,6105	0,6802	2,6591	3,5392	6,0744	7,3222
1,2	—2,0501	0,5370	2,6843	3,8181	6,1014	7,5740
1,4	—2,4981	0,3599	2,6953	4,1000	6,1625	7,8451
1,6	—2,9528	0,1590	2,6916	4,3719	6,2603	8,1346
1,8	—3,4129	—0,0591	2,6744	4,6236	6,3969	8,4418
2,0	—3,8774	—0,2903	2,6449	4,8491	6,5726	8,7658
2,2	—4,3455	—0,5317	2,6048	5,0469	6,7845	9,1057
2,4	—4,8168	—0,7811	2,5556	5,2193	7,0271	9,4606
2,6	—5,2907	—1,0371	2,4989	5,3711	7,2931	9,8294
2,8	—5,7668	—1,2985	2,4357	5,5075	7,5757	10,2112
3,0	—6,2450	—1,5644	2,3672	5,6328	7,8693	10,6048
3,2	—6,7248	—1,8341	2,2942	5,7505	8,1698	11,0092
3,4	—7,2063	—2,1070	2,2175	5,8628	8,4743	11,4234
3,6	—7,6890	—2,3827	2,1378	5,9714	8,7811	11,8463
3,8	—8,1730	—2,6608	2,0554	6,0775	9,0888	12,2769
4,0	—8,6581	—2,9409	1,9708	6,1817	9,3967	12,7145
4,2	—9,1441	—3,2229	1,8844	6,2847	9,7044	13,1583
4,4	—9,6311	—3,5065	1,7964	6,3868	10,0117	13,6074
4,6	—10,1188	—3,7914	1,7070	6,4882	10,3184	14,0614
4,8	—10,6073	—4,0776	1,6165	6,5892	10,6244	14,5196
5,0	—11,0964	—4,3649	1,5250	6,6897	10,9298	14,9815
5,2	—11,5861	—4,6532	1,4327	6,7901	11,2346	15,4468
5,4	—12,0764	—4,9424	1,3396	6,8902	11,5388	15,9150
5,6	—12,5672	—5,2323	1,2458	6,9902	11,8425	16,3858
5,8	—13,0585	—5,5230	1,1515	7,0900	12,1457	16,8590

Appendix (continued)

h	ε_1	ε_2	ε_3	ε_4	ε_5	ε_6
$\alpha = 90°$						
0,4	—0,3992	0,7348	2,6942	2,7587	6,4381	6,4381
0,6	—0,8054	0,7973	2,7343	2,9286	6,5041	6,5059
0,8	—1,2321	0,7665	2,7693	3,1639	6,5953	6,6018
1,0	—1,6731	0,6664	2,7944	3,4393	6,7111	6,7266
1,2	—2,1244	0,5187	2,8074	3,7312	6,8494	6,8824
1,4	—2,5835	0,3387	2,8078	4,0225	7,0080	7,0711
1,6	—3,0485	0,1359	2,7961	4,3022	7,1848	7,2943
1,8	—3,5183	—0,0835	2,7733	4,5633	7,3774	7,5526
2,0	—3,9919	—0,3153	2,7406	4,8026	7,5837	7,8450
2,2	—4,4685	—0,5568	2,6991	5,0199	7,8017	8,1693
2,4	—4,9477	—0,8060	2,6502	5,2164	8,0299	8,5220
2,6	—5,4291	—1,0615	2,5949	5,3950	8,2666	8,8989
2,8	—5,9123	—1,3220	2,5341	5,5583	8,5106	9,2961
3,0	—6,3971	—1,5869	2,4686	5,7093	8,7609	9,7099
3,2	—6,8832	—1,8553	2,3990	5,8504	9,0165	10,1374
3.4	—7.3705	—2,1269	2,3261	5,9835	9,2768	10,5757
3,6	—7,8588	—2,4011	2,2501	6,1104	9,5411	11,0230
3,8	—8,3481	—2,6776	2,1717	6,2324	9,8088	11,4776
4,0	—8,8382	—2,9561	2,0910	6,3503	10,0795	11,9382
4,2	—9,3289	—3,2364	2,0085	6,4651	10,3528	12,4037
4,4	—9,8203	—3,5182	1,9242	6,5773	10,6285	12,8733
4,6	—10,3123	—3,8014	1,8385	6,6875	10,9062	13,3463
4,8	—10,8048	—4,0859	1,7516	6,7959	11,1856	13,8223
5,0	—11,2979	—4,3714	1,6635	6,9030	11,4667	14,3008
5,2	—11,7912	—4.6579	1,5744	7,0089	11,7492	14,7814
5,4	—12,2850	—4,9454	1,4844	7,1139	12,0330	15,2638
5,6	—12,7792	—5,2336	1,3936	7,2181	12,3179	15,7478
5,8	—13,2737	—5,5225	1,3022	7,3217	12,6039	16,2332

REFERENCES

1. L.S. Korniyenko, and A.M. Prokhorov, ZhETF, 1959, 36, 919.
2. J.E. King, and R.W. Terhune, J. Appl. Phys., 1959, 30, 1844.
3. L.S. Korniyenko, and A.M. Prokhorov, ZhETF, 1957, 33, 805.
4. G.S. Bogle, and H.F. Symmons, Proc. Phys. Soc., 1959, 73, 531.
5. N. Bloembergen, S. Shapiro, P.S. Pershan, and J.O. Artman, Phys. Rev., 1959, 114, 445.
6. B. Bleaney, and R.S. Trenam, Proc. Roy. Soc., A. 1954, 223, 1.
7. V.M. Vinokurov, M.M. Zaripov, and N.R. Yafayev, ZhETF, 1959, 37, 312.

Submitted to editors 29 March 1960

BRIEF COMMUNICATIONS

INCREASE IN THE TRANSMISSION RANGE OF PULSE SIGNALS OF GIVEN ENERGY IN THE PRESENCE OF NOISE WITH AN ARBITRARY SPECTRUM

F.I. Khaytun

1. FORMULATION OF THE PROBLEM

When the transmission of pulsed radio signals is accompanied by noise with a constant spectral density in the operating frequency range (for example, fluctuation noise in a vacuum-tube receiver), the limiting range attained under optimal signal-reception conditions is determined by the energy of the radiated pulse [1]. There is no transformation of a radiated pulse of given energy capable of increasing this limiting range, corresponding to realization of the required signal/noise ratio on the receiving end. However, noise acting on the receiver may also have a nonuniform spectral density (for example, noise in semiconductor amplifiers or certain external interference).

We show in this article that in the presence of noise with a nonuniform spectrum, the range of transmission can be increased by rational shaping of the radiated pulses, keeping their energy constant (or by keeping constant the average transmitter power for a specified pulse repetition frequency).

We also consider briefly the transmission of light (optical) pulse signals; this case is quite distinct, owing to the peculiarities of the transformation of light signals into electric signals.

2. DERIVATION OF GENERAL EXPRESSION FOR THE THEORETICALLY ATTAINABLE IMPROVEMENT IN THE SIGNAL/NOISE RATIO AND INCREASE IN THE TRANSMISSION RANGE.

Assume that it is necessary to transmit a radio signal in the form of a pulse, characterize by a certain function $f_1(t)$, which is the time dependence of the instantaneous value of the radiated power. Further, let the initial pulse of radiation be transformed so that its amplitude increases as λ, and its duration decreases as $1/\lambda$, while the energy and waveform of the pulse remain constant.

It is easy to show that in this case the transformed pulse is described by the function

$$f_2(t) = \lambda f_1(\lambda t). \tag{1}$$

The radiation pulses induce voltage (or current) pulses in the receiving antenna. The initial and transformed pulses are denoted by $x_1(t)$ and $x_2(t)$, respectively.

The signal voltage produced in the receiving antenna is proportional to the field intensity, i.e., to the square root of the power of the electromagnetic wave. Consequently, if the radiated pulse is subjected to transformation (1), the corresponding voltage (or current) signal pulses in the receiving antenna will be related by

$$x_2(t) = \sqrt{\lambda}\, x_1(\lambda t). \tag{2}$$

We now undertake to determine theoretically the attainable improvement in signal/noise ratio under this transformation of the radiated pulse, in the case of noise having an arbitrary spectral-density distribution. We start from the premise that the transfer function (frequency characteristic) of the receiver amplifier is chosen every time to be optimal for the given pulse signal, and that a maximum possible ratio (M) of peak signal to mean-squared noise is obtained at the output of the amplifier.

The maximum signal/noise ratio can be represented in the form [2]

$$M = \sqrt{\frac{1}{\pi}\int\limits_{0}^{\infty} [\Phi^2(\omega)/G(\omega)]\, d\omega}\,, \tag{3}$$

where $\Phi(\omega)$ is the spectrum of the signal amplitudes and $G(\omega)$ is the energy spectrum of the noise.

We are considering such combinations of the working-signal and noise spectrum, under which the integral in (3) converges.

Let us now see how M changes if the input signal pulse is subjected to transformation (2).

On the basis of (3), the quantity characterizing the relative change in the signal/noise ratio can be represented in the form

$$\frac{M_2}{M_1} = \alpha = \sqrt{\frac{\int\limits_{0}^{\infty}[\Phi_2^2(\omega)/G(\omega)]\, d\omega}{\int\limits_{0}^{\infty}[\Phi_1^2(\omega)/G(\omega)]d\omega}}\,, \tag{4}$$

where M_1 and M_2 are the maximum attainable signal/noise ratios for the pulses $x_1(t)$ and $x_2(t)$ respectively; $\Phi_1(\omega)$ and $\Phi_2(\omega)$ are the amplitude spectra of pulses $x_1(t)$ and $x_2(t)$.

We shall designate the efficiency of transformation by a quantity α. Since the spectrum of the function $x_1(\lambda t)$ is $\frac{1}{\lambda}\Phi_1(\frac{\omega}{\lambda})$, the spectrum of the transformed pulse, taking (2) into account, is expressed by

$$\Phi_2(\omega) = \frac{1}{\sqrt{\lambda}}\,\Phi_1\left(\frac{\omega}{\lambda}\right). \tag{5}$$

From (4) and (5) we obtain after elementary transformations

$$\alpha = \sqrt{\beta}\,, \tag{6}$$

where

$$\beta = \frac{\int\limits_{0}^{\infty}[\Phi_1^2(\omega)/G(\lambda\omega)]d\omega}{\int\limits_{0}^{\infty}[\Phi_1^2(\omega)/G(\omega)]d\omega}. \tag{7}$$

This is the general expression for the efficiency of conversion of pulsed signals.

When $\alpha > 1$ the signal/noise ratio is improved, so that the maximum transmission range can be increased. When the flux density of the electromagnetic power decreases as the square of the transmitted distance, the intensity of the magnetic and electric fields, and consequently the signal voltage in the receiver, decrease as the first power of the distance.

The gain in the maximum distance is then given by

$$\gamma = \frac{D_2}{D_1} = \alpha = \sqrt{\beta}\,, \tag{8}$$

where D_1 and D_2 are the maximum transmission distances of the initial and transformed signals, respectively.

3. CALCULATION OF POSSIBLE INCREASE IN SIGNAL/NOISE RATIO IN THE TRANSMISSION OF RADIO PULSES IN THE PRESENCE OF SOME TYPICAL NOISE SPECTRA

Let us consider the case of noise, whose energy spectrum has the form

$$G(\omega) = \frac{1}{a^n + \omega^n}, \tag{9}$$

where a = const.

Taking (7) into account, we get

$$\beta = \frac{a^n m_0 + \lambda^n m_n}{a^n m_0 + m_n},$$ (1

where

$$m_0 = \int_0^\infty \Phi_1^2(\omega)\, d\omega;$$ (1

$$m_n = \int_0^\infty \Phi_1^2(\omega)\, \omega^n\, d\omega.$$ (1

Putting

$$q = \frac{m_n}{m_0},$$ (13

we obtain on the basis of (6) and (10)

$$\alpha = \sqrt{\frac{a^n + \lambda^n q}{a^n + q}}.$$ (1

When n = 0, corresponding to the case of "white" noise ($G(\omega) = \text{const}$), we obtain $\alpha \equiv 1$, [this follows directly from (6) and (8)], i.e., we reach the well-known conclusion that the maximum signal/noise ratio cannot be improved by similarity transformations of a radiated pulse of given energy.

If n > 1, i.e., in the case of noise with decreasing spectral density, a value $\alpha > 1$ is reached when $\lambda > 1$. In other words, it is possible to increase the signal/noise ratio (and the transmission range) in this case by increasing the amplitude and accordingly shortening the duration of the radiation pulse. The efficiency of transformation of the pulse signal increases here with increasing exponent n.

The quantity q in (14) depends on the waveform of the working pulse. When a = 0, i.e., i the case of a noise in the form $G(\omega) = 1/\omega^n$, we obtain $\alpha = \lambda^{n/2}$ independently of the form of the pulse signal. In particular, for noise with an energy spectrum $G(\omega) = 1/\omega$, which is customarily used to characterize noise of the semiconductor type [4], we have $\alpha = \sqrt{\lambda}$.

Let us determine now, by way of an example, the value of α as applied to noise given by (9) and a working signal of "bell-shaped" form

$$x_1(t) = e^{-b^2 t^2}.$$

The signal spectrum has a form [3]

$$\Phi_1(\omega) = \frac{\sqrt{\pi}}{b} e^{-\frac{\omega^2}{4b^2}}.$$

Calculating m_0 and m_n in accordance with (11) and (12), and taking (13) into account, we get

$$q = \frac{2^{\frac{n}{2}} b^n}{\sqrt{\pi}} \Gamma\left(\frac{n+1}{2}\right),$$

where Γ is the gamma function.

After substituting the resultant value of q in (14), we determine the quantity of interest to us, namely the transformation efficiency α.

The table lists the results of calculations of the efficiency of transformation for two typical noise spectra.

4. TRANSMISSION OF OPTICAL PULSED SIGNALS AT A DISTANCE

Most light-energy receivers (for example, photocells with external photoeffect, photoresistances) effect linear conversion, within the operating range, of the light flux (radiant power) into signal current or voltage. Consequently, the signal voltage at the input of a photoelectric amplifier is proportional to the first degree of the radiant power, and not to the square root of the power, as in the case of radio signal reception.

Accordingly, if a pulse of optical radiation is subjected to transformation (1), the converted and initial electric signal pulses at the output of the receiving amplifier will be related by the equation

$$x_2(t) = \lambda x_1(\lambda t). \tag{15}$$

A deduction analogous to that made above leads to the following expression for the efficiency of transformation of pulsed light signals, α_1 :

$$\alpha_1 = \sqrt{\lambda\beta} = \alpha\sqrt{\lambda}, \tag{16}$$

where α and β are given, as before, by (6) and (7). Thus, for example, for noise with constant spectral density we have

corresponding to the result obtained in [5], and indicating that the limiting range of transmission of light pulses of given energy can be increased, in the presence of white noise, by increasing the intensity and simultaneously reducing the duration of the light pulses.

REFERENCES

1. V.I. Siforov, Effect of Noise on the Reception of Pulsed Radio Signals, Radiotekhnika, 1946, 1, 1,5.
2. B.M. Dwork, Detection of a pulse superposed on fluctuation noise, Proc. I.R.E., 1950, 38, 7,771.
3. A.A. Kharkevich, (Spectra and Analysis), GITTL, 1957.
4. A. Van der Ziel, Fluctuations in Radio and in Physics, GEI, 1958.
5. F.I. Khaytun, B.E. Snolyanskii, Possibility of Increasing the Transmission Range of Pulsed Light Signals, (Optical-Mechanical Industry), 1957, 3, 13.

Submitted to editors 21 April 1960.

METHOD FOR IDEAL MEASUREMENT OF OSCILLATION PARAMETERS

B.A. Dubinskiy

An analysis of the errors of an ideal receiver (in the sense of Kotel'nikov, see [1]), carried out in reference [2], has suggested one method of measuring the parameters of oscillations distorted by additive Gaussian noise. For the sake of brevity we shall describe this method without preliminary derivations, and then prove that it is ideal in the sense indicated above.

In the general case, a proposed processing of the distorted signal is ideal only if the oscillation is a linear function of the parameters, if it has the form

$$L(\lambda;t) = L(\lambda_1;\lambda_2;\ldots;\lambda_n;t) = D_0(t) + \sum_{i=1}^{n} D_i(t)\lambda_i\,, \tag{1}$$

where $L(\lambda; t)$ is the true signal, a known function of the time and of the n parameters λ_1, λ_2, $\ldots$; λ_n; $D_0(t)$; $D_1(t)$;...; $D_n(t)$ are known functions of the time, which are independent of the parameter λ_i.

The oscillation $L(\lambda; t)$ has a finite duration from t_1 to t_2, and is identically zero outside this interval. It is assumed that the parameters of the signal can assume with equal probability all values within certain limits.

The signal at the receiver output will be denoted by x(t):

$$x(t) = L(\lambda; t) + w(t), \tag{2}$$

where w(t) is the noise — the realization of a random Gaussian process with known energy spectrum $\sigma^2(\omega)$.

The processing of the signal x(t) consists in the following.

1. The difference signal $\Delta x(t)$ is formed:

$$\Delta x(t) = x(t) - D_0(t). \tag{3}$$

This signal is then passed through a filter having a frequency characteristic $Y(\omega)$

$$|Y(\omega)| = \frac{1}{\sigma(\omega)}. \tag{4}$$

The phase characteristic is immaterial.

We shall denote the signals at the output of the filter (4) by the same symbol as at the input, but with a bar above.

2. The signal $\overline{\Delta x(t)}$ is then applied to the input of an n-channel device, in each channel of which $\Delta x(t)$ is multiplied by the suitable oscillation $D_i(t)$ $(i = 1, 2, \ldots, n)$ and the product integrated during the interval from t_1 to $t_2 + \tau$, where τ is the duration of the response of the filter (4). At the output of the channels we obtain the quantities

$$V_i = \int_{t_1}^{t_2+\tau} \overline{\Delta x(t)}\,\overline{D_i(t)} \quad (i = 1, 2, \ldots, n).$$

3. The concluding stage in the processing of the signal is the solution of the system of n linear equations

$$V_i = \sum_{j=1}^{n} p_{ij}\lambda_{j0} \quad (i = 1, 2, \ldots, n). \tag{5}$$

The coefficients p_{ij} are calculated beforehand by means of the formulas

$$p_{ij} = \int_{t_1}^{t_2+\tau} \overline{D_i(t)}\,\overline{D_j(t)}\,dt \quad (i, j = 1, 2, \ldots, n).$$

As a result of solution of the system of equations, we obtain estimates for the sought parameters λ_{i0} $(i = 1, 2, \ldots, n)$.

In the particular case when $p_{ij} \equiv 0$ and $i \neq j$ [all the $D_i(t)$ are mutually orthogonal], the parameters are estimated by means of the formulas

$$\lambda_{i0} = \frac{V_i}{p_{ii}} \quad (i = 1, 2, \ldots, n).$$

In other words, the output of the aforementioned channels can be calibrated directly in values of the corresponding parameters.

The resultant estimates of the parameters λ_{i0} differ from the true values of the parameters λ_i $(i = 1, 2, \ldots, n)$ by the magnitude of the error

$$\delta\lambda_i = \lambda_{i0} - \lambda_i \quad (i = 1, 2, \ldots, n).$$

Let us prove now that in the above-described processing (measurement) method the errors in the parameters $\delta\lambda_i$ will be equal to the errors of an ideal receiver.

For this purpose we represent the signal x(t) in the following form (see [1] and [2])

$$x(t) = D_0(t) + \sum_{i=1}^{n} D_i(t)\lambda_i + w(t)$$

and perform on it the operations described in Items 1 and 2. As a result we obtain

$$V_i = \sum_{j=1}^{n} p_{ij}\lambda_j + v_i \quad (i = 1, 2, \dots, n). \tag{6}$$

where

$$v_i = \int_{t_1}^{t_1+\tau} w(t)\, D_i(t)\, dt.$$

It follows from (6) that the true values of the parameters λ_i are found by solving the system of equations

$$V_i - v_i = \sum_{j=1}^{n} p_{ij}\lambda_j \quad (i = 1, 2, \dots, n). \tag{7}$$

On the basis of (5) and (7) we can readily verify that

$$v_i = \sum_{j=1}^{n} p_{ij}\delta\lambda_j \quad (i = 1, 2, \dots, n). \tag{8}$$

The system of equations (8) determines uniquely the errors in the parameters $\delta\lambda_i$ [for a fixed noise w(t)].

Comparing (8) with the analogous system of equations for the error in the estimate of the parameters by an ideal receiver (see [2]), we see that these systems of equations are identical; consequently, the method proposed for the measurement of the oscillation parameters is ideal, i.e., it realizes the potential interference immunity.

In conclusion we note that the possible practical application of the proposed processing is not restricted to the case when the oscillation depends on the parameters linearly, but can be extended to include the case when this dependence is nonlinear, provided that rough values of the parameters are known in advance (for example, as a result of a preliminary rough processing). In this case the signal processing proposed above should yield merely the corrections to the rough values of the parameters. With the problem so formulated, the role of the sought-after parameters will be assumed by the corrections, and the oscillation can be represented in the form (1). Actually, let $A(\lambda; t)$ be an oscillation that depends nonlinearly on the parameters $\lambda_1, \lambda_2, \dots, \lambda_n$, and let λ_i (i = 1, 2, ..., n) be the rough values of the parameters; then, expanding this oscillation in a Taylor series in the parameters and dropping terms of second order and above, we obtain the following expressions:

$$A(\lambda; t) = A(\lambda'; t) + \sum_{i=1}^{n} F_i(t)\,\Delta'\lambda_i = B(\Delta\lambda; t),$$

where

$$F_i(t) = \left[\frac{\partial A(\lambda; t)}{\partial \lambda_i}\right]_{\lambda = \lambda'} \tag{9}$$

$$i = 1, 2, \dots, n. \quad \Delta\lambda_i = \lambda'_i - \lambda_i .$$

The oscillation $B(\Delta\lambda; t)$ is a linear approximation of the oscillation $A(\lambda; t)$ and corresponds to the form (1); consequently, its parameters (the corrections $\Delta\lambda_i$) can be estimated in an ideal manner by the method described above.

The validity of the linear approximation (9) depends on the properties of the oscillation $A(\lambda; t)$ as a function of the parameters, and on the accuracy of the rough values of the parameters, i.e., on the values of $\Delta\lambda_i$. We note that in the case when the values of the parameters are too rough, it is necessary to refine these rough values after determining the corrections, to obtain a new linear approximation of the oscillations, and to repeat the refinement of the parameters by using the same processing method. This refinement can be repeated several times. The process of successive approximations obtained thereby is analogous to the well-known process of successive approximations used in the least-squares method.

I am thankful to V.I. Bunimovich for many valuable hints concerning the exposition in the present paper.

REFERENCES

1. V.A. Kotel'nikov, Theory of Potential Interference Immunity, GEI, 1956.
2. B.A. Dubinskiy. On the Question of Accuracy of Measurement of Parameters of an Oscillation Distorted by a Guassian Noise of Low Intensity, Radiotekhnika i elektronika 1959, 4, 12, 1959.

Submitted to editors 28 July 1960

CHARACTERISTIC RESISTANCE AND ATTENUATION OF A TEM WAVE PROPAGATING ALONG A MULTICONDUCTOR LINE MADE UP OF RECTANGULAR CONDUCTORS

B.A. Sukhov

We develop below a method for calculating the characteristic resistance and the damping o a TEM mode in a line made of rectangular conductors. Since we know the solution of the probl of the TEM mode in a multiconductor line with strip conductors lying in a single plane [1], the present problem reduces to finding a conformal mapping that converts the exterior of this line into the exterior of a multiconductor periodic line, consisting of rectangular conductors. Such a conformal mapping, when the periods of both lines are equal to 2π, is realized by the function $\xi + j\eta = f(x + jy)$, which converts the external region of Figure 1 into the external region

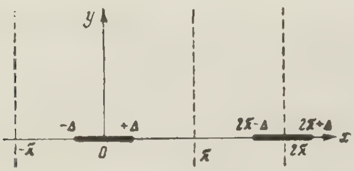

Figure 1

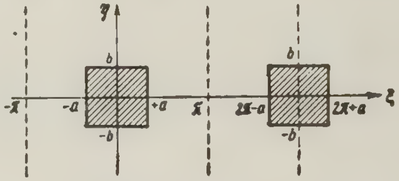

Figure 2

of Figure 2. For $-\pi \leqslant x, \xi \leqslant \pi; 0 \leqslant y, \eta$ we can represent this function in the following form

$$\xi + j\eta = C \int\limits_0^{\sin\left(\frac{x+jy}{2}\right)} \frac{\sqrt{1 - \varkappa^2 t^2}}{\sqrt{(1 - k^2 t^2)(1 - t^2)}}\, dt + jb, \tag{1}$$

where $\frac{1}{k} = \sin\frac{\Delta}{2}$; $0 < \frac{1}{\varkappa} < \frac{1}{k}$.

Considering that $f\left(2 \arcsin \frac{\pm 1}{\varkappa}\right) = jb \pm a$, $f(\pm\Delta) = \pm a$ and $f(\pm\pi) = \pm\pi$, we can obtain one-parameter families of curves $a(\varkappa)$, $b(\varkappa)$ and $C(\varkappa)$ with parameter Δ from the following system of equations

$$a = C\frac{(\mu - \nu)}{\gamma\sqrt{l}}\left[(1 - \varkappa^2\mu)\, F\left(\frac{\pi}{2}; \sqrt{\frac{m}{l}}\right) + (\mu - \nu)\,\varkappa^2 \Pi\left(\frac{\pi}{2}; \sqrt{\frac{m}{l}}; -\frac{1}{l}\right)\right],$$

$$\pi - a = C\frac{(\mu - \nu)}{\gamma\sqrt{l}}\left[(\varkappa^2\nu - 1)\, F\left(\frac{\pi}{2}; \sqrt{\frac{m}{l}}\right) + \varkappa^2(\mu - \nu)\, \Pi\left(\frac{\pi}{2}; \sqrt{\frac{m}{l}}; -m\right)\right].$$

$$b = 2C\frac{(\mu - \nu)}{\gamma\beta n}\left\{\left[\varkappa^2\mu - 1 - \varkappa^2\frac{(\mu - \nu)\sqrt[4]{ml}}{\sqrt[4]{ml} - 1}\right] F\left(\frac{\pi}{2}; \frac{1}{n^2}\right) + \right.$$

$$\left. + 2\varkappa^2\frac{(\mu - \nu)\sqrt[4]{ml}}{\sqrt[4]{ml} - 1}\, \Pi\left[\frac{\pi}{2}; \frac{1}{n^2}; -\left(\frac{\sqrt[4]{ml} - 1}{\sqrt[4]{ml} + 1}\right)^2 \frac{1}{n^2}\right]\right\},$$

where $F\left(\frac{\pi}{2}; k\right)$ and $\Pi\left(\frac{\pi}{2}; k; n\right)$ are the complete elliptic integral of the first and third kind, respectively,

$$\mu, \nu = \frac{\varkappa^2 \pm \sqrt{(\varkappa^2 - 1)(\varkappa^2 - k^2)}}{\varkappa^2 k^2 + \varkappa^2 - k^2};$$

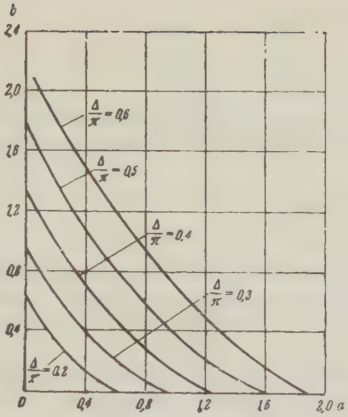

Figure 3

$$m=\left(\frac{1-\mu}{1-\nu}\right)^2;\quad l=\left(\frac{\mu}{\nu}\right)^2;\ n=\frac{\sqrt[4]{l}+\sqrt[4]{m}}{\sqrt[4]{l}-\sqrt[4]{m}};$$

$$\gamma=\sqrt{(1-k^2\nu)(1-\nu)(1-\varkappa^2\nu)\,\nu};$$

$$\beta=\sqrt{l}-\sqrt{m},$$

In the limiting case, when a = 0 (see Figure 2), the conformal mapping assumes a simple form

$$\xi+j\eta=\arcsin\left[\frac{2\cos(x+jy)}{1+\cos\Delta}+\frac{1-\cos\Delta}{1+\cos\Delta}\right]-\frac{\pi}{2}\qquad(1')$$

and b is given by the formula

$$b=\operatorname{arc\,ch}\frac{3-\cos\Delta}{1+\cos\Delta}.\qquad(2')$$

By virtue of the one-to-one correspondence between a and $\varkappa$, it is more convenient to determine b and C for a given value of Δ in the form of functions of a with Δ as a parameter. The curves b = b(a) (Figure 3) define families of multiconductor lines of rectangular conductors the characteristic resistances of which are equal to the characteristic resistance of a multiconductor strip line with strip width 2Δ.

The characteristic resistance of a strip line can be represented in the form

$$K_t(s)=K_{t_0}(s)\,R_t(s),\qquad(3)$$

where s is the phase shift over the period in the cross-section plane, divided by 2π;

$$K_{t_0}(s)=\frac{1}{4}\sqrt{\frac{\varepsilon}{\mu}}\frac{1}{s\pi};$$

$R_t(s)$ is a function that depends on the parameter Δ and on s. Parts of these functions are shown in Figure 4 for different values of Δ.

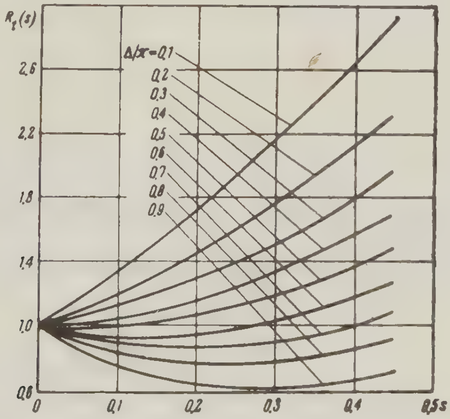

Figure 4

Thus, using the plots of Figures 3 and 4, we can determine by means of formula (3) the characteristic resistance of a multiconductor line made up of rectangular conductors. Obviously, the characteristic resistance of a system having a period other than 2π can be readily determined, since it is invariant under the similarity transformation.

The damping factor of such systems is inversely proportional to the similarity coefficient, and, consequently, it is enough to calculate the damping for systems with period 2π.

The damping coefficient α is determined from the formula

$$2\alpha = \frac{P}{W}, \tag{4}$$

where P is the loss per unit conductor length; W is the energy flux through the strip bounded by the lines ξ, $x = -\pi$ and ξ, $x = \pi$ (Figures 1 and 2). Substituting P and W in explicit form into (4), we obtain

$$2\alpha = R\sqrt{\frac{\varepsilon}{\mu}}\,\frac{2\sin(s\pi)\,L}{\pi^2 P_{-s}(\cos\Delta)\,P_{-s}(-\cos\Delta)}, \tag{5}$$

where R is the specific surface resistance of the conductor; $P_u(v)$ is the Legendre function on the section $-1 < v < 1$; L is determined by the shape of the conductors of the slow-wave system, obtained with the aid of conformal mapping from a strip line with conductors of width 2Δ; the period of both systems is 2π.

It is more convenient to seek the ratio α/α_0, where α_0 is the attenuation coefficient of a TEM wave in an anisotropically conducting plane having a surface resistance R along the direction of propagation and an infinite surface resistance perpendicular to the direction of propagation

$$2\alpha_0 = R\sqrt{\frac{\varepsilon}{\mu}}\,s.$$

Let us denote α/α_0 by $R_\alpha(s)$. Then

$$R_\alpha(s) = \frac{2L\sin(s\pi)}{\pi^2 s P_{-s}(\cos\Delta)\,P_{-s}(-\cos\Delta)}. \tag{6}$$

In the case of conductors with rectangular cross section we have

$$Z_{\text{rect}} = \frac{2k^2(\mu - \nu)}{\gamma C}\left[\frac{F\left(\frac{\pi}{2};\sqrt{\frac{m}{l}}\right)}{\sqrt{l}} + \frac{2F\left(\frac{\pi}{2};\frac{1}{n^2}\right)}{n\beta}\right]. \tag{7}$$

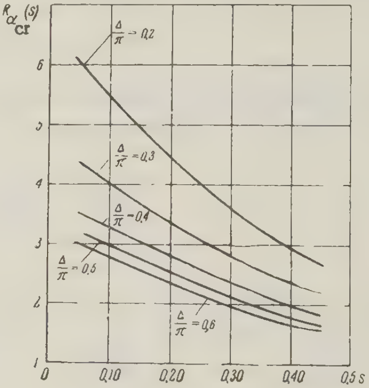

Figure 5

As can be seen from (7), L depends both on Δ and on a. In this connection, it is convenient to break up $R_{\alpha\,\text{rect}}(s)$ into two factors

$$R'_\alpha(s) = \frac{2L'\sin(s\pi)}{\pi^2 s P_{-s}(\cos\Delta)\,P_{-s}(-\cos\Delta)}$$

and

$$\frac{L_{\text{rect}}}{L'},$$

where L' depends only on Δ. We choose for L' the value of L for round conductors [1],

$$L_{\text{cr}} = \left(\frac{1}{M\sin\frac{\Delta}{2}}\right)F\left(\frac{\pi}{2};\,k_1\right),$$

where

$$M = \frac{1}{1 + \frac{2}{\Delta}\operatorname{arc\,ch}\left(\sec\frac{\Delta}{2}\right)}; \qquad k_1 = \frac{\left[M^2 - (1 - M)^2\cos^2\frac{\Delta}{2}\right]^{1/2}}{M}.$$

Obviously, with such a choice of L', the value of $R'_\alpha(s)$ is equal to that of $R_{\alpha r}(s)$, i.e., it is the ratio of the attenuation coefficient of a system of round wires of radius $r = (1 - M)\Delta$ to α_0. Plots of $R_{\alpha r}(s)$ are given in reference [1]; they have been replotted in more convenient form in Figure 5. Figure 6 shows the dependence of the ratio of L_{rect}/L_r on a and Δ.

Thus, by using Figures 5 and 6, we can calculate $R_{\alpha\,\text{rect}}(s)$ from the following formula

$$R_{\alpha_{\text{пр}}}(s) = R_{\alpha_{\text{кр}}}(s)\,\frac{L_{\text{пр}}}{L_{\text{кр}}}. \tag{8}$$

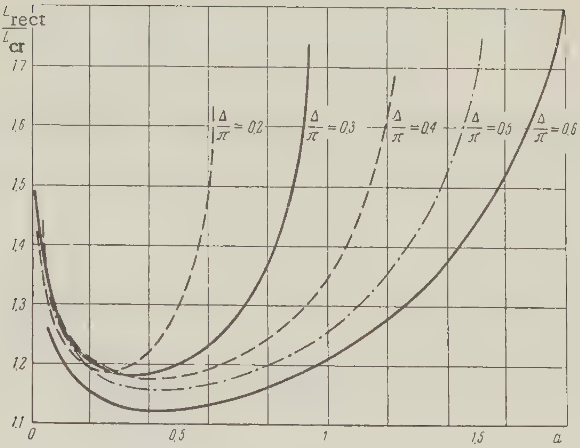

Figure 6

Knowing $R_{\alpha\,\mathrm{rect}}(s)$, we can readily determine the coefficient of attenuation of a slow-wave system made up of rectangular conductors.

REFERENCES

1. Chiao-Min Chu, J. Appl. Phys., 1958, 29, 88.

Submitted to editors 28 April 1960.

REMARKS ON THE CALCULATION OF CASCADE CONNECTIONS OF n- SIMILAR TWO-PORTS

L.R. Yavich

We have remarked earlier [1] that a nonreciprocal two-port, described by a matrix [X], can be represented in the form of a cascade connection of a reciprocal two-port with matrix $[X_0]$ and an ideal power converter with transformation coefficient k:

$$[X] = [X_0]\,\frac{1}{k},$$

where

$$[X_0] = \begin{bmatrix} X_{110} & X_{120} \\ X_{210} & X_{220} \end{bmatrix}; \quad k = \frac{1}{\sqrt{|X|}};$$

$$|X| = \det[X].$$

By the matrix [X] is meant one of the following matrices

$$[X]=\begin{cases}[a],\\ [A],\\ [T],\end{cases}$$

where [a] is the classical transmission matrix, [A] is the normalized matrix [a], and [T] is the transmission wave matrix.

To calculate the resultant transmission matrix $[X]^n$ of n similar two-ports connected in cascade, we used the formula

$$[X]^n=[X_0]^n\frac{1}{k^n}.$$

Thus, the problem reduces to raising the matrix of the reciprocal part of the two-port, $[X_0]$, to the n-th power.

Let us transform the expressions for $[X_0]^n$ (see 1/, 2/), to the form

$$[X_0]^n=\begin{bmatrix}\operatorname{ch} nU+\beta\frac{\operatorname{sh} nU}{\operatorname{sh} U} & X_{120}\frac{\operatorname{sh} nU}{\operatorname{sh} U}\\ X_{210}\frac{\operatorname{sh} nU}{\operatorname{sh} U} & \operatorname{ch} nU-\beta\frac{\operatorname{sh} nU}{\operatorname{sh} U}\end{bmatrix}, \tag{1}$$

where

$$U=\operatorname{arch}\alpha=\operatorname{arch}\left[\frac{1}{2}(X_{110}+X_{220})\right]; \tag{2}$$

$$\beta=\frac{1}{2}(X_{110}-X_{220}).$$

It should be noted that (1) coincides with the expression obtained by Fel'dshteyn [3].

Substituting (2) into (1) and recognizing that the Chebyshev polynomials of the first kind are given by

$$T_n(\alpha)=\operatorname{ch}(n\operatorname{arch}\alpha),$$

and the Chebyshev polynomials of the second kind are given by [4]

$$U_n(\alpha)=\frac{\operatorname{sh}[(n+1)\operatorname{arch}\alpha]}{\sqrt{\alpha^2-1}}=\frac{1}{n+1}T'_{n+1}(\alpha),$$

where n = 0, 1, 2, ..., we obtain, after simple transformations,

$$[X_0]^n=\begin{bmatrix}T_n(\alpha)+\beta U_{n-1}(\alpha) & X_{120}U_{n-1}(\alpha)\\ X_{210}U_{n-1}(\alpha) & T_n(\alpha)-\beta U_{n-1}(\alpha)\end{bmatrix}. \tag{3}$$

The form (3) has the advantage over previously used forms that it contains polynomials tha can be expanded in finite series in powers of α. This makes it possible to avoid cumbersome trigonometric transformations. The simplifications are particularly noticeable in the case of two-ports of general form, described by the complex elements of the matrix $[X_0]$ (α and β are complex numbers).

It is interesting to compare (3) with the matrix equation [5] that is derived from the result obtained in [6]. In our notation

$$[X_0]^n=\begin{bmatrix}X_{110}R_n(2\alpha)-R_{n-1}(2\alpha) & X_{120}R_n(2\alpha)\\ X_{210}R_n(2\alpha) & X_{220}R_n(2\alpha)-R_{n-1}(2\alpha)\end{bmatrix}, \tag{4}$$

where

$$R_n(2\alpha)=\frac{T_{n+1}(\alpha)-T_{n-1}(\alpha)}{2(\alpha^2-1)};\ \alpha\neq\pm 1.$$

Expression (4) contains a new function $R_n(2\alpha)$, which has a singularity. At the same time, the properties of the Chebyshev polynomials of the first and second kinds have been thoroughly investigated. By virtue of the foregoing circumstances, relation (3) is more convenient for use.

Let us make several remarks regarding a broad class of two-ports made up of purely reactive elements. The matrix $[A_0]$ ($[a_0]$) has in this case the following structure

$$[A_0]=\begin{bmatrix}A & jB\\ jC & D\end{bmatrix},$$

where A, B, C, and D are real. Consequently, according to (2), the coefficients α and β are real numbers and their values are

$$\alpha = \frac{1}{2}(A + D); \quad \beta = \frac{1}{2}(A - D).$$

At the same time, the matrix [T$_0$] obeys the relations [7]

$$\begin{aligned} T_{110} &= \xi + j\varepsilon = T^*_{220}, \\ T_{120} &= T^*_{210}, \end{aligned} \tag{5}$$

therefore (see (2))

$$\alpha = \xi; \quad \beta = j\varepsilon;$$

in addition

$$\det [T_0] = 1;$$

consequently, the working attenuation function is

$$L = |T_{110}|^2 = 1 + |T_{120}|^2. \tag{6}$$

Let us write the expression for the modulus of the coefficient of reflection of the cascade connection of n identical lossless two-ports. Taking (3) and (6) into account, we obtain

$$|\Gamma| = \sqrt{\frac{L^{(n)} - 1}{L^{(n)}}},$$

where

$$L^{(n)} = 1 + |T_{120} U_{n-1}(\alpha)|^2.$$

Certain simplifications (3) take place for symmetrical two-ports. In this case

$$a_{110} = a_{220} = A_{110} = A_{220},$$

and therefore [see (2)].

$$\alpha = a_{110}, \ \beta = 0.$$

Thus,

$$[a_0]^n = \begin{bmatrix} T_n(a_{110}) & a_{120} U_{n-1}(a_{110}) \\ a_{210} U_{n-1}(a_{110}) & T_n(a_{110}) \end{bmatrix}.$$

We recall that

$$[T_0]^n = \begin{bmatrix} 1 & 1 \\ 1 & -1 \end{bmatrix}^{-1} [A_0]^n \begin{bmatrix} 1 & 1 \\ 1 & -1 \end{bmatrix}.$$

REFERENCES

1. L.R. Yavich. Certain Relations for a Cascade Connection of n Similar Nonreciprocal Two-ports. Radiotekhnika i elektronika 1960, 5, 4, 633.
2. W. Proctor Wilson, Some matrix theorems, Electronic and Radio Engineer (New series), 1957, 34, 6, 229.
3. A. L. Fel'dshteyn, Generalized Matrix Theory of Inhomogeneous Lines, Radiotekhnika, 1960, 15, 6, 10.
4. V.L. Goncharov (Theory of Interpolation and Approximation of Functions), GITTL, 1954.
5. L.R. Yavich, Use of Chebyshev Polynomials for the Calculation of a Cascade Junction of n Similar Two-ports, Elektrosvyaz', 1960, 10, 70.
6. Václav Doležal, Vyšetřent vlastnosti řetězů stejných obecných čtyřpolů, Slaboproudy obzor, 1958, 19, 4, 253.
7. L.R. Yavich, Wave Matrices of a Two-Port, Radiotekhnika i elektronika, 1957, 2, 7, 870.

Submitted to editors 18 August 1960.

ON THE FORM OF THE FIELD IN A BACKWARD WAVE TUBE IN THE PRESENCE OF DISTRIBUTED ATTENUATION

M.B. Tseytlin and Ye. M. Il'ina

The analysis of the operation of a backward wave generator, carried out in [1], can be generalized to include losses in the line.

The power-balance equation in the presence of distributed attenuation in the tube can be written, in analogy with equation (18) of reference [2], as

$$\frac{E_1^2(z)}{2} = \frac{m}{\beta_q}\int_l^z E_1(x)\,dx\int_0^z E_1(t)\sin k(x-t)\sin\beta_q(x-t)\,dt - \frac{\beta_e Cd}{2}\int_l^z E_1^2(x)\,dx, \tag{1}$$

where $E_1(z)$ is the amplitude of the intensity of the high frequency field; $k = \beta_e bC$; $m = \beta_e\beta^2C^3$; $C^3 = \frac{KI_0}{4u_0}$, $\beta_q = \frac{\omega_q}{v_0}$; $\beta_e = \frac{\omega}{v_0}$; ω_q is the frequency of plasma oscillations in the beam; v_0 is the velocity of the electron; b is the nonsynchronism parameter; d is the attenuation parameter, d = L/54.5 CN; L is the attenuation of the line in decibels, and $z = l$ corresponds to the collector end of the line.

Equation (1) reduces to the fifth-order differential equation

$$\frac{d^5E_1}{dz^5} - \beta_e Cd\frac{d^4E_1}{dz^4} + 2(k^2+\beta_q^2)\frac{d^3E_1}{dz^3} - 2(k^2+\beta_q^2)\beta_e Cd\frac{d^2E_1}{dz^2} + \\ + [(k^2-\beta_q^2)+2km]\frac{dE_1}{dz} - (k^2-\beta_q^2)\beta_e CdE_1 = 0. \tag{2}$$

With initial conditions

$$z = 0,\quad E_1(z) = E_1(0),\quad \frac{dE_1}{dz} = \beta_e CdE_1(0),\quad \frac{d^2E_1}{dz^2} = (\beta_e Cd)^2E_1(0), \tag{3}$$

$$\frac{d^3E_1}{dz^3} = (\beta_e Cd)^3E_1(0),\quad \frac{d^4E_1}{dz^4} = -2kmE_1(0).$$

The solution of equation (2) can be represented in the form

$$E_1(z) = \sum_{i=1}^{5} C_i e^{\lambda_i z}, \tag{4}$$

where λ_i are the roots of the characteristic equation corresponding to equation (2).

Assuming that the perturbations introduced by the small losses are themselves small, we set, as an approximation,

$$\lambda_i = \lambda_{0i}(1-\delta_i), \tag{5}$$

where λ_{0i} are the roots of the corresponding characteristic equation for d = 0. We retained terms quadratic in δ_i in the calculation of λ_i.

The integration constants C_i are determined by substituting in (4) the initial conditions

$$C_1 = \frac{2km + \lambda_{02}\lambda_{03}\lambda_{04}\beta_e Cd - (\lambda_{03}\lambda_{04} + \lambda_{02}\lambda_{03} + \lambda_{02}\lambda_{04}(\beta_e Cd)^2}{\lambda_{01}(\lambda_{02}-\lambda_{01})(\lambda_{03}-\lambda_{01})(\lambda_{04}-\lambda_{01})}, \tag{6}$$

C_2, C_3, and C_4 are determined from (6) by cyclic permutation of the indices:

$$C_5 = 1 - \sum_{i=1}^{4} C_i. \tag{7}$$

Figure 1 shows the distribution of the relative amplitude of the intensity of the high-frequency field along the tube for different values of the attenuation parameter d and for negligibly small space charge (QC = 0). Figure 2 shows an analogous dependence for a space charge different from zero (QC = 0.25). It is seen from these plots that in the case of losses the relative amplitude of the field in the backward wave tube has a maximum

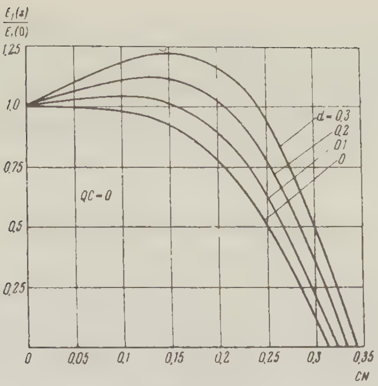

Figure 1

hich increases with increasing losses. The presence of the maximum can be explained as llows. The amplitude of the field in the backward wave tube has a near-cosinusoidal variation the absence of losses, i.e., it remains practically constant at the input to the tube. The tenuation of the "cold" wave in the line is exponential, the amplitude decreasing in the direc-on of the energy flux. Consequently, the loss-power flux will increase continuously in this rection, and the increase in the field amplitude brought about by the interaction with the electron eam will be compensated at some point by a decrease in the amplitude due to the losses, after hich the field amplitude begins to decrease.

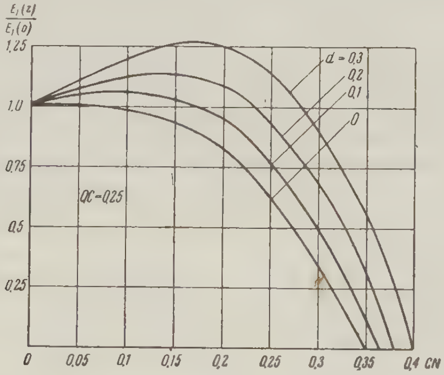

Figure 2

The starting values of CN are determined from the condition that the field vanish on the ollector end of the tube.

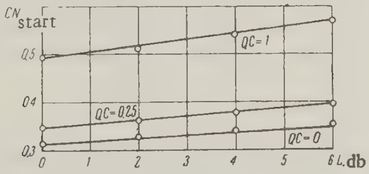

Figure 3

Figure 3 shows the dependence of the starting values of CN on the distributed losses L for different values of the space charge parameter QC. The points denote the results of calculations on the basis of the data of reference [3]. As can be seen from the plot, the results are in full agreement with the rigorous theory.

REFERENCES

1. M.B. Tseytlin, Ye.M. Il'ina, Radiotekhnika i elektronika, 1960, 5, 6, 1010.
2. M.B. Tseytlin, Ye.M. Il'ina, ibid., 1960, 5, 4, 700.
3. H. Johnson, Proc. I.R.E., 1955, 43, 6, 684.

Submitted to editors 9 September 1960

ONE METHOD OF MEASURING THE FLUCTUATION OF THE PHASE OF RADIO WAVES IN A STUDY OF TROPOSPHERIC SCATTER PROPAGATION

A.A. Shur, and G.S. Maksimov

Results of measurements of phase fluctuations of radio waves propagating in the troposphere are of considerable interest both in theory and in practice. The known methods of such measurements are exceedingly complicated and cumbersome ([1, 2] and others). We have employed a simple measurement method, based on the Nyquist principle [3]. In this method the loop between the input and output of the investigated two-port is unnecessary (by two-port is meant in this case the medium in which the radio wave propagates).

A block diagram of the measuring apparatus is shown in the figure. The transmitting apparatus consists of a transmitter 1, modulator 2, and receiver-filter 3. The receiving apparatus includes the receiver 4, the phase-meter 5 with visual-indication oscilloscope 6, and receiver-filter 7.

The measurement principle consists in the following. On the transmitting end of the investigated path, the receiver-filter 3 receives a signal from a certain radio broadcast station 8. Amplifying only the carrier voltage of this signal, the receiver-filter suppresses all the remaining spectrum components. In view of the fact that the receiver-filter 3 is connected to the input of a frequency modulator 2, the transmitter 1 is modulated by the carrier of the broadcast station. On the receiving end of the path, the radio broadcast station carrier voltage, separated after passing through the receiver 4, is compared in phase with the carrier frequency of the same station produced at the output of the receiver-filter 7. The time variation of the phase between these oscillations will obviously depend only on the conditions of radio wave propagation along the investigated portion. The phase of the broadcast-station signal can differ on the receiving end from the phase of the same signal on the transmitting end, but the phase difference is, first, equal to a constant quantity and, second, remains unchanged in time. In addition to the fact that the transmitter is modulated by the carrier frequency of the broadcast station, its own carrier frequency swings within definite limits. Consequently, one can observe on the oscillograph screen the overall phase characteristic of the medium and of the apparatus. The influence of the apparatus is accounted for by first plotting the phase characteristics of the transmitting and receiving apparatus.

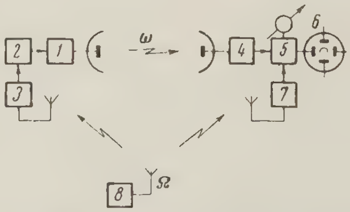

Block diagram of measuring apparatus.

According to the Nyquist principle, the spectrum of the transmitter signal is taken here to be much smaller than the bandwidth of the whole apparatus. In this case the phase shift acquired by the signal passing through the investigated two-port is

$$\varphi = \Omega T(\omega),$$

where Ω is the circular frequency of the modulating oscillation; $T(\omega)$ is the group time delay of the two-port at the given carrier frequency; ω is the carrier frequency.

As can be seen from this formula, the phase shift is simply related to the group time dela Thus, by measuring the fluctuations in the phase of the frequency-modulated signal we can simultaneously determine the fluctuations in the group time delay of the same signal. Thus, we have chosen a broadcast station operating at frequency $\Omega = 263$ kc; the maximum angle measured by the phase meter was $\varphi_{max} = 180°$. From the formula given above it is easy to see that the maximum measured delay time is $T(\omega)_{max} = 1.92$ microseconds. Experience has shown that in the case of UHF tropospheric scatter propagation this quantity exceeds the dicated figure, and consequently, measurement of angles greater than 180° is unnecessary. he minimum measured delay time $T(\omega)_{min}$ is limited by the resolving power of the phase eter. For $\varphi_{min} = 1°$ we have $T(\omega)_{min} = 0.0106$ microsecond.

It can be shown that the delay time between two waves scattered or reflected from inhomo- eneities located at heights that differ by an amount Δh, is

$$T(\omega) = \frac{R\Delta h}{R_{eq}c},$$

here R is the length of the path; R_{eq} is the equivalent radius of the earth, and c is the velocity f light in free space ($c = 3 \times 10^5$ km/sec).

It is easy to see from this formula that the delay time makes it possible to estimate the dimension of inhomogeneities." Thus, by assuming $T(\omega) = T(\omega)_{min}$, R = 300 km, and R_{eq} = 500 km, we find that the minimum value of Δh is approximately 90 meters.

This measurement method has been realized in an experimental path for which tropo- pheric propagation was used. The signals were transmitted and received by the standard elay-line equipment to which only the receiver-filters and phase meter were added. The nterval of the experimental path amounted to 300 km. The measurements were carried out t 1,000 Mc. The transmitter carrier was varied within a band of 5 Mc at a frequency of 50 ps. The receiver-filter was a three-stage direct-amplification receiver using 6ZhlP tubes with quartz filter, the bandwidth of which was 80 cps. The fluctuations were registered by photo- graphic and motion-picture cameras.

REFERENCES

1. J.W. Herbstreit, and M.C. Thompson, Measurements of the phase of radio waves received over transmission paths with electrical lengths varying as a result of atmospheric turbulence, Proc. I.R.E., 1955, 43, 10, 1391.
2. A.P. Dean, and B.M. Fannin, Phase-difference variations in 9350-megacycle radio signals arriving at spaced antennas., Proc. I.R.E., 1955, 43, 10, 1402.
3. H. Nyquist, and S. Brand, Bell System Techn. J., 1930, 9, 522.

Submitted to editors 16 February 1960

SINGLE-LOOP PARAMETRIC AMPLIFIER

Ye.M. Gershenzon, N.G. Ptitsyna, G.I. Rozhkova and V.S. Etkin

Much attention is paid at present in radio engineering to the use of low-noise parametric amplifiers with semiconductor diodes [1 - 4].

We give below certain results of an investigation of a single-loop parametric amplifier using a semiconductor diode. These results are based on investigations made in the 'thirties by the students of L.I. Mandel'shtam and N.D. Papaleksi [5, 8, 11].

Usually a single-loop parametric microwave amplifier is connected to the circuit through a ferrite circulator [1,4]. Inasmuch as the amplifier carries in this case one incident and one reflected wave, the equivalent circuit of the single-loop parametric amplifier can be drawn as in Figure 1 [10]. Here, E is the emf of the equivalent signal source whose internal resistance is equal to the wave impedance Z of the supply feeder:

$$E = E_0 \sin(\omega_c t + \varphi_c); \quad C = \frac{C_0}{1 + m \sin(\omega_p t + \varphi_p)}.$$

In connection with the fact that the amplified signal is in the form of a reflected wave, the amplification coefficient is equal to the power reflection coefficient

$$K = \frac{P_{\text{ref}}}{P_{\text{inc}}} = \left| 1 - \frac{ZI}{U_{\text{inc}}} \right|^2, \tag{1}$$

where $P_{\text{ref, inc}}$ stands for the power of the reflected and incident waves; U_{inc} is the amplitude of the incident voltage wave; I is the current in the loop [10]. In the case of high gain ($K \gg 1$) we have

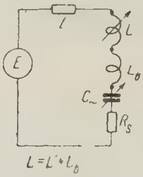

Figure 1. Equivalent circuit of single-loop parametric amplifier - regenerated LCR tank circuit.

$$K \simeq \frac{4Z^2 I^2}{E_0^2} = \frac{4Z^2 \omega_c^2 Q^2}{E_0^2}, \tag{2}$$

where Q is the amplitude of the charge on the capacitor; ω is the frequency of the signal.

The equation describing the oscillations in the amplifier tank circuit is of the form

$$L \frac{d^2 q}{dt^2} + R \frac{dq}{dt} + \frac{1}{C_0} [1 + m \sin(\omega_p t - \varphi_p)] q = E_0 \sin(\omega_c t - \varphi_c), \tag{3}$$

where L is the equivalent inductance of the tank circuit; $R = Z + R_S$, R_S is the diode loss resistance, responsible for the main losses in the amplifier tank circuit. As is well known [11], in similar circuits with periodically varying parameters one observes near the instability regions ($\omega_p \simeq 2\omega_0$, $\omega_p \simeq \omega_0$ ...) the parametric regeneration, which has been investigated for the particular cases $\omega_p = 2\omega_{\text{sig}}$ and $\omega_p = 2\omega_0$ in references [5] and [7].

Using the procedure of reference [7], we investigate equation (3) for the general case when $\omega_p \simeq 2\omega_0 \simeq 2\omega_{\text{sig}}$. For this purpose, using the notation of reference [7],

$$y = \frac{q}{C_0 U_0}; \quad \lambda = \frac{E_0}{U_0}; \quad 2\Theta = \frac{R}{\omega_0 L}; \quad \omega_0^2 = \frac{1}{LC_0}; \quad \omega_p = 2\omega_1;$$

$$t = t_1 + \frac{\varphi_p}{\omega_p}; \quad \frac{\omega_0}{\omega_1} = 1 + \xi_0; \quad \frac{\omega_c}{\omega_1} = 1 + \xi; \quad \tau = \omega_1 t \quad \Psi = \varphi_c - \frac{\omega_c}{\omega_p} \varphi_p,$$

where U_0 is a normalizing factor, we reduce equation (3) to the following simplified form:*

$$\ddot{y} + y = \lambda \cos[(1 + \xi)\tau - \Psi] - 2\Theta \dot{y} - 2\xi_0 y - my \sin 2\tau. \tag{4}$$

If we seek a solution in the form

$$y = a \sin\tau + b \cos\tau, \tag{5}$$

where a and b are functions that vary slowly compared with $\sin\tau$ and $\cos\tau$, we can obtain for a and b the expressions**

$$a = \frac{\lambda}{2(4\xi^2\Theta^2 + C^2)} \left\{ \left[2\xi\Theta \left(\Theta - \frac{m}{4} \right) - C(\xi_0 + \xi) \right] \sin(\xi\tau - \Psi) + \right.$$
$$\left. - \left[C \left(\Theta - \frac{m}{4} \right) + 2\xi\Theta(\xi_0 - \xi) \right] \cos(\xi\tau - \Psi) \right\},$$

---

*Since the maximum possible depth of modulation of the capacitance of the diode is $m \simeq 0.4 - 0.6$ [14], we have $\Theta_{\max} \leqslant 0.1$ and $\xi, \xi_0 \leqslant 0.1$, while the value of λ can be made small by suitable choice of U_0 in [7]. Consequently, the terms $\sim \Theta^2, \xi^2, \xi_0^2, \lambda^2$ can be neglected to a first approximation.

**We have described the details of the solution in reference [15].

$$b = \frac{\lambda}{2(4\xi^2\Theta^2 + C^2)}\left\{\left[C\left(\Theta + \frac{m}{4}\right) + 2\xi\Theta(\xi_0 + \xi)\right]\sin(\xi\tau - \Psi) + \right.$$
$$\left. + \left[C(\xi_0 + \xi) - 2\xi\Theta\left(\Theta + \frac{m}{4}\right)\right]\cos(\xi\tau - \Psi)\right\}, \tag{6}$$

where $C = \xi_0^2 - \xi^2 + \Theta^2 - \left(\frac{m}{4}\right)^2$.

For the mean square of the amplitude we obtain

$$\overline{A^2} = \bar{a}^2 + \bar{b}^2 = \lambda^2 \frac{\Theta^2 + \left(\frac{m}{4}\right)^2 + (\xi_0 + \xi)^2}{4(4\xi^2\Theta^2 + C^2)}. \tag{7}$$

The phenomena occurring in the amplifier are quite different when $\xi = 0$ from those occurring when $\xi \neq 0$. If $\xi = 0$, i.e., the equality $\omega_p = 2\omega_{sig}$ is rigorously satisfied, we have the amplifier working in synchronism and the oscillations in the tank circuit have a single frequency while their amplitude depends on the phase difference between the pumping frequency and the signal frequency Ψ:

$$A^2 = \frac{\lambda^2}{4C^2}\left[\left(\xi_0^2 + \left(\Theta + \frac{m}{4}\right)^2\right)\sin^2\Psi + \right.$$
$$\left. + \left(\xi_0^2 + \left(\Theta - \frac{m}{4}\right)^2\right)\cos^2\Psi - \xi_0\frac{m}{4}\sin 2\Psi\right]. \tag{8}$$

In the case of a high degree of regeneration ($m \simeq 4\Theta$) as a function of the value of Ψ, the value of A changes from $A_{max} = \sqrt{2A}$ to $A_{min} = \lambda/4\Theta$, but a considerable amplification takes place on the aberage (in phase).

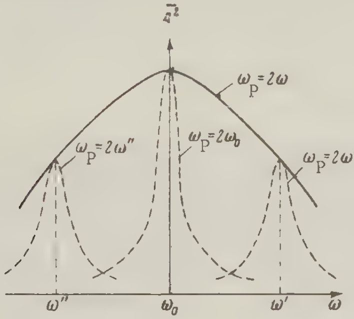

Figure 2. Resonant curve of single-loop parametric amplifier in synchronous line) and biharmonic (dotted) modes.

In the case when $\xi \neq 0$ ($\omega_p \neq 2\omega_{sig}$), the oscillations in the tank circuit occur at two frequencies, $1 + \xi$ (ω_{sig}) and $1 - \xi$ ($\omega_d = \omega_p - \omega_{sig}$), i.e., a biharmonic mode sets in, given by equation (8). The square of the amplitudes of the harmonics can be represented in the form

$$A_{1+\xi}^2 = \lambda^2 \frac{\Theta^2 + (\xi_0 + \xi)^2}{4(4\xi^2\Theta^2 + C^2)}, \quad A_{1-\xi}^2 = \lambda^3 \frac{\left(\frac{m}{4}\right)^2}{4(4\xi^2\Theta^2 + C^2)}. \tag{9}$$

The resonant curves characterizing the amplifier in the synchronous and biharmonic modes (for three values of ξ) are shown in Figure 2; here m = 0.99 × 4θ. In the biharmonic mode $\xi = 0.4 \times 10^{-3}$, $\omega' = \omega_0 (1 + \xi_0)$, and $\omega'' = \omega_0 (1 - \xi_0)$.

We see that the maximum amplification in the biharmonic mode is obtained near $\omega_{sig} = \omega_p/2$; the resonant curve of the synchronous mode is the envelope of the curves of the biharmonic mode. It follows, therefore, that in the biharmonic mode it is possible to tune the amplifier by changing the pumping frequency, the tuning range being determined by the bandwidth of the resonant curve of the synchronous mode.

The following simple expressions can be obtained for the maximum values of the gain and bandwidth of the amplifier for the case of large regeneration [by using relations (3), (7), and (9)].

In the synchronous mode, the gain is

$$K = K_{av}(1 - \cos 2\Psi), \quad K_{av} = \frac{2Q^2}{n^2 Q_{ext}^2}, \quad Q = \frac{\omega_0 L}{R}; \quad Q_{ext} = \frac{\omega_0 L}{Z}; \quad n = 1 - \frac{m}{m_{cr}}, \tag{10}$$

where $m_{cr} = 2/Q$ is the depth of modulation at which the amplifier becomes self-oscillating. The bandwidth of the amplifier (the tuning band in the biharmonic mode) is

$$2\Delta\xi_{tun} = \sqrt{2(\sqrt{2} - 1)}\sqrt{n}\frac{1}{Q}. \tag{11}$$

In the biharmonic mode, the gain for each harmonic (ω_s or ω_d) is

$$K_1 = \frac{K_{av}}{2} = \frac{Q^2}{n^2 Q^2_{ext}},$$

The bandwidth is

$$2\Delta\xi_{amp} = \frac{n}{Q}, \tag{12}$$

and the product

$$\sqrt{K_1}\, 2\Delta\xi_{amp} = \frac{1}{Q_{ext}} \tag{13}$$

is thus independent of the degree of regeneration if n is small.

The main advantage of parametric amplifiers with semiconductor diodes is their low noise figure. Actually, only the resistance noise R_s is of importance for semiconductor diodes operating in the microwave band [16]. We can therefore assume the amplifier tank circuit to contain a noise voltage

$$E_n^2 = \varepsilon^2_{n,\,ext} + \varepsilon^2_{n,\,int} = 4kTZ\Delta f + 4kTR_s\Delta f.$$

The fluctuation noise can be regarded as an oscillation of frequency $\omega_p/2$ with random-modulated amplitude and phase [17]. The noise amplification coefficient is in this case equal to K_{av}, and, therefore, the noise factor of the amplifier in the receiver circuit will depend on whether the next stage of the receiver receives both harmonics, ω_{sig} and ω_d, or only one.

In the case when a signal is received from the amplifier output at frequencies ω_{sig} and ω_d, while the input receives noise with a continuous spectrum (i.e., both ω_{sig} and ω_d), the noise factor has the form

$$F = 1 + \frac{R_s T_s{}^{*}}{Z T_0},$$

which coincides with the expression obtained in reference [3].

If only the signal ω_{sig} of ω_d is received, the noise factor can be written as

$$F = 2 + \frac{2R_s T_s}{Z T_0},$$

where T_s is the diode temperature and T_0 is the standard temperature.

If no noise at the frequency ω_d is received at the input of the amplifier,** then

$$F = 1 + \frac{2R_s T_s}{Z T_0}.$$

When the useful signal at the input of the amplifier contains both ω_{sig} and ω_d (for example, random radio emission in radio astronomy or a noise signal from a noise generator used to measure the noise factor by the standard procedure), then the amplifier noise factor will be

$$F = 1 + \frac{R_s T_s}{Z T_0}$$

or when $T_s = T_0$

$$F = \frac{Q_{ext}}{Q},$$

independently of the frequency to which the output of the amplifier is tuned.

In practice the main possible characteristics of the amplifier are best expressed in terms of the diode parameters, particularly through the characteristic parameter $f_{cr} = \frac{m_{max}}{2}$, i.e., in terms of the frequency at which modulation of the diode capacitance can compensate only the losses introduced by the diode itself.

---

*In the present communication we mean by "noise factor of a parametric amplifier" the ratio of the total noise power at the output of the amplifier to that part of the power which is due to the antenna noise at the input of the amplifier in the useful bandwidth of the amplifier.

**For example, if a filter is used to cut off the signal ω_d at the input to a circulator with a "cold load," say in the form of an antenna directed toward the zenith.

The simplest resonator for an amplifier with diode is shown in Figure 3a, while the equivalent

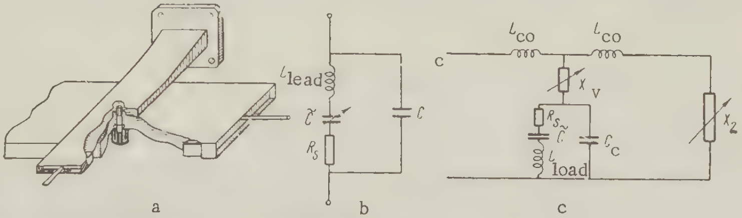

Figure 3. Simplest resonator for parametric amplifier, equivalent circuits of the diodes and of the amplifier with diode.

circuit of the diode [9,13] is shown in Figure 3b, and the equivalent circuit of the diode amplifier is shown in Figure 3c. In Figures 3b and 3c, L_{lead} is the inductance of the diode lead-in, R_s is the loss resistance in the diode, C is a nonlinear capacitance, C_c is the cartridge capacitance, and L_{co} is the equivalent inductance of the cut off waveguides, while X_1 and X_2 are trimming reactances.

If the cartridge capacitance is small compared with the diode capacitance, or if its effect is eliminated in parallel resonance with the aid of a rear plunger (X_2), and the capacitance between the diode and the bottom of the pumping waveguide (X_1) tunes C and L_{lead} in series resonance at the frequency ω_{sig}, then the equivalent circuit of the amplifier can actually be represented in the form shown in Figure 1. Using f_{cr} and the condition for large gain $\frac{m}{2}\frac{1}{\omega_s C_0} \simeq R = Z + R_s$, we can obtain expressions for the maximum possible product $\sqrt{K_1}\ 2\Delta\xi_{amp}$ for the minimum noise factor attainable at a frequency f with the aid of diodes having specified f_{cr} and m_{max}:

$$\sqrt{K_1}\Delta\xi_{amp} = \frac{m_{max}}{2}\left(1 - \frac{f}{f_{cr}}\right),$$

$$F_{min} = 1 + \frac{1}{\frac{f_{cr}}{f} - 1}\frac{T_s}{T_0}.$$

An experimental investigation of single-loop amplifiers was carried out in installations analogous to those described by us in [15] at frequencies 3,000 and 4500 Mc. A spectrum analyzer was used as an additional indicator.

The investigations have shown that the two harmonics ω_{sig} and ω_d were actually observed at the output of the parametric amplifier, so that the possibility of tuning the amplifier has been confirmed. The table lists the values of the Q of one of the amplifier breadboards, and the corresponding data on the measurement of the amplifier parameters at 4500 Mc, using the diodes described in [12]. Analogous data were obtained also at 3,000 Mc.

Measurements have actually shown that at large K we get $\sqrt{K_1}\ \frac{\Delta f}{f} = \frac{1}{Q_{ext}}$, as follows from the calculations.

Tentative measurements of the noise factor, carried out with a noise generator at 3,000 Mcs, yielded $F_{min} \simeq 1.5$ to 3 (1 to 4 db), which is more than the calculated value for the given amplifier, $F_{min} = Q_{ext}/Q = 1.3 - 1.4$ owing to the instability of the amplifier and to other factors. By modulating the pumping frequency, it is possible to attain a unique "super-regenerative mode," in which the stable gain and the bandwidth of the amplifier increase.

Modulation of the pumping frequency (by changing the voltage on the pumping klystron repeller) at an "audio" frequency (20 kc) resulted in a broadening of the bandwidth by three times with an increase of 5 - 10 db in the gain.

f_{op} Mc	Q	Q_{ext}	K, db	Δf_{amp} Mc	Δf tun Mc	$\sqrt{K_1}\,\frac{\Delta f_{exp}}{f}$
4500	25—30	30—35	27 (500 times)	7		$155/4500 \simeq \frac{1}{30}$
	25—30	30—35	20 (100 times)	15	40*	$150/4500 \simeq \frac{1}{30}$

*Calculated value (see [11]) of Δf_{tun} for $Q = 30$:

$$\Delta f\ \text{tun} = \frac{f\sqrt{n}}{Q}\sqrt{2\left(\sqrt{2}-1\right)} = 4500\,\frac{\sqrt{0{,}1}}{30}\,0{,}4 \simeq 40\ \text{Mc}\ .$$

In conclusion, I am grateful to K.A. Merkur'yev, N.E. Skvortsova, A.V. Kresilov, V.M. Val'd-Perlov, and A.A. Rabinovich-Vizel' for aid and counsel in the performance of the work.

REFERENCES

1. H. Heffner, G. Kotzebue, Proc. I.R.E., 1958, 46, 6, 1301.
2. G. Herrman, H. Uenohara, and A. Uhlir, Proc. I.R.E., 1958, 46, 6, 1301.
3. S. Blooms, and K.K. Chang. RCA Rev., 1957, 18, 4, 578.
4. V.S. Etkin (Parametric Amplifiers), Radio Electronic Industry, 1959, 9, 3.
5. L.I. Mandel'shtam, N.D. Papaleksi, On the Question of Parametric Regeneration, Communications Electrical Engineering News, 1935, 3, 1.
6. E.M. Rubchinskiy, ibid, 1935, 3, 7.
7. M. Duvil'kovskiy, and S. Rytor, On the Problem of Self-Excitation and Resonance in a System with Periodically Varying Self-Inductance, ZhTF (Journal of Technical Physics) 1936, 6, 3, 474.
8. V.A. Lazarev, Oscillations in Coupled Systems with Periodically Varying Parameters, ZhTF, 1940, 10, 11, 918.
9. I. Rusin, N.Ye.Skvortsova, and Yu.A. Sokolov, Semiconductor Devices and Their Applications, edited by Ya.A. Fedotov, Soviet Radio Press, Collection No. 3, 1958.
10. Waveguide Handbook (MIT Series, v. 10), Russian Translation, Soviet Radio Press, 1952.
11. G.S. Gorelik, Resonant Phenomena in Systems with Periodically Varying Parameters, ZhTF, 1934, 4, 10; 1935, 5, 2, 3.
12. Ye.M. Gershenzon, and V.S. Etkin, Parametric Regeneration in the Microwave Band Using a Semiconductor Diode, Izv. Vuzov MVO SSSR (Radiofizika), News of the Colleges, Ministry of Higher Education, USSR (Radiophysics), 1959, 2, 5, 835.
13. S.N. Ivanov, N.Ye.Skvortsova, and Yu.A. Sokolov, Radiotekhnika i elektronika, 1959, 4, 9, 1538.
14. A.A. Kulikovskiy, (Linear Radio Receiver Stages) GEI, 1958.
15. Ye.M. Gershenzon, N.G. Ptitsyna, G.I. Rozhkova, and V.S. Etkin, Fundamentals of Theory, Design, and Problems in Research Procedures for Single-Loop Parametric Microwave Amplifiers Using Semiconductor Diodes, (Radio Electronic Industry) 1950, 17, 3.
16. A. Uhlir, Proc. I.R.E., 1956, 44, 4, 557.
17. V.I. Bunimovich, Fluctuation Processes in Radio Receiving Devices, Soviet Radio Press, 195 1951.

V.I. Lenin Moscow State Pedagogical
Institute, Faculty of Experimental
Physics.

Submitted to editors 2 July 1959,
after revision 3 March 1960.

EXPERIMENTAL INVESTIGATION OF FORCED OSCILLATION IN A PARAMETRICALLY REGENERATED TANK CIRCUIT

A.N. Vakhrameyev

1. The processes that take place in an oscillating system with periodically varying parameters (capacitance or inductance), under the influence of an external sinusoidal signal and in the absence of an integral ratio between the frequency of the signal and the frequency of variation of the parameter, have not been sufficiently investigated. Some information on such processes are found in the papers by G.S. Gorelik [1], S.M. Rytov, and M.A. Davil'kovskiy [2]. V.V. Migulin [3] calculated the forced oscillations in a system with periodically varying capacitance (or inductance). He calculated the components of the oscillations in a parametrically under-excited tank circuit, tuned exactly to half the parameter-variation frequency, in the linear approximation, for an external-signal frequency close to the natural frequency of the tank circuit. For a parametrically excited oscillating system, which calls for a nonlinear analysis, the mathematical difficulties are such that a rigorous explanation of the presence of three components in the spectrum of the forced oscillations could be justified for only a rather small signal, and it was possible to show qualitatively the existence of a process wherein the external signal suppresses the component having the parametric-excitation frequency. To clarify the real character of these processes, it is very important to verify experimentally the applicability of the calculations in the under-excited system and to investigate the forced oscillations in a parametrically excited system which does not lend itself to a consistent theoretical analysis.

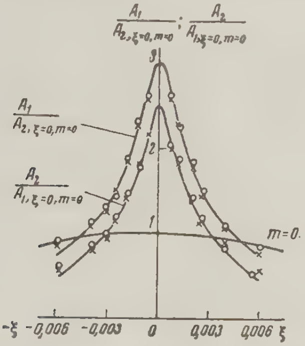

Figure 1. Dependence of the amplitudes of the components of forced oscillations on the detuning. Damping $\vartheta = 69 \times 10^{-4}$.

○ – $A_{\substack{\xi=0\\m=0}} = 0{,}06$ V; × – $A_{\substack{\xi=0\\m=0}} = 0{,}12$ V, $m/m_{cr} = 0{,}82$

2. We have studied in the present investigation the forced oscillations in a tank circuit with periodically varying inductance. The inductance was modulated by changing the permeability of a small portion of a toroidal ferrite core by means of a transverse magnetic field. The modulating field was applied perpendicular to the magnetic field, which in turn was produced in the core by an inductance winding. This method of modulation ensures in practice almost no induced component having the same frequency as the parameter in the oscillations investigated in the resonant circuit [5]. The external periodic signal was injected into the tank circuit by a current generator whose internal resistance was much greater than the resonant resistance of the tank circuit. The parameter-variation frequency was set by a crystal-stabilized generator, and amounted to $2\omega_0 = 75$ kc, where ω_0 is the average natural frequency of the tank circuit. The damping decrement of the tank circuit was determined from the rate of attenuation of shock-excited free oscillations produced in the tank circuit in the range of investigated amplitudes. The parameter-modulation coefficient m was determined from the damping decrement, for which the determined depth of modulation became critical, i.e., for which the condition $m = d/2$ was satisfied.*

---

* The condition for excitation of parametric oscillations in response to a jump-like change in the parameter [4].

This method determined the effective modulation coefficient more accurately than the method used in [5].

For $m < m_{cr}$, the tank circuit was operated in the linear part of its characteristic, so that the experimental results could be quantitatively compared with the calculations. The variation of the parameter used by the author was not sinusoidal, and was closer to a square wave with equal half cycles. Consequently, to make sure that the sinusoidal and square-wave modulations are equivalent from the energy point of view, we used in the theoretical formulas obtained for sinusoidal variation of the parameter a modulation coefficient $4m_s/\pi$, where $m_s = (L_{max} - L_{min})/(L_{max} + L_{min})$ is the modulation coefficient for the employed square-wave modulation.

Figure 1 shows the dependence of the amplitude of the components of the forced oscillation, namely A_1 with frequency p and A_2 with frequency $2\omega_0 - p$, on the detuning ξ; these relations were obtained experimentally and also calculated by means of the formulas cited in reference [3],

$$\frac{A_1^2}{A^2_{1,\xi=0,\ m=0}} = \frac{16\vartheta^2(\xi^2+\vartheta^2)}{\left(4\xi^2+4\vartheta^2+\frac{m^2}{4}\right)^2-4\vartheta^2 m^2},$$

$$\frac{A_2^2}{A^2_{1,\xi=0,\ m=0}} = \frac{m^2\vartheta^2}{\left(4\xi^2+4\vartheta^2+\frac{m^2}{4}\right)^2-4\vartheta^2 m^2},$$

where ϑ is the attenuation of the tank circuit and m is the relative depth of modulation. As can be seen from Figure 1, when the parameter is modulated, the amplitude of the forced oscillations increases, and the experimental values of the component A_1 and A_2 agree quite wel with the calculated values.

The slight deviation at low amplitudes and large values of detuning may be due to signals induced from the modulation system. The tank-circuit modulation spectrum contained not only the components with frequencies p and $2\omega_0 - p$, but also combination frequencies $3\omega_0 - p$, 2p, etc., but at appreciably lower amplitudes. Owing to the relative smallness of the amplitudes with sideband combination frequencies, their influence on the principal components was practically unnoticeable.

3. As was already indicated, it is shown in reference [3] that the spectrum of the forced oscillations of a parametrically excited tank circuit ($m > m_{cr}$) contain components having the same frequency as the parametric excitation; the possibility of suppressing this component by means of the signal has also been suggested. To clarify the real character of these processe we used the apparatus described above to investigate the spectral composition of the forced oscillations for the parametrically excited tank circuit, at different amplitudes of the signal.

Figure 2 shows the dependence of the amplitudes of the oscillation components in the tank circuit for a given mode, on the signal emf at three fixed values of the detuning.

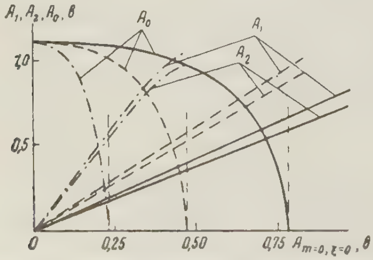

Figure 2. Dependence of amplitudes of components of forced oscillations on the external signal. Damping $\vartheta = 56 \times 10^{-4}$:

Continuous lines – $\xi = 0.0040$; dashed lines – $\xi = 0.0022$; dash-dot lines – $\xi = 0.0013$, $m/m_{cr} = 1.150$.

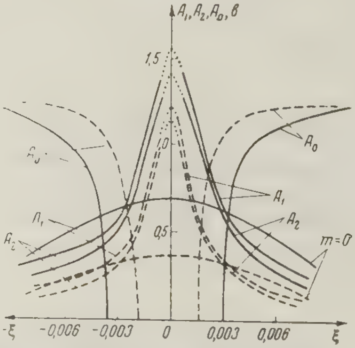

Figure 3. Dependence of amplitudes of components of forced oscillations on the detuning. Damping $\vartheta = 53 \times 10^{-4}$, $m/m_{cr} = 1.150$.

From an examination of these relations we see that as the external signal increases, the components A_1 and A_2, with respective frequencies p and $2\omega_0$ - p, also increase, while the component A_0 with frequency ω_0 diminishes to zero. The "quenching" of the component A_0 occurs after the components A_1 and A_2 reach a value which is quite fixed for a given value of m/m_{cr}. At a greater value of m/m_{cr} the quenching amplitude increases accordingly. Thus, the extinction of the component A_0, a component to the parametric excitation of the tank circuit, is produced by the external emf not directly, but via the components A_1 and A_2, the magnitudes of which depend not only on the signal emf amplitude, but also on the detuning of its frequency relative to the natural frequency of the tank circuit. The reduction in the component A_0 and its quenching are apparently all closely related to the reduction in the effective induction-modulation coefficient rather than to the drift of the average natural frequency of the tank circuit due to the currents of the components A_1 and A_2, since additional tuning of the tank circuit did not bring about any excitation of the already quenched oscillations. The reduction in the effective modulation coefficient is apparently due to the nonlinear conditions in that part of the core which is under the influence of the transverse modulating field and the longitudinal magnetic field produced by the currents of the components A_1 and A_2. Therefore, an increase in A_1 and A_2 reduces the depth of inductance modulation due to the change of the permeability of this portion by the transverse field. Quenching of the component is observed also when the detuning of the signal emf (the amplitude of which is constant) is varied relative to the central frequency of the tank circuit. The experimentally-obtained variations of the components A_1, A_2, and A_0 are shown in Figure 3, as functions of the detuning of the external signal, whose amplitude is kept constant. For small detunings the amplitudes A_1 and A_2 are sufficiently large while there is no component A_0. With increasing detuning, the amplitudes A_1 and A_2 increase, and when they reach the values that are characteristic of the given m/m_{cr}, the component A_0 appears. Further increase in the detuning causes an increase in A_0, which reaches its maximum value, determined by the parameters of the tank circuit and by the depth of modulation.

In the spectrum of the forced oscillations of a parametrically excited system, which we have investigated, there is found, as in any underexcited system, not only the fundamental components considered above, but also components having other combination frequencies. Since these components are quite small in amplitude (owing to the relatively small nonlinearity of the characteristic of the tank circuit), we have disregarded them.

Conclusion. The experimentally obtained results have fully confirmed the conclusions that follow from a linear analysis of forced oscillations in parametrically underexcited systems, and the correctness of the assumptions made in such an analysis.

An investigation of the forced oscillations in a parametrically excited circuit has also confirmed the correctness of the conclusions of reference [5], concerning the spectral composition and the possibility of suppressing, by means of an external signal, the component having the same frequency as the parametric excitation.

The author takes this opportunity to acknowledge his indebtedness to V. V. Migulin for suggesting the topic and for interest in the work.

REFERENCES

1. G.S. Gorelik, ZhTF, 1934, 4, 1783; ZhTF, 1935, 5, 195; ZhTF, 1935, 5, 489.
2. S.M. Rytov, and M.A. Davil'kovskiy, ZhTF, 1936, 6, 474.
3. V.V. Migulin, Radiotekhnika i elektronika, 1960, 5, 6, 955.
4. L.I. Mandel'shtam, Collected Works, v. II, Academy of Sciences Press, 1947.
5. V.V. Migulin, and A.N. Vakhrameyev, NDVSh (Scientific Reports of the Universities - Physical and Mathematical Sciences), 1958, 1, 138.

Physics Faculty, M.V. Lomonosov,
Moscow State University, Department of Theory of Oscillations.

Submitted to editors 2 February 1960.

SPECTRAL AND AMPLITUDE-FREQUENCY CHARACTERISTICS OF SUPERREGENERATIVE PARAMETRIC AMPLIFIERS

Ye.M. Gershenzon and V.S. Etkin

Many recent papers describe the application of the superregenerative mode in parametric regenerative amplifiers using semiconductor diodes [1, 2, 3]; this application increases both the stable gain coefficient and the bandwidth of the amplifier.

Regenerative parametric amplifiers can be viewed as regenerative amplifiers with negative resistance for each of the frequencies obtained in the amplification, namely f_s and $f_d = f_p - f_s$, where f_p, f_s, and f_d are the pumping, signal, and difference frequencies, respectively.

For a single-loop parametric amplifier [3], the expressions for the gain coefficient of each harmonic, at a large degree of regeneration, have the form

$$k = \frac{Z^2}{(R - R_-)^2},$$

where Z is the wave impedance of the line feeding the amplifier, R is the total resistance of the equivalent circuit of the amplifier, and R is the negative resistance

$$R \quad - \frac{m}{2} \frac{1}{\omega_0 \; c_0}$$

(ω_0 is the tank-circuit frequency, and C_0 is the capacitance at the operating point). If the pumping voltage, controlling the diode capacitance, is modulated with a low frequency $\Omega = 2\pi F$ (or, what is practically the same, if C_0 is modulated), one can speak of slow modulation of the value of the negative resistance. Therefore, the behavior of a parametric superregenerative receiver is qualitatively described by the theory previously developed by G.S. Gorelik for the case of an ordinary superregenerator with modulated negative resistance [4]. In this connection, one can expect the spectrum at the output of the amplifier to consist of two families of spectra, $f_s \pm nF$, and $f_d \pm nF$, $n = 0, 1, 2, \ldots$, and that the frequency characteristic acquires additional maxima at the frequencies $f_p/2 \pm nF$.

We have verified these conclusions by using the parametric amplifiers previously described [3].

In producing the superregenerative mode we used a "high" pumping modulation frequency (2 - 5 Mc), comparable with the bandwidth of the amplifier. It was found that actually two families of spectra are produced at the output of the amplifier in the case of "superposition," and the frequency characteristics broaden and acquire new maxima. The ordinate of the frequency characteristic is in this case the total intensity of oscillation of all the frequencies excited in the parametric superregenerative receiver by a signal of frequency ω. This intensity is measured by determining the current of a video detector at the output of the amplifier. Figure 1 shows spectrograms obtained with the aid of a spectrum analyzer for the regenerative and superregenerative modes: the left group (reading down): frequencies f_s and f_d close to $|f_s - f_d| \approx 3$ Mc. 1) Spectrum in regenerative mode. 2) Spectrum in superregenerative mode at $F_{mod} = 5$ Mc. 3) Spectrum in superregenerative mode for $F_{mod} = 2.2$ Mc. In the right group, the frequencies f_s and f_d are remote, $|f_s - f_d| \approx 12$ Mcs; the spectra are the same as for the right group.

Figure 2 shows oscillograms of the frequency characteristics of the amplifier, obtained with the aid of a swinging-frequency generator, in the regenerative and superregenerative modes: 1) Resonance curve of nonregenerative amplifier. 2) Resonance curve of regenerative amplifier. 3) and 4) Resonance curve of superregenerative amplifier; $F = 2.2$ and 5 Mc.

Thus, the use of the superregenerative mode increases the gain (for example, in the experiments described, for the same average pumping level the increase was from 20 to 35 - 40 db) and the bandwidth (by a factor 2 - 4), but is accompanied by so considerable a distortion of the signal spectrum at the output of the amplifier and of the frequency characteristics that the use of superregenerative parametric amplifiers becomes impossible in many radio installations.

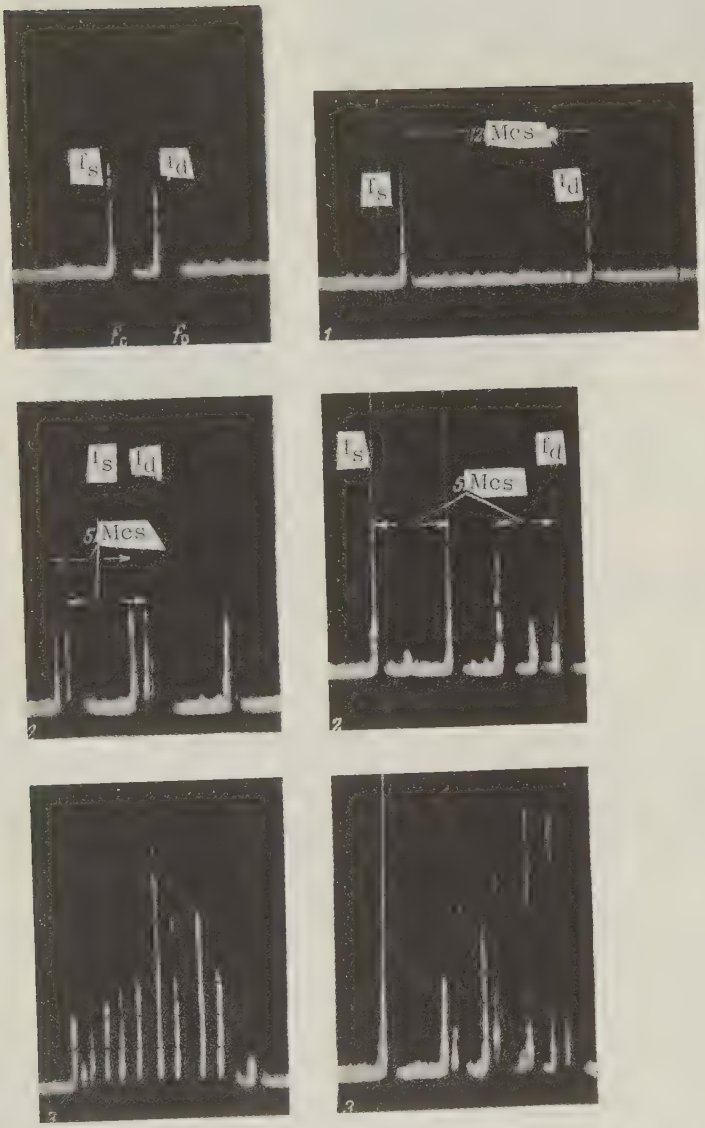

Figure 1

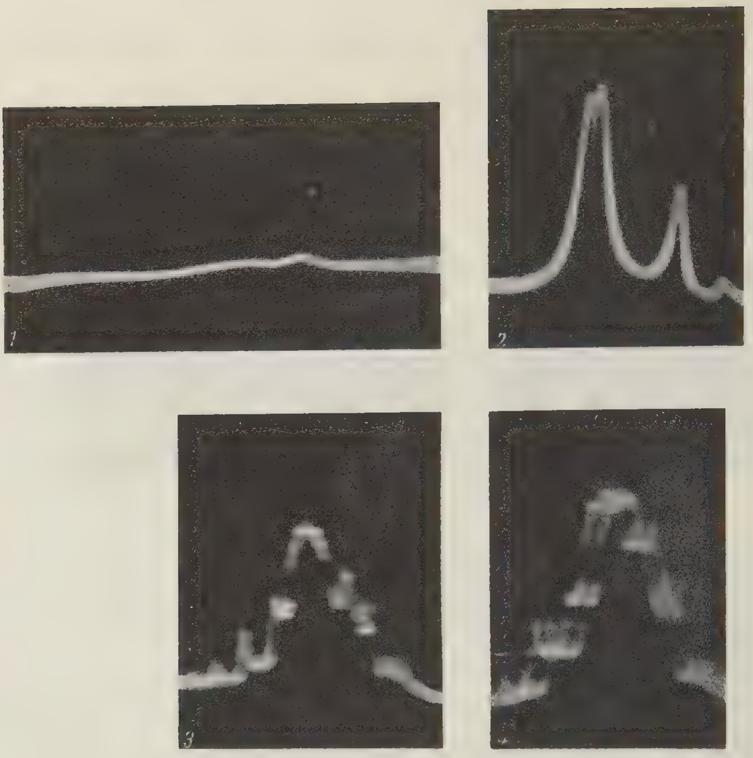

Figure 2

REFERENCES

1. H. Heffner, and G. Wade, Proc. I.R.E., 1959, 47, 7, 1971.
2. B. Bossard, Proc. I.R.E., 1959, 47, 7, 1969.
3. Ye.M. Gershenzen, N.G. Ptitsyna, G.I. Rozhkova, and V.S. Etkin, Concerning a Single-Loop Parametric Amplifier, Radiotekhnika i elektronika, 1961, 6, 5, 829.
4. G.S. Gorelik, Linear Resonant Phenomena in a Superregenerative Receiver, Elektrosvyaz' 1929, 6.

Submitted to editors 9 March 1960.

TRANSFER FUNCTION OF A SUPERREGENERATIVE PARAMETRIC AMPLIFIER

Yu.Ye. D'yakov

The determination of the transfer function of a single-loop superregenerative parametric amplifier reduces to a solution of the differential equation

$$\ddot{q} + 2h\dot{q} + \omega_0^2\{1 - \eta(t)\cos[\Omega t + \psi + \lambda(t)]\}\, q = \exp j\omega t, \tag{1}$$

where η (t) and λ (t) are slow functions of the time $(\dot{\eta} \ll \omega_0\eta,\ \dot{\lambda} \ll \omega_0\lambda)$.

We shall henceforth assume that $\lambda = \psi = 0,\ \Omega = 2\omega_0,\ Q = \omega_0 / 2h \gg 1$ and use the following notation

$$\delta = \omega - \omega_0 \ll \omega_0,\ z = 1 + \frac{j\delta}{h},\ \alpha = \dot{\eta} / 2\eta h,\ h_{1,2} = h\left(1 \mp \frac{\bar{\eta}Q}{2}\right),$$

$$\mu = \frac{hQ}{2}\int \tilde{\eta}\, dt,\ f_1 = (z - 2\alpha) / 4jQ,\ f_2 = \eta / 8,$$

$$p_1 = 2h(z - \alpha),\ p_2 = h^2\left(z^2 - \frac{\eta^2 Q^2}{4} - 2z\alpha\right),\ \rho = h^2\left(\frac{\eta^2 Q^2}{4} + \alpha^2 - \frac{\dot{\alpha}}{h}\right),$$

where $\tilde{\eta}$ and $\bar{\eta}$ are the alternating and constant components of the function η (t).

The solution of equation (1) for $\omega > 0$ will be sought in the form

$$q = e^{j\omega t}(k_1 + k_2 e^{-j2\omega_0 t}), \tag{2}$$

assuming $k_{1,2}$ to be slow functions of the time, so that $\dot{k}_{1,2} \ll \omega_0 k_{1,2}$. The factor following exp $j\omega t$ in equation (2) is called the "transfer function". Substituting (2) in (1) and equating to zero the coefficients of exp($j\omega t$) and exp [$j\omega t(\omega - 2\omega_0)t$], we obtain

$$\frac{\ddot{k}_1}{\omega_0^2} + \left(\frac{1}{Q\omega_0} + \frac{2j\omega}{\omega_0^2}\right)\dot{k}_1 + \left[1 - \left(\frac{\omega}{\omega_0}\right)^2 + \frac{j\omega}{Q\omega_0}\right]k_1 - \frac{1}{2}\eta k_2 = \omega_0^{-2},$$

$$\frac{\ddot{k}_2}{\omega_0^2} + \left(\frac{1}{Q\omega_0} + \frac{2j(\omega - 2\omega_0)}{\omega_0^2}\right)\dot{k}_2 + \left[1 - \left(\frac{\omega - 2\omega_0}{\omega_0}\right)^2 + \frac{j(\omega - 2\omega_0)}{Q\omega_0}\right]k_2 - \frac{1}{2}\eta k_1 = 0.$$

In view of the assumed slowness of $k_{1,2}$ and the large value of Q in this system, we can neglect the first two terms of each equation, after which we readily find the equations separately for k_1 and k_2 :

$$\ddot{k}_n + p_1(t)\dot{k}_n + p_2(t)k_n = f_n,\ n = 1, 2. \tag{3}$$

It follows from (3) that the asymptotic values of k_n (corresponding to t → ∞) are

$$k_n(t) = \int\limits_{-\infty}^{t} \frac{y_2(t)y_1(\theta) - y_2(\theta)y_1(t)}{\Delta(\theta)} f_n(\theta)\, d\theta, \tag{4}$$

where $y_{1,2}$ are the linearly independent solutions of equation (3) without the right half, and $\Delta = y_1\dot{y}_2 - \dot{y}_1 y_2$.

After making the substitution $y = w\exp\left(-\frac{1}{2}\int p_1\, dt\right)$, the equation $\ddot{y} + p_1\dot{y} + p_2 y = 0$ assumes the form $\ddot{w} - \rho(t)w = 0$, where $\rho(t) = p_2 - (p_1^2 + 2\dot{p}_1) / 4$. It can be shown (see, for example [1, 2]) that if the function ρ(t) is sufficiently slow, namely, when

$$\frac{1}{\rho}\frac{d\sqrt{\rho}}{dt} \sim a,\quad \frac{1}{\rho^{3/2}}\frac{d^2\sqrt{\rho}}{dt^2} \sim a^2,\ a \ll 1, \tag{5}$$

the linearly independent solutions of the equation $\dot{w} - \rho(t)w = 0$ are $w_{1,2} = g^{-1/2}\exp\left(\pm\int g\, dt\right)$ where $g = \sqrt{\rho} + O(a^2)$. In the case of a superregenerative parametric amplifier, conditions (5) are usually satisfied, and, in addition,

$$4(\alpha^2 - \dot{\alpha}h^{-1})\,\eta^{-2}Q^{-2} \sim a^2 \ll 1 \tag{6}$$

(see below), so that it is necessary to assume in the approximate expression for $w_{1,2}$ that $g = \sqrt{p} \simeq hQ\eta/2$. As a result we obtain

$$y_{1,2} = \exp\left[-h\left(z \mp \frac{Q\bar{\eta}}{2}\right)t \pm \mu(t)\right] = \exp\left[-(h_{1,2} + j\delta)t \pm \mu(t)\right]. \tag{7}$$

As follows from (7), $\Delta(t) = -hQ\eta \exp(-2hzt)$. . The function $\mu(t)$ in (7) does not have a constant component; thus, the parametric system, described by equation (1), is characterized by two damping factors, h_1, and h_2 (if we neglect the corrections of order $h0(a^2)$ to $h_{1,2}$, [see (5) and (6)].

Expressions (2), (4) and (7) determine the dependence of the sought transfer function on the coefficients of equation (1).

Let us examine several examples.

1. The value of η in equation (1) is independent of the time (the parametric amplifier is in the usual regeneration mode). In this case $\eta = \bar{\eta}$, $\mu = 0$, $f_1 = z/4jQ$ and $f_2 = \bar{\eta}/8$. From (4) we get

$$\left.\begin{matrix} k_1 = z/4jQ \\ k_2 = \bar{\eta}/8 \end{matrix}\right\} \times \frac{2}{\bar{\eta}\omega_0}\left[\frac{1}{h_1 + j\delta} - \frac{1}{h_2 + j\delta}\right]. \tag{8}$$

Usually the value of $\bar{\eta}$ is chosen close to 2/Q, so that $h_1 \ll h_2$ and we can assume $\delta \sim h$. According to (8) we have here $k_1 \simeq [4j\omega_0(h_1 + j\delta)]^{-1}$, $k_2 \simeq [4\omega_0(h_1 + j\delta)]^{-1}$, $|k_1| = |k_2|$.

2. The value of η is constant and equal to zero (tank circuit with constant parameters). Going to the limit $\eta = \eta \to 0$ in (8), we find, as is to be expected,

$$k_1\,[2j\omega_0(h + j\delta)]^{-1},\ k_2 = 0.$$

3. Let us assume that $\eta(t) = \bar{\eta}(1 + \varkappa\cos\nu t)$, $\varkappa < 1$. In this case

$$\tilde{\eta} = \bar{\eta}\varkappa\cos\nu t,\ \alpha = -\frac{\varkappa\nu\sin\nu t}{2h(1 + \varkappa\cos\nu t)},\ \mu = \beta\sin\nu t,\ \beta = \frac{\bar{\eta}Q}{2}\,\frac{h\varkappa}{\nu}. \tag{9}$$

It follows from (9) that the role of the small parameter a in (5) and (6) is played by the ratio ν/h (under the condition that the coefficient $\varkappa$ is not too close to unity, and we can assume that $(1 + \varkappa\cos\nu t)^{-1} \sim 1$). The inequality $\nu \ll h$ is usually well satisfied in superregenerative parametric amplifiers. Inasmuch as $\dot{\alpha} \sim \varkappa\nu/h$, we can put in (4) $f_1 = \text{const} = z/4jQ$.

Substituting the expression (9) in (7) and (4), we obtain

$$y_{1,2} = \exp[-(h_{1,2} + j\delta)t \pm \beta\sin\nu t],\ \Delta = -hQ\bar{\eta}(1 + \varkappa\cos\nu t)\exp(-2hzt),$$

$$k_1 = \frac{-z}{4jhQ^2\bar{\eta}}\int_{-\infty}^{t}\{\exp[(h_2 + j\delta)(\theta - t) + \beta(\sin\nu\theta - \sin\nu t)] -$$

$$-\exp[(h_1 + j\delta)(\theta - t) - \beta(\sin\nu\theta - \sin\nu t)]\}(1 + \varkappa\cos\nu\theta)^{-1}\,d\theta. \tag{10}$$

Inasmuch as $(-\beta\sin\nu\theta) = \sum\limits_{n=-\infty}^{\infty} J_n(j\beta)\,e^{jn\nu\theta}$, we obtain from (10), by setting $(1 + \varkappa\cos\nu\theta)^{-1} \simeq 1 - \varkappa\cos\nu\theta$ and using the relation $J_{n+1}(j\beta) + j_{n-1}(j\beta) = (2n/j\beta)\,J_n(j\beta)$,

$$k_1 = \frac{z}{4jhQ^2\bar{\eta}}\left\{e^{\beta\sin\nu t}\sum_n \frac{e^{jn\nu t}}{h_1 + j(\delta + \nu n)}\left(1 + \frac{j\varkappa n}{\beta}\right)J_n(j\beta) -\right.$$

$$\left.-\,e^{-\beta\sin\nu t}\sum_n \frac{e^{-jn\nu t}}{h_2 + j(\delta - \nu n)}\,J_n(j\beta)\left(1 - \frac{j\varkappa n}{\beta}\right)\right\}, \tag{11}$$

for $\bar{\eta} \simeq 2/Q$ we have

$$k_1 \simeq \frac{z}{4j\omega_0}\,e^{\beta\sin\nu t}\sum_n \frac{\left(1 + \frac{jn\nu}{h}\right)J_n(j\beta)}{h_1 + j(\delta + n\nu)}\,e^{jn\nu t}.$$

An analogous expression is obtained for k_2:

$$k_2 \simeq \frac{1}{4\omega_0}\,e^{\beta\sin\nu t}\sum_n \frac{J_n(j\beta)}{h_1 + j(\delta + n\nu)}\,e^{jn\nu t}.$$

REFERENCES

1. S.M. Rytov, Modulated Oscillations and Waves, Transactions of the Physics Institute, Academy of Sciences USSR, 1940, 2, 1.
2. L. Brillouin, M. Parodi, Propagation of Waves in Periodic Structures (Russian Translation), IL, 1959.

Submitted to editors 21 April 1960

AN ERROR IN THE ANALYSIS OF A TWO-LOOP M PARAMETRIC AMPLIFIER

Yu.Ye. D'yakov

In the analysis of a two-loop regenerative parametric amplifier it is usually assumed that the oscillations in one of the loops occurs at a signal frequency $\omega - \Omega_1$, while in the other, so-called balanced loop, the oscillations are at the difference frequency $|\omega - \Omega_3| \simeq \Omega_2$, where Ω_3 is the pumping frequency and $\Omega_{1,2}$ are the natural frequencies of the loops. Such an assumption is justified when the loops are of high Q and are weakly coupled, the latter condition calling not only for the satisfaction of the inequality $C_3 \ll C_{1,2}$, but also for the frequency difference $\Omega_1 - \Omega_2$ to be not too small.

In the degenerate case $\Omega_1 = \Omega_2$ each loop will carry oscillations not at one but at two frequencies, ω and $\omega - \Omega_3$, similar to what takes place in a single-loop parametric amplifier. It follows, therefore, that in the case of the synchronous mode ($2\omega = \Omega_3$), for example, the degenerate two-loop parametric amplifier will have selectivity with respect to the phase of the amplified voltage U(t). The double-frequency character of the oscillations in the loops of the parametric amplifier for $\Omega_1 - \Omega_2$ is not taken into account in references [1, 2], and the results of these papers pertinent to this case are in error.

The analogy between the degenerate two-loop and single-loop parametric amplifiers can also easily be verified mathematically. Let us assume for simplicity that the loops of the circuits shown in the figure are perfectly identical and let us put $C_n - C$, $(L_n C_n)^{-1/2} = \Omega_0$, $R_n/2L_n - h$ and $v_n = C^{-1} \int i_n \, dt$ $(n - 1,2)$. Writing down the Kirchhoff equations, we obtain for v_n the following system of differential equations:

$$\ddot{v}_n + 2h\dot{v}_n + \Omega_0^2 v_n - \Omega_0^2 F(t)(v_1 + v_2) = \begin{cases} \Omega_0^2 U(t), & n = 1, \\ 0, & n = 2, \end{cases} \tag{1}$$

where $F(t) = C_3(t)C^{-1}[1 + C_3(t)C^{-1}]$. Adding equations (1) with n = 1, and n = 2, and setting $v = v_1 + v_2$, we get

$$\ddot{v} + 2h\dot{v} + \Omega_0^2 [1 - 2F(t)] v = \Omega_0^2 U(t). \tag{2}$$

As is known, this is precisely the equation for a single-loop parametric amplifier, whose capacitance is modulated in proportion to $[1 - 2F(t)]^{-1}$, thus proving the aforementioned analogy.

If the function v, satisfying equation (2), has been determined, then, as can be seen from (1), the determination of v_1 and v_2 reduces to the elementary problem of solving a second-order differential equation with constant coefficients, with a known right half. In particular, when the amplitude of the time-dependent component of the coupling capacitance C_3 is close to its threshold value, corresponding to the start of parametric oscillation, we have $v_1 \simeq v_2$ and $i_1 \simeq i_2$.

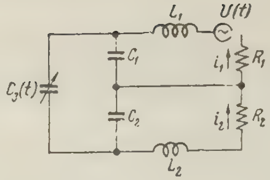

REFERENCES

1. S. Bloom, and K.K.N. Chang, Theory of parametric amplification using nonlinear reactances, RCA Rev., 1957, 18, 4, 578.
2. V.I. Zubkov, and Ya.A. Monosov, Some Problems in the Theory of Parametric Amplifiers, Radiotekhnika i elektronika 1960, 5, 1, 75.

Submitted to editors 21 April 1960

CONSIDERATION OF COMBINATION FREQUENCIES IN SYSTEMS WITH PERIODICALLY VARYING REACTANCE

Yu. A. Kravtsov

As is well known, the steady-state response of a linear system with periodically varying parameters to a harmonic signal

$$i(t) = I e^{i\omega t} \tag{1}$$

is expressed by a Fourier series in the harmonics of the fundamental pumping frequency

$$u(t) = \left(\sum_{-\infty}^{+\infty} k_n(\omega) e^{in\Omega t}\right) I e^{i\omega t} . \tag{2}$$

For systems having high selectivity, it is necessary to take into account in expression (2) only those combination frequencies, which lie in the passband of the system. In particular, in a one-loop parametric amplifier, and also in a two-loop regenerative amplifier, it is possible to retain only terms with index n = 0 and − 1, while in a double-loop nonregenerative amplifier the indices n = 0 and + 1 need be retained. In multiloop parametric amplifiers, sometimes a larger number of harmonics is taken into account.

It is of interest to calculate the amplitudes of all the combination frequencies in the expansion (2), at least for a system with a single periodically varying capacitance (Figure 1). For this system, the voltage on the capacitance u(t) and the current i(t) are related by

$$Y[u(t)] + \frac{d}{dt}[C(t)\, u(t)] = i(t), \tag{3}$$

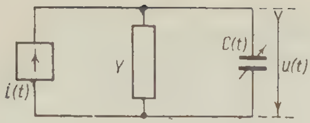

Figure 1

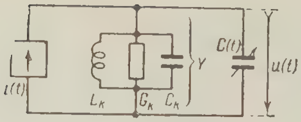

Figure 2

where C(t) is the periodically varying capacitance:

$$C(t) = \bar{C} + 2\tilde{C}\cos\Omega t, \tag{4}$$

and Y is the linear admittance operator of the part of the circuit having constant parameters. Substituting (1) and (2) and (4) into (3) and equating the coefficients of exp $[i(\omega + n\,\Omega)]$ in the left and right halves, we obtain for the coefficients $k_n(\omega)$ the system of equations

$$Y_n k_n(\omega) + y_n[k_{n-1}(\omega) + k_{n+1}(\omega)] = \begin{cases} 1, & n = 0, \\ 0, & n \neq 0, \end{cases} \tag{5}$$

where

$$Y_n = Y(\omega_n) + i\omega_n \bar{C}; \quad y_n = i\omega_n \tilde{C};$$

$$\omega_n = \omega + n\Omega \quad (n = 0, \pm 1, \pm 2, \ldots).$$

The solution of the system (5), which can be found first for a finite number of unknowns $(-N < n < N)$, and then expanded to include the case $N = \infty$, has the form

$$\begin{aligned} k_0(\omega) &= \frac{1}{\hat{Y}_0}, \\ k_n(\omega) &= -\frac{y_n}{\hat{Y}_n} k_{n-1}(\omega), \quad n > 0, \\ k_n(\omega) &= -\frac{y_n}{\hat{Y}_n} k_{n+1}(\omega), \quad n < 0, \end{aligned} \tag{6}$$

where

$$\hat{Y}_0 = Y_0 - \frac{y_0 y_1}{\hat{Y}_1} - \frac{y_0 y_{-1}}{\hat{Y}_{-1}};$$

$$\hat{Y}_n = Y_n - \cfrac{y_n y_{n+1}}{Y_{n+1} - \cfrac{y_{n+1} y_{n+2}}{Y_{n+2} - \cdots}}, \quad n > 0;$$

$$\hat{Y}_n = Y_n - \cfrac{y_n y_{n-1}}{Y_{n-1} - \cfrac{y_{n-1} y_{n-2}}{Y_{n-2} - \cdots}}, \quad n < 0. \tag{7}$$

In the case of small capacitance deviation $\tilde{C}$ $(\tilde{C} \ll \bar{C})$ and a sufficiently high harmonic number n (such that the frequency $\omega_n = \omega + n\,\Omega$ lies outside the passband of the system), the ratio y_n/Y_n, contained in the recurrence formulas (6), is a small quantity on the order of $\tilde{C}/\bar{C}$:

$$|y_n / \hat{Y}_n| \sim \frac{\tilde{C}}{\bar{C}} \ll 1,$$

and the amplitudes of the harmonics $|k_0(\omega)|$ decrease one order of magnitude with respect to $\tilde{C}/\bar{C}$ whenever n is increased by one. Under these conditions we can confine ourselves to only a few terms in the expansion (2).

The contribution of the individual combination components to the amplitude of the fundamental harmonic $|k_0(\omega)|$ (the harmonic at the signal frequency ω) is also determined by the magnitude of the ratio y_n/Y_n, by virtue of which the continuous fractions in (7) can be terminated, starting with a certain index n. In particular, in a one-circuit parametric amplifier (Figure 2),

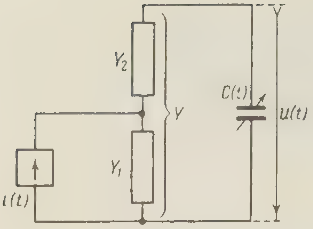

Figure 3

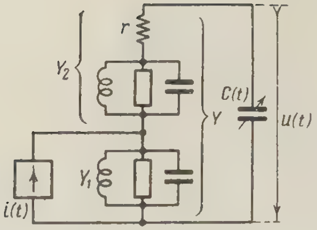

Figure 4

in which the signal frequency is approximately half the pumping frequency and is close to the frequency to which the circuit is tuned $[\omega \simeq \Omega/2 \simeq 1/\sqrt{L_{\text{к}}(C_{\text{к}}+\overline{C})}]$the most important roles are played by the admittances Y_0 and Y_{-1} at the frequencies $\omega_0 \equiv \omega$ and $\omega_{-1} = \omega - \Omega \simeq -\omega$, so that

$$\hat{Y}_0 \simeq Y_0 - \frac{y_0 y_{-1}}{Y_{-1}}, \quad \hat{Y}_{-1} \simeq Y_{-1},$$

$$k_0(\omega) \simeq \frac{1}{Y_0 - \frac{y_0 y_{-1}}{Y_{-1}}}, \quad k_{-1}(\omega) = -\frac{y_{-1}}{Y_{-1}} k_0(\omega).$$

The system shown in Figure 1 can be made more complicated by adding the signal source to part of the admittance Y (Figure 3). Expression (1) - (7) remain in force, provided the current i(t) is replaced by $i'(t) = \frac{i(t)}{1+\frac{Y_1}{Y_2}}$,and the admittance Y is replaced by $\frac{Y_1 Y_2}{Y_1 + Y_2}$. The circuits shown in Figure 3 can be used for the calculations of a two- loop parametric amplifier, in which the coupling element comprises a capacitance C(t) connected in series with a resistance R (Figure 4).

Naturally, the results obtained for the circuit shown in Figure 1 can also be extended to include a system with periodically varying inductance.

The author is grateful to S. M. Rytov for interest in this work.

Submitted to editors 20 August 1960

EFFECT OF ASYMMETRY ON THE OPERATION OF PUSH-PULL, SEMICONDUCTOR CONVERTERS WITH EXTERNAL EXCITATION

G.N. Berestovskiy

In high-power, push-pull converters (Figure 1a), which as a rule are externally excited, there is frequently observed a substantial difference between the collector currents of the two transistors, i.e., the presence of a dc component in the current flowing in the transformer collector winding. This phenomenon frequently causes one of the transistors to be overloaded or even to fail. The appearance of a dc component I is due to the asymmetry of both the circuit and the switching mode, and the considerable value of I is due to the small resistance of the conducting transistor and to the presence of the inductance L of the collector winding, connected between the two transistors.

The inductance L causes the current in the steady-state mode to be so distributed among the transistors, that the inductance voltage u_L (and consequently the load voltage) has no dc component:

$$\int_0^T u_L\,dt = 0, \tag{1}$$

where T is the period of the oscillations in the circuit.

The dc component, more accurately, the monotonically varying component, of the voltage u_L will be present only during the settling time of the oscillations. The magnetizing current i_L will also have a slowly increasing unipolar component, which grows until the change in the voltage drop on the collector-circuit resistance causes equation (1) to be satisfied.

Let us calculate the dc component I of the current i_L taking into account both the asymmetry of the circuit and the asymmetry of the output voltage, i.e., the voltages on the inductance. To simplify the calculations we shall assume that a) the duration of the voltage front is equal to zero during switching; b) the maximum value of the current i_L is much less than E/r, where r is the resistance of the circuit through which the collector current of one of the transistors flows. The latter assumption, as shown by calculation, enables us to regard the current i_c of a conducting transistor as constant and equal to the value averaged over the time of the pulse.

On the basis of these assumptions, expression (1) can be represented in a simpler form:

$$u_{L1}\tau_1 = u_{L2}\tau_2, \tag{2}$$

where u_{L1} and τ_1 are respectively the amplitude and duration of the voltage half wave of one polarity; u_{L_2} and τ_2 are the same for the other polarity. On the other hand,

$$u_{L1} = E - e_1 - (I_{\text{H}} - I)r_1, \quad u_{L2} = E - e_2 - (I_{\text{H}} + I)r_2, \tag{3}$$

where e_1 and e_2 are the residual voltages on the transistor collectors, voltages that depend on the collector and base currents; I_ℓ is the current I'_ℓ referred to the collector winding. The current I flows through the following closed loop: transistor T1, transformer winding - transistor T2. Therefore, in one transistor I is added to I_ℓ, whereas in the other it is subtraced. From equations (2) and (3), we obtain, neglecting the small quantities and assuming that $\left|\frac{\tau_2-\tau_1}{\tau_2}\right| \ll 1$, we have the following expression for the current I:

$$I = \frac{E}{r_1 + r_2} \quad \frac{\tau_2 - \tau_1}{\tau_2} + \frac{(e_1 + r_1 I\ell) - (e_2 + I\ell\, r_2)}{r_1 + r_2}. \tag{4}$$

To gain a clearer idea of the order of magnitude of I, let us consider the following example: E = 25 v, $r_1 + r_2 = 0.5$ ohm, relative difference in durations of the voltage half waves is 1%. Here I = 0.5 amp and consequently the current I_{C2} is found to be 1 amp greater than the current I_{C1}. We see that even a very slight asymmetry in switching leads to a large difference in currents. The second term in equation (4), due to the asymmetry in the circuit, is as a rule small in value, since the voltage losses in the primary circuit are usually small.

However, the same asymmetry can lead to the appearance of the first term, too, i.e., to an inequality in the half-waves of the output voltage even though the control voltage is perfectly symmetrical. To explain this effect, let us examine the switching process in the circuit of Figure 1a.

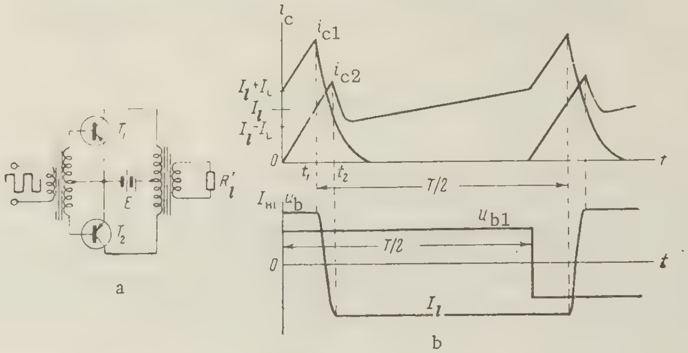

Figure 1

a — diagram of converter with external excitation, b — current and voltage curves

When the transistor base voltages reverse signs, the cutoff transistor, say T2, starts conducting and its collector current i_{c2} increases in accordance with the transient characteristi of the transistor, while the conducting transistor T1 begins to cut off. But since transistor T1 was previously in the saturation mode, a certain time t_1 (Figure 1b) elapses before it goes into the active region of the characteristics. Only starting with that time will the voltage on the transformer windings begin to change, meaning also the load current I'_ℓ. In order to determine the character of variation of the currents, let us turn to the equation relating the currents in the circuit

$$i_{c1} - i_{c2} = i_l + i_L. \tag{5}$$

Assuming the inductance L to be sufficiently large, we neglect the change in the current i_L during the switching time. Then, up to the instant t_1, the difference in transistor currents will remain constant, i.e., both i_{c1} and i_{c2} will increase in accordance with the law governing the variation of the current i_{c2}. After the transistor T_1 goes out of the saturation mode, both currents i_{c1} and i_{c2} vary independently of each other, each in accordance with its own law: i_{c1} decreases while i_{c2} increases. Their difference determines the magnitude of the current i_ℓ and accordingly the voltages on the transistor collectors. This process continues until the transistor T2 becomes saturated (instant t_2 on Figure 1b). Then the load current reverses sign and reaches its stationary value I_ℓ. Thus, the time interval $t_2 - t_1$ corresponds to the duration of the voltage front across the load. After T_2 becomes saturated it turns into a passive element, and now its current i_{c2} duplicates the course of the current i_{c1} in such a way that their difference remains equal to $I_\ell - I_L$. After a half-cycle, the current i_{c2} increases to a value $I_\ell + I_L$ and the entire process of switching is repeated again.

If the transistors have unequal characteristics, then both the durations of the fronts and the times required for the transistors to go out of the saturation mode will be different, and this leads to asymmetry in the output-voltage half-waves. With increasing switching frequency, the relative difference in the voltage half-waves increases, since the durations of the fronts remain constant while the period decreases.

In self-oscillating operation of the converter, a dc current component also appears if the circuit is not symmetrical, but owing to the automatic regulation of the ratio of the half-cycle durations, this dc component can be much smaller. Moreover, the use of an inductive element with a core made of a material having a rectangular hysteresis loop, the saturation of which determines the instant of flipping of the circuit, almost completely eliminates the dc component in such a circuit. In a separately excited generator, naturally, such an element cannot help since the switching mode is imposed from the outside.

Thus, the main cause of the dc component of the current is the difference in the durations of the output-voltage half-cycles, and also the differences in the transistor characteristics (particularly at high commutation frequency).

The symmetry of the switching voltage can be attained by selecting the transistors in the master oscillator (converter in self-oscillating mode) and by using in the oscillator a transformer with a rectangular-hysteresis-loop core. The difference in the converter transistor switching times can be greatly reduced by reducing the switching time, this being accomplished by using a control voltage with a large peak at the start of each half cycle.

Physics Faculty, M.V. Lomonosov
Moscow State University

Submitted to editors 16 December 1960

PARAMAGNETIC AMPLIFIER FOR THE TEN-CENTIMETER BAND USING Fe3+ IONS IN CORUNDUM

N.V. Karlov, Yu.P. Pimenov, A.M. Prokhorov

The possibility of using Fe^{3+} ions in corundum in paramagnetic amplifiers for the three-centimeter band has by now been experimentally established [1,2]. It is interesting to ascertain whether this material can produce a resonant parametric amplifier for the ten centimeter band. In this case we can choose several different levels of the Fe^{3+} ion. We have experimentally investigated only one version, in which we used a paramagnetic amplifier resonating system already on hand. The trigonal axis of the electric field of the crystal was perpendicular to the external constant magnetic field. In this case the energy levels of the two nonequivalent Fe^{3+} ion systems coincide. We use for the amplification the transition between the lower levels, which could be characterized by the quantum numbers $M = \pm 1/2$ in the case of parallel orientation. The auxiliary transition used was $-1/2 \rightarrow -3/2$. The frequency of the auxiliary radiation was about 14,000 Mc. In the cavity used, the high-frequency magnetic field of the signal was perpendicular to the external magnetic field and to the trigonal axis of the crystal.

The amplification and generation were observed at a temperature 2° K. The constant magnetic field was approximately 380 oersteds. The product of the gain by the bandwidth was small in this case, principally because the corundum specimen which we possessed contained a small number of iron ions. From these preliminary experiments we conclude that corundum with Fe^{3+} is apparently a suitable material for paramagnetic amplifiers for the decimeter band.

REFERENCES

1. L.S. Korniyenko, and A.M. Prokhorov, ZhETF, 1959, 36, 919.
2. J.E. King, and R.W. Terhune, J. Appl. Phys., 1959, 30, 1844.

Submitted to editors 26 September 1960

MICROWAVE REGENERATION IN A FERRITE IN RESPONSE TO LONGITUDINAL PUMPING

A.L. Mikaelyan, A.A. Vasil'yev, V.V. D'yachenko

In reference [1] the authors have investigated phenomena that take place in a magnetized ferrite subject to the action of an alternating magnetic field with circular polarization of large amplitude (that is, the pumping field).

The gist of these phenomena, the mechanism of which was first considered by H. Suhl [2], is the following. When "magnetostatic" oscillations at frequencies ω_1 and ω_2, related by the equation

$$\omega_1+\omega_2=\omega_p, \tag{1}$$

(ω_p is the pumping-field frequency) are excited in a ferrite, the natural-oscillation losses at the frequencies ω_1 and ω_2 can be offset by the pumping-field energy; here the pumping field plays the role of a source that gives rise to periodic variations in the properties of the ferrite. At certain "threshold" values of the pumping field, when the losses in the ferrite are compensated for, oscillations will be generated at frequencies ω_1 and ω_2.

Articles [1, 2] treat only the case when the pumping field is homogeneous and circularly polarized in the plane perpendicular to the magnetization axis (type 1, $\overline{1}$, 0).

The present communication is devoted to an investigation of analogous phenomena in a ferrite sphere, acted upon by a pumping field h_p oriented along the magnetizing field H_0^e (the direction of this field coincides with that of the z axis).

When the pumping field has this direction, magnetostatic oscillations other than those considered in reference [1], can now interact with each other.

As in [1], we shall consider a small ferrite sphere, whose dimensions are such that the magnetostatic approximations are applicable.

By determining the magnetization $4\pi M_1$ at the frequency ω_1 from the system of equations

$$\frac{d\vec{M}}{dt}=-\gamma\,[\vec{M}\vec{H}],\quad \operatorname{rot}\vec{H}=0,\quad \vec{H}=\operatorname{grad}\Psi \tag{2}$$

we obtain*

$$\begin{aligned} 4\pi M_{x_1}&=\chi_1\frac{\partial\Psi_1}{\partial x}-jk_1\frac{\partial\Psi_1}{\partial y}-\alpha\,h_p\frac{\partial\Psi_2^*}{\partial x}+j\beta h_p\frac{\partial\Psi_2^*}{\partial y},\\ 4\pi M_{y_1}&=\chi_1\frac{\partial\Psi_1}{\partial y}+jk_1\frac{\partial\Psi_1}{\partial x}-\alpha h_p\frac{\partial\Psi_2^*}{\partial y}-j\beta h_p\frac{\partial\Psi_2^*}{\partial x}, \end{aligned} \tag{3}$$

where

$$\chi_1=\frac{\omega_0\omega_M}{\omega_0^2-\omega_1^2};\quad k_1=-\frac{\omega_1\omega_M}{\omega_0^2-\omega_1^2};\quad \alpha=\frac{\gamma\omega_M(\omega_0^2-\omega_1\omega_2)}{2(\omega_0^2-\omega_1^2)(\omega_0^2-\omega_2^2)};$$

$$\beta=\frac{\gamma\omega_M\omega_0(\omega_2-\omega_1)}{2(\omega_0^2-\omega_1^2)(\omega_2^2-\omega_2^2)}. \tag{4}$$

With the aid of the equation $\operatorname{div}\vec{B}=0$ and expressions (3) we readily obtain the following system of equations for the magnetostatic-oscillation potentials at the frequencies ω_1 and ω_2:

---

*We use everywhere the same notation as in [1].

$$\mu_1\left(\frac{\partial^2}{\partial x^2}+\frac{\partial^2}{\partial y^2}\right)\Psi_1+\frac{\partial^2\Psi_1}{\partial z^2}=\alpha h_p\left(\frac{\partial^2}{\partial x^2}+\frac{\partial^2}{\partial y^2}\right)\Psi_2^*,$$

$$\mu_2\left(\frac{\partial^2}{\partial x^2}+\frac{\partial^2}{\partial y^2}\right)\Psi_2+\frac{\partial^2\Psi_2}{\partial z^2}=\alpha h_p\left(\frac{\partial^2}{\partial x^2}+\frac{\partial^2}{\partial y^2}\right)\Psi_1^*. \tag{5}$$

If there is no pumping field ($h_p = 0$), then the system (5) separates into two independent equations, describe the free magnetostatic oscillations at frequencies ω_1 and ω_2. In the presence of a pumping field, these oscillations are coupled to each other.

The method for the investigation of this system of equations is fully analogous to the method used in [1]. We, therefore, leave out all the intermediate mathematical derivations and give only the final results, which determine the types of interacting oscillations and the amplitude of the pumping field corresponding to the oscillation threshold.

1. Oscillations with a zero second index, that is,

$$2,0,1;\ 3,0,1;\ 4,0,1 \tag{6}$$

etc., interact "with each other." This is the so-called "degenerate" case when $\omega_1 = \omega_2 = \frac{1}{2}\omega_p = \omega$. It must be noted that inasmuch as the index can assume different values for oscillations of the higher types,* a "nondegenerate" case is also possible. The interacting pair 4, 0, 1 - 4, 0, 2 is an example.

For the sake of illustration, let us examine the formula for the threshold of oscillations of type 2, 0, 1. This formula reads

$$\frac{h_p}{\Delta H} \geqslant 2\,\frac{\omega_0^2+\omega^2}{\left|\omega_0^2-\omega^2\right|}=\frac{5}{2}\,\frac{H_0^e-\frac{4}{3}\pi M}{4\pi M}\left(1+\frac{\omega^2}{\omega_0^2}\right) \tag{7}$$

if the resonant tuning is of the type 2, 0, 1, when $\omega_0^2-\omega^2 = -\frac{4}{5}\omega_0\omega_M$ (see, for example, reference [1]). Results of calculations based on this formula for different external magnetizing fields are illustrated in Figure 1.

2. The second group of interacting oscillations contain the pairs

$$3,\bar{1},0—3,1,1 \quad 4,\bar{1},0—4,1,1, \quad 4,\bar{2},0—4,2,1 \tag{8}$$

etc., that is, circularly polarized oscillations with oppositely directed rotation.

It must be noted that the third index can also have a nonzero value, if such an oscillation exists (an example is the interacting pair 3, $\bar{1}$, 1 - 3, 1, 1).

The formula for the oscillation threshold of the lowest pair of oscillations 3, $\bar{1}$, 0 - 3, 1, 1 has the form

$$h_p^2 \geqslant \frac{\left(8\mu_1\mu_1''-4\mu_1k_1''-4k_1\mu_1''+27\mu_1''-k_1''\right)\left(8\mu_2\mu_2''+4\mu_2k_2''+4\mu_2''k_2+27\mu_2''+k_2''\right)}{\left[\alpha\left(4\mu_1+k_1-4\mu_2+27\right)-\beta\left(4\mu_2+1\right)\right]\left[\alpha\left(4\mu_2+4k_2+4\mu_1+27\right)-\beta\left(4\mu_1+1\right)\right]}. \tag{9}$$

The calculation was carried out with each of the oscillations tuned to resonance, as determined by the relations

$$k_1-27\mu_1-4\mu_1^2+4\mu_1k_1-4=0,\ k_2+27\mu_2+4\mu_2^2+4\mu_2k_2+4=0. \tag{10}$$

The first equation has two roots, corresponding to oscillations of type 3, 1, 0 and 3, $\bar{1}$, 1. The results of the calculations for the pair 3, $\bar{1}$, 0 - 3, 1, 1 are shown in Figure 2. We see that the oscillation threshold has the same order as in the case of pumping with circular polarization, considered in [1].**

---

*These oscillations have different natural frequencies.

**The threshold values of the pumping field for the pair 3, 1, 1 - 3, 1, 1 have been calculated to be of the same order of magnitude.

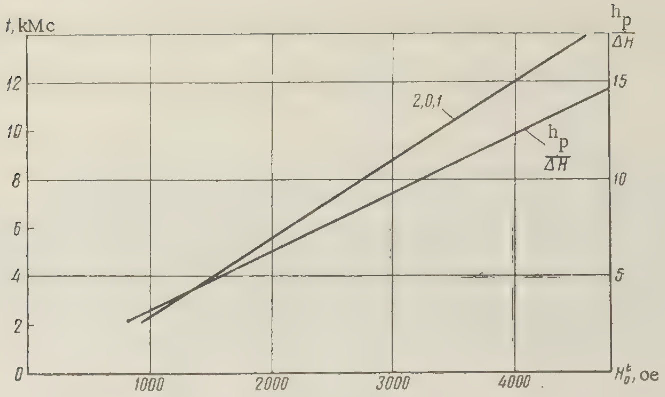

Figure 1

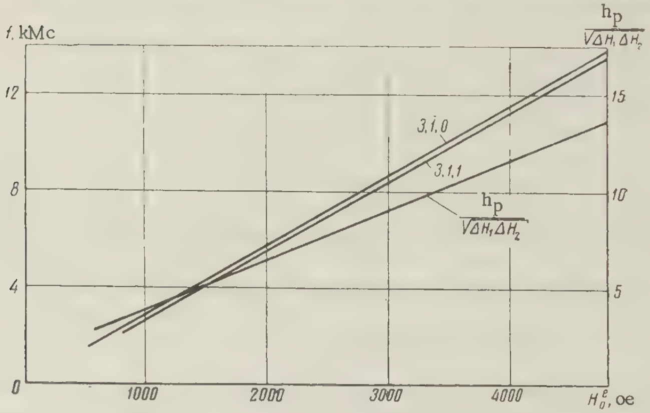

Figure 2

In conclusion we note that oscillation in ferrites was recently observed experimentally [3] also for oscillations 3, $\overline{1}$, 0 - 3, 1, 1 with a power on the order of 1 watt (the frequencies of these types were 4626 and 4570 Mc, respectively).

Calculation by means of the plot given in Figure 2 yields under these conditions $h_p = 5.5\Delta H$. For the experimentally used half-wave pumping resonator and a ferrite with $2\Delta H = 0.4$ oersted, this corresponds to about 0.6 watt, which is close to the experimental figure indicated above.

Analogous preliminary experiments, carried out by the authors, also confirm the possibility of amplification and generation of oscillations. Gain for the degenerate case (oscillation of type 2, 0, 1) on the order of 20 db, with a bandwidth of 20 Mc were observed with a single-crystal sphere 1.9 mm in diameter at a pulse pumping power of 20 watts. The oscillation threshold at half frequency, determined by formula (7) with a 3 oersted width for the curve of the investigated ferrite, amounts to approximately 50 watts.

REFERENCES

1. A.L. Mikaelyan, and A.A. Vasil'yev, Interaction Between Magnetostatic Oscillations in a Ferrite Specimen in Regeneration, Parts I - II, Radiotekhnika i elektronika, 1961, 6, 4, 5, 639, 789.
2. H. Suhl, Theory of ferromagnetic microwave amplifier, J. Appl. Phys., 1957, 28, 11, 1225.
3. R.T. Denton, A ferromagnetic amplifier using longitudinal pumping, Proc. I.R.E., 1960, 5, 937.

Submitted to editors 24 June 1960

A SPIN GENERATOR

V.G. Veselago

The spin generator is a self-oscillating system whose oscillating frequency is determined by the precession of nuclear or electronic spins in a magnetic field. Such a system can cause a frequency variation in accordance with a definite law, depending on the variation of the magnetic field, as first proposed by Schmelzer [1]. Considerable promise is afforded also by the use of a spin generator for the measurement and stabilization of a magnetic field in nuclear-magnetic-resonance installations of high resolution. It is essential here that the operating substance of the spin generator be stationary, since the oscillation frequency of a spin generator with moving specimen [2,3,4] depends on the rate of its flow and on the variation of the field at different points of the path of the working substance. A brief theory of a spin generator with stationary specimen is given in references [5, 6].

A block diagram of the spin generator which we have constructed is shown in Figure 1. The coil with specimen is placed in the field of a permanent magnet of intensity H = 5000 oersteds. The magnitude of the field can be varied slightly by using magnetizing coils. The proton precession frequency in the field H is about 20.3 Mc. The coil with the specimen comprises an arm of a double-T bridge. The output of the bridge is connected to its input through a resonant amplifier tuned to 20.3 Mc. The overall frequency characteristic of the entire channel, including the bridge with the specimen and the amplifier, is shown in Figure 2. The central narrow peak ± 100 cps in width corresponds to the unbalance in the bridge circuit, due to the nuclear magnetic resonance in the specimen, while the broad maxima on the edges are due to incomplete balance of the bridge over a broad range. For successful operation of the spin generator it is essential that the central peak be greater than the side maxima, or else the spin generator will operate on a sideband frequency which is not under control of the NMR signal. Since the T-bridge customarily used [7] has a very narrow bandwidth, we used the "idle tuned circuit" shown in Figure 3 [3]. The bridge is balanced by adjusting the trimming capacitors C_1 and C_2, which should be very precise in order to attain high stability. The attenuation of the bridge at the resonant frequency is ~80 db and is maintained for a time on the order of several hours.

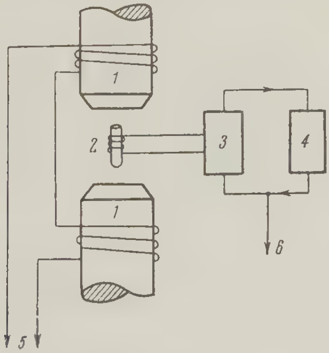

Figure 1

Block diagram of spin generator:

1 - magnet; 2 - coil with specimen; 3 - bridge circuit; 4 - amplifier; 5 - bias of magnetic field; 6 - output to wavemeter-heterodyne

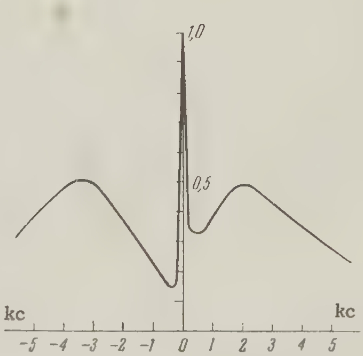

Figure 2

Frequency characteristic of spin generator.

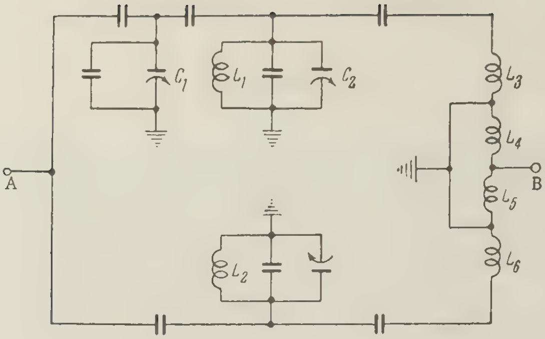

Figure 3

Bridge circuit.

A - input; B - output; C_1, C_2 - balance adjustment; L_1 - coil of "idle tank circuit," L_2 - coil with specimen; L_{3-6} - phase transformer.

The amplifier used in the spin generator was a revamped type KVM receiver, tuned to 20.3 Mc. The voltage at the "IF output" socket was fed to a special balanced mixer. The voltage from the heterodyne of the KVM receiver is also applied to the same mixer, and the result is a signal of the same frequency as at the receiver input, i.e., 20.3 Mc. The bandwidth of the receiver is ±3 kc, and the total gain necessary for operation of the spin generator is about 10^3. The oscillation frequency was measured with the aid of a wavementer-heterodyne, to which voltage was applied from the input of the bridge circuit.

To trigger the spin generator, the bridge circuit was tuned to maximum damping of the 20.3-Mc signal, with the field tuned away from resonance. The field was then set equal to the resonant value and the amplifier gain increased until oscillations set in. The oscillation amplitude was ~ 0.01 v. The signal/noise ratio was greater than 10. The oscillation frequency is proportional to the magnetic field and "follows" the field in a range ±500 cps. A change of 2 - 3 kc in the setting of the KVM receiver changes the oscillation frequency by merely 20 - 25 cps.

To increase the interval in which the spin-generator frequency follows the variation of the magnetic field, it is necessary to use a bridge with greater bandwidth, something that can be accomplished by equating the Q's of the working and the "idle" tank circuits.

In conclusion, the author expresses his great indebtedness to A.M. Prokhorov and K.V. Vladimirskiy for much advice and discussion; to Yu.V. Kosichkin, a student at the Moscow State University, for help in plotting the characteristics of the spin generator; and to M.S. Matyaev and L.V. Zav'yalov for aid in erection of the apparatus.

REFERENCES

1. O. Schmelzer, Lectures on the theory and design of an alternating-gradient proton synchrotron, Geneva, 1953.
2. F.I. Skripov, Dokl. AN SSSR, 1958, 121, 998.
3. H. Benoit, P. Grivet, L. Guibe, and M. Sauzade, J. phys. et radium. 1958, 19, 905.
4. M. Pettig, Optik aller Wellenlängen, Berlin, 1959, 68.
5. K.V. Vladimirskii, ZhETF, 1957, 33, 532.
6. S.S. Kurochkin, Radiotekhnika i elektronika, 1958, 3, 2, 198.
7. H.L. Anderson, Phys. Rev., 1949, 76, 1460.
8. G.E. Pake, J. Chem. Phys., 1948, 16, 327.

P.N. Lebedev Physics Institute
Academy of Sciences USSR

Submitted to editors 21 November 1960

CHRONICLE

THIRD ALL-UNION CONFERENCE ON ELECTRON MICROSCOPY

From the 24th to the 29th of October, 1960, the Commission on Electron Microscopy of the Academy of Sciences, USSR conjointly with the A. S. Popov Scientific Technical Society of Radio Engineering and Telecommunication convened the 3rd All-Union Conference on Electron Microscopy in the city of Leningrad. One hundred and sixty reports were delivered in the five sections, dealing with 1) electron optics and physical applications, 2) instrument design and general preparatory methods, and applications in the fields of 3) metallurgy, 4) chemistry and technology, and 5) biology and medicine.*

The conference was opened by the representative of the organizing committee, Academician A. A. Lebedev.

At the first plenary session a survey report "Contemporary Electron Microscopy," was made by Yu. M. Kushnir. As in the past, X-ray methods continue to occupy a leading position in electron microscopy. Along with a trend toward increased resolving power in the instruments may be observed a striving for greater and greater standardization (in heating and cooling systems, objective length, photographic processes, gas microchamber, etc.) Domestic and foreign microscopes of recent manufacture were enumerated.

Ever-increasing knowledge is being acquired in the fields of high- and low-voltage microscopy. High voltage permits the study of coarse objects and microdiffraction investigations of regions fractions of a micron in cross section (smaller regions cannot be studied by electron microscopes due to the effect of the magnetic field of the intermediate lens), and, finally, allows the obtaining of stereophotographs for investigation of the spatial structure of objects. The greatest results in the field of high-voltage microscopy have been achieved in the USSR. Low-voltage microscopy (5—15 kv) is promising because it heightens image contrast (the contrast is increased by, approximately, a factor of 10, but the resolution is cut in half). Possibilities of investigating living and wet objects were opened up by the work conducted in the USSR toward development of the gas chamber, in which objects may be studied under pressures close to atmospheric. Encouraging results were obtained in the application of brightness amplifiers in studies at low voltage

Along with the development of X-ray microscopes, both in the USSR and outside it, promising work is being conducted toward direct investigation of macroscopic objects (emission, reflection, mirror and scanning microscopes).

In his conclusion, the speaker remarked on the present state of development of several other electron-optical instruments: electronographs, energy spectrum analyzers, interference and phase microscopes, X-ray shadow microscopes, and microanalyzers. The entire report stressed the progress made of late in the design of such instruments in the USSR, but took note of a number of inadequacies, which can and should be eliminated, if there is to be further progress in electron microscopy in our country.

In the section on Electron Optics and Physical Applications of Electron Microscopy, a number of theoretical reports were heard. A great deal of interest was elicited by the communication of A.G. Vlasov and D. M. Krupp entitled "Field Calculations for Electronic Lenses," in which the Dirichlet problem was solved and a method of dividing the investigated region into cells was used, these cells being bounded by planes in an orthogonal coordinate system of a type that allows the Laplace equation to be integrated by separation of the variables.

In answer to the questions of A. M. Strashkevich and G. V. Der-Shvarts concerning the possibility of extensive use of computers and the generality of the method and approximations proposed by Vlasov, it was stated that complex problems may be solved approximately, that it is best to set up individual programming for each case, but standard programming may also be used.

---

* The present article is a digest of material given us by the leaders of all sections with the exception of the biology and medicine section.

In the discussion between A. G. Ulasov and G. V. Der-Shvarts, permissible assumptions in calculation, and the degree of accuracy of results were appraised.

The work of G. V. Der-Shvarts and V. P. Rachkov, "Calculations for Lenses Excited by Permanent Magnets" contained a method for calculating the field of magnetostatic lenses by the simplifying assumption of a uniform field intensity; using this calculation the optimal dimensions of a magnet are found to sufficient practical accuracy.

In the discussion that followed it was brought out that not in every case is such a simplification of the boundary conditions permissible (e. g., angles, edges, etc., were not considered).

P. P. Kas'yankov and K. P. Dutova presented the work entitled "The Problem of Aberration in Electron-Optical Systems." The work had intrinsic interest because it took up the general case of third-order aberration. A formula for the aberration factor was derived by the trajectory method, without assuming the presence of an object or an image in the field or in the field-free space.

G. G. Dritov and Yu. V. Vorob'yev took part in the discussion. The question arose: to what degree can Kas'yankov's formula yield the results appearing in Glaser's works? Kas'yankov asserted that Glaser's formula was obtainable as a special case of his own, but the coefficients were a bit different.

O. I. Seman pointed out that the report had been interesting in two of its aspects: 1) the linking of systems exploying beams not limited by diaphragms with those containing diaphragms, and 2) the application of the trajectory method to systems with magnetic immersion.

A. G. Vlasov noted that it is unwise to choose any beam inclined from the principal plane for calculation purposes.

A. N. Pilyankevich in his communication "Calculation of the Scattering Characteristics of Electrons in Free Atoms" presented a theory of the scattering of medium-energy electrons. This question is of interest in the appraisal of contrast in electron microscope images. The self-consistent Hartree-Fock wave function was utilized for calculations and spatial relations and asymmetry in the distribution of electrons in the atom were taken into account.

The calculations were made by assuming the presence of scattering in free atoms. The dependence of the scattering cross section on the aperture angle of the objective lens was discussed in the report. It appears that at large aperture angles the pertinent results of Lenz are not accurate.

In the ensuing discussion, A. Ya. Vyat-skin was interested in the effect of displacement of the parent atoms and molecules of the scattered electrons. Pilyankevich explained that he did not consider this effect, although it does indeed have value in matters concerning the resolving power of electron microscopes.

A. M. Strashkevich in a report, "Investigation of Hyper-Gaussian Trajectories in the Field of an Electrostatic Quadrupole Lens," derived equations for the trajectories of charged particles in the hyper-Gaussian region. He corrected an error made by Bernard and Hugh. It was shown that, in quadrupole lenses and many other fields, the trajectory of least deviation is that which is symmetrical with respect to the plane of symmetry of the field. In the Gaussian region this does not hold true.

In discussing the results of this work, P. P. Kas'yankov and O. I. Seman clarified certain details concerning the structure of the field along the axis of a rectangular coordinate system and defined the limits of the speaker's assumption that the dimensions of spherical electrodes are small in comparison to the distance between them.

G. G. Dutov in a report entitled "Electron Optics for Probe Systems" considered the problem of creating an electron beam of small dimensions, explained the role of aberration, in particular, spherical aberration in the secondary lens of a system and established the expediency of applying nonaxially symmetric devices in probe systems.

In the succeeding discussion in which G. V. Der-Shvarts, I. S. Sbitnikova, and others took part, were established: the magnitude of the limiting current (without considering space charge effects); the applicability of the formula of Liebman and Durando; the possibility of calculating spherical aberration of the terminal lens of a fine-beam system.

Theoretical investigations on electron optics were heard which reflected the intense efforts toward deeper knowledge of the nature of aberration with the aim of reducing and suppressing it, and the search for better and simpler focusing systems for modern X-ray, emission and scanning microscopes

A number of reports concerned with physical applications of electron microscopy were also heard.

Yu. M. Kushnir and A. N. Kabanov spoke of the application of an electron analyzer to studies of the energy spectrum of electrons reflected from metals. The 75v analyzer constructed previously by the authors has a sensitivity of 0.5v. Registration was made not only by a photographic method, but more thoroughly, by using an FEU and an EPV electronic potentiometer, which gave precise measurements of the intensity of lines in the electron energy spectrum. By varying the angles of incidence and reflection, they determined the ratio of elastically and inelastically reflected electrons. The temperature dependence of the characteristic losses in iron, titanium, aluminum alloys and other materials was studied.

In the discussion that followed (A. Ya. Vyat-skin and G. V. Spivak) the value of the work was noted, but also the desirability of improving conditions on the surface of the investigated objects; the materials had not been degassed and thoroughly cleaned. In particular, in the measurements on titanium the extraneous phenomenon of absorption of gas from the instrument might have been superimposed. The original authors of the report established that in the spectrum of α-Fe, there are two series of characteristic losses: one series is radically altered on change of the crystal structure, i.e., in the transition from $\alpha-\gamma$-Fe. The results are in good agreement with the theory of pair collisions. As for titanium, on change of its crystal structure and the resultant change of temperature of α- and β-Ti, the spectrum is also qualitatively changed.

A number of reports were connected with the application of electron microscopy to semiconductor physics: 1) structure and photoelectric properties of thin layers of lead sulfide (R. Ya. Bergala and M. I. Rudenok); 2) investigation of the mechanism of formation of lead sulfide layers (G. I. Distler, S. A. Daryusina); 3) electron microscopic and electronographic studies of Ge surfaces (P. Ya. Bergala, P. P. Konorov and M. I. Rudenok); 4) studies of the absorption of ions from water in the washing of Ge and Si (V. S. Sotnikov and F. B. Nikishova); 5) study of semiconductor whiskers (monocrystalline filaments) with the aid of an electron microscope (I. G. Sorotenko, G. V. Spivak, I. G. Stoyanova and G. M. Osad'ko); 6) application of an electron mirror to the investigation of electrical inhomogeneities on semiconductor surfaces (D. V. Kormilitsyn and P. K. Oshchenkov).

In the first report R. Ya. Bergala stated that needle-shaped formations distributed parallel to the molecular beam may be observed with an electron microscope. He explained the great significance of profiles, which give more valuable information than prints.

In the subsequent discussion V. N. Vertsner did not agree with the author's assertion concerning needles on the surfaces. The most acceptable surface process should be dendrite formation.

The author of the second theme said the lead sulfide layers were obtained by chemical means. Electron microscopy permitted following the development of the layer from a nucleus. The observations of the author concerning the essential role of the sublayer (crystalline or amorphous) were interesting.

In the third work, presented by P. P. Konorov, the connection between the velocity of surface recombination and the nature of the surface etching was established. In answer to a question, the researcher noted that the surface was polished with abrasive particles, 100μ in diameter, and this certainly led to the presence of coarse nonuniformities in the germanium surfaces.

The fourth communication in this cycle was given by F. B. Nikishova, in which she noted the presence of copper, silver and gold impurities from previous technological treatment and cleaning of the semiconductors.

The fifth report was made by I. G. Sirotenko, who spoke of investigations, in a gas chamber developed by I. G. Stoyanova, of the structure of monocrystalline filaments of tungstic and molybdic oxide, prepared by ignition in air. The studies were made in an autoelectronic emission projector under a high vacuum.

I. L. Sokol'skaya, Yu. M. Polukatov and D. V. Ignatov wanted to know about the individual emission pictures of the whiskers and the effect of temperature on the evaporation and dimensions of the monocrystals.

The final communication in this series was given by D. V. Kormilitsyn. Photographs were used to illustrate the application of electron mirrors to the observation of p-n junctions in Ge and Si; p-n junctions were observed as fine bands (magnification 100 ×) at the cleavage boundaries.

The author was deluged with questions concerning the construction of the instrument, its supply line, methods of preparing the objects of investigation and possibilities of observing structural details of the p-n junction.

In the discussion period G. V. Spivak remarked on the importance of this work for the study of the nature of p-n junctions, the necessity of improving the construction of the mirror and increasing the light power of the instrument and the usefulness of further studies in this direction as a promising method for investigating microfield structures.

Three other reports were devoted to investigations in electrical and magnetic microfields. The first one — "Electron-Optical Measurements of Electrical and Magnetic Microfields on Surfaces" — was presented by N. N. Sedov, G. V. Spivak and N. F. Isayeva. A quantitative relationship was established between the brightness of a picture obtained from secondary or photo emission and the local field at the emitter. The image on the screen of an electron microscope was objectively recorded by a photomultiplier or even a Faraday cell. The method permits the field distribution over the surface of a solid to be measured and studied.

In the communication of A. B. Druzhinin and B. N. Popov, "Determination of the Work Function of Microregions of Thermionic Cathodes," measurements of current in the image plane of pressed and L-cathodes in a high-vacuum emission microscope ($p \simeq 5 \cdot 10^{-7}$ mm Hg), constructed by the authors, were reported. From these measurements, the local work functions were calculated by Richardson's formula.

G. V. Spivak noted that image contrast, even in the given strong electric field, is a function of the tangential components ("field spots") and this leads to errors in determining the work function.

The author of the report agreed with this, stating that measurements made at the center are more reliable than those at the edges.

In the report of L. V. Lazareva and G. V. Spivak, "Electron Microscopic Observation of Microfields Using Photographic Prints," was indicated the possibility of observing magnetic inhomogeneities with the aid of replicas. The possibility may be realized because magnetic nonuniformities and surface deformations are closely interrelated. A correspondence was found between powder patterns and electron-microscope pictures.

Yu. A. Skakov called attention to the system of bands in the electron-microscope photographs and their connection with the direction in which the material had been rolled (worked), while N. N. Buinov noted the desirability of making observations in the presence of an applied magnetic field.

V. E. Yurasova, A. A. Predvoditelev and N. A. Tyapunina told of the application of ion bombardment for revealing dislocations in cadmium crystals. In this report, delivered by Tyapunina, the substantial advantages of this method over others were given.

Yu. A. Skakov, N. N. Buinov, Polyakov and others were interested in the temperature control of the sample, the shape of the ionic etch patterns, and the character of the spiral entities among the surface patterns formed.

The communication of V. G. Bravinskiy, V. P. Ivanov and A. M. Reshetnikov was concerned with the application of electron microscopy to the investigation of fractures in ceramics. The samples were submitted to bending tests. Their surfaces were studied with lacquer replicas, tinted with chrome.

K. N. Namitokov investigated metallic powders with the electron microscope. The powders had been obtained by several methods, including electrical corrosion.

V. B. Ostroumov felt studies of fine iron carbonyl would be desirable; N. N. Buinov thought the temperature gradient and other experimental particulars might be better controlled.

In the section, Instrument Design and General Preparatory Methods, and subsection, X-Ray Microscopes, a number of reports were heard.

In the report, "Optics of Electron Microscopes EM-5 and EM-7," V. N. Vertsner, Yu. V. Vorob'yev, G. A. Bogdanovskiy, Yu. M. Voron and Yu. V. Chentsov described the construction of these two instruments. They feature: a) a condenser that reduces the region irradiated by the electrons to 6—10 microns; b) an unregulated stigmator in the condenser and intermediate lenses, and an electromagnetic stigmator with a rotating field in the objective and movable pole shoes in the intermediate lens; d) alignment in which a 50 cycle alternating voltage is applied to the accelerating voltage. The resolving power is 12—15 Å.

In answer to the questions of G. V. Der-Shvarts, A. G. Vlasov, P. P. Kas'yankov and V. N. Vertsner, Yu. M. Vorona stated that the basic difference between the EM-5 and EM-7 lies in the power supply. The EM-7 uses a high-frequency circuit and the accelerating voltage is increased to 80 kv.

Achromatic lenses in multilens magnetic electron microscopes were considered by

P. A. Stoyanov. To suppress chromatic aberration in the field, a double intermediate lens is used. The objective and projecting lenses are achromatized by the usual method.

Answering the questions of G. V. Der-Shvarts, A. G. Vlasov, P. P. Kas'yankova and V. N. Vertsner, the author declared that there was no distortion. The presence of two intermediate lenses gives no trouble in focusing. The total aberration may be taken equal to the arithmetic sum of all the aberrations. Chromatic aberration of rotation is compensated for by opposing coils in the two intermediate lenses.

Yu. V. Vorob'yev remarked that field chromatic aberration, which can be corrected by achromatization in microscopes of high resolution, is negligibly small in comparison to axial chromatic aberration. The appraisal of the field chromatic aberration of the intermediate lens (0.5 Å) given by the author for a microscope with 5 Å resolution was in error by at least an order of magnitude. In the opinion of Vorob'yev, introduction of the two intermediate lenses was unjustified.

In the communication entitled "The Photoelectronic Microscope EM-6," V. N. Vertsner, V. A. Nikiforov, G. A. Bogdanovskiy, V. V, Kozelkin and Yu. V. Shchetnev described the structural details of this instrument. The machine is a combination of an electromagnetic objective, and a monocrystalline screen of high resolution with a photomicroscope. Photography is performed at magnifications of 3,000, 5,000, and 10,000 × and exposures of 3 to 20 sec with the aid of an attachment employing a "Zenit C" photochamber. The resolving power is better than 100 Å.

Responding to questions from Yu. M. Kushnir, I. G. Stoyanova, A. M. Strashkevich, P. A. Stoyanov, and A. I. Makarova, researcher Shchetnev added that the instrument could be made portable if desired. Essentially, the current density at the objective is at least 2 to 3 orders lower than that in the usual electron microscope. The small loss of sharpness observed at the periphery of photomicrographs is due to quality defects in the optical objective lens. The vacuum is created by a diffusion pump with air cooling. Advantages of the EM-6 are simplicity of construction and ease in handling. A. N. Kabanov noted that it might be possible to further simplify and decrease the dimensions of the instrument. A. E. Protsenko felt that the microscope should be of great interest to biologists.

In the report "Study of Magnetic Circuits for Electron Microscope Lenses," P. A. Stoyanov and L. Yu. Vol'fson made a comparison of the leakage fields of lenses with various magnetic circuits. It was noted that permalloy circuits sharply reduce the leakage field.

A. G. Vlasov noted that it was not clear from the diagrams presented that the angles of the magnetic circuit are of importance. This is a defect in the method. G. G. Der-Shvarts said the work was very important since the quality of images is essentially determined by the stray field.

Yu. V. Vorob'yev presented the report "Analysis of Aberration Due to Faulty Installation and Adjustment of Electron Microscopes." Errors in setting up the objective lens leads to axial astigmatism and other aberrations. A compensator for suppressing aberration was proposed. Methods of adjusting the microscope were compared and it was indicated that, to ensure high resolution, the distance between the voltage and magnetic centers should not exceed 3 to 4 microns.

Answering the questions of G. V. Der-Shvarts and P. A. Stoyanov, the researcher said that the stray field is the source of the divergence of the two centers. The permissible variations in alignment depend on the operating regime. Sometimes there are no criteria for controlling the calculated aberration. Pole shoe astimatic control is insufficient for realizing the limiting resolution. New control means must be found.

P. A. Stoyanov remarked that the work was highly significant and that creation of pole shoes with a small astigmatic difference in the focal length would ensure high resolution. V. N. Vertsner interjected that at the present time there has been no noticeable advance in raising the limiting resolution of instruments. The condition is similar to the situation with astigmatism in his own time before the invention of the stigmator. There are several uncorrected aberrations, and until methods of compensation and control are created, there can be no significant advance.

The work "Alignment of Electron Microscopes by Means of Electromagnetic Fields" was reported by P. A. Stoyanov. Electromagnetic systems for aligning the instruments by deflection of the electron beam (equivalent in effect to two prisms) were considered.

G. V. Der-Shvarts remarked that, in his experience, such systems are very difficult to adjust. V. N. Vertsner recalled that electromagnetic alignment has already been used for a number of years in the electron microscopes EM-5 and EM-7. However, it is necessary to consider that since the stray field is a nonlinear function of the excitation, any transition to a different accelerating voltage upsets the alignment.

S. V. Bezlepkin, Yu. M. Kushnir, G. V. Der-Shvarts, P. V. Zaytsev and L. B. Rozenfel'd reported on the modernization of the UEM-100 microscope. An intermediate lens has been developed which is placed in the objective tube. There is a "cat's eye" type selector diaphragm. The instrument is adaptable to observation or microdiffraction.

P. A. Stoyanov and N. M. Grishina gave a report "Elimination of Astigmatism in the Intermediate Lens in Microdiffraction Work by Means of a Stigmator." For improving the quality of microdiffraction pictures from the UEMB-100 microscope, an electromagnetic stigmator, composed of two pairs of coils, is inserted in the intermediate lens. No distortion of the electronogram scale was observed.

At the meeting of the instrument design section devoted to electron microscopes of various types and other instruments for studying microstructure, the following communications were heard.

G. V. Spivak, I. A. Pryamkova, D. V. Fetisov, A. N. Kabanov, L. V. Lazareva and A. I. Shilina presented a work entitled "Mirror Electron Microscopes for Studying Surface Structure of Solids." Data on all-metal models of mirror electron microscopes were presented with the most recent structural developments of these devices for observing the microgeometry of electrical and magnetic microfields on the surfaces of solids. A feature of the instrument is its high sensitivity and the possibility of detailed investigation of surface microstructures permitted by the fact that the electrons, for the most part, linger near the surface under investigation, are strongly modified by the surface fields, and depart, bearing information on the microstructures. The report was illustrated by pictures of the domain structures of cobalt, ferrites and ferroelectrics and surfaces of Ge and Cu single crystals, etched by ion bombardment. The mirror microscope has an illumination system with a condenser, photochamber, intermediate lens, electronic mirror, and an alignment mechanism; the sample may be moved in three dimensions; it may be heated, its temperature measured or a magnetic field may be superimposed. The light-gathering power of the instrument is enhanced by a magnetic field in the region of the object.

In answer to questions, posed by Z. Ya. Berestneva and G. V. Der-Shvarts, G. V. Spivak informed the gathering that the sample may be of any form; surfaces are preliminarily cleaned by mild ionic bombardment, which is done outside the instrument.

Speaking on the report, V. N. Vertsner observed the great promise of the work. New possibilities are emerging with the development of such instruments. With this method, it is now possible to directly observe and evaluate the magnitude of microfields, whereas other methods only permit evaluation from indirect observations.

On the theme "Certain Topics in Reflection Electron Microscopy," Yu. M. Kushnir, C. Z. Bezlepkin, G. V. Der-Shvarts, I. V. Zaytsev, Yu. V. Kulikov, L. B. Rozenfel'd, L. A. Titov and I. S. Trutneva presented a report concerning a developed instrument in which the sample is inclined at an angle of 20—30° to the microscope axis. The electron beam ensures a high electron density over the object. The image may be observed on a brightness amplifier screen. The permissible tolerances in accuracy of preparing the lenses and aligning them were calculated. In answering the questions of Z. Ya. Berestneva, G. V. Spivak, G. G. Dutova, A. V. Smirnova and B. A. Ostroumov, G. V. Der-Shvarts informed them that to protect certain samples, the voltage must be lowered. In the future the temperature of objects will be measured automatically; at present this is done pyrometrically. The beam aperture is on the order of $5 \cdot 10^{-3}$ radians; the electronic brightness was not determined. The diameter of the crossover is 14 microns. The scale ratio in two directions is equal to 3. Irradiation at wide angles from the instrument axis gives pictures of poor quality.

A. M. Solov'yev and V. N. Vertsner spoke of certain problems encountered in the development of X-ray microanalyzers. Depending on operating conditions of the microanalyzer, the secondary lens should have a long focal length and a specified coefficient of spherical aberration. For obtaining maximum current density in a spot of given diameter, the electron optical system should operate with a reduction $M = d_{source}/d_{probe}$. Three adjustment mechanisms are necessary and sufficient: a shifting of the Venel't cylinder relative to the anode; an inclination of the beam between lenses, and mobility of the diaphragm of the secondary lens.

Answering the questions of G. V. Der-Shvarts and I. S. Sbitnikova, the researcher A. M. Solov'yev reported that the diameter of the source was taken equal to the "half-width" of the crossover for calculation purposes. To compensate for spherical aberration, a nonaxially symmetric optical system was designed and installed.

A report on the theme "Certain Problems of Scanning Microscopes with X-Ray Microanalyzers" was presented by Yu. M. Kushnir, D. V. Fetisov, K. K. Raspletin, B. I. Pochtarev, F. U. Spektor and A. N. Kabanov. The optical system of the instrument developed by them consists of two reducing electrostatic lenses and is equipped with a stigmator. A probe measuring a few tenths of a micron was made. The receiver is a secondary electron multiplier, the GOI(VEU). The assembled machine was tested as a scanning microscope. The X-ray microanalyzer is located outside the machine.

In answering the questions of M. I. Isypin, B. N. Malyshev, G. V. Saparin, G. V. Spivak and N. N. Buynov, researcher Kushnir gave the additional information that the limits of the analyzing element are identical with those of a static probe. Due to the scattering of electrons in the sample, use of a probe less than 0.5 micron would be unreasonable. Although only electron-beam images were obtained, in the future X-ray images will be attempted. At present nothing is known concerning the nature of the contrast formed at p-n junctions which was observed during the experiments.

The communication "Objective Method of Registering Energy Spectra with an Electrostatic Analyzer" was presented by A. N. Kabanov, Yu. M. Kushnir, D. V. Fetisov and M. P. Moiseyeva. Up to accelerations of 75 kv, constant resolution is maintained by smooth control of the potential of the analyzing lens, which further ensures invariance in the trajectory of electrons with different energies. In this way there is no intensity distortion in the electron distribution.

The receiver may be an FEU or a VEU. Characteristic losses were examined for a host of objects under conditions of transmission and reflection.

In answering questions from P. D. Tokarev and A. Ya. Vyat-skin, Kabanov informed them that the current passing through the second aperture was about 10^{-9} amperes. Tokarev suggested that a modulator could be inserted behind the second aperture to give a few cycles of alternation to the recording beam current. In that way an AC amplifier could be used and currents of 10^{-12} to 10^{-14} amperes could be measured with high stability and sufficient accuracy.

A report on a magnetic objective attachment for electron emission microscopes was made by A. M. Rozenfel'd and P. V. Zaytsev. With their magnetic objective, due to the absence of screening by a Venel't cylinder, it should be possible to increase the resolving power of the EEM-7 emission microscope. Structural details of the objective and photomicrographs obtained with it were demonstrated.

To the questions of V. V. Polivanov and G. V. Spivak, Rozenfel'd replied that the magnitude of the power supply instability at 100 Å was not determined. It was probably the same as that for ordinary microscopes. Unfortunately, if there was also great distortion at the objective, some of the magnetic field was lost.

In his report "Analysis of X-Ray Microscope Manufacture and Employment," Kh. I. Mamadzhanov reproduced the familiar literature data on the contrast and resolving power of X-ray microscopes with diverse systems.

The third meeting of the instrument design section dealt with experimental methods, apparatus for preparing the material, and photographic supplies.

I. S. Renskiy and P. A. Stoyanov told of studies made with certain types of photographic plates used in electron microscope work. They gave the results of nuclear research with electronographic and photographic plates.

Answering the questions of Yu. S. Chentsov and N. G. Sushkin, Renskiy said he and his colleague had little data on the contrast and resolving power of the electronographic plates; the resolving power of the nuclear plates was 40 tracks per mm.

I. A. Fomina spoke of the latest developments in photographic materials for electron microscopes. Sensitometer investigations of fine-grained nuclear plates of type MK and MR, in the entire range of intensities used, gave no deviation from the rule of interchangeability. The plates have high sensitivity and contrast, plus excellent resolution. She presented some formulas for developers.

The questions of Z. Ya. Berestneva, B. S. Kolchev, S. B. Stefanov, I. S. Mel'nikova and A. K. Pakidin brought out that MR plates are more sensitive than MK, and have high resolving power. They are good for six months.

A great deal of interest was created by the report of I. G. Stoyanova, entitled "The Physicotechnical Fundamentals of the Gas Microchamber Method in Electron Microscopy." The chamber, installed in the UEMB-100 instrument, allows preparations found in gaseous media to be investigated. If the radiation time can be made small enough, the vital functions of microorganisms may be preserved. The kinetics of reactions between solid and gas phases can be followed, using this chamber. During the discussion period, V. M. Kushnarev observed that the photomicrographs of bacterial cells presented had very poor definition. The sequence of changes occurring in the organism, denoted by the author of the report, were debatable. But, as A. D. Gil'man pointed out, the remarks of Kushnarev in no way lessens the importance of the chamber for biologists and others. G. O. Bagdykyants agreed that the chamber is a valuable addition to microscopy. It will be especially useful in research on the kinetics of chemical reactions, requiring only some very simple manipulator for bringing the components into contact. Recording could be made with a kinematograph. Yu. M. Kushnir pointed out that development of the gas chamber is the first step toward the study of living objects in the electron microscope. I. G. Stoyanova has made great steps forward in the development of the original chamber.

V. N. Vertsner was the last to speak on the paper. He admitted that the gas chamber is an interesting new development. However, even allowing that at present it may be applied to chemical materials, in the field of biology, the basic problem is still unsolved, i. e., how to lower the X-ray dose, which kills microorganisms even on brief exposure. In this connection, a television method of observing images might be employed — a television electron microscope. Using it, the current density around an object could be reduced by 3 or 4 orders of magnitude.

The report, "Concerning the UMD-4 Ultramicrotome" was made by A. M. Rubinshteyn and M. I. Dashevskiy. The UMD-4 microtome, working on magnetostriction principles, is capable of making cuts 50 to 500 angstroms thick at a rate of 15 to 60 per min; micron cuts can also be made. The area of the section may be as much as 4 mm^2. The microtome uses a thermal feed. In reverse motion, the object is deflected 4 microns from the knife, due to magnetostriction. The slicing speed is variable from 18 to 60 cm/min.

Answering V. M. Kushnarev and A. M. Reshetnikov, researcher Rubinshteyn said that the slicing speed is selected following data on the earlier microtome of M. I. Dashevskiy. Fairly hard objects, such as catalysts and soft minerals were required. Kushnarev pointed out that, to obtain sections of biological material, a higher slicing speed would be necessary. A Swedish microtome has a slicing speed of 50 mm/sec.

Ya. Yu. Komissarchik and V. F. Mashanskiy spoke on experience in operation of the mass— produced Soviet ultramicrotome, the UMT-2. Six months of work with the UMT-2. and a variety of histological objects showed that reliable production of a series of identical, undeformed sections, 100Å thick with an area from 1 to 1.5 mm^2, can be obtained. Photomicrographs showed fine definition. Certain faults were noted: the arrangement of the motor and the binocular microscope is unfortunate; there are too few object holders; there is no way to smoothly vary the cutting speed.

In answer to a question from M. I. Dashevskiy, researcher Komissarchik replied that the cutting speeds are 25 and 50 mm/sec, and that the sections are not wrinkled, if the knife is set properly.

S. V. Stefanov noted that the UMD-4 microtome holds a number of advantages over the UMT-2: there is no motor or drive mechanism, and the slicing speed can be altered in a continuous fashion.

Those in attendance showed great interest in the report, "Device for Etching the Surfaces of Metals, Dielectrics and Semiconductors by Ionic Bombardment (the UIT-3)," presented by G. V. Spivak, F. F. Kushnir, and V. E. Yurasova. A new model was described. The possibilities of the device were illustrated by photomicrographs revealing grain structure, the symmetry of crystal planes, slide figures, details of grain structure, dislocations, and so on. Structural investigations may be made on samples heated to 1200°C and under the influence of mechanical forces such as compression or tension. Observation of the etching process is made with a long-focus optical microscope; photographs are made without removing the sample from the vacuum. For electron-microscope studies, the sample, while in the vacuum, can be directly coated with a carbon, quartz, or other type of film, thus producing a replica. Ionic bombardment has several advantages over other etching methods.

Answering a flood of questions, V. E. Yurasova added that the etch time varied within wide limits and on it depended the depth of etching. The degree of etching was also a linear function of the current density. The samples can have any shape or thickness. Investigations of mechanically deformed objects are still only tentative. The etching was done in neon and argon, which were not previously purified. There was no local heating of the samples.

D. V. Ignatov remarked that oxides may be formed during ionic etching and decompose the basic material of the object. Therefore, the composition must be controlled electronographically. Later, I. P. Sokolskiy declared that the proposed method could be of great use to metallography, especially in conjunction with deformation of the sample. But it must be carefully worked out to avoid the creation of oxidation products.

K. P. Bondarenko, B. N. Grechushnikov, G. I. Distler, V. S. Chudakov and G. D. Shnyrev described a universal vacuum vaporizer. The device provides for vacuum evaporation and cathode dispersion. Objects placed in it can be cooled to —170°C and heated to 500°C. During evaporation the placement angle of the sample relative to the vaporizer can be changed, and the sample may be set to rotate at a given speed. The vacuum achievable without freezing is $2 \cdot 10^{-5}$ mm Hg, and with freezing, it is $5 \cdot 10^{-6}$ mm Hg.

Answering questions, researcher Shnyrev stated that the device could also be used to evaporate difficultly fusible metal powders.

L. B. Rozenfel'd and A. I. Makarov presented a paper entitled "Ion-Optical Method for Preparing Diaphragms of Small Aperture." With the aid of the ion gun developed by them, which gives a beam 2 to 3 microns across, it is possible to obtain apertures of truly circular form, having diameters of from 2 to 100 microns, in metals, dielectrics, and semiconductors.

In answer to questions asked by A. A. Petrova, Yu. M. Vorony and Yu. S. Veselyanskiy, Rozenfel'd reported the amount of deviation from circular form depended on the basic structure of the metal. In an aperture of 50 microns, the ellipticity is insignificant. Good diaphragms were not obtainable from molybdenum plate. To all appearances, ionic etching can be used to clean diaphragms with apertures.

The following communications were presented in the section on instrument manufacture on the subjects of supply sources for electron microscopes and development of structural details.

"Supply Source for Electron Lenses with High Resolution," V. V. Polivanov, V. V. Il'in and R. V. Pogudina. In the developed feed, the current instability through the objective lens does not exceed 0.0004%. Smoothness and accuracy of regulation of the current (within 0.0008%) is secured within wide limits.

P. A. Stoyanov noted that the authors have created a circuit of high stability. Furthermore, the design of their control system is such that a series of photographs in the immediate neighborhood of the focus may be made by given variations of the current. This possibility increases the quantity of usable photographs.

A. V. Iz'yurov described a high-voltage supply for electron microscopes of high resolution. It involves the insertion in cascade of a high-frequency rectifier allowing a total instability, including pulsations, of 0.0005%. The instability is measured continuously by a circuit of 0.0001% sensitivity. This source gives a resolving power of 5 Å.

Discussing this, V. V. Polivanov stated that, in the accepted method for calculating instability, only the peak voltage at the time of the determination is used, ignoring its duration. This leads to an unjustifiably large value for the instability.

V. N. Vertsner pointed out the need for a rational approach to this determination through the use of statistical weights for observed peaks, that is to say, by making allowance for their number and duration.

In a communication delivered by D. V. Fetisov and A. N. Kabanov, "Small-Scale Armoring of High Voltage Leads," an armored construction made and tested by the authors was presented.

P. A. Stoyanov and V. V, Kozelkin noted that a porcelain—organic glass seal in a high-voltage lead will not contain the voltage, and testing of the proposed lead even with doubled dimensions showed their unsuitability of these materials at 60—70 v.

There followed a report, "Vacuum Switches" by D. V. Fetisov, B. I. Pochtarev and A. N. Kabanov, concerning the structural design of semiautomatic vacuum switches found in many electronoptical devices.

As was noted by V. N. Vertsner, D. V. Fetisov is a pioneer among us in the development and application of vacuum tube switches, not employing sylphons. The work of his entire group in this direction has been extremely fruitful.

Below we give a brief survey from "The Applications of Electron Microscopy to Chemistry." Most of the chemistry papers heard in this section were devoted to studies of polymer and silicate materials.

K. A. Begnovskaya, L. G. Senatorskaya, B. Z. Berman and B. A. Dogadkin made an electron microscopic investigation of latex mixtures.

Z. Ya. Birestneva, M. B. Konstantinopol'skaya and V. A. Kargin conducted an investigation of fibrous inorganic substances, using fibrous aluminum hydroxide as an example. Comparing electron microscopic and electronographic data, the authors detected differences in the structure of the preparation, according to which method was chosen for structure determination.

L. N. Rashkovich and V. P. Varganov studied the crystallization of certain hydrosilicates of calcium under hydrothermal treatment. The authors established the factors that determine the time required for conversion of the hydrosilicates and showed that these conversions proceed only by means of the solution of one and crystallization of another phase. The electron microscope allowed the course of the process of change of form in the crystals to be followed.

Z. M. Larionova completed an investigation on the hydration of various binders, including sulfate, quick—setting and torsion cements. Here the electron microscope makes possible the observation of kinetic processes, such as the formation of calcium aluminum hydrosulfate in certain cements in the early stages, when the newly formed crystals are practically invisible in an optical microscope. There is every reason to believe that the results obtained will give builders more confidence in applying specified binders in the production of steel and concrete details.

A positive feature of the last two works is their complexity: besides the electron microscope, the authors used a variety of other physical and chemical methods, all of which gave depth and richness to the information collected concerning the systems under investigation. To a lesser degree, this complexity was present in a study of the structure of glass (V. I. Shelyubskiy and N. M. Vaysfel'd), although, indeed, here the electron microscope recommended itself as an extremely effective tool for the development of glass—crystal materials with specified properties. Finally, the carefully performed, definitely interesting, electron—microscopic investigations of soils (N. I. Gorbunov and B. P. Gradusov) and argillaceous materials (D. D. Kotel'nikov) still lost something of their value by the omission of other methods in the research.

Among other works might be mentioned the well—conducted study of the secondary structure of iron carbonyl (A. A. Petrova, et al.), in which the authors established a connection between the structure of the preparations and the technological conditions under which they are obtained. M. L. Petrova made a detailed electron—microscopic and electronographic investigation of pyrolitic carbon films, and as a result she succeeded in establishing a relationship between the film structure and the conditions of their formation; she proposed new theories for the mechanism of pyrolitic carbon formation.

The new methods presented at the Conference were extremely interesting.

V. I. Kasatochkin, V. M. Luk'yanovich, N. M. Popov and K. V. Chmutov used an electron microscope—electronograph with an accelerating voltage of 400 kv to make microdiffraction studies on the structure of carbon—black particles. The authors were able to obtain electronograms of regions no more than 0.06 micron wide, whereas the microdiffraction selectivity of the ordinary microscope of 100 kv accelerating voltage is about 1 micron. There is no doubt that high-voltage microdiffraction is an extremely effective method for investigating the mosaic structure of materials.

The new possibilities offered by X-ray microscopes were exemplarily demonstrated by G. O. Bagdykyants and M. A. Tsepova in their study of a number of fillers in organic media.

The conference showed that electron microscopy in chemical investigation is a very important tool, affording information concerning the dimensions, form, and character of aggregations of particles in colloidal dispersion. As distinct from a number of indirect methods, at the present time it is only electron microscopy that permits the direct and reliable obtaining of the above-mentioned information, information that is prerequisite for the solution of many theoretical and applied problems. The raised methodological level of work conducted in recent times should be noted. In addition to studies of powder samples, which require very simple preparation, the Conference was the recipient of no small number of works devoted to the qualitative examination of the surfaces of solids by means of the replica method (carbon and quartz). Microtome methods are beginning to find more frequent use in chemical investigations.

Below we give a brief description of material presented in the section on the applications of electron microscopy to metallography.

In the reports of S. T. Kishkin, N. S. Gorchikova, E. V. Polyak, I. S. Mel'nikova, A. V. Smirnova, M. I. Vinograd, G. A. Kokorin and G. L. Gromova, data were presented which evidenced successful application of electron microscopy to the investigation and treatment of heat-resistant alloys. The method permits qualitative indexes to be established, characterizing the structural composition of metals submitted to various thermal treatments and high-temperature deformations.

Differentiation of particles with various carbide and intermetallic contents was made possible by applications of electrolytic phase separation, hardening methods and ultrasonic segregation of alloy precipitates. The study of intermetallic inclusions in certain cast alloys established the causes of lowered plasticity in individual cases, on the basis of structure and method of production.

L. M. Utevskiy and M. P. Usikova made investigations of their films of stainless steel on the UEMB-100 electron microscope. They revealed the distribution of dislocations after various deformations and after annealing.

In another report, L. G. Utterskiy applied the thin—foil method to the study of dislocations in iron.

Yu. A. Skakov and Tyan Shu-Sen reported an investigation of the mosaic structure and distribution of dislocations in aluminum by the thin-foil method, and in oxide impressions by the X-ray method. It was stated that X-ray findings on the magnitude and disorientation of the blocks is connected with the distribution of dislocations in the interior of the fragments.

A study of changes in the fine structure of aluminum and its alloys after deformation and annealing was reported by R. M. Lerinman, V. I. Dobatkin and S. I. Seletskaya. The authors used the etch figures in the oxide prints to judge the composition of the materials. It was found that the first recrystallized regions are formed at the boundaries of distorted blocks.

M. F. Longinov and V. A. Zverev told of a method developed by them for thinning metal plates for direct study of structures with the X-ray microscope.

A series of communications by L. G. Orlov and L. M. Utevskiy, V. R. Golik and Yu. S. Veselyanskiy, and Yu. I. Demkin, were devoted to electron-microscopic investigations of the surface geometry of steel fractures. The material presented confirmed the usefulness of electron microscopy in fractography, and permitted establishing the fine structure of ductile and brittle metal fractures and the connection between dislocations and rupture processes.

E. S. Kosyakina and V. S. Ivanova reported on structural changes as a result of fatigue testing of steels 10 and E Ya—IT.

A number of reports dealt with phase identification in different systems. Among those carried out with electronographic analysis were: Investigation of Thin Fe—C Films (L. S. Palatnik, G. V. Fedotov, and A. G. Ravlik); Study of the Transition Layer between Tin Metal and Electrolytic Tin Precipitates (G. A. Kokorin and N. I. Vitkin); Electronographic Investigation of Carbide Formation in Steels (S. S. D'yachenko); Study of Phase Separation on Aging Technical Steel (Yu. A. Skakov and S. K. Maksimov).

In the report of V. V. Polotnyuk, L. A. Nikolayeva and E. I. Rabinovich, interesting results from the electron microscopic investigation of the structure of low-carbon steel after deformation and age hardening were presented. Unfortunately the authors were unable to obtain an electronographic analysis for identification of the separated phases.

A communication on an electron-microscopic investigation of low-carbon steel after aging and tempering was given by P. G. Serdyuk.

In the work of S. S. D'yachenko and R. S. Kaplan, electron microscopy was used in conjunction with a number of other methods (X-ray analysis of fine matrix structure, chemical and structural analysis of carbide inclusions) for revealing the source of differences in the endurance of cast and forged chrome-molybdenum-vanadium steels.

In reports by M. A. Kotkis including a large number of investigations of special steels, cermets, fatigue fractures and phosphate coatings, electron microscopy was shown to be expedient for the successful solution of many technological problems. Thus, the cause of different workability of gears, and the parameters of the phosphate process were defined. G. V. Kvyatkovskaya presented interesting data on the structure of construction steel, prepared by different pickling methods.

The reports of O. N. Repkova, V. N. Boloslovskiy and O. K. Shabalina were devoted to electron—microscopic investigations of details in ferrite powders and iron oxides. D. I. Layner, M. A. Tsypin and A. S. Bay investigated the structure of slags in titanium by the cross-sectional cut method.

A number of reports were concerned with methodology: Method for Obtaining Replicas from a Given Section (P. V. Churayev); Electron Microscopic Investigation of the Principal Orientation of Polycrystalline Metals (D. I. Layner, E. I. Krupnikova, and A. S. Bay); Structure of Electrolytically Finished Surfaces (G. S. Vozdvizhenskiy, G. P. Dozider'yev, and

G. A. Gorbachuk); Nature of Etched Sections in Carbon Steels (V. V. Polotnyuk and L. A. Nikolayeva). The interesting properties of carbon and quartz impressions from polished surfaces were noted: often the impressions do not reveal the sample structure (L. V. Lazareva, T. V. Filipova); X-ray microscopy (B. M. Rovinskiy and V. G. Lyutsan).

The review of the reports in the metallography section presented here shows that electron microscopy has been chiefly applied to determinations of the structure of heat-resistant alloys, and alloys in which separation processes occur, studies of dislocation distribution, and to studies of structural changes after plastic deformation or rupture of metals.

As far as methods are concerned, we may mention the promising direct investigations with foils obtained by thinning bulk samples and the wide application of electronography, although, unfortunately, microdiffraction was applied in only a few isolated cases.

There was a complete absence of reports devoted to direct surface investigations by emission or reflection microscopes, even though there are a number of well-known works indicating the great promise of such methods in metallography.

G. V. Spivak, V. N. Vertsner, V. M.
Luk'yanovich, E. E. Levin and Yu. A. Skakov

INTERDEPARTMENTAL SEMINAR ON CATHODE ELECTRONICS (17th MEETING)

At the meeting of the Interdepartmental Seminar on Cathode Electronics, convened on the 28th of November, 1960 at the Institute of Radio Engineering and Electronics, Acad. Sci. USSR, 6 reports on thermal and secondary electron emission were delivered.

The report of I. A. Rezgol' was concerned with those points on the volt-ampere characteristic of a thermoelectronic energy converter which represent optimal operation, from the point of view of power and efficiency. By means of an artificial division of the load voltage into two components, equations for the regimes of maximum available power and maximum efficiency in conversion were obtained, both for electron-retarding and electron-accelerating fields. The resultant equations were transcendental in relation to the load voltage, but the speaker presented a physically demonstrable and uncomplicated method for solving them. Furthermore, he proposed finding the operating points of general, rather than particular, volt-ampere characteristics given in reduced coordinates.

The paper by I. M. Dykman and P. M. Tomchuk dealt with questions of the electroconductivity and thermoelectronic emission of hot electrons in semiconductors. The speakers considered a uniform electron conductor with a sufficiently large concentration of n-type conductivity existing in a uniform electric field. From kinetic equations they calculated the pulse distribution of electrons with allowance for scattering by optical and acoustic phonons, ion impurities and n-type conductivity. The criterion for Maxwellian distribution of average-energy electrons at a temperature T_e, which exceeds the lattice temperature T, was obtained. At sufficiently high energies (greater than kT_e) the distribution function is also Maxwellian) but the temperature is that of the lattice, T. It was stated that the second region of the distribution function is important for thermal emission of hot electrons, while for semiconductor electron conductivity, the first region is significant. Calculations were given for semiconductor electroconductivity with heated electron gas and its dependence on the concentration of n-type conductivity, the field, and the sample temperature. Special attention was given to low-temperature regions in the lattice.

In the ensuing discussion, M. I. Yelinson and V. B. Sandomirskiy pointed out the need for carefully, considering shock ionization processes, the role of scattering by optical phonons, and the possibility of obtaining large hot-electron emission currents from semiconductors with extensive n-type conductivity.

G. V. Dudko and O. V. Mitrofanov told of their investigations on the thermoemissive properties of certain monocrystalline tungsten faces. By the straight-line method of Richardson they determined the work function Ψ and the constant A for flat surfaces (~ 0.5 cm^2 in area) with various crystallographic indices. Using the X-ray method they were able to determine the crystallographic orientation of these surfaces with great accuracy. The report contained a detailed explanation of the methods used to prepare the samples and the construction of the experimental apparatus. The measurements were conducted in a sealed tube at a vacuum of the order of $1 \cdot 10^{-8}$ to $5 \cdot 10^{-9}$ mm Hg.

The experimental results showed a marked difference in the magnitude of the thermal emission constant for different faces of the tungsten monocrystal, both in the presence and in the absence of a barium film.

Taking part in the discussion of the report, V. P. Shrednik, B. N. Popov, A. R. Shul'man and L. N. Dobretsov gave a number of factors which would tend to lower the accuracy of the emitter temperature determination and they took note of the inadequacy of the given vacuum conditions for experiments of this nature.

O. V. Mitrofanov gave a report entitled "Experimental Studies of Continuous Secondary-Electron Amplification" concerning a cylindrical multiplier with continuous voltage drop over the layer, without central focusing of the electrode. An analytical expression was given for the amplification factor M of the multiplier for a range of tolerances, and the results of investigations on a multiplier with an antimony-cesium emitter, and another with a specially developed solid, nonfilm emitter of magnesium orthotitanate ($2MgO \cdot TiO_2$), were presented.

For selected parameters, the $2MgO \cdot TiO_2$ multiplier gives linear characteristics and has the value $M = 10^5$ for a channel voltage of approximately $U_k = 4500$ v. Studies of the secondary emission of flat samples gave $\sigma_{max} = 1.8$ at $U = 400$ v.

In the discussion that followed, N. L. Yansnopol'skiy stated that the principles of operation of the instrument were first established and applied, in the photoelectric multiplier RS in 1939, by G. S. Vil'dgrube and V. S. Parkhomenko.

In the report of E. S. Mashkova and V. A. Timofeeva, "Secondary Emission of Certain Ferroelectric Monocrystals," data was presented from an investigation of the temperature dependence of secondary electron emission from ferroelectric and nonferroelectric modifications of potassium niobate ($KNbO_3$).

The investigators found that, for the nonferroelectric modifications, in the interval from 250 to 650°C, the coefficient of secondary emission was practically independent of temperature, which is in agreement with results on the temperature dependence in semiconductors the energy distribution of the secondary electrons was of the same type as that in semiconductors.

The coefficient of secondary emission for the ferroelectric modifications had a minimum in the vicinity of the Curie point.

K. A. Akopov, N. A. Karelina, V. I. Pokalyakin
and G. V. Stepanov

CORRECTION

In issue No. 4, 1961, page 680, 1st line from the bottom should appear: V. L. Patrushev.

RADIO ENGINEERING AND ELECTRONIC PHYSICS

Institute of Radio Engineering and Electronic Physics,
Academy of Sciences of the USSR

EDITORIAL BOARD

Editor-in-Chief: V.A. Kotel'nikov
Associate Editors: D.V. Zernov, Yu.B. Kobzarev

A.I. Berg
B.A. Vvedenskiy
I.S. Gonorovskiy
V.L. Granovskiy
L.A. Zhekulin
N.D. Devyatkov
L.N. Dobretsov
A.N. Kazantsev
S.G. Kalashnikov
P.L. Kapitsa
V.V. Migulin
A.L. Mikaelyan
A.A. Pistol'kors
A.M. Prokhorov
S.M. Rytov
V.I. Siforov
Ya.N. Fel'd
S.E. Khaykin
B.M. Tsarev

Scientific Secretary of Editorial Board: G.A. Bernashevskiy

The English Edition of Radio Engineering and Electronic Physics is mailed to subscribers within 18 weeks after the publication of the original Russian issue.

Russian electronic journals published by the
American Institute of Electrical Engineers
Translated by Royer and Roger, Inc.

	Subscription rates			
	Individuals		Libraries	
	$	£	$	£
Radio Engineering and Electronic Physics	28.50	10	57.00	20
Radio Engineering	14.25	5	28.50	10
Telecommunications	14.25	5	28.50	10

Royer and Roger translates and produces
the following Russian scientific journals:

Biophysics
Entomological Review
Geochemistry
Geodesy and Cartography
Izvestiya, Academy of Sciences of the USSR, Geologic Series
Pavlov Journal of Higher Nervous Activity
Problems of Oncology
Radio Engineering
Radio Engineering and Electronic Physics
Refractories
Sechenov Physiological Journal of the USSR
Soil Science
Telecommunications

Comments and inquiries regarding *Radio Engineering and Electronic Physics* and other translation journals should be sent to:

International Division
Royer and Roger, Inc.

1000 Vermont Avenue, N.W.
Washington 5, D.C.

41 East 28th Street
New York 16, New York

RADIO ENGINEERING AND ELECTRONIC PHYSICS

РАДИОТЕХНИКА И ЭЛЕКТРОНИКА

NUMBER 5 196

CONTENTS

V.M. Lopukhin, The Kinetic Power Theorem and its Application to Electron Beam Devices 60
B.N. Mityashev, Interference Immunity of Two Methods of Reception of Pulse Signals 62
G.V. Druzhinin, Supply of Spare Parts for Electronic Circuits on the Basis of Load 63
A.I. Kalinin, Effect of Earth in UHF Tropospheric-Scatter Propagation 64
V.V. Novikov and G.I. Makarov, Propagation of Pulsed Signals over a Homogeneous Flat Earth 64
Yu.L. Kokurin, A.N. Sukhanovskiy et al., Investigation of a Model of Large-Scale Ionospheric Inhomogeneities by a Radio Astronomical Method 65
G.N. Krylov, Structure of Electromagnetic Field of Directional Antennas above a Flat Earth with Finite Conductivity 66
A.Ya. Yashkin, A Method of Calculation of Characteristic Modes and Dispersion in Straight and Bent Waveguides of Complex Cross Section 66
L.N. Loshakov, Coupling Coefficient between Electron Beam and Transverse Electromagnetic Field in a Microwave Waveguide 67
A.K. Musin, Plasma Motion in Crossed Electric and Magnetic Fields 68
M.D. Karasev, Influence of Parasitic Parameters of a Semiconductor Diode upon the Operation of a Parametric Amplifier 68
A.L. Mikaelyan and A.A. Vasil'yev, Interaction of Magnetostatic Oscillations in a Ferrite Sample in the Case of Regeneration. Part II—Conditions of Excitation of Oscillations in General 69
N.G. Basov, V.V. Nikitin, et al., Investigation of Maser Frequency Dependence upon Different Parameters. Part I—(Theory, Line $J=3$, $K=2$) 70
G.A. Siulina and G.A. Feshchenko, Fe^{3+} Spin Levels in Corundum 71

BRIEF COMMUNICATIONS

F.I. Khaytun, Increase in the Transmission Range of Pulse Signals of Given Energy in the Presence of Noise with an Arbitrary Spectrum 72
B.A. Dubinskiy, Method for Ideal Measurement of Oscillation Parameters 72
B.A. Sukhov, Characteristic Resistance and Attenuation of a TEM Wave Propagating along a Multiconductor Line Made Up of Rectangular Conductors 72
L.R. Yavich, Remarks on the Calculation of Cascade Connections of n- Similar Two-Ports 72
M.B. Tseytlin and Ye.M. Il'ina, On the Form of the Field in a Backward Wave Tube in the Presence of Distributed Attenuation 73
A.A. Shur and G.S. Maksimov, One Method of Measuring the Fluctuation of the Phase of Radio Waves in a Study of Tropospheric Scatter Propagation 73
Ye.M. Gershenzon, N.F. Ptitsyna, et al., Single-Loop Parametric Amplifier . . . 73
A.N. Vakhrameyev, Experimental Investigation of Forces Oscillation in a Parametrically Regenerated Tank Circuit 74
Ye.M. Gershenzon and V.S. Etkin, Spectral and Amplitude-Frequency Characteristics of Superregenerative Parametric Amplifiers 74
Yu.Ye. D'yakov, Transfer Function of a Superregenerative Parametric Amplifier . . 74
Yu.Ye. D'yakov, An Error in the Analysis of a Two-Loop M Parametric Amplifier . . 74
Yu.A. Kravtsov, Consideration of Combination Frequencies in Systems with Periodically varying Reactance 75
G.N. Berestovskiy, Effect of Asymmetry on the Operation of Push-Pull Semiconductor Converters With External Excitation 7
N.V. Karlov, Yu.P. Pimenov, et al., Paramagnetic Amplifier for the Ten-Centimeter Band Using Fe^{3+} Ions in Corundum 7
A.L. Mikaelyan, A.A. Vasil'yev, et al., Microwave Regeneration in a Ferrite in Response to Longitudinal Pumping. 7
V.G. Veselago, A Spin Generator 7

CHRONICLE

Third All-Union Conference on Electron Microscopy. 7
Interdepartmental Seminar on Cathode Electronics (17th Meeting). 7